An investigation of factors that regulate the cytoskeleton in the first mitotic division of the *C. elegans* embryo

By
Megha Bajaj

A thesis submitted in partial fulfillment of the requirements for the degree of

Doctor of Philosophy

In

Molecular Biology and Genetics

Department of Biological Sciences
University of Alberta

©Megha Bajaj, 2017

Abstract

Microtubule dynamics is regulated by naturally occurring microtubule-associated proteins occurring in the cellular environment as well as by natural and synthetic compounds. These compounds target the microtubule cytoskeleton and serve as anti-mitotic drugs. Therefore, microtubules continue to be one of the most effective targets for developing new anti-mitotic agents. Laulimalide is one such anti-mitotic agent that was isolated from the marine sponge, *Cacospongia mycofijiensis*. Laulimalide has been shown to disrupt microtubules in a manner similar to paclitaxel, by causing bundling of microtubules and inducing microtubule stabilization. However, the acute effects of laulimalide on microtubules and its mode of action are unclear. The *C. elegans* embryo is an excellent model to characterize microtubule-targeted drugs, and herein, I report the first analysis of laulimalide in this system. My work indicates that laulimalide induces a concentration-dependent, biphasic change in microtubule polymer dynamics in the embryo. This analysis provides novel information about the acute *in vivo* effects of laulimalide on the microtubule polymer and helps distinguish this anti-mitotic drug from the widely-used chemotherapeutic paclitaxel.

In the *C. elegans* embryo, CYK-1 formin is required for a late step in cytokinesis. Based on the localization of CYK-1, it has been proposed to function in cytokinesis by bridging microtubules and microfilaments at the cleavage furrow. This bridging role of CYK-1 could stabilize the cytokinetic cleavage furrow by binding to spindle microtubules at the mid-zone on one side and actin, which is associated with the plasma membrane, on the other side. CYK-1 has also been implicated in cortical functions prior to cytokinesis, suggesting that it has a more global role in regulating the actin cytoskeleton. Using live-cell imaging and reverse-genetics, I found that depletion of CYK-1 resulted in exaggerated spindle pole oscillations during anaphase

in the one-cell *C. elegans* embryo, suggesting that CYK-1 normally limits cortical forces in the embryo. UV laser-induced ablation of the cortex during mitosis showed that *cyk-1* contributes to an increase in cortical rigidity. Thus, the effect of *cyk-1* on spindle forces was likely due to changes in cortical elasticity. Additional experiments involving known components of the G-protein coupled cortical force generators also indicated that *cyk-1* likely does not alter cortical forces by modulating this pathway directly. This work contributes additional insight into how microtubules and the actin cytoskeleton coordinately modulate spindle forces during asymmetric cell division.

Preface

Some of the results presented in Chapter 2 of this thesis have been previously published as Bajaj M. and Srayko M. (2013) Laulimaldie induces dose-dependent modulation of microtubule behavior in the *C. elegans* embryo. PLoS One **8**(8): e71889. I was responsible for designing experiments, carrying out expriments and interpreting the results.

The results presented in chapter 3 and Appendix are an original work and have not been previously published.

Acknowledgements

I would like to thank my supervisor, Dr. Martin Srayko for accepting me into his lab. His guidance and support throughout my graduate program has been invaluable to me and I have learnt a lot from my discussions with him. I also want to acknowledge the guidance offered by my supervisory committee members: Dr. Shelagh Campbell and Dr. Gordon Chan. I would like to thank Dr. Gordon Chan for providing me with the reagents to finish my publication.

A big thanks to the members of the Srayko lab, both past and present. Karen L., Maryam, Tegha, Cheryl, Ellen, Eva, Jens and Rudra- thank you for all the help in the lab, your funny stories and making my stay in the lab so enjoyable. And to all those friends who lent an ear and helped me through this.

I would like to thank my parents and sister, Deepti for supporting me throughout my graduate program. A special thank you to my mother, for her unconditional love. Mumma- you are immensely missed and you continue to be my guiding light.

Lastly, I thank my loving husband, Ninad for the constant encouragement and support through the years. This would not have been possible without him by my side, thank you for everything. Words will never fully express my gratitude to him.

Table of contents

List of Tables

List of Figures

List of abbreviations and symbols

° C	degree Celsius
µl	microliter
µM	micromolar
nm	nanomolar
µm	micrometer
AAA+	ATPase associated with diverse activities
bp	basepair
dhc	dynein heavy chain
DIC	Differential interference contrast
DNA	Deoxyribonucleic acid
dsRNA	double stranded RNA
Gα	G-alpha
Gβ	G-beta
Gγ	G-gamma
GDP	guanine diphosphate
GTP	guanine triphosphate
GPR	G protein regulator
GFP	green fluorescent protein
IPTG	isopropyl β-D-1-thiogalactopyranoside
MAS	Martin A Srayko (lab designation for *C. elegans* strains)
MAP	Microtubule-associated protein
ml	milliliter
MTOC	Microtubule organizing centre
NEBD	Nuclear Envelope Breakdown
NGM	Nematode growth medium
NMY	Non-muscle myosin
pN	piconewton
RNA	Ribonucleic acid
RNAi	RNA interference
WT	Wild type

1. Introduction

Cells exhibit a myriad of behaviors that help them to adapt to their environment. Often correlated with a change in behavior is a change in cell morphology. Cells change their morphology as part of normal differentiation, during cell migration, and during cell division. At the molecular level, it is the cytoskeleton that provides the basis for these morphological changes. There are three main types of cytoskeletal polymers: microtubules, actin filaments and intermediate filaments. Together these polymers regulate the shape and mechanics of eukaryotic cells. All three types of polymers are highly organized into cellular networks that resist cellular deformation but can also respond to external forces and rearrange themselves in response to internal forces. These three components have rather different structural and physical properties, enabling specific cellular functions. However, there is growing evidence that interaction of these individual subsystems is required for various cellular functions (Swan, Severson et al. 1998, Rodriguez, Schaefer et al. 2003, Rosales-Nieves, Johndrow et al. 2006). The dynamic polymerization and depolymerization of actin and microtubule polymers drives the changes in cell shape, and other intracellular functions such as molecular-motor based transport of cellular cargo. Intermediate filaments can be cross-linked to each other as well as to microtubules and actin filaments. Intermediate filaments help to resist tensile forces and form organized structures in response to mechanical stress, *e.g.*, keratin intermediate filaments provide strength and support to epithelial cells. The 3 different types of cytoskeletal structures are coordinated to orchestrate a number of complex processes in the cell. During cell division, microtubules are essential for forming the division plane and assembling the mitotic spindle. In anaphase, the central spindle is formed of bundled microtubules and microtubule-associated motors and other accessory proteins, which promotes the assembly of filamentous actin to form the contractile

ring for cytokinesis. Thus, microtubules and the actin cytoskeleton interact with each other to establish the division plane. Guanine nucleotide exchange factors (GEFs) and GTPase activating proteins (GAPs) help to regulate the interactions between actin and microtubules. However, we currently do not completely understand how this crosstalk is regulated at the mechanistic level.

The cytoskeleton plays an important role in cell division. During the development and adult life of multicellular organisms, cell division is essential to replenish cells that have a limited life span. Cell division is tightly regulated and subjected to many quality control checkpoints, as any errors can lead to cell death, tumor formation, or developmental defects. In many cases, cellular diversity occurs during cell division, resulting in daughter cells that differ in their developmental potential, via an asymmetric cell division. This form of cell division involves the partitioning of different developmental determinants into the future daughter cells and requires a coordinated regulation of the cytoskeleton to ensure that the cell division plane is correctly oriented during division. In many systems such as neuroblasts in *Drosophila* and the *C. elegans* one-cell embryo, the orientation of the mitotic spindle is precisely regulated during asymmetric cell division, which offers an opportunity to understand the molecular pathways that facilitate cellular asymmetry and spindle positioning.

1.1 Introduction to asymmetric cell division

Asymmetric cell division is an evolutionarily conserved mechanism for generating cell diversity during development. Asymmetric cell divisions can generate two daughter cells that are different in size, protein content and have different developmental fate. There are a number of examples of asymmetric cell division, which have been well studied in various organisms. For example, the development of neuroblasts in *Drosophila*, asymmetric cell division in mammalian epidermis, bud formation in *Saccharomyces cerevisiae* and the first mitotic division in the *C. elegans* embryo are all extensively studied systems that have already provided many clues on how this type of cell division is achieved.

Conklin first described asymmetric cell division in ascidian embryos (Conklin 1905). He described the development of the larval tail muscle in the early embryo and reported the presence of yellow colored cytoplasm that always segregated with the presumptive tail muscle cells (Conklin 1905). The yellow pigment worked as a cell lineage marker and this study helped to establish that the egg is inhomogeneous in composition. This was followed by investigation of cell asymmetry in a number of model organisms. In 1988, a screen done to identify mutations that affect *C. elegans* asymmetric cell division was reported (Kemphues, Priess et al. 1988). Four of the mutants were the par (abnormal embryonic partitioning of cytoplasm) genes, *par-1*, *par-2*, *par-3* and *par-4* that were identified in this screen. This was followed by identification of *par-5*, *par-6* and *pkc-3* (atypical protein kinase C) (Watts, Etemad-Moghadam et al. 1996, Tabuse, Izumi et al. 1998, Morton, Shakes et al. 2002). *pkc-3* is also classified as a *par* gene because removal of its product from the embryo also causes phenotypes similar to the *par* mutant embryos (Tabuse, Izumi et al. 1998). Embryos that lack functional PAR proteins divide symmetrically and also show similar distribution of cell-fate determinants in both the daughter cells. In 1994, the NUMB protein was described in the *Drosophila* external sensory organ (Uemura, Shepherd et al. 1989). Numb localized only on one edge of the cell, forming a crescent shape and segregated into only one of the daughter cells, which later develops into sensory neurons (Uemura, Shepherd et al. 1989).

In a simplistic model, asymmetric cell division is described in three simple steps (figure 1.1). During interphase, a set of proteins determines the polarity axis of the embryo; during mitosis the polarity axis is used to specify spindle orientation and segregation of cell fate determinants. This is followed by telophase, during which spindle orientation and asymmetric localization serve as a compass for the cell to ensure that the polarized factors are segregated only to one daughter cell. These polarized factors are important for the generation of cell diversity.

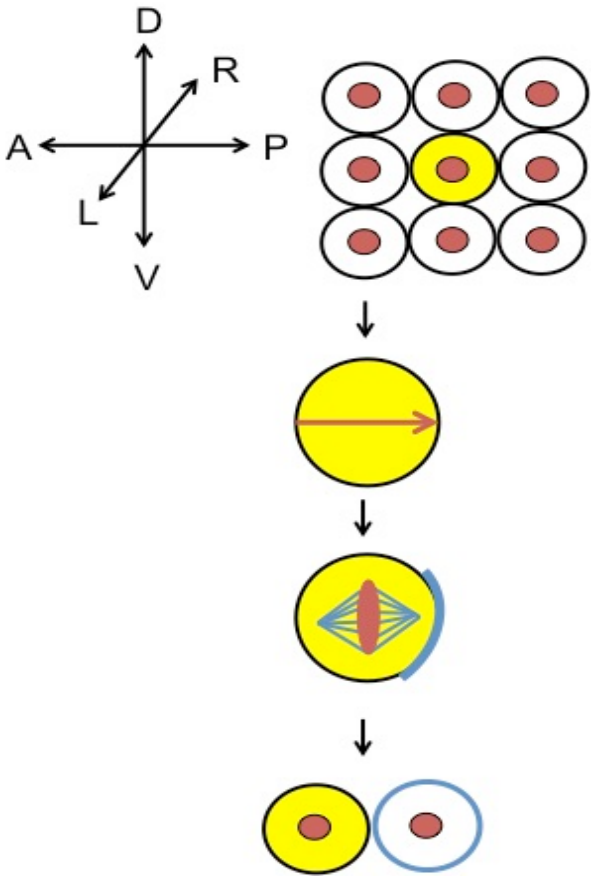

Figure 1.1: Simplistic model of asymmetric cell division. An axis of polarity is first established to provide orientation of cell division. Cell fate determinants (proteins, mRNA or signaling molecules) are localized in an asymmetric manner. During mitosis, the spindle orients along the axis in such a way that cytokinesis creates daughter cells with different concentrations of cell fate determinants. Adapted from Knoblich J.A., 2001.Nat Rev Mol Cell Biol.

Our understanding of asymmetric cell division has been refined since then due to emerging research in a number of organisms. The basics of asymmetric cell division in *Drosophila* and *C. elegans* are described below.

1.1.1 Asymmetric cell division in *Drosophila* neuroblast

In *Drosophila melanogaster*, a well-studied model of asymmetric cell division is the neuroblast, which generates the majority of cells of the central nervous system. The neuroblast undergoes about 20 rounds of asymmetric cell division to form the neurons of the larval nervous system. There are several types of larval neuroblasts.

The most prevalent ones are the type I neuroblasts. Type I neuroblasts undergo asymmetric division, forming a larger daughter cell that retains the stem cell identity and continues to divide asymmetrically. The smaller daughter cell is called the ganglion mother cell (GMC). The GMC forms two terminally differentiated neurons or glial cells. The type II neuroblast is located in the dorso-posterior region of the central brain hemisphere. The smaller cell arising from the type II neuroblast forms an intermediate neural precursor (INP). The INP undergoes self-renewal and forms one INP and one GMC.

The mechanism of asymmetric cell division in *Drosophila* neuroblast involves asymmetric localization of proteins. The NUMB protein and the translation inhibitor Brain tumor (BRAT) accumulate in the basal plasma membrane during late prometaphase. Two adaptor proteins help facilitate the asymmetric localization of NUMB (Spana, Kopczynski et al. 1995) and BRAT (Lee, Wilkinson et al. 2006). BRAT localizes by binding Miranda (Lee, Wilkinson et al. 2006), (Betschinger, Mechtler et al. 2006) and NUMB localization is facilitated by the adaptor protein Partner of Numb (PON) (Lu, Rothenberg et al. 1998). Miranda also localizes a transcription factor Prospero into the GMC. After these basal determinants are localized, the spindle is oriented in the apical-basal plane so that these determinants are inherited by the GMC.

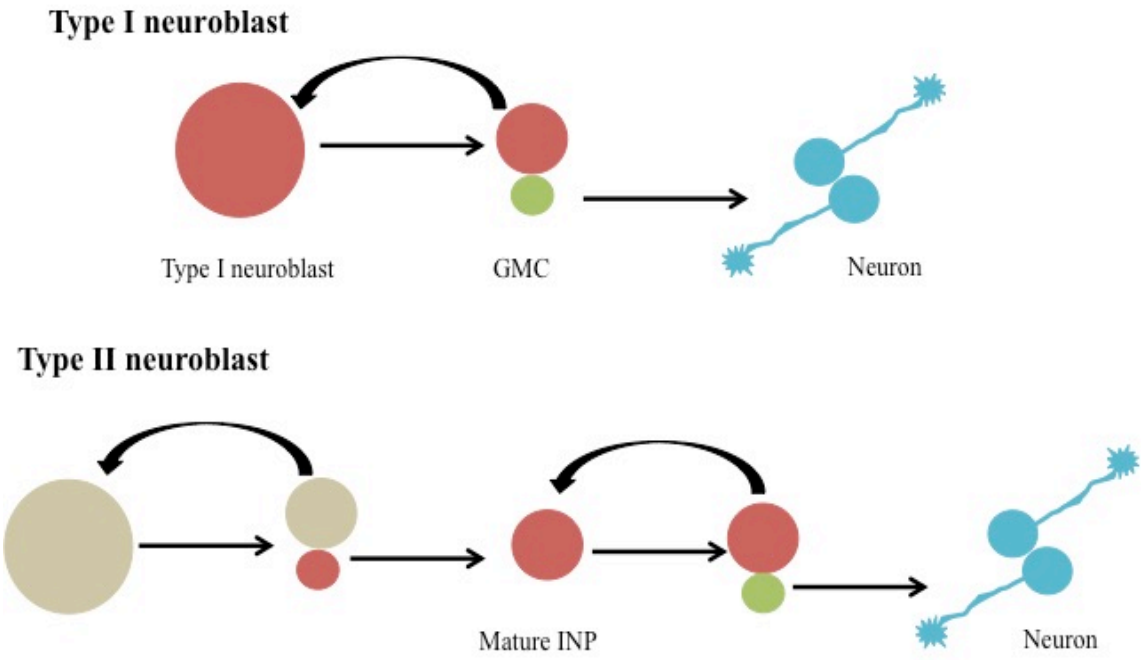

Figure 1.2: Asymmetric cell division in the *Drosophila* neuroblast. A wild type neuroblast undergoes asymmetric division to self-renew and to generate a Ganglion mother cell (GMC). The GMC then differentiates and forms the neuron. In case of abnormal division, the neuroblast divides to form symmetric neuroblast-like daughter cells which self-renew and lead to neuroblast overgrowth.

The PAR proteins localize to the apical cell cortex before mitosis. The localization of PAR proteins at the apical cortex also specifies the asymmetric localization of basal determinants. PAR-3, PAR-6 and the aPKC localize to the apical cortex in the neuroblast. The adaptor protein Inscuteable is required for linking the PAR-3-PAR-6-aPKC complex to a second protein complex that contains heterotrimeric G proteins (Kraut and Campos-Ortega 1996). The PAR proteins are also involved in asymmetric cell division in the *C. elegans* embryo. In Drosophila they act as a major regulator of asymmetric cell division. In case of the *C. elegans* embryo they are involved in both regulating asymmetric cell division as well as in the symmetry-breaking event; this is explained below.

1.1.2 Asymmetric cell division in the *C. elegans* embryo

In *C. elegans*, the first asymmetric cell division generates an anterior AB cell and a posterior P1 cell. The size and fate of these daughter cells are different and the mechanism that generates the asymmetry is similar to the *Drosophila* neuroblast. In the hermaphrodite *C. elegans* gonad, the acentriolar oocytes arrest in meiosis I until they get fertilized. Fertilization occurs when the oocyte passes through the spermatheca and gets fertilized by a sperm cell.

The sperm typically enters the embryo on the opposite side of the female pronucleus. The entry of the sperm releases the meiosis arrest followed by completion of meiosis I and II (Hubbard and Greenstein 2000). In addition to the male pronucleus, the sperm cell also contributes a pair of centrioles**.** The centriole assembles the pericentriolar material (PCM) to form a centrosome that nucleates microtubules. Sperm entry also specifies the future posterior domain of the embryo by initiating an organization of the PAR proteins to two complementary domains. PAR-3, PAR-6 and aPKC are initially uniform throughout the cortex. However, after sperm entry they concentrate at the anterior domain of the cortex forming the anterior- (PAR-3/PAR-6/PKC; protein kinase C) and the posterior- (PAR-1/PAR-2) embryo cortex (Cowan and Hyman 2004). The mutual exclusion of the PAR proteins from each domain ensures a polarized distribution in the embryo.

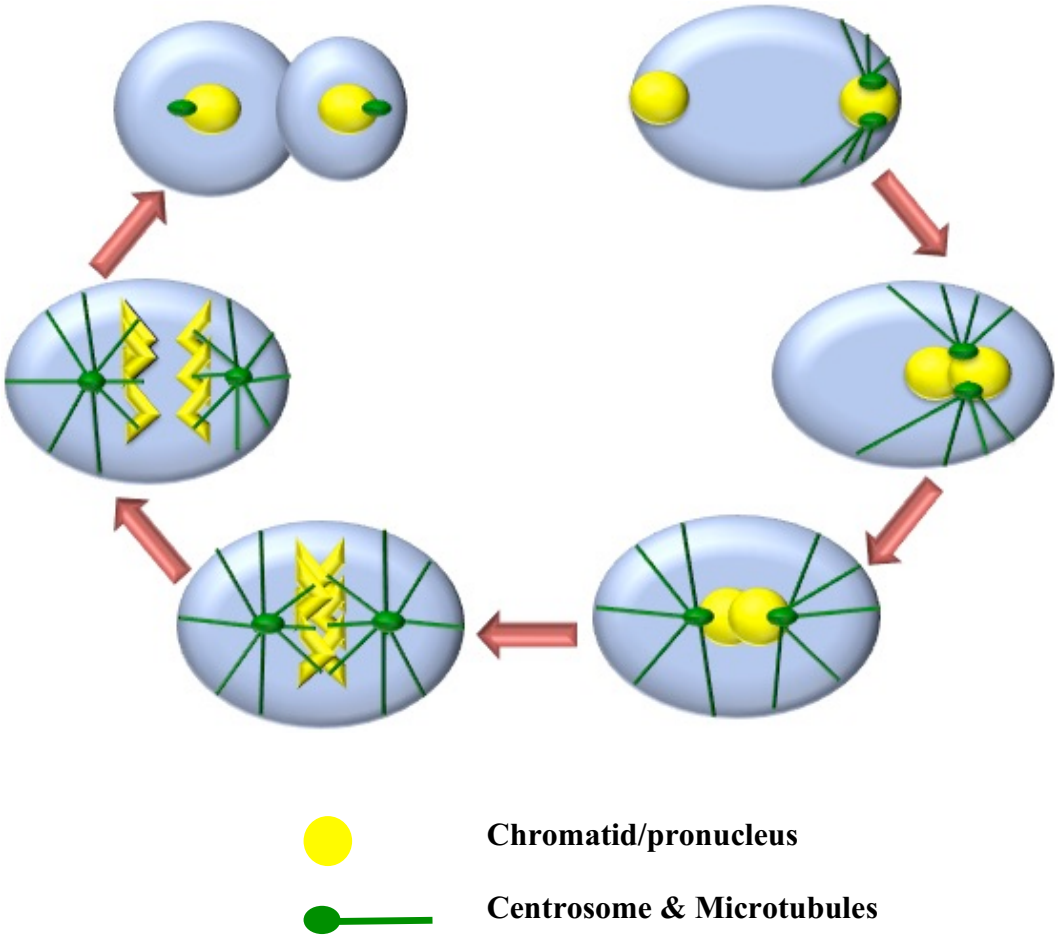

Figure 1.3: First cell division in the *C. elegans* embryo. The main events in the first mitotic cell division are shown.

After fertilization, the anterior cortical actin in the *C. elegans* embryo undergoes surface contractions. These contractions are called “cortical ruffling” which induces cytoplasmic streaming into the posterior cortex. Cytoplasmic streaming causes slow movement of the female pronucleus towards the posterior of the embryo. Once the microtubules from the sperm-donated centrosomes contact microtubule motor proteins on the oocyte nuclear envelope, the male pronucleus also starts moving towards the female pronucleus. This causes the male and the female pronuclei to meet in the posterior domain of the embryo (Tsou, Hayashi et al. 2003). This is followed by centration and rotation of the pronuclei. As evidenced by modeling studies, centration in the *C. elegans* embryo occurs by pushing forces generated by microtubules and dynein motor protein (Kimura and Onami 2005). It was shown that depletion of a light chain subunit of dynein, DYRB-1 blocks the minus-end directed motion of dynein and this also blocks movement of early and late endosomes in the cytoplasm. Once the pronuclei reach the cell center these anterior directed forces cease to act. This can possibly be explained by the buildup of higher pulling forces on the posterior side acting on the centrosome during late prophase (Labbe, McCarthy et al. 2004). At this time, the spindle remains in the center of the embryo. The reason for the central localization of the spindle at this point has been explained by an anterior ‘tether’ that possibly holds the anterior centrosome in place, preventing the movement of spindle to the posterior at this stage (Labbe, McCarthy et al. 2004). Centration and rotation of the pronuclei also causes alignment of the mitotic spindle along the anterior-posterior axis of the embryo (Cowan and Hyman 2004, Labbe, McCarthy et al. 2004).

This is followed by nuclear envelope breakdown (NEBD), which allows microtubules to attach to chromosomes. During metaphase, the centrosomes separate to a small extent and the spindle moves slightly towards the posterior domain of the embryo. This indicates that, although forces are applied throughout the mitotic spindle, there is net posterior-directed force acting on the spindle apparatus (Cowan and Hyman 2004, Labbe, McCarthy et al. 2004). At the same time there is a resistant force active on the anterior cortex, which opposes higher cortical forces to prevent excessive movement of the spindle in the posterior domain, as discussed above

(Labbe, McCarthy et al. 2004). At anaphase initiation, the mitotic spindle starts oscillating in the transverse plane and these oscillations are maintained throughout anaphase. During this time, the chromosomes have separated. In many organisms, anaphase is completed in two phases, anaphase A and anaphase B. During anaphase A, chromosomes separate as a result of shortening of the kinetochore microtubules (Desai, Maddox et al. 1998). During anaphase B, separation of the spindle pole takes place, and sister chromatids that are attached to opposite poles move away from each other. In *C. elegans*, the majority of the force contribution for chromosome segregation is from anaphase B (Oegema, Desai et al. 2001) and cortical pulling forces. During chromosome segregation, higher force acting on the posterior cortex pulls the posterior spindle pole to the posterior of the embryo. At this time, the anterior spindle pole remains stationary and this creates an off-centered spindle mid-zone. The positioning of the spindle as well as other cortical factors determines the location of the cytokinetic cleavage furrow (Glotzer 2003, Bringmann and Hyman 2005).

1.2 Spindle positioning and movement during asymmetric cell division

In the *C. elegans* embryo, during the movement of the mitotic spindle towards the posterior domain, the spindle oscillates in the transverse plane. At this time, the anterior and posterior spindle poles move perpendicular to the A-P axis of the embryo and the oscillations of the two poles are out of phase. The amplitude of these transverse oscillations builds up slowly and reaches a peak as the spindle approaches most-posterior position. The amplitude of oscillations then starts decreasing and finally dies down. Because of the sinusoidal movement, it seems like the mitotic spindle is rocking around a point closer to the anterior pole. This oscillatory movement of the spindle is also referred to as ‘spindle rocking’.

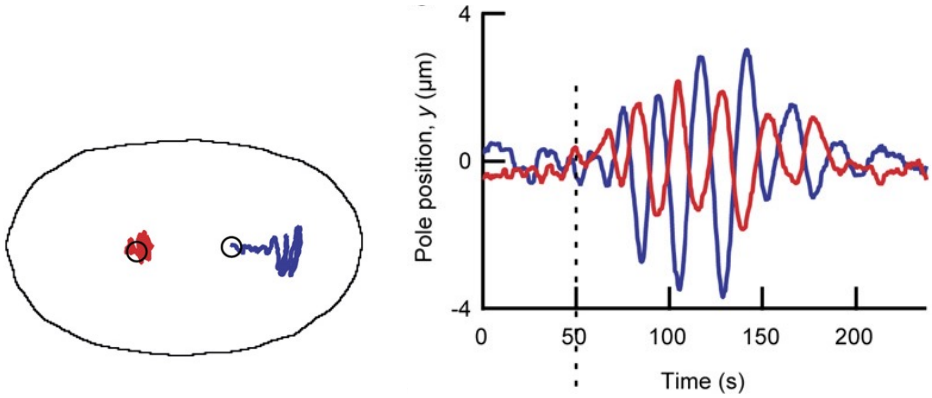

Figure 1.4: Spindle Oscillations during asymmetric cell division in the *C. elegans* embryo. The embryo shows movement of the anterior and posterior spindle poles during anaphase. The graph shows the build -up and die down of the spindle oscillations during anaphase. The red indicates anterior spindle pole and blue indicates posterior spindle pole.

Source: License number: 3984630402771. Reprinted from Spindle Oscillations during Asymmetric Cell Division Require a Threshold Number of Active Cortical Force Generators, 16 (21), Pecreaux J. *et al*., p2111-2122. Copyright (2006), with permission from Elsevier.
Reprinted from The Lancet, 16. 21, Pecreaux J. *et al*, Spindle Oscillations during Asymmetric Cell Division Require a Threshold Number of Active Cortical Force Generators, p2111-2122.

The exact function of the oscillations remains unknown; however, mitotic spindle oscillations have been associated to asymmetric divisions in many organisms (Haydar, Ang et al. 2003). In *C. elegans*, a model has been put forth to explain how the oscillations occur during asymmetric cell division. The model explains that the oscillations occur due to a combination of microtubule elasticity and the force generators attaching and detaching from the astral microtubules that contact the cortex. Based on mathematical modeling, it has been predicted that a critical number of force generators undergo binding and detachment with the astral microtubules stochastically at the cortex. In addition, the posterior cortex has more force generators compared to the anterior cortex. However, the total number of force generators remains constant throughout metaphase and anaphase but the activity of motors increases over the course of time (during anaphase). Therefore, the model predicts that an increase in the motor activity of force generators is responsible for the increase in oscillations in the embryo. Though, spindle oscillations are not necessary for asymmetric cell division, it is possible that the occurrence of spindle oscillations during anaphase is used by the cell as a read-out of sufficient force generation (Grill, Kruse et al. 2005, Pecreaux, Roper et al. 2006).

Proper positioning of the mitotic spindle is crucial for successful asymmetric cell division in the *C. elegans* embryo. The most prominent component of the mitotic spindle is microtubules and the forces that orient the spindle asymmetrically act through microtubules and the proteins that bind to them. Microtubules are filamentous polymers formed of α and β tubulin heterodimers. Microtubules are polarized and they have a slow growing 'minus end' and a highly dynamic 'plus end'. The slow-growing minus end is embedded in the centrosome while the fast growing plus end approaches the inner cortex of the embryo. The polymerization rate of microtubules in *C. elegans* embryo is approximately 0.7 μm/s (Srayko, Kaya et al. 2005). Therefore, this allows the microtubules to reach the inner cortex within approximately 20 seconds after nucleation from the centrosome (Srayko, Kaya et al. 2005). After the plus end of microtubule contacts the inner cortex, microtubule depolymerization occurs in approximately 1.4 seconds (Kozlowski, Srayko et al. 2007). Until cell

division is completed, the plus ends of the microtubules continue a cycle of polymerization/depolymerization. Therefore, the plus end of microtubules transiently contacts the inner embryonic cortex, where the force generators for anaphase-pulling forces are located. Laser ablation studies done in *C. elegans,* where either the mitotic spindle was severed or the centrosomes were ablated; show that the spindle/centrosome fragments are pulled towards the cortex. (Grill, Gonczy et al. 2001, Grill, Howard et al. 2003). Statistical analysis of the mean and variance of the fragment velocities show that after ablation, the fragments moving towards the posterior moved with a higher velocity compared to the fragments moving towards the anterior cortex (Grill, Howard et al. 2003). This suggests that anaphase forces are generated by pulling on astral microtubules that touch the embryonic inner cortex.

A study that investigated the role of EFA-6, a putative guanine nucleotide exchange factor, shows that it can regulate microtubule dynamics at the cortex (O'Rourke, Christensen et al. 2010). Embryos that were depleted of EFA-6 showed an increased number of microtubules contacting the cortex. In addition, the residence time of microtubules at the cortex was increased in these embryos. EFA-6 is enriched on the anterior side of the embryo (O'Rourke, Dorfman et al. 2007). It would be interesting to investigate whether the asymmetric distribution of EFA-6 contributes to the asymmetry in anaphase pulling forces in the embryo.

Cortical pulling forces presumably require the interaction of microtubule ends with force generators at the embryo cortex, it is possible that more force is generated on the posterior cortex because more microtubules grow from the posterior centrosome or they grow faster than the microtubules emanating from the anterior centrosome. However, a study that investigated the number of microtubules and the growth rate of microtubules in the *C. elegans* embryo showed that both the number of microtubules as well as their growth rate is identical on the anterior and posterior side throughout the cell cycle (Srayko, Kaya et al. 2005). This suggests that the asymmetry in the cortical forces during anaphase is due to the interaction of microtubules with

the force generators at the cortex. These force generators are discussed in the next section.

1.3 Asymmetric forces arise from an asymmetry in the embryo cortex

At the end of the first mitotic division of the *C. elegans* embryo results in the formation of a larger anterior cell called AB (25% larger) and a smaller posterior cell called P1. In *C. elegans* one-cell embryos, the mitotic spindle is asymmetrically positioned because of an imbalance of net pulling forces on the spindle poles during anaphase (Grill, Gonczy et al. 2001). The majority of the force in the embryo is derived from the microtubule-based force generators that involve heterotrimeric G proteins, dynein motor protein and other associated proteins at the inner cortex.

1.3.1 The role of dynein motor protein in cortical force generation

Dynein is a minus-end directed microtubule motor protein, it moves along the microtubule minus end, *i.e.,* the movement of dynein is towards the centrosome (Vallee, Williams et al. 2004). The motor protein was identified more than 50 years ago in *Tetrahymena pyriformis* cilia (Gibbons 1963). Dynein was named after the greek word *"dyne"* meaning force (Gibbons and Rowe 1965) because of its role in cilary movement. The class of dynein present in flagella and cilia is also called axonemal dynein. Cytoplasmic dynein is structurally and functionally different than axonemal dynein. It is a homodimer consisting of 2 identical heavy chains, also referred to as dynein heavy chain (DHC). The dynein heavy chain consists of a 350-400 kDa ring-shaped motor domain. The motor domain belongs to a large family of related AAA+ proteins (ATPases associated with diverse activities). There are 6 AAA+ modules linked together into a large polypeptide. There is a tail domain for dimerization and binding accessory proteins and a microtubule-binding domain, which is a coiled-coil stalk.

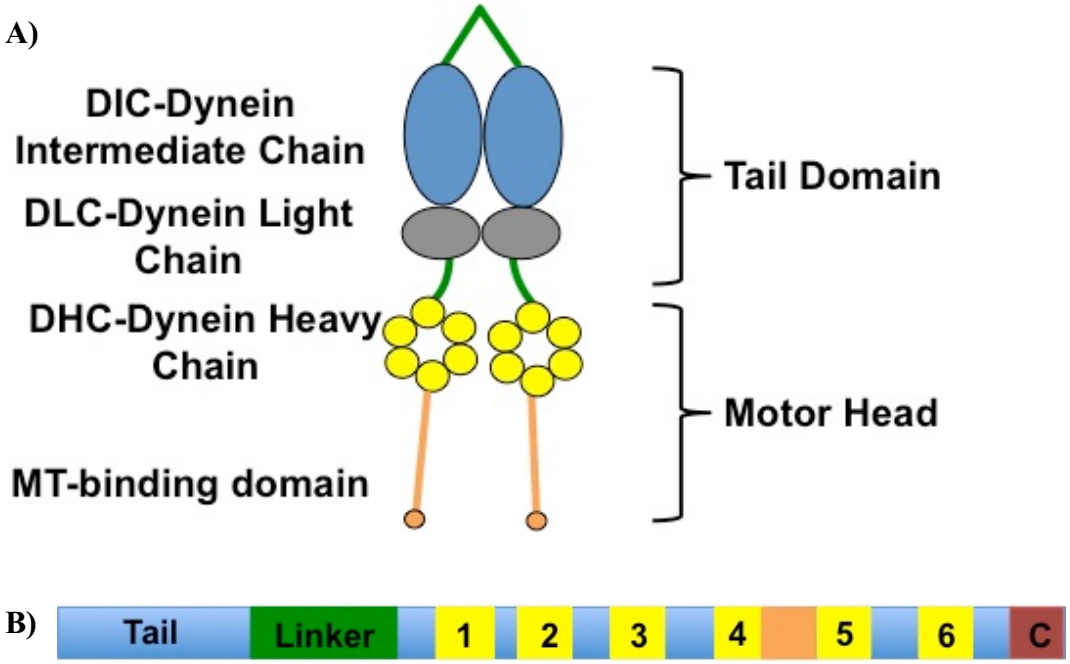

Figure 1.5: Cytoplasmic Dynein Structure. A) Dynein motor complex is shown with its intermediate, light and heavy chains.
B) Organization of the domains in the motor head. The 6 AAA+ modules are shown in yellow blocks. Microtubule binding domain is the stalk shown in orange. C stands for the C-terminus sequence of DHC

The ATP hydrolysis cycle is coupled to dynein movement, which is characterized by conformational change in the motor domain and microtubule-binding domain. In the absence of ATP, the 6 AAA+ modules are present in a "straight" conformation with the N-terminus of the polypeptide linker on the AAA+ ring. At this time, the microtubule-binding domain is attached strongly to the microtubule. When ATP binds to AAA+, the linker bends and microtubule-binding domain of dynein loses its attachment to microtubule. After ATP hydrolysis, dynein motor rebinds to microtubule and this causes the linker to undergo the powerstroke. The transition of the linker from a bent to straight conformation produces force which propels the cargo for movement (Schmidt and Carter 2016).

Dynein is involved in a number of cellular processes like intracellular trafficking, microtubule organization, chromosome segregation and organelle positioning. Dynein is present at the cell cortex, kinetochore, centrosomes, nuclear envelope, spindle microtubules and this localization at different sub-cellular locations is possible because of dynein's interaction with a number of adaptor proteins.

An important regulator of dynein is dynactin protein. Dynactin is a multi-subunit protein and is about 1MDa in size. Dynactin interacts with dynein to help in transportation of cargo along microtubules. The p150 glued subunit of dynactin tethers and recruits dynein on the microtubules. In an in-vitro assay it has been shown that the N-terminus of the p150-glued subunit of Dynactin is essential for promoting sustained interaction of dynein with microtubules. Point mutations in the CAP-Glycine (Cytoskeletal associated protein- glycine rich domain) of p150 subunit increased the detachment rate of dynein from microtubules (Ayloo, Lazarus et al. 2014). The CAP-Glycine domain of dynactin is important to enrich dynactin distally on the axons where dynactin can interact with cargo such as late endosomes, lysosomes for the dynein-driven transport of cargoes from the distal end of axons. Point mutations in the CAP-Glycine domain of dynactin have been implicated in neurodegenerative diseases.

Dynactin binds both microtubules and dynein, it has been implicated in increasing dynein motor's processivity along the microtubule lattice (King and Schroer 2000). In *C. elegans* embryo depletion of dynactin causes defects in pronuclear/centrosome complex centration and the pronuclear centrosome complex remains on the posterior of the embryo (Skop and White 1998, O'Rourke, Carter et al. 2011).

1.3.2 Dynein interacts with the G-protein complex to generate cortical force

The heterotrimeric G protein complex consists of Gα, Gβ and Gγ and are found either associated in a single complex, or dissociated into Gα and Gβγ, the latter of which remains as a dimer (Gotta and Ahringer 2001, Srinivasan, Fisk et al. 2003, Nguyen-Ngoc, Afshar et al. 2007). The heterotrimeric G proteins are normally inactive, in this state Gα is bound to GDP. Upon activation by a GEF, GDP is exchanged for GTP, which causes Gα to dissociate from Gβγ. The dissociated partners may then activate target effectors, which vary depending on the system. With respect to force generation in *C. elegans* embryos, subsequent hydrolysis of Gα-GTP to Gα-GDP promotes a physical interaction between Gα and GPR-1/2, which forms part of an active force-generator complex that includes other proteins, including LIN-5 and dynein as shown in figure 1.6 (Gotta and Ahringer 2001, Srinivasan, Fisk et al. 2003, Nguyen-Ngoc, Afshar et al. 2007).

Previous work done in *C. elegans* has shown that depletion of Gα and GPR-1/2 by RNAi results in loss of spindle oscillations and greatly reduced spindle movement (Gotta and Ahringer 2001). On the other hand, depletion of Gβ protein causes an increase in spindle oscillations, which can be suppressed by *Gα(RNAi)* (Gotta and Ahringer 2001). This suggests that Gα is the activator of cortical forces and Gβγ opposes Gα activity and suppresses cortical forces. The activator protein, GPR-1/2 and the dynein binding protein, LIN-5 are asymmetrically localized and enriched on the posterior cortex (Grill, Howard et al. 2003, Park and Rose 2008), suggesting that this is a key mechanism for increasing pulling forces on the posterior pole during

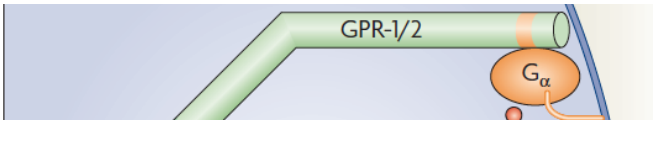

anaphase. Previous work indicated that this complex generates force in the embryo by interacting with the dynein motor protein.

Dynein generates spindle oscillations and is required for posterior spindle displacement during anaphase (Grill, Howard et al. 2003, Schmidt, Rose et al. 2005, Nguyen-Ngoc, Afshar et al. 2007). There is interesting data from a number of studies that provides insight into how dynein might be working to generate cortical force in the *C. elegans* embryo. Co-immunoprecipitation experiments have shown that LIN-5 protein associates with dynein. In addition, upon depletion of the components of the ternary complex, the presence of dynein at the cortex is also affected (Nguyen-Ngoc, Afshar et al. 2007). Dynein is anchored to the embryo cortex by the G-protein complex and it has been hypothesized that the motor activity of dynein generates the cortical pulling force. The G-protein complex is anchored to the plasma membrane via the myristoyl and palmitoyl lipid modification in the Gα protein. As shown in figure 1.7, dynein being a minus-end directed motor protein attempts to move on the astral microtubule from the plus end towards the minus end. In doing so it pulls on the astral microtubules and generates the pulling force (Nguyen-Ngoc, Afshar et al. 2007, Kotak and Gonczy 2013, di Pietro, Echard et al. 2016). However, another interesting report indicates that cortical dynein and its lattice-interaction with microtubules (as shown in figure 1.8) is not sufficient to generate spindle-pulling forces during anaphase (Gusnowski and Srayko 2011). In this study, an elegant assay was developed to measure the motor activity of dynein at the embryo cortex.

As shown in figure 1.6 microtubules that reach the cortex of the embryo can either interact with dynein in a lateral manner or in an end-on manner. Depending on how dynein interacts with microtubules, two different models for force generation were predicted in the *C. elegans* embryo (shown in figure 1.8) (Gusnowski and Srayko 2011).

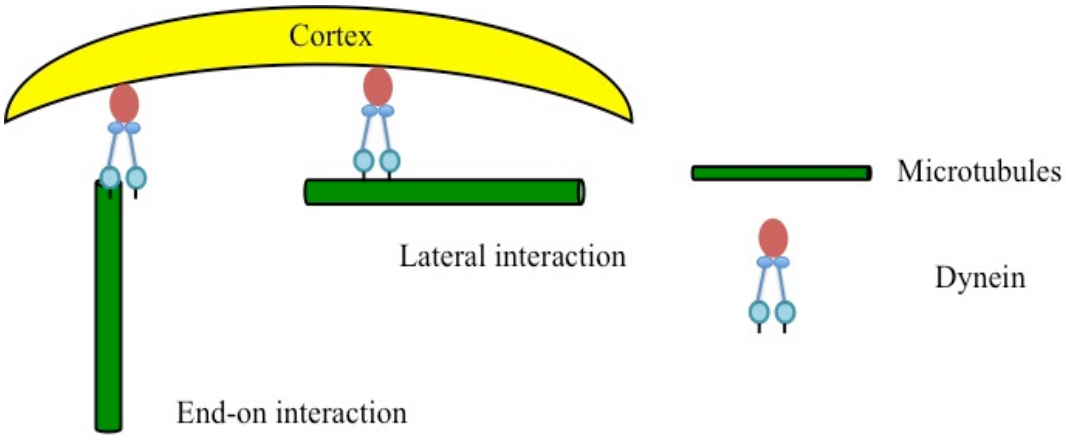

Figure 1.6: Dynein microtubule interaction at the cortex. In end-on interaction dynein motor protein holds onto the plus end of microtubules. This type of microtubule interaction is common during metaphase-anaphase when the microtubule ends approach the cortex at an orthogonal angle. During pronuclear migration and centering, microtubules approach the cortex at a shallow angle, in this case, dynein motors walk from plus end of microtubules towards the minus end.

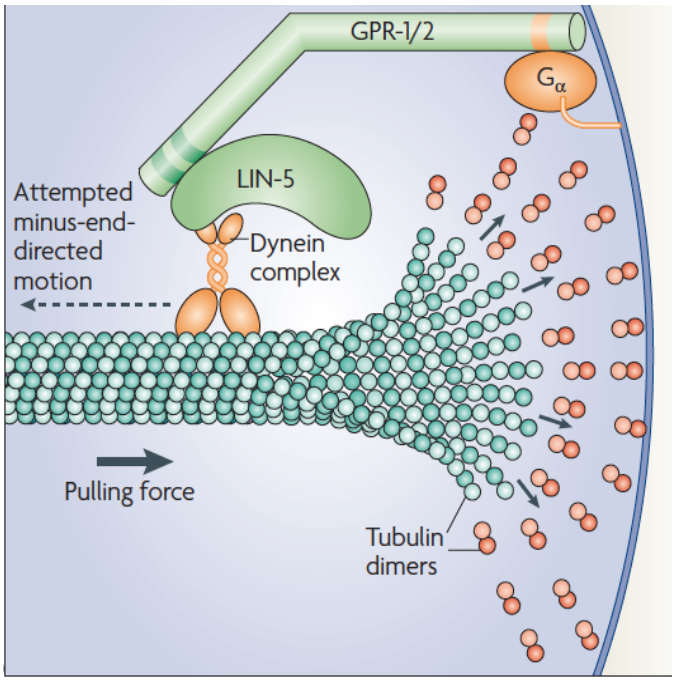

Figure 1.7: Heterotrimeric G-protein complex in the *C. elegans* embryo. Dynein complex associates with LIN-5, which then interacts with GPR-1/2. In turn, GPR-1/2 binds to Gα, which is present at the embryo cortex thus recruiting the dynein-LIN-5-GPR-1/2 complex to the cortex. Since dynein is a minus-end directed motor it moves towards the minus end of microtubule, in turn, generating a pulling force on the astral microtubule at the cortex.

Source: License number: 3950560915190. Reprinted by permission from Macmillan Publishers Ltd: Nat Rev Mol Cell Biol,**9**(5): p. 355-66. Mechanisms of asymmetric cell division: flies and worms pave the way. Gonczy, P., copyright (2008).

During anaphase, most of the microtubules emanating from the centrosome approach the cortex at an orthogonal angle. This angle is more likely to result in an end-on microtubule-dynein interaction. At this time, anaphase-pulling forces occur primarily through end-on interaction of dynein with the plus end of microtubules. On the other hand, during pronuclear centering stage, most of the microtubules approach the embryo cortex at shallow angle. Therefore, this angle is more amenable to lateral interactions between dynein and microtubules. Due to the lateral contact, dynein can walk along the microtubule lattice, which generates a force contributing to pronuclear centration. In addition, it is also possible that these two modes of force generation are not mutually exclusive and both types of interactions occur at both stages of cell cycle. However, it is possible that the end-on interaction is more productive during anaphase and lateral interaction is more prevalent during pronuclear centration stage (Gusnowski and Srayko 2011). This model presents an important contrast on the assumptions that the minus-end directed movement of dynein on microtubule alone generates anaphase-pulling forces. Interestingly, data from budding yeast indicates that spindle positioning and displacement employs both end-on interaction and lateral interaction of microtubules with force generators (Carminati and Stearns 1997, Adames and Cooper 2000).

Another hypothesis regarding force generation by dynein motor proteins is related to the dynamic nature of microtubules. An *in vitro* assay where dynein was tethered to micro-fabricated chamber shows that the microtubule plus end interacts with dynein, this interaction inhibits their growth and causes microtubule depolymerization (Laan, Pavin et al. 2012). The interaction of dynein with microtubule plus ends helps in positioning of the spindle. A computer-simulation study done in the *C. elegans* embryo suggests that dynein at the cortex could hold onto depolymerizing microtubules to generate cortical pulling force (Kozlowski, Srayko et al. 2007).

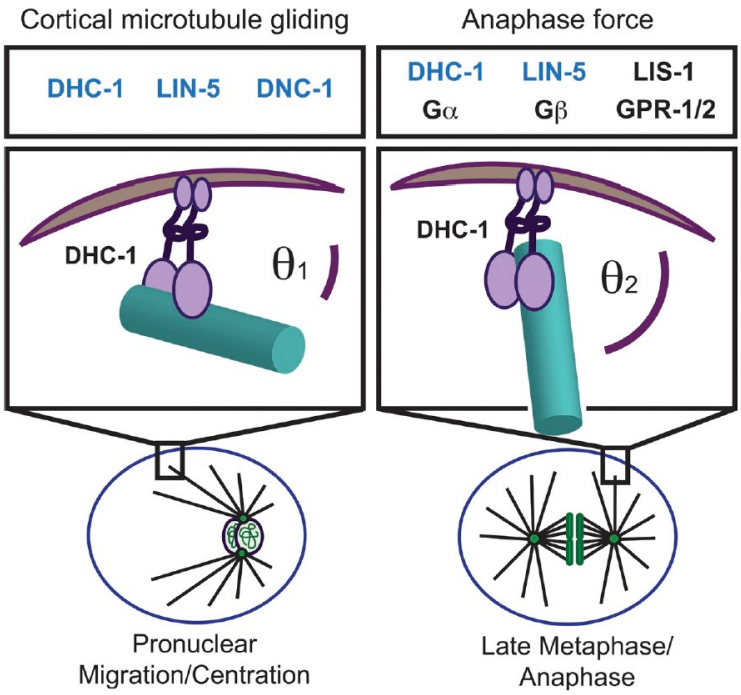

Figure 1.8: The angle between microtubule and the cortex could determine the type of interaction between dynein and microtubule. During pronuclear migration/centration the microtubule approached the cortex at a shallow angle and dynein possibly interacts laterally with microtubules. During anaphase, microtubules reach the cortex at right angle and dynein and microtubules interact in an end-on manner.
Source: License number: 3986710224796. Reprinted by permission from Rockefeller University Press. Copyright 2011. Gusnowski and Srayko. Visualization of dynein-dependent microtubule gliding at the cell cortex: implications for spindle positioning. JCB. 194 (3): PP 377-386. doi: 10.1083/jcb.201103128

An *in-vitro* study done using yeast cytoplasmic dynein has shown the end-on pulling of microtubules by dynein motor protein (Laan, Pavin et al. 2012). In this study, immobilized and purified dynein on microfabricated barrier was used to observe the interaction of centrosome-nucleated microtubules. When the microtubule plus ends hit a dynein-coated barrier, they switched to catastrophe; however, the rate of microtubule depolymerization rate was reduced after catastrophe. Because of this reduction in microtubule depolymerization rate, there was an extended period of interaction between microtubule depolymerizing end and the dynein. The depolymerization of microtubule was also accompanied by centrosome pulling toward the barrier. The measured pulling force was ~ 5 pN. There was no lateral microtubule interaction with the dynein barrier observed in this study. The reason for this is currently not known, however some speculation has been made. During end-on interaction of dynein-microtubule it is possible that 2 or more dynein molecules interact with the protofilament on opposite sides. This type of interaction is absent during lateral MT-dynein interaction at the cortex, as there are no physical constraints available to keep dynein molecules associated with the microtubule polymer on both the ends. This could be one of the reasons no lateral-dynein-microtubule interaction was observed in this microfabricated barrier study (Laan, Pavin et al. 2012).

The ternary G-protein complex and dynein motor proteins locate to the inner cortex of the embryo and are important for cortical force generation during anaphase. However, there is another important factor that regulates cortical force. The acto-myosin network also characterizes the inner cortex. The contribution of the acto-myosin network in cortical force generation is discussed below.

1.3.3 The physical characteristics of the cortex plays a role in force generation

The physical composition and properties of the eukaryotic cortex is not completely understood. However, a lot of work has been done in various systems to identify the components and physical properties of the cortex. These studies have established that the cortex consists of a thin layer of actin filament, myosin motor

protein and other proteins that associate with the plasma membrane (Mayer, Depken et al. 2010, Ramalingam, Franke et al. 2015). This acto-myosin derived cortex is highly dynamic and myosin motors generate active stresses in the network by interacting with the actin filament (Mayer, Depken et al. 2010). Expansion and contraction of the acto-myosin cortex generates tension, which has important roles in cell division, cell migration and for tissue reorganization (Salbreux, Charras et al. 2012, Vinzenz, Nemethova et al. 2012).

In *C. elegans* embryo, the acto-myosin network characterizes the inner cortex. This meshwork provides rigidity to the inner cortex and also serves as a substrate for attachment of various proteins that are anchored to the cortex. In addition to actin, the non-muscle myosin protein, NMY-2 is also localized at the inner cortex of the embryo. Actin and NMY-2 overlap and form the acto-myosin network surrounding the cortex as depicted in figure 1.9.

After the sperm enters the oocyte and the embryo is fertilized, NMY-2 is required to maintain cortical contractility (Munro, Nance et al. 2004). Cortical localization of both NMY-2 foci and actin foci often show spatial overlap (as shown in figure 1.3). The NMY-2 and actin foci together bring about cortical surface contractions. These surface contractions are important for polarization of the embryo (Munro, Nance et al. 2004, Werner, Munro et al. 2007). Upon anaphase onset, the NMY- 2 patches form a contractile network via the connecting actin foci (Werner, Munro et al. 2007). Acto-myosin is not only important for cortical contractility and cytoplasmic streaming but it also influences microtubule-based forces on the mitotic spindle (Munro, Nance et al. 2004). Furthermore, in a computer-modeling study of the *C. elegans* embryo, by altering the cortical rigidity/elasticity of the embryo the spindle pole oscillations and spindle displacement were simulated. Based on the results, the authors postulated that a softer (more elastic and less rigid) posterior cortex could result in sustained pulling forces acting on the posterior spindle (Kozlowski, Srayko et al. 2007). In addition, when an actin destabilizing drug, latrunculin A was applied to

the embryos during anaphase, the anterior spindle pole experienced a higher cortical force (Afshar, Werner et al. 2010). Moreover, a study that investigated the movements of the centrosome during centration/rotation in the first mitotic division found that application of latrunculin caused small disruptions in the acto-myosin network. In this study, embryos with perturbed acto-mysoin network showed exaggerated movements of the centrosome (Spiro, Thyagarajan et al. 2014). In addition, another study showed that it is possible to visualize the sites of force generation in embryos where the actomysoin network has been perturbed (Redemann, Pecreaux et al. 2010). By partial depletion of NMY-2 and other regulators of the actin cytoskeleton, membrane invaginations extended from the cortex and were directed towards the centrosome. These membrane invaginations are generated by microtubules, because treatment of these embryos with nocodazole eliminated these extensions (Redemann, Pecreaux et al. 2010).

Thus, in addition to heterotrimeric proteins and dynein, the structural integrity of the acto-myosin cortex also plays an important role in maintaining the spindle oscillations and posterior spindle displacement during anaphase. Therefore, cortical elasticity of the embryo also plays a significant role in determining the differential cortical forces.

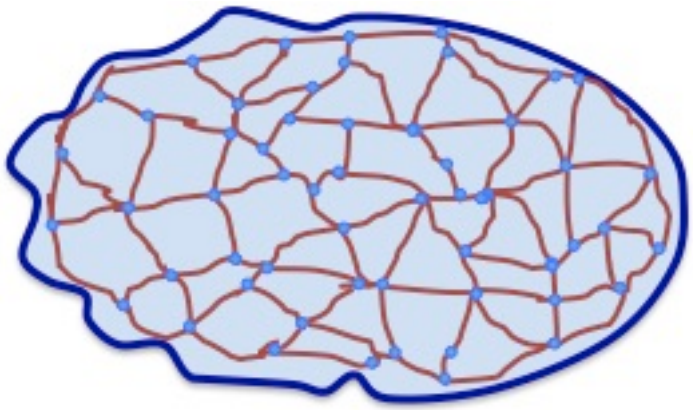

Figure 1.9: The cortical acto-myosin network. Acto-myosin is present as a meshwork surrounding the embryo cortex. NMY-2 foci are shown in light blue and actin is shown in brown.

1.4 Spindle positioning and cleavage formation

The role of spindle positioning and furrow formation was first examined over 100 years ago. Hertwig discovered that sea urchin embryos undergo spindle orientation along the long axis of the cell (Lu and Johnston 2013, Moorhouse and Burgess 2014). His model stated that cells sensed shape changes, oriented the mitotic spindle along the longest axis in the cell and divided perpendicular to the longest axis of the cell (Lu and Johnston 2013, Moorhouse and Burgess 2014). Later on, micromanipulation experiments done by Rappaport in Sand dollar embryos indicated that positioning of the mitotic spindle is capable of forming cleavage furrow (Oegema and Mitchison 1997). These experiments indicated that astral microtubules are capable of inducing a cleavage furrow at the cortex.

1.4.1 Cleavage furrow induction

Over the last 100 years, it has been tested and experimentally verified that the mitotic spindle plays a significant role in positioning the division plane (Rappaport 1961, Rappaport 1996). The simplest example comes from the early studies done by Rappaport in marine invertebrate embryos (Rappaport 1961, Rappaport 1996). In his experiment, when the spindle was displaced to a new position, the old furrow regressed and the new cleavage furrow coincided with the new spindle position.

In another micromanipulation experiment, Rappaport showed that multiple cleavage furrows could be formed in a cell when the mitotic spindle is moved closer to the cell cortex (Rappaport 1997). When physical blocks (e.g.- oil droplet) were kept in the centre of the mitotic spindle, the furrow formed at its usual position at the cortex. These early experiments indicated that microtubules from the spindle midzone are not required for furrow formation and that astral microtubules of the spindle are sufficient to induce cleavage furrow formation (Rappaport 1983). Though the above results show that astral microtubules are sufficient to form the cleavage furrow, the

mode of cleavage specification is likely specific to the model organism. The spindle midzone plays an important role in furrow formation in other systems. For example, asterless mutants of *Drosophila* spermatocytes do not form astral microtubules, however, the spindle midzone microtubules are normal in these mutants (Bonaccorsi, Giansanti et al. 1998) and they are able to undergo furrow formation and cytokinesis. Thus, these experiments indicate that different organisms and cell types use different methods to form the cytokinesis furrow.

C. elegans provides some interesting results in the role of the central spindle and aster microtubules for the formation of the furrow. The central spindle consists of two proteins, ZEN-4 (a kinesin-like protein) and CYK-4, a GTPase activating protein. Both proteins are required for the formation of the central spindle in *C. elegans* embryos (Jantsch-Plunger, Gonczy et al. 2000). However, embryos depleted of either protein forms cleavage furrows, suggesting that the central spindle is dispensable for the formation of the cleavage furrow. A study in *C. elegans* shows that a local minimum density of microtubules at the cortex is required for furrow formation (Dechant and Glotzer 2003). The radial distribution of microtubules around the mitotic spindle is not homogenous. Moreover, the central spindle as well as spindle elongation, contribute to the spatial distribution of microtubules around the mitotic spindle in the embryo. Based on data from measuring microtubule density at the presumptive furrow site, centrosome-separation measurements and initiation of furrow formation, authors in the study show that when the central spindle component ZEN-4 was simultaneously depleted with the PAR-2 protein (required for asymmetric division and centrosome separation), furrow initiation was inhibited (as shown in figure 1.10).

However, furrow initiation was not affected when these proteins were depleted individually. These results led them to propose that low microtubule density, generated by proper centrosome separation is key for cleavage furrow formation and the signals from the central spindle are required subsequently for furrow ingression (Dechant and Glotzer 2003).

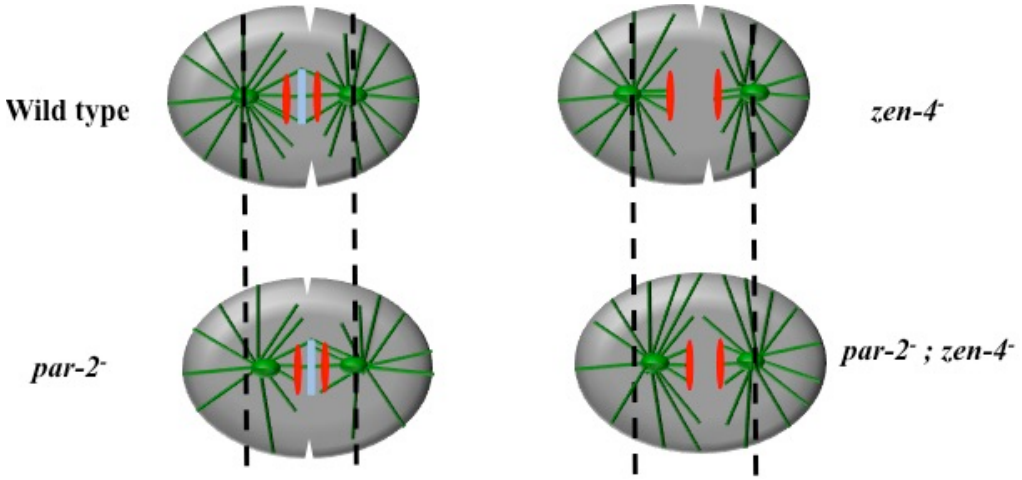

Figure 1.10 The model for initiation of furrow formation. The chromosomes are shown here in red and spindle mid-zone in light blue. The broken black line compares the extent of centrosome separation in embryos. Based on the model in Dechant and Glotzer, 2003.

1.4.2 Cytokinesis

The final step of mitosis, cytokinesis, is initiated during late anaphase. The assembly of an equatorial contractile ring is triggered by signals from the anaphase spindle. This leads to the enrichment of actin and NMY-2 at the equatorial ring, which is followed by constriction of the contractile ring (Glotzer 2005). The microtubule and actin cytoskeleton components that contribute to cytokinesis in the *C. elegans* embryo were broadly divided into 3 classes based on the phenotype obtained on depleting the genes. The original classification divided the proteins functioning in cytokinesis into 3 broad classes. Class 1 includes proteins involved in initiation of cytokinesis and contractile events. The class 2 proteins are required for central spindle formation and completion of cytokinesis and class 3 proteins are the components of the chromosomal passenger complex, which are also required for central spindle formation (www.wormbook.org) (Glotzer 2005).The class 1 proteins initially included the following proteins. NMY-2 protein localizes to the equatorial contractile ring, it provides the force for contraction of the actin filaments (Munro, Nance et al. 2004). NMY-2 is activated by phosphorylation of MLC-4 (myosin light chain). MLC-4 phosphorylation activates NMY-2 and allows it to interact with actin filaments (Shelton, Carter et al. 1999). The small GTPase RHO-1 and its guanine exchange factor ECT-2 are considered main regulators of cortical contractility in the one-cell embryo (Piekny, Werner et al. 2005, Motegi and Sugimoto 2006). A RHO binding kinase, called LET-502 localizes to the contractile ring. LET-502 promotes phosphorylation of MLC-4 and thereby indirectly helps in NMY-2 mediated contractility in the embryo. Previous studies have reported that depletion of LET-502 slows down the rate of furrow ingression; however it does not completely inhibit it (Piekny and Mains 2002). Cytokinesis failure does occur at random in these embryos but a lot of embryos also show normal cell division (Piekny and Mains 2002). In embryos depleted of RHO-1 all contractile events prior to first mitosis, *i.e.* cortical ruffling and polar body formation as well as cleavage ingression during cytokinesis is

blocked. PFN-1 (profilin) is required for assembly and maintenance of cortical actin. PFN-1 binds to another protein, CYK-1 (cytokinesis defective) that is also required for actin assembly. Depletion of PFN-1 and CYK-1 also causes defects in cytokinesis (Severson, Baillie et al. 2002). Another actin-binding protein, ANI-1 (Anillin) also belongs to this group. ANI-1 localizes to the contractile ring, however, embryos depleted of ANI-1 do not show cytokinesis defects (Monen, Maddox et al. 2005). ANI-1 is required for pseudocleavage, cortical ruffling and polar body formation during early embryo development. Imaging and immunofluorescence experiments have shown that ANI-1 is required for targeting the septin proteins to the site of cytokinesis furrow but not for targeting NMY-2 (Monen, Maddox et al. 2005, Piekny and Glotzer 2008). Anillin promotes the organization of cortical myosin into large foci and is required for its polarization along the anterior-posterior axis (Tse, Piekny et al. 2011). Thus, anillin acts as a molecular scaffold by interacting with F-actin, myosin, septins and formins to organize the cytoskeleton (Piekny and Glotzer 2008, Watanabe, Okawa et al. 2010).

The spindle midzone forming proteins were grouped into class 2 proteins. As cytokinesis progresses, the two daughter cells remain connected for some time by a transient structure called the midbody. The midbody is formed by the compaction of the central spindle microtubules. The spindle midzone is formed of an array of microtubules that bundle between the separating chromosomes. A kinesin protein ZEN-4 and a GTPase activating protein, CYK-4 together form a complex and localize at the central spindle midzone. Both of these proteins are required for the organization of the spindle midzone and cytokinesis completion. However, depletion of these proteins does not affect furrow initiation (Jantsch-Plunger, Gonczy et al. 2000, Severson, Hamill et al. 2000). The aurora-related kinase AIR-2 also plays an important part in midzone formation and is required for completion of cytokinesis (Severson, Hamill et al. 2000). The chromosomal passenger proteins were grouped into class 3. The chromosomal passenger proteins form a complex and localize to the chromosomes during mitosis and to the central spindle and mid body during anaphase and telophase. The members of this complex in *C. elegans* are ICP-1, CSC-1 and

BIR-1. BIR-1 and ICP-1 are required for successful chromosome segregation during anaphase, assembly of the spindle midzone and for completion of cytokinesis (Romano, Guse et al. 2003) (Kaitna, Mendoza et al. 2000). ICP-1 is phosphorylated by AIR-2 kinase (Bishop and Schumacher 2002).

The SPD-1 protein initially formed a class of its own and was not grouped into any of the classes as described above. SPD-1 localizes to the spindle midzone and also to astral microtubules. It has been reported that depletion of SPD-1 causes cytokinesis failure in the 4-cell stage and is non-essential for cytokinesis in the one-cell stage.
Initially, the cytokinesis proteins were divided into three classes to reflect their involvement in different stages of cytokinesis, such as furrow formation, ingression and abscission. However, recent work has shown that proteins from these classes interact with each other to collectively orchestrate cytokinesis. During cytokinesis, ECT-2 activation requires its interaction with CYK-4 (a component of the centralspindlin complex). CYK-4 binding to the N-terminus of ECT-2 relieves auto-inhibition and activates ECT-2 (Wolfe, Takaki et al. 2009). ECT-2 is a guanine exchange factor for the small G-protein, RHO-1. When Rho is bound to GTP, a conformational switch results in an increased affinity of Rho for downstream effector proteins. There are two main Rho effectors involved in cytokinesis, the formin family member CYK-1, and Rho-dependent kinase, ROCK (Piekny, Werner et al. 2005). Activated RHO-1 binds CYK-1 in the GTPase binding domain (GBD) on the N-terminus and this activates CYK-1. As a formin family member, CYK-1 is thought to promote actin polymerization for the formation of the actomyosin contractile ring. The FH1 and FH2 domains of CYK-1 bind to profilin and actin, respectively, to facilitate the polymerization of actin. In the absence of active RHO, CYK-1 would be expected to remain in an autoinhibited state through binding between the C-terminal and N-terminal domains. This has been shown for the formin Diaphanous, whereby N-terminal DID (diaphanous inhibitory domain) and C-terminal DAD (diaphanous autoregulatory domain) interact to inhibit its activity (Chesarone, DuPage et al. 2010).

Another activator of RHO-1 in *C. elegans* is NOP-1. NOP-1 is thought to be part of a pathway that is parallel to CYK-4, which promotes events downstream of

RHO activation. NOP-1 is also required for earlier events like maintaining cortical contractility in the embryo and for normal pseudocleavage formation (Tse, Werner et al. 2012). During polarization, NOP-1 is required for all RHO-1 dependent events. During cytokinesis, the main function of NOP-1 is to activate RHO-1 and initiate cytokinetic furrow ingression in the embryo (Tse, Werner et al. 2012).

The *C. elegans* one-cell embryo serves as an excellent model to study asymmetric cell division. As part of its normal development, it undergoes stereotypical rounds of cell division in a highly reproducible manner (Kaltschmidt and Brand 2002, Pearson and Bloom 2004). The one-cell embryo is large (~50 μm along the anterior-posterior axis) and its optical clarity makes it suitable to study the mechanics of asymmetric cell division and early events can easily be tracked. In addition, a sequenced genome, advancement of techniques like RNAi, CRISPR and sophisticated live-cell microscopy has further contributed to the success of this model organism in studying various cellular processes. Furthermore, there are about 21,000 protein coding genes identified in the *C. elegans* genome and ~7500 of these genes have human orthologs (Shaye and Greenwald 2011). Therefore, studies done in *C. elegans* can lead to a better understanding of biological processes in humans.

1.5 Goals of this thesis

As part of my efforts to understand microtubule dynamics in the one-cell embryo, I used a specialized microscopy assay to study microtubule-binding drugs in *C. elegans* embryo. Specifically, I tested the acute effects of a potential anti-mitotic agent laulimalide on the first mitotic division in the one-celled embryo and compared it with a known microtubule stabilizer, paclitaxel and microtubule destabilizer, nocodazole. The results from this project are presented in chapter 2 of this thesis and have been published earlier (Bajaj and Srayko 2013). I worked on another project, where I elucidated the role of a formin homology gene, *cyk-1* in first asymmetric cell division in the one-celled *C. elegans* embryo. I investigated the function of CYK-1 in cortical force generation during anaphase in the first asymmetric cell division in the embryo. The results from this project are presented in chapter 3 of this thesis. Testing the acute effects of the drug laulimalide on microtubules and studying the role of

CYK-1 protein in *C. elegans* mitosis will lead to better understanding of the contribution these factors make in regulating microtubule dynamics.

Aamodt, E. J. and J. G. Culotti (1986). "Microtubules and microtubule-associated proteins from the nematode Caenorhabditis elegans: periodic cross-links connect microtubules in vitro." J Cell Biol **103**(1): 23-31.

Adames, N. R. and J. A. Cooper (2000). "Microtubule interactions with the cell cortex causing nuclear movements in Saccharomyces cerevisiae." J Cell Biol **149**(4): 863-874.

Afshar, K., M. E. Werner, Y. C. Tse, M. Glotzer and P. Gonczy (2010). "Regulation of cortical contractility and spindle positioning by the protein phosphatase 6 PPH-6 in one-cell stage C. elegans embryos." Development **137**(2): 237-247.

Andreu, J. M. and S. N. Timasheff (1986). "Tubulin-colchicine interactions and polymerization of the complex." Ann N Y Acad Sci **466**: 676-689.

Bajaj, M. and M. Srayko (2013). "Laulimalide induces dose-dependent modulation of microtubule behaviour in the C. elegans embryo." PLoS One **8**(8): e71889.

Bennett, M. J., K. Barakat, J. T. Huzil, J. Tuszynski and D. C. Schriemer (2010). "Discovery and characterization of the laulimalide-microtubule binding mode by mass shift perturbation mapping." Chem Biol **17**(7): 725-734.

Bennett, M. J., G. K. Chan, J. B. Rattner and D. C. Schriemer (2012). "Low-dose laulimalide represents a novel molecular probe for investigating microtubule organization." Cell Cycle **11**(16): 3045-3054.

Betschinger, J., K. Mechtler and J. A. Knoblich (2006). "Asymmetric segregation of the tumor suppressor brat regulates self-renewal in Drosophila neural stem cells." Cell **124**(6): 1241-1253.

Bishop, J. D. and J. M. Schumacher (2002). "Phosphorylation of the carboxyl terminus of inner centromere protein (INCENP) by the Aurora B Kinase stimulates Aurora B kinase activity." J Biol Chem **277**(31): 27577-27580.

Bollag, D. M., P. A. McQueney, J. Zhu, O. Hensens, L. Koupal, J. Liesch, M. Goetz, E. Lazarides and C. M. Woods (1995). "Epothilones, a new class of microtubule-stabilizing agents with a taxol-like mechanism of action." Cancer Res **55**(11): 2325-2333.

Bonaccorsi, S., M. G. Giansanti and M. Gatti (1998). "Spindle self-organization and cytokinesis during male meiosis in asterless mutants of Drosophila melanogaster." J Cell Biol **142**(3): 751-761.

Bringmann, H. and A. A. Hyman (2005). "A cytokinesis furrow is positioned by two consecutive signals." Nature **436**(7051): 731-734.

Brogdon, C. F., F. Y. Lee and R. M. Canetta (2014). "Development of other microtubule-stabilizer families: the epothilones and their derivatives." Anticancer Drugs **25**(5): 599-609.

Carminati, J. L. and T. Stearns (1997). "Microtubules orient the mitotic spindle in yeast through dynein-dependent interactions with the cell cortex." J Cell Biol **138**(3): 629-641.

Carvalho, A., S. K. Olson, E. Gutierrez, K. Zhang, L. B. Noble, E. Zanin, A. Desai, A. Groisman and K. Oegema (2011). "Acute drug treatment in the early C. elegans embryo." PLoS One **6**(9): e24656.

Chen, J., T. Liu, X. Dong and Y. Hu (2009). "Recent development and SAR analysis of colchicine binding site inhibitors." Mini Rev Med Chem **9**(10): 1174-1190.

Clark, E. A., P. M. Hills, B. S. Davidson, P. A. Wender and S. L. Mooberry (2006). "Laulimalide and synthetic laulimalide analogues are synergistic with paclitaxel and 2-methoxyestradiol." Mol Pharm **3**(4): 457-467.

Corley, D. G., R. Herb, R. E. Moore, P. J. Scheuer and V. J. Paul (1988). "Laulimalides. New potent cytotoxic macrolides from a marine sponge and a nudibranch predator." The Journal of Organic Chemistry **53**(15): 3644-3646.

Cowan, C. R. and A. A. Hyman (2004). "Asymmetric cell division in C. elegans: cortical polarity and spindle positioning." Annu Rev Cell Dev Biol **20**: 427-453.

D'Agostino, G., J. del Campo, B. Mellado, M. A. Izquierdo, T. Minarik, L. Cirri, L. Marini, J. L. Perez-Gracia and G. Scambia (2006). "A multicenter phase II study of the cryptophycin analog LY355703 in patients with platinum-resistant ovarian cancer." Int J Gynecol Cancer **16**(1): 71-76.

De Brabander, M., G. Geuens, R. Nuydens, R. Willebrords and J. De Mey (1981). "Taxol induces the assembly of free microtubules in living cells and blocks the organizing capacity of the centrosomes and kinetochores." Proc Natl Acad Sci U S A **78**(9): 5608-5612.

Dechant, R. and M. Glotzer (2003). "Centrosome separation and central spindle assembly act in redundant pathways that regulate microtubule density and trigger cleavage furrow formation." Dev Cell **4**(3): 333-344.

Desai, A., P. S. Maddox, T. J. Mitchison and E. D. Salmon (1998). "Anaphase A chromosome movement and poleward spindle microtubule flux occur At similar rates in Xenopus extract spindles." J Cell Biol **141**(3): 703-713.

Desai, A. and T. J. Mitchison (1997). "Microtubule polymerization dynamics." Annu Rev Cell Dev Biol **13**: 83-117.

Dhamodharan, R., M. A. Jordan, D. Thrower, L. Wilson and P. Wadsworth (1995). "Vinblastine suppresses dynamics of individual microtubules in living interphase cells." Mol Biol Cell **6**(9): 1215-1229.

di Pietro, F., A. Echard and X. Morin (2016). "Regulation of mitotic spindle orientation: an integrated view." EMBO Rep **17**(8): 1106-1130.

Don, S., N. M. Verrills, T. Y. Liaw, M. L. Liu, M. D. Norris, M. Haber and M. Kavallaris (2004). "Neuronal-associated microtubule proteins class III beta-tubulin and MAP2c in neuroblastoma: role in resistance to microtubule-targeted drugs." Mol Cancer Ther **3**(9): 1137-1146.

Dumontet, C. and M. A. Jordan (2010). "Microtubule-binding agents: a dynamic field of cancer therapeutics." Nat Rev Drug Discov **9**(10): 790-803.

Dumontet, C., M. A. Jordan and F. F. Lee (2009). "Ixabepilone: targeting betaIII-tubulin expression in taxane-resistant malignancies." Mol Cancer Ther **8**(1): 17-25.

Gapud, E. J., R. Bai, A. K. Ghosh and E. Hamel (2004). "Laulimalide and paclitaxel: a comparison of their effects on tubulin assembly and their synergistic action when present simultaneously." Mol Pharmacol **66**(1): 113-121.

Gerth, K., N. Bedorf, G. Hofle, H. Irschik and H. Reichenbach (1996). "Epothilons A and B: antifungal and cytotoxic compounds from Sorangium cellulosum (Myxobacteria). Production, physico-chemical and biological properties." J Antibiot (Tokyo) **49**(6): 560-563.

Glotzer, M. (2003). "Cytokinesis: progress on all fronts." Curr Opin Cell Biol **15**(6): 684-690.
Glotzer, M. (2005). "The molecular requirements for cytokinesis." Science **307**(5716): 1735-1739.

Gornstein, E. and T. L. Schwarz (2014). "The paradox of paclitaxel neurotoxicity: Mechanisms and unanswered questions." Neuropharmacology **76 Pt A**: 175-183.
Gotta, M. and J. Ahringer (2001).
Distinct roles for Galpha and Gbetagamma in regulating spindle position and orientation in Caenorhabditis elegans embryos." Nat Cell Biol **3**(3): 297-300.

Greene, L. M., M. J. Meegan and D. M. Zisterer (2015). "Combretastatins: More Than Just Vascular Targeting Agents?" Journal of Pharmacology and Experimental Therapeutics **355**(2): 212-227.

Grill, S. W., P. Gonczy, E. H. Stelzer and A. A. Hyman (2001). "Polarity controls forces governing asymmetric spindle positioning in the Caenorhabditis elegans embryo." Nature **409**(6820): 630-633.

Grill, S. W., J. Howard, E. Schaffer, E. H. Stelzer and A. A. Hyman (2003). "The distribution of active force generators controls mitotic spindle position." Science **301**(5632): 518-521.

Grill, S. W., K. Kruse and F. Julicher (2005). "Theory of mitotic spindle oscillations." Phys Rev Lett **94**(10): 108104.

Gusnowski, E. M. and M. Srayko (2011). "Visualization of dynein-dependent microtubule gliding at the cell cortex: implications for spindle positioning." J Cell Biol **194**(3): 377-386.

Hastie, S. B. (1991). "Interactions of colchicine with tubulin." Pharmacol Ther **51**(3): 377-401.

Haydar, T. F., E. Ang, Jr. and P. Rakic (2003). "Mitotic spindle rotation and mode of cell division in the developing telencephalon." Proc Natl Acad Sci U S A **100**(5): 2890-2895.

Horvitz, H. R., S. Brenner, J. Hodgkin and R. K. Herman (1979). "A uniform genetic nomenclature for the nematode Caenorhabditis elegans." Mol Gen Genet **175**(2): 129-133.

Hubbard, E. J. and D. Greenstein (2000). "The Caenorhabditis elegans gonad: a test tube for cell and developmental biology." Dev Dyn **218**(1): 2-22.

Jantsch-Plunger, V., P. Gonczy, A. Romano, H. Schnabel, D. Hamill, R. Schnabel, A. A. Hyman and M. Glotzer (2000). "CYK-4: A Rho family gtpase activating protein (GAP) required for central spindle formation and cytokinesis." J Cell Biol **149**(7): 1391-1404.

Johnson, I. S., J. G. Armstrong, M. Gorman and J. P. Burnett, Jr. (1963). "The Vinca Alkaloids: A New Class of Oncolytic Agents." Cancer Res **23**: 1390-1427.

Johnson, I. S., H. F. Wright, G. H. Svoboda and J. Vlantis (1960). "Antitumor principles derived from Vinca rosea Linn. I. Vincaleukoblastine and leurosine." Cancer Res **20**: 1016-1022.

Jordan, M. A., K. Wendell, S. Gardiner, W. B. Derry, H. Copp and L. Wilson (1996). "Mitotic block induced in HeLa cells by low concentrations of paclitaxel (Taxol) results in abnormal mitotic exit and apoptotic cell death." Cancer Res **56**(4): 816-825.

Kaitna, S., M. Mendoza, V. Jantsch-Plunger and M. Glotzer (2000). "Incenp and an aurora-like kinase form a complex essential for chromosome segregation and efficient completion of cytokinesis." Curr Biol **10**(19): 1172-1181.

Kaltschmidt, J. A. and A. H. Brand (2002). "Asymmetric cell division: microtubule dynamics and spindle asymmetry." J Cell Sci **115**(Pt 11): 2257-2264.
Kamath, R. S. and J. Ahringer (2003). "

Genome-wide RNAi screening in Caenorhabditis elegans." Methods **30**(4): 313-321.
Kamath, R. S., M. Martinez-Campos, P. Zipperlen, A. G. Fraser and J. Ahringer (2001).

Effectiveness of specific RNA-mediated interference through ingested double-stranded RNA in Caenorhabditis elegans." Genome Biol **2**(1): RESEARCH0002.

Kavallaris, M., A. S. Tait, B. J. Walsh, L. He, S. B. Horwitz, M. D. Norris and M. Haber (2001).Multiple microtubule alterations are associated with Vinca alkaloid resistance in human leukemia cells." Cancer Res **61**(15): 5803-5809.

Kemphues, K. J., J. R. Priess, D. G. Morton and N. S. Cheng (1988). "Identification of genes required for cytoplasmic localization in early C. elegans embryos." Cell **52**(3): 311-320.

Kimura, A. and S. Onami (2005). "Computer simulations and image processing reveal length-dependent pulling force as the primary mechanism for C. elegans male pronuclear migration." Dev Cell **8**(5): 765-775.

Kotak, S. and P. Gonczy (2013). "Mechanisms of spindle positioning: cortical force generators in the limelight." Curr Opin Cell Biol **25**(6): 741-748.

Kozlowski, C., M. Srayko and F. Nedelec (2007). "Cortical microtubule contacts position the spindle in C. elegans embryos." Cell **129**(3): 499-510.

Kraut, R. and J. A. Campos-Ortega (1996). "inscuteable, a neural precursor gene of Drosophila, encodes a candidate for a cytoskeleton adaptor protein." Dev Biol **174**(1): 65-81.

Laan, L., N. Pavin, J. Husson, G. Romet-Lemonne, M. van Duijn, M. P. Lopez, R. D. Vale, F. Julicher, S. L. Reck-Peterson and M. Dogterom (2012). "Cortical dynein

controls microtubule dynamics to generate pulling forces that position microtubule asters." Cell **148**(3): 502-514.

Labbe, J. C., E. K. McCarthy and B. Goldstein (2004). "The forces that position a mitotic spindle asymmetrically are tethered until after the time of spindle assembly." Journal of Cell Biology **167**(2): 245-256.

Lakhani, N. J., M. A. Sarkar, J. Venitz and W. D. Figg (2003). "2-Methoxyestradiol, a promising anticancer agent." Pharmacotherapy **23**(2): 165-172.

Lambier, A. and Y. Engelborghs (1980). "A quantitative analysis of tubulin-colchicine binding to microtubules." Eur J Biochem **109**(2): 619-624.

Leandro-Garcia, L. J., S. Leskela, I. Landa, C. Montero-Conde, E. Lopez-Jimenez, R. Leton, A. Cascon, M. Robledo and C. Rodriguez-Antona (2010). "Tumoral and tissue-specific expression of the major human beta-tubulin isotypes." Cytoskeleton (Hoboken) **67**(4): 214-223.

Lee, C. Y., B. D. Wilkinson, S. E. Siegrist, R. P. Wharton and C. Q. Doe (2006). "Brat is a Miranda cargo protein that promotes neuronal differentiation and inhibits neuroblast self-renewal." Dev Cell **10**(4): 441-449.

Liu, J., M. J. Towle, H. Cheng, P. Saxton, C. Reardon, J. Wu, E. A. Murphy, G. Kuznetsov, C. W. Johannes, M. R. Tremblay, H. Zhao, M. Pesant, F. G. Fang, M. W. Vermeulen, B. M. Gallagher, Jr. and B. A. Littlefield (2007). "In vitro and in vivo anticancer activities of synthetic (-)-laulimalide, a marine natural product microtubule stabilizing agent." Anticancer Res **27**(3B): 1509-1518.

Lu, B., M. Rothenberg, L. Y. Jan and Y. N. Jan (1998). "Partner of Numb colocalizes with Numb during mitosis and directs Numb asymmetric localization in Drosophila neural and muscle progenitors." Cell **95**(2): 225-235.

Lu, M. S. and C. A. Johnston (2013). "Molecular pathways regulating mitotic spindle orientation in animal cells." Development **140**(9): 1843-1856.

Marty, M., P. Fumoleau, A. Adenis, Y. Rousseau, Y. Merrouche, G. Robinet, I. Senac and C. Puozzo (2001). "Oral vinorelbine pharmacokinetics and absolute bioavailability study in patients with solid tumors." Ann Oncol **12**(11): 1643-1649.

Mayer, M., M. Depken, J. S. Bois, F. Julicher and S. W. Grill (2010). "Anisotropies in cortical tension reveal the physical basis of polarizing cortical flows." Nature **467**(7315): 617-621.

Monen, J., P. S. Maddox, F. Hyndman, K. Oegema and A. Desai (2005). "Differential role of CENP-A in the segregation of holocentric C. elegans chromosomes during meiosis and mitosis." Nat Cell Biol **7**(12): 1248-1255.

Mooberry, S. L., G. Tien, A. H. Hernandez, A. Plubrukarn and B. S. Davidson (1999). "Laulimalide and isolaulimalide, new paclitaxel-like microtubule-stabilizing agents." Cancer Res **59**(3): 653-660.

Moorhouse, K. S. and D. R. Burgess (2014). "How to be at the right place at the right time: the importance of spindle positioning in embryos." Mol Reprod Dev **81**(10): 884-895.

Morton, D. G., D. C. Shakes, S. Nugent, D. Dichoso, W. Wang, A. Golden and K. J. Kemphues (2002). "The Caenorhabditis elegans par-5 gene encodes a 14-3-3 protein required for cellular asymmetry in the early embryo." Dev Biol **241**(1): 47-58.

Motegi, F. and A. Sugimoto (2006). "Sequential functioning of the ECT-2 RhoGEF, RHO-1 and CDC-42 establishes cell polarity in Caenorhabditis elegans embryos." Nat Cell Biol **8**(9): 978-985.

Munro, E., J. Nance and J. R. Priess (2004). "Cortical flows powered by asymmetrical contraction transport PAR proteins to establish and maintain anterior-posterior polarity in the early C. elegans embryo." Dev Cell **7**(3): 413-424.

Nguyen-Ngoc, T., K. Afshar and P. Gonczy (2007). "Coupling of cortical dynein and G alpha proteins mediates spindle positioning in Caenorhabditis elegans." Nat Cell Biol **9**(11): 1294-1302.

Noble, R. L., C. T. Beer and J. H. Cutts (1958). "Role of chance observations in chemotherapy: Vinca rosea." Ann N Y Acad Sci **76**(3): 882-894.

Nogales, E., M. Whittaker, R. A. Milligan and K. H. Downing (1999). High-resolution model of the microtubule." Cell **96**(1): 79-88.

Nogales, E., S. G. Wolf, I. A. Khan, R. F. Luduena and K. H. Downing (1995). "Structure of tubulin at 6.5 A and location of the taxol-binding site." Nature **375**(6530): 424-427.

O'Rourke, S. M., S. N. Christensen and B. Bowerman (2010). "Caenorhabditis elegans EFA-6 limits microtubule growth at the cell cortex." Nat Cell Biol **12**(12): 1235-1241.

O'Rourke, S. M., M. D. Dorfman, J. C. Carter and B. Bowerman (2007). "Dynein modifiers in C. elegans: light chains suppress conditional heavy chain mutants." PLoS Genet **3**(8): e128.

Oegema, K., A. Desai, S. Rybina, M. Kirkham and A. A. Hyman (2001). "Functional analysis of kinetochore assembly in Caenorhabditis elegans." J Cell Biol **153**(6): 1209-1226.

Oegema, K. and T. J. Mitchison (1997). "Rappaport rules: cleavage furrow induction in animal cells." Proc Natl Acad Sci U S A **94**(10): 4817-4820.

Olson, S. K., G. Greenan, A. Desai, T. Muller-Reichert and K. Oegema (2012). "Hierarchical assembly of the eggshell and permeability barrier in C. elegans." J Cell Biol **198**(4): 731-748.

Owellen, R. J., C. A. Hartke, R. M. Dickerson and F. O. Hains (1976). "Inhibition of tubulin-microtubule polymerization by drugs of the Vinca alkaloid class." Cancer Res **36**(4): 1499-1502.

Park, D. H. and L. S. Rose (2008). "Dynamic localization of LIN-5 and GPR-1/2 to cortical force generation domains during spindle positioning." Dev Biol **315**(1): 42-54.

Pearson, C. G. and K. Bloom (2004). "Dynamic microtubules lead the way for spindle positioning." Nat Rev Mol Cell Biol **5**(6): 481-492.

Pecreaux, J., J. C. Roper, K. Kruse, F. Julicher, A. A. Hyman, S. W. Grill and J. Howard (2006). "Spindle oscillations during asymmetric cell division require a threshold number of active cortical force generators." Curr Biol **16**(21): 2111-2122.

Piekny, A., M. Werner and M. Glotzer (2005). "Cytokinesis: welcome to the Rho zone." Trends Cell Biol **15**(12): 651-658.

Piekny, A. J. and M. Glotzer (2008). "Anillin is a scaffold protein that links RhoA, actin, and myosin during cytokinesis." Curr Biol **18**(1): 30-36.

Piekny, A. J. and P. E. Mains (2002). "Rho-binding kinase (LET-502) and myosin phosphatase (MEL-11) regulate cytokinesis in the early Caenorhabditis elegans embryo." J Cell Sci **115**(Pt 11): 2271-2282.

Poi, M. J., M. Berger, M. Lustberg, R. Layman, C. L. Shapiro, B. Ramaswamy, E. Mrozek, E. Olson and R. Wesolowski (2013). "Docetaxel-induced skin toxicities in breast cancer patients subsequent to paclitaxel shortage: a case series and literature review." Support Care Cancer **21**(10): 2679-2686.

Pryor, D. E., A. O'Brate, G. Bilcer, J. F. Diaz, Y. Wang, Y. Wang, M. Kabaki, M. K. Jung, J. M. Andreu, A. K. Ghosh, P. Giannakakou and E. Hamel (2002). "The microtubule stabilizing agent laulimalide does not bind in the taxoid site, kills cells resistant

to paclitaxel and epothilones, and may not require its epoxide moiety for activity." Biochemistry **41**(29): 9109-9115.

Ramalingam, N., C. Franke, E. Jaschinski, M. Winterhoff, Y. Lu, S. Bruhmann, A. Junemann, H. Meier, A. A. Noegel, I. Weber, H. Zhao, R. Merkel, M. Schleicher and J. Faix (2015). "A resilient formin-derived cortical actin meshwork in the rear drives actomyosin-based motility in 2D confinement." Nat Commun **6**: 8496.

Rappaport, R. (1961). "Experiments concerning the cleavage stimulus in sand dollar eggs." J Exp Zool **148**: 81-89.

Rappaport, R. (1983). "Cytokinesis: Effects of blocks between the mitotic apparatus and the surface on furrow establishment in flattened echinoderm eggs." Journal of Experimental Zoology **227**: 213-227.

Rappaport, R. (1996). "Cytokinesis in Animal Cells." Cambridge: Cambridge University Press.

Rappaport, R. (1997). "Cleavage furrow establishment by the moving mitotic apparatus." Dev Growth Differ **39**(2): 221-226.

Redemann, S., J. Pecreaux, N. W. Goehring, K. Khairy, E. H. Stelzer, A. A. Hyman and J. Howard (2010). "Membrane invaginations reveal cortical sites that pull on mitotic spindles in one-cell C. elegans embryos." PLoS One **5**(8): e12301.

Roberts, W. N., M. H. Liang and S. H. Stern (1987). "Colchicine in acute gout. Reassessment of risks and benefits." JAMA **257**(14): 1920-1922.

Romano, A., A. Guse, I. Krascenicova, H. Schnabel, R. Schnabel and M. Glotzer (2003). "CSC-1: a subunit of the Aurora B kinase complex that binds to the survivin-like protein BIR-1 and the incenp-like protein ICP-1." J Cell Biol **161**(2): 229-236.

Rowinsky, E. K. and R. C. Donehower (1995). "Paclitaxel (taxol)." N Engl J Med **332**(15): 1004-1014.

Salbreux, G., G. Charras and E. Paluch (2012). "Actin cortex mechanics and cellular morphogenesis." Trends Cell Biol **22**(10): 536-545.

Schierenberg, E. and W. B. Wood (1985). "Control of cell-cycle timing in early embryos of Caenorhabditis elegans." Dev Biol **107**(2): 337-354.

Schiff, P. B., J. Fant and S. B. Horwitz (1979). "Promotion of microtubule assembly in vitro by taxol." Nature **277**(5698): 665-667.
Schiff, P. B. and S. B. Horwitz (1980). "Taxol stabilizes microtubules in mouse fibroblast cells." Proc Natl Acad Sci U S A **77**(3): 1561-1565.

Schmidt, D. J., D. J. Rose, W. M. Saxton and S. Strome (2005). "Functional analysis of cytoplasmic dynein heavy chain in Caenorhabditis elegans with fast-acting temperature-sensitive mutations." Mol Biol Cell **16**(3): 1200-1212.

Severson, A. F., D. L. Baillie and B. Bowerman (2002). "A Formin Homology protein and a profilin are required for cytokinesis and Arp2/3-independent assembly of cortical microfilaments in C. elegans." Curr Biol **12**(24): 2066-2075.

Severson, A. F., D. R. Hamill, J. C. Carter, J. Schumacher and B. Bowerman (2000). "The aurora-related kinase AIR-2 recruits ZEN-4/CeMKLP1 to the mitotic spindle at metaphase and is required for cytokinesis." Curr Biol **10**(19): 1162-1171.

Shaye, D. D. and I. Greenwald (2011). "OrthoList: a compendium of C. elegans genes with human orthologs." PLoS One **6**(5): e20085.

Shelton, C. A., J. C. Carter, G. C. Ellis and B. Bowerman (1999). "The nonmuscle myosin regulatory light chain gene mlc-4 is required for cytokinesis, anterior-posterior polarity, and body morphology during Caenorhabditis elegans embryogenesis." J Cell Biol **146**(2): 439-451.

Smoter, M., L. Bodnar, R. Duchnowska, R. Stec, B. Grala and C. Szczylik (2011). "The role of Tau protein in resistance to paclitaxel." Cancer Chemother Pharmacol **68**(3): 553-557.

Spana, E. P., C. Kopczynski, C. S. Goodman and C. Q. Doe (1995). "Asymmetric localization of numb autonomously determines sibling neuron identity in the Drosophila CNS." Development **121**(11): 3489-3494.

Spiro, Z., K. Thyagarajan, A. De Simone, S. Trager, K. Afshar and P. Gonczy (2014). "Clathrin regulates centrosome positioning by promoting acto-myosin cortical tension in C. elegans embryos." Development **141**(13): 2712-2723.

Srayko, M., A. Kaya, J. Stamford and A. A. Hyman (2005). "Identification and characterization of factors required for microtubule growth and nucleation in the early C. elegans embryo." Dev Cell **9**(2): 223-236.

Srinivasan, D. G., R. M. Fisk, H. Xu and S. van den Heuvel (2003). "A complex of LIN-5 and GPR proteins regulates G protein signaling and spindle function in C elegans." Genes Dev **17**(10): 1225-1239.

Tabuse, Y., Y. Izumi, F. Piano, K. J. Kemphues, J. Miwa and S. Ohno (1998). "Atypical protein kinase C cooperates with PAR-3 to establish embryonic polarity in Caenorhabditis elegans." Development **125**(18): 3607-3614.

Tanaka, S., T. Nohara, M. Iwamoto, K. Sumiyoshi, K. Kimura, Y. Takahashi and N. Tanigawa (2009). "Tau expression and efficacy of paclitaxel treatment in metastatic breast cancer." Cancer Chemother Pharmacol **64**(2): 341-346.

Torres, K. and S. B. Horwitz (1998). "Mechanisms of Taxol-induced cell death are concentration dependent." Cancer Res **58**(16): 3620-3626.

Tozer, G. M., C. Kanthou, C. S. Parkins and S. A. Hill (2002). "The biology of the combretastatins as tumour vascular targeting agents." International Journal of Experimental Pathology **83**(1): 21-38.

Tsou, M. F., A. Hayashi and L. S. Rose (2003). "LET-99 opposes Galpha/GPR signaling to generate asymmetry for spindle positioning in response to PAR and MES-1/SRC-1 signaling." Development **130**(23): 5717-5730.

Uemura, T., S. Shepherd, L. Ackerman, L. Y. Jan and Y. N. Jan (1989). "numb, a gene required in determination of cell fate during sensory organ formation in Drosophila embryos." Cell **58**(2): 349-360.

Vallee, R. B., J. C. Williams, D. Varma and L. E. Barnhart (2004). "Dynein: An ancient motor protein involved in multiple modes of transport." J Neurobiol **58**(2): 189-200.

van Vuuren, R. J., M. H. Visagie, A. E. Theron and A. M. Joubert (2015). "Antimitotic drugs in the treatment of cancer." Cancer Chemother Pharmacol **76**(6): 1101-1112.

Vasquez, R. J., B. Howell, A. M. Yvon, P. Wadsworth and L. Cassimeris (1997). "Nanomolar concentrations of nocodazole alter microtubule dynamic instability in vivo and in vitro." Mol Biol Cell **8**(6): 973-985.

Verdier-Pinard, P., S. Shahabi, F. Wang, B. Burd, H. Xiao, G. L. Goldberg, G. A. Orr and S. B. Horwitz (2005). "Detection of human betaV-tubulin expression in epithelial cancer cell lines by tubulin proteomics." Biochemistry **44**(48): 15858-15870.

Vinzenz, M., M. Nemethova, F. Schur, J. Mueller, A. Narita, E. Urban, C. Winkler, C. Schmeiser, S. A. Koestler, K. Rottner, G. P. Resch, Y. Maeda and J. V. Small (2012). "Actin branching in the initiation and maintenance of lamellipodia." J Cell Sci **125**(Pt 11): 2775-2785.

Watts, J. L., B. Etemad-Moghadam, S. Guo, L. Boyd, B. W. Draper, C. C. Mello, J. R. Priess and K. J. Kemphues (1996). "par-6, a gene involved in the establishment of asymmetry in early C. elegans embryos, mediates the asymmetric localization of PAR-3." Development **122**(10): 3133-3140.

Wendell, K. L., L. Wilson and M. A. Jordan (1993). "Mitotic block in HeLa cells by vinblastine: ultrastructural changes in kinetochore-microtubule attachment and in centrosomes." J Cell Sci **104 (Pt 2)**: 261-274.

Werner, M., E. Munro and M. Glotzer (2007). "Astral signals spatially bias cortical myosin recruitment to break symmetry and promote cytokinesis." Curr Biol **17**(15): 1286-1297.

Wilson, L., M. A. Jordan, A. Morse and R. L. Margolis (1982). "Interaction of vinblastine with steady-state microtubules in vitro." J Mol Biol **159**(1): 125-149.

Yvon, A. M., P. Wadsworth and M. A. Jordan (1999). "Taxol suppresses dynamics of individual microtubules in living human tumor cells." Mol Biol Cell **10**(4): 947-959.

2. Laulimalide induces dose-dependent modulation of microtubule behavior

2.1 Introduction- Structure of microtubules

Microtubules are hollow tube-like polymers of tubulin subunits. It is made of α/β tubulin heterodimers, which interact in a "head-to-tail" manner to form the protofilaments. The protofilaments interact laterally to form the hollow cylinder approximately 25 nm in diameter (figure 2.1a). The microtubule polymer is polarized due to the arrangement of α and β subunits. At one end, termed the minus end the α subunit is exposed and the other end, termed the plus end β subunit is exposed (Mitchison 1993). Microtubules exhibit both structural and functional polarity. The plus end is more dynamic than the minus end. Microtubules have an intrinsic property called dynamic instability where they undergo polymerization and depolymerization and can switch between growing and shrinking phases (Mitchison and Kirschner 1984, Walker, O'Brien et al. 1988). The transition from growing to shrinking is called catastrophe and the transition from shrinking to growing is called rescue.

A number of factors contribute to the dynamic instability of microtubules. However, the rate of GTP hydrolysis is the primary factor that influences the growth and shrinkage of microtubules. In its stable state, microtubule is predominantly composed of GTP-bound β tubulin protofilaments. Upon hydrolysis of GTP, the GDP-bound lattice depolymerizes (Hyman, Chretien et al. 1995). The GDP-bound β tubulin has a curved conformation and it has been shown that this curved conformation makes the protofilament unstable, followed by depolymerization (figure 2.1b). Based on this it has been postulated that the polymer has a GTP-"cap" that provides structural stability and through hydrolysis of this GTP-"cap", the microtubule becomes unstable and switches to disassembly through a catastrophe (Desai and Mitchison 1997).

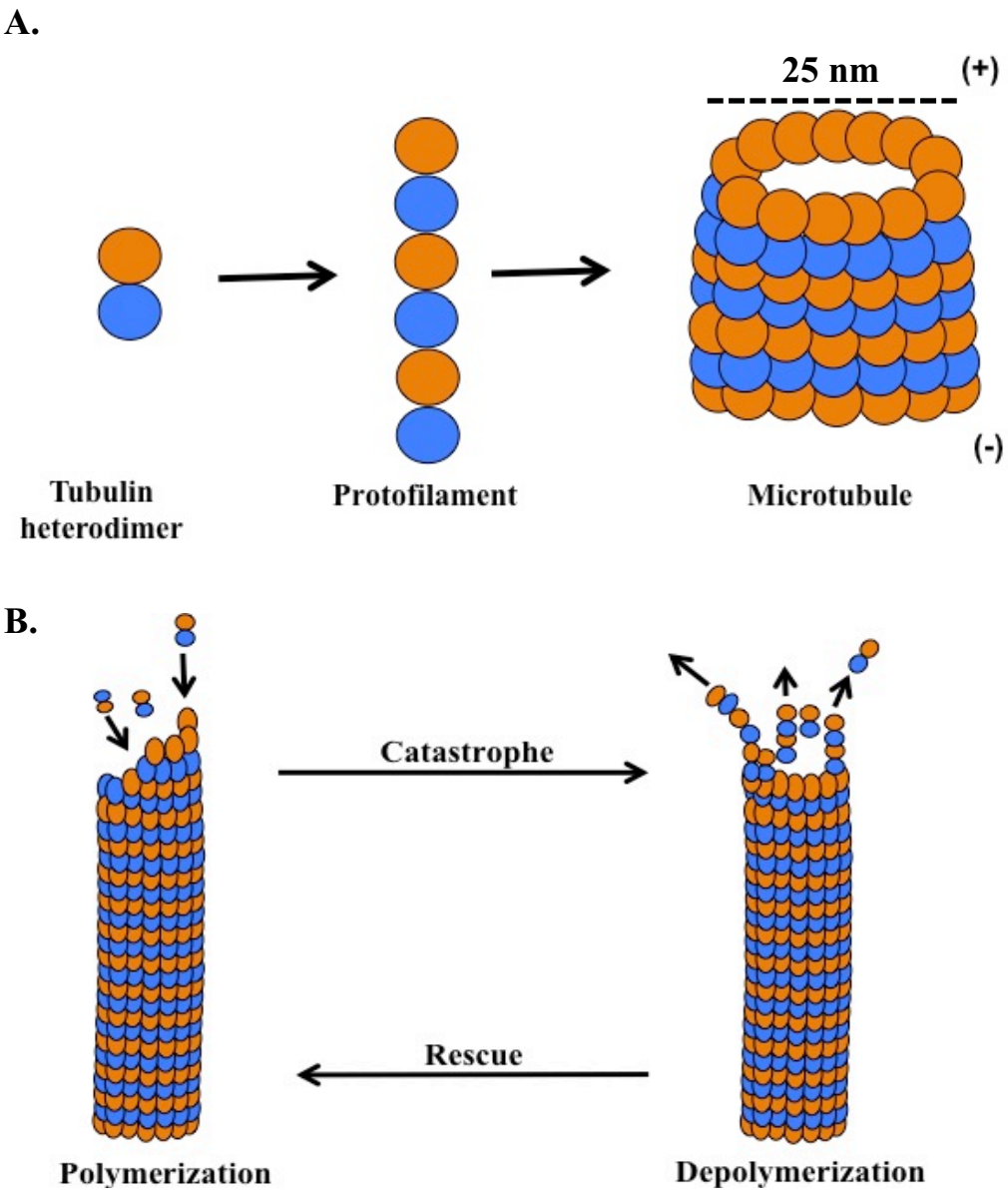

Figure 2.1 Microtubule structure and dynamics
A) α/β tubulin monomers assemble and form the heterodimer. The heterodimer assemble into a protofilament. The protofilaments join laterally and form the microtubule structure. B) Dynamic instability of microtubule switching between polymerization and depolymerization.

2.1.1 Microtubule dynamics and MAPs

Microtubule associated proteins (MAPs) that naturally occur in the cellular environment influence microtubule dynamics (Desai and Mitchison 1997). In living cells and cell extracts, MAPs primarily regulate the formation of higher order structure like the mitotic spindle. Understanding how these regulators affect microtubule dynamics is important to understand how microtubules form complex structures in the cell.

2.1.1.1 Contribution of MAPs in regulating microtubule dynamics

MAPs control microtubule polymerization, depolymerization, nucleation and stabilization in the cell. Gamma-tubulin is the best-characterized protein that promotes microtubule nucleation in the cell. Gamma tubulin forms the gamma tubulin ring complex, which functions as a template for microtubule nucleation (Oakley, Paolillo et al. 2015). However, gamma tubulin is not absolutely necessary for nucleation of microtubules. A study done in *C. elegans* has shown that embryos depleted of gamma tubulin microtubules can also nucleate microtubules around the centrosomes, though the organization of these arrays is disorganized (O'Toole, Greenan et al. 2012).

Microtubule growth is required for cell proliferation and differentiation. Microtubule polymerization occurs when tubulin subunits are added on at the plus end of a microtubule. XMAP215 is a microtubule polymerizing protein, which promotes microtubule polymerization by acting as a tubulin-shuttle to add tubulin subunits to the microtubule polymer (Brouhard, Stear et al. 2008). Thus, XMAP215 helps in promoting longer microtubules and formation of the mitotic spindle (Widlund, Stear et al. 2011).

Microtubule destabilizing proteins induce catastrophe, promote microtubule disassembly and inhibit microtubule polymerization. One of the best-studied families of microtubule depolymerizers is the kinesin-13 family. MCAK is a kinesin-13 family protein that uses ATP hydrolysis to promote microtubule depolymerization

(Ohi, Sapra et al. 2004). MCAK associates with the plus-end of microtubules and shows high affinity to curved protofilaments that resemble the shrinking microtubules (Moores, Yu et al. 2002). MCAK binding brings about a conformational change in the protofilaments and makes the lateral interaction between them weak. This induces catastrophe and microtubule disassembly (Burns, Wagenbach et al. 2014). In *C. elegans* embryo loss of the microtubule destabilizer, KLP-7 causes an increase in the number of microtubules, in both, mitosis (Srayko, Kaya et al. 2005) and meiosis (Han, Adames et al. 2015). Another mechanism to promote microtubule disassembly is by lowering the concentration of free tubulin. The stathmin protein binds tubulin and sequesters it to lower the effective concentration of tubulin; this in turn induces microtubule depolymerization (Jourdain, Curmi et al. 1997). Inactivation of stathmin by phosphorylation promotes microtubule stability and assembly (Gadea and Ruderman 2006). In addition, microtubule-severing enzyme like katanin converts long microtubules into short microtubule fragments by severing it near the centrosome, during meiosis (Srayko, O'Toole E et al. 2006).

Cells use various mechanisms to stabilize microtubules. For example, the HURP protein directly interacts with the microtubule lattice to stabilize the interaction between protofilaments and thus prevents microtubule destabilization (Yang and Fan 2008). Another study has shown that MCRS1 protein localizes at the minus end of chromosomal microtubules and stabilizes them. And MCRS1 promotes microtubule stabilization by interfering with the microtubule depolymerizing activity of the MCAK protein. By antagonizing the interaction of MCAK with microtubules, MCRS1 decreases the overall catastrophe of microtubules (Meunier and Vernos 2011). A recent study has shown that hSAXO1, a member of the MAP-6 family of protein localizes specifically at the cilia, centriole and axoneme microtubules and stabilizes microtubules through its Mn domain. However, the mechanism of stabilization currently remains unknown (Dacheux, Roger et al. 2015).

2.1.2 Contribution of microtubule binding drugs in regulating microtubule dynamics

In addition to MAPs that naturally occur in the cellular environment, synthetic and naturally occurring chemicals, are also able to influence microtubule dynamics. These compounds act as antimitotic agents because they target the microtubule-based cytoskeletal structures that are essential for proper cell division. For this reason, microtubules continue to be one of the most effective targets for developing anticancer drugs. There are various classes of microtubule-binding compounds; they are classified on the basis of the domain that binds to tubulin and/or microtubules, *e.g.,* the taxol domain binders, vinca-domain binders and colchicine domain binders. The antimitotic microtubule-binding agents are also often broadly classified into two major classes depending on how they specifically affect the microtubule polymer mass at high concentrations: microtubule stabilizers and destabilizers. The role of various microtubule-binding chemicals in the regulation of microtubule dynamics is discussed below.

2.1.2.1 Inhibitors of microtubule polymerization

The inhibitors of microtubule polymerization dynamics are further classified into two main sub-categories: drugs with a vinca binding site (also known as vinca alkaloids) and drugs with a colchicine-binding site. These classes are discussed below.

2.1.2.1.1 Vinca site binding drugs

The vinca alkaloid was first isolated from the periwinkle plant *Catharanthus roseus* at the University of Western Ontario (Noble, Beer et al. 1958). Its chemotherapeutic potential was then developed by the research group at Western Ontario and the company Eli Lilly (Johnson, Wright et al. 1960). The vinca alkaloids bind to the β-subunit of tubulin; a region termed the vinca-binding domain. One tubulin dimer has two vinca binding sites. One of the vinca alkaloids, vinblastine,

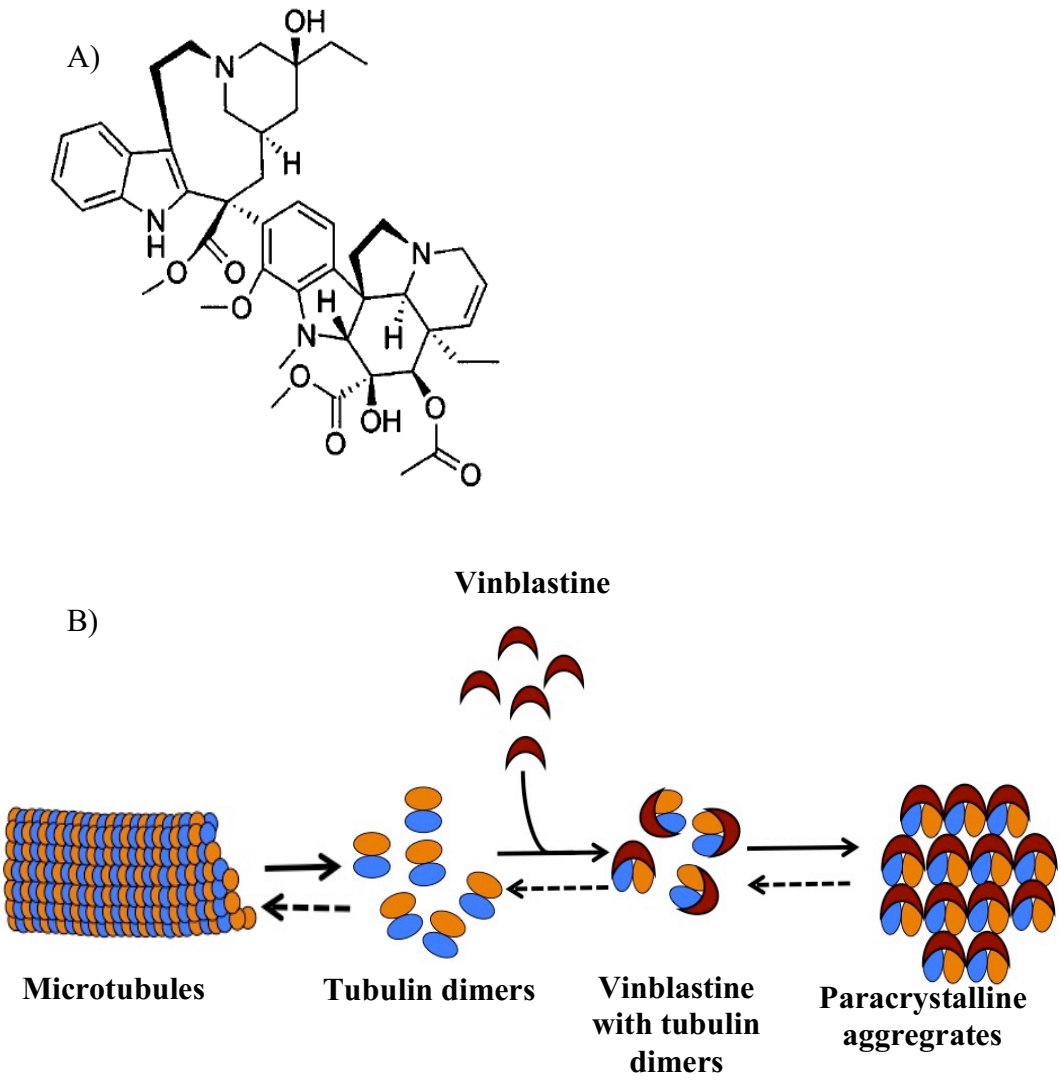

Figure 2.2 Vinblastine structure and mechanism of action
A) Vinblastine structure

Source: License number: 3994531046614. Reprinted by permission from John Wiley & Sons Inc. Copyright 2011.Stanton, RA. *et al.* Drugs that target dynamic microtubules: A new molecular perspective. Med. Res. Rev. 31(3): 443-81. doi: 10.1002/med.20242.

B) Formation of tubulin-vinblastine paracrystals
Vinblastine binds soluble tubulin, changes its conformation and forms paracrystalline aggregates of tubulin-vinblastine. Free tubulin is no longer available for microtubule assembly and this shifts the equilibrium to microtubule depolumerization.

binds to soluble tubulin and induces a conformational change in tubulin (Wilson, Jordan et al. 1982).

This conformational change forms tubulin-vinca alkaloid paracrystals, thereby decreasing the pool of free tubulin available for microtubule assembly. This shifts the equilibrium to microtubule disassembly and depolymerization of the polymer, which has been verified in HeLa cells at 10-100 nM (Owellen, Hartke et al. 1976). At low concentrations (0.8 nM in HeLa cells), vinblastine binds to microtubule ends and reduces the dynamic instability of microtubules- i.e. it reduces the rate and extent of microtubule growth and shrinkage and leaves it in a state of 'stability' (Wendell, Wilson et al. 1993, Dhamodharan, Jordan et al. 1995). Thus, by suppressing the microtubule dynamics, the mitotic spindle is either not able to form, or it fails to function properly as cells transit from metaphase to anaphase; these cells eventually die by apoptosis. Thus, the vinca alkaloids can act as both microtubule-stabilizing and destabilizing agents, depending on the concentration used. In terms of clinical applications, the Vinca drugs are used to treat a variety of tumors. Vincristine is used against hodgkins's disease, all lymphomas and various solid tumors (Johnson, Armstrong et al. 1963). Vinorelbine is used against breast cancer and non-small cell lung cancer (Marty, Fumoleau et al. 2001).

2.1.2.1.2 Drugs with colchicine-binding site

Colchicine is an alkaloid extracted from two plants, meadow saffron and glory lily. It has been used in the treatment of gout for centuries (Roberts, Liang et al. 1987). It was the first compound identified to be a tubulin binder. Colchicine first binds to soluble tubulin and forms a complex, which then copolymerizes onto the ends of the microtubule. This suppresses microtubule dynamics at the ends as the colchicine-tubulin complex binds more tightly to its tubulin neighbors than free tubulin. Colchicine binding to β-tubulin results in curved tubulin dimers, which cannot assume the straight structure due to steric hindrance between colchicine and α-

tubulin. This prevents microtubule assembly (Lambier and Engelborghs 1980, Andreu and Timasheff 1986, Hastie 1991).

Though colchicine itself has failed clinical trials (for use as an anticancer agent) due to high toxicity (Chen, Liu et al. 2009), there are other colchicine-site binding agents, which are either used as anticancer agents or are currently under investigation. 2-methoxyestradiol has been shown to prevent tumor growth in a variety of cell lines (Lakhani, Sarkar et al. 2003). Combretastatins is another colchicine-site binding agent. It is a naturally occurring phenol extracted from *Combretum caffrum*. Combretastatins have also been developed as anti-angiogenic agents and this unique property has overshadowed its development for cancer therapy (Tozer, Kanthou et al. 2002). However, there is an ongoing clinical trial of combretastatin investigating its potential for the development as an anticancer agent (Greene, Meegan et al. 2015).

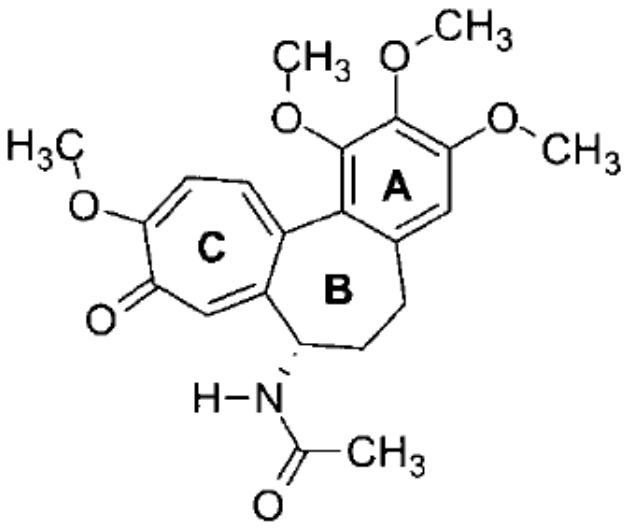

Figure 2.3 Colchicine structure

Source: License number: 3994531046614. Reprinted by permission from John Wiley & Sons Inc. Copyright 2011.Stanton, RA. *et al.* Drugs that target dynamic microtubules: A new molecular perspective. Med. Res. Rev. 31(3): 443-81. doi: 10.1002/med.20242

2.1.2.2 Microtubule stabilizing agents

In cancer therapy, microtubule-stabilizing agents are of great interest due to the significant anticancer activities of the taxane group of compounds. Most of the classes of microtubule stabilizers bind at or near the taxane site. However, new structural classes of stabilizing agents have also been discovered, many of which are being clinically developed. Some of the important classes of microtubule-stabilizing agents are discussed below.

2.1.2.2.1 Taxanes

Taxanes are plant alkaloids. The most important and widely used taxane is paclitaxel (with the trade name Taxol). Paclitaxel was first isolated from the bark of yew tree in 1967 (Wani, Taylor et al. 1971). It binds poorly to soluble tubulin, however, it binds with high affinity to tubulin along the length of the microtubule polymer. It has been thought to access the binding site by diffusing through small openings in the microtubule polymer. The binding of paclitaxel to β-subunit of tubulin on the inner surface of microtubule lattice induces a conformation change in tubulin and increases its affinity for neighboring tubulin molecules (Nogales, Wolf et al. 1995). This in turn stabilizes the microtubule polymer and prevents it from depolymerization. In 1979 it was discovered that paclitaxel could also induce microtubule polymerization (Schiff, Fant et al. 1979). Within cells, paclitaxel at micromolar concentrations is able to override the microtubule organizing centre (MTOC) function and promote the formation of short microtubule bundles in the cytoplasm. These microtubule bundles are not linked to the centrosome and are independent of the MTOC (De Brabander, Geuens et al. 1981).

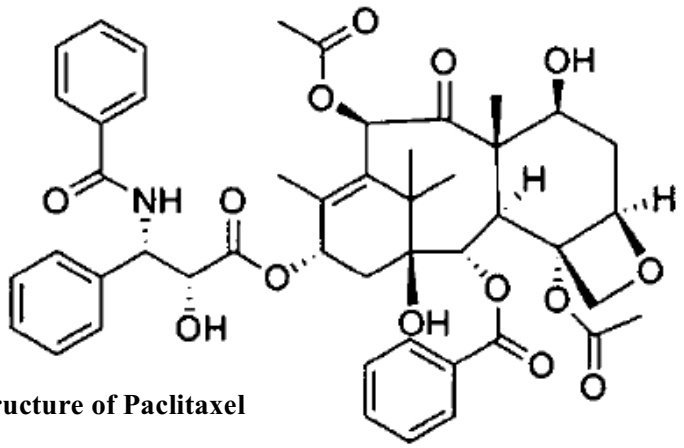

Figure 2.4 Structure of Paclitaxel

Source: License number: 3994531046614. Reprinted by permission from John Wiley & Sons Inc. Copyright 2011.Stanton, RA. *et al.* Drugs that target dynamic microtubules: A new molecular perspective. Med. Res. Rev. 31(3): 443-81. doi: 10.1002/med.20242

Paclitaxel binds tubulin and locks the microtubules in a polymerized state. This prevents the cells from transitioning from G2 to M phase of the cell cycle. Thus the cells arrest in the G2/M phase of the cell cycle and this induces mitotic arrest (Yvon, Wadsworth et al. 1999). Paclitaxel has been developed as a potent anticancer agent against a variety of tumors. It has been particularly effective against ovarian and breast cancer (Rowinsky and Donehower 1995). The IC_{50} value of most drugs varies depending on the cell lines used. For paclitaxel, the IC_{50} was found to be between 2.5-7.5 nM for HeLa (cervical cancer), HT-29 (colon adenocarcinoma) and MCF-7 (Breast adenocarcinoma) cell lines (Liebmann, Cook et al. 1993).

2.1.2.2.2 Epothilones

Epothilones are naturally occurring 16-membered macrolides that were isolated in 1987 from *Sorangium cellulosum,* gram-negative soil bacteria at the Society for Biotechnological Research, Germany (Gesellschaft für biotechnologische Forschung, GBF). Epothilone was first identified because of its anti-fungal property but a cytotoxic property was later reported in 1996 (Gerth, Bedorf et al. 1996). The mechanism of action of epothilone is similar to paclitaxel and a competitive binding study indicated that it binds to the same site as paclitaxel (Bollag, McQueney et al. 1995). Similar to paclitaxel, epothilone causes cell-cycle arrest at the G2-M transition phase (Bollag, McQueney et al. 1995). In spite of the similarities between paclitaxel and epothilones, there are also important differences between the two drugs. Though epothilones also bind β-tubulin on the inner surface of microtubule lattice in the same binding pockets, the β-tubulin amino acids that bind epothilones are distinct as compared to taxanes (Brogdon, Lee et al. 2014).

Ixabepilone (with the trade name Ixempra) is the first and only epothilone to be approved for clinical use. It is used for the treatment of advanced breast cancer that is resistant to taxanes (van Vuuren, Visagie et al. 2015).

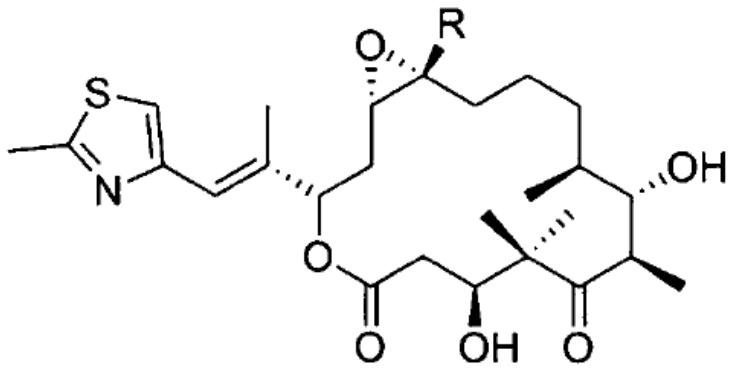

Figure 2.5 Structure of Epothilone
Source: License number: 3994531046614. Reprinted by permission from John Wiley & Sons Inc. Copyright 2011.Stanton, RA. *et al.* Drugs that target dynamic microtubules: A new molecular perspective. Med. Res. Rev. 31(3): 443-81. doi: 10.1002/med.20242

2.1.3 Toxicity and drug resistance associated with microtubule-binding agents

Though microtubule-targeting agents have been developed as important anticancer drugs, there are some challenges in their use. Toxicity and development of resistance to these drugs are two important and unsolved questions in the field that are discussed below.

2.1.3.1Toxicity of microtubule targeted drugs

A major limitation of using microtubule-targeting drugs for cancer therapy is that they often produce side effects. The evaluation of some microtubule binding drugs has been discontinued due to their excessive toxicity and two examples are discussed below.

The first clinical trial study with both naturally isolated and synthetic Crytophycin (a microtubule-stabilizing agent) showed severe neurological toxicity in patients and no improvement in patients with ovarian cancer (D'Agostino, del Campo et al. 2006). Novartis conducted clinical trials on patients with solid tumors with the drug discodermolide, a microtubule-stabilizing agent. The phase I clinical trial reports were promising and there were no reported toxicities at that time. However, the clinical trial was discontinued because of several cases of severe pulmonary toxicity reported later in the clinical trial (Dumontet and Jordan 2010). Apart from the example above, most of the successful microtubule-binding drugs in cancer therapy also show various side effects. For example, paclitaxel shows neutropenia, neuropathy and fatal allergic reactions in patients (Gornstein and Schwarz 2014). Breast cancer patients treated with docetaxel developed severe dermatologic toxicity (Poi, Berger et al. 2013). Some toxicities are compound-specific, for example fluid retention observed in patients treated with docetaxel and diarrhoea observed in patients after patupilone therapy (Dumontet and Jordan 2010).

In spite of the reported toxic side effects of some of the microtubule-targeting compounds, studies are being done to discover new analogs of the drug. In addition, combination therapies with drugs of other classes are also being carried out.

2.1.3.2 Mechanisms of resistance to microtubule-targeted drugs

One of the important drawbacks of using microtubule-targeting drugs for cancer therapy is the tendency for the cancerous cells to develop resistance to these drugs (Dumontet and Jordan 2010). Some of the reasons for development of resistance for microtubule-binding drugs are overexpression of transporter proteins and tubulin isotypes and altered expression of microtubule-associated proteins. These mechanisms are discussed below.

One of the important mechanisms for development of drug resistance is through overexpression of the multidrug transporter, P-glycoprotein (Pgp). The cells acquire resistance to drugs because Pgp pumps the drug out of the cell, thereby decreasing their intracellular concentration and therapeutic effects. Pgp belongs to the ATP-binding cassette (ABC) family of transporter proteins and uses the energy from ATP for drug efflux (Dumontet and Jordan 2010). There are different Pgp proteins that confer resistance for various drugs. However, in most cases, cells that increase the rate of export of one drug will often act on many others and, in such cases, multi-drug treatment of cancer is often ineffective.

Most animals have more than one gene that encodes alpha and beta tubulin. Depending on the tissue or developmental stage, different tubulin isotypes can form dimers and polymerize to generate microtubules with slightly different properties. For example the human β-tubulin has 8 different isotypes. Class II, III and IV are expressed mainly in the neurons and class VI is hematopoietic cell-specific (Verdier-Pinard, Shahabi et al. 2005). In addition, a study to develop a quantitative PCR method to determine the mRNA expression of the isotypes of human β-tubulin found that isotype IVa is primarily expressed in the brain and isotype of class I, IVb and V were expressed at similar levels across all tissue types (Leandro-Garcia, Leskela et al. 2010). In cancers, deregulation of gene expression can lead to mis-expression of tubulin isotypes, thus altering the affinity of microtubule-binding agents on the microtubule polymer. A reduced effect of taxane drugs is correlated with increased expression of class II and class III- β-tubulin. This reduced efficacy of taxanes has been observed in lung, breast and ovarian cancers (Dumontet and Jordan 2010).

Similarly decreased level of expression of class III- β-tubulin is associated with resistance to vinca alkaloids (Kavallaris, Tait et al. 2001). Epothilones are unaffected by β-tubulin overexpression (Dumontet, Jordan et al. 2009).

Another important factor that contributes to microtubule-targeting drug resistance is microtubule-associated proteins (MAPs). MAPs such as tau and MAP2 bind to microtubules and stabilize them. Increased expression of tau protein is associated with paclitaxel resistance in breast cancer (Smoter, Bodnar et al. 2011). Though the exact molecular basis of resistance is not completely understood, tau (in its unphosphorylated form) is thought to bind to the outer microtubule wall, which limits paclitaxel from accessing its binding site on the inner surface of the microtubule lattice (Tanaka, Nohara et al. 2009). MAP2 protein functions in neuronal morphogenesis and regulation of cytoskeleton dynamics. It binds to both microtubules and microfilaments through its tubulin-binding domain. Down-regulation of MAP2c, one of the splice variants of MAP2, is associated with vincristine resistance in a neuroblastoma cell line. Decrease in expression of MAP2c is thought to favor the production of hyperstable microtubules, which become resistant to the microtubule destabilizing agent, vincristine (Don, Verrills et al. 2004).

Due to the prevalence of drug resistance in cancers, it is desirable to identify new microtubule targeting drugs that are effective on resistant cell lines and suitable for *in vivo* use. In addition to their use in cancer therapy, drugs with novel mechanisms of action could potentially identify relationships between specific subsets of cellular pathways and polymer ultrastructure. Therefore, in addition to their development as an anticancer agent, these drugs could be developed as important research tools.

2.1.4 Laulimalide: A microtubule-targeting drug

Laulimalide was originally isolated from a marine sponge, *Cacospongia mycofijiensis* (Corley, Herb et al. 1988). Chemically, laulimalide is a polyketide macrolide. In 1988, the structure of laulimalide and its analogue, Isolaulimalide was published (Corley, Herb et al. 1988). In 1999, Mooberry et al., published that

laulimalide had a similar effect on microtubules as paclitaxel. It stabilized microtubules and also induced microtubule polymerization. The published IC_{50} value for laulimalide in a human prostrate cancer cell line is in the range of 12-15 nM (Liu, Towle et al. 2007).

In vivo and *in vitro* studies done using mammalian cell lines show that laulimalide stabilizes microtubules and also induces an increased rate of apoptosis in a cell population, similar to paclitaxel (Jordan, Wendell et al. 1996, Torres and Horwitz 1998, Gapud, Bai et al. 2004). However, there are clues that suggest that the two drugs have different effects on cells. For example, although mammalian cells treated with laulimalide and paclitaxel both have abnormal spindle morphology, the laulimalide-treated cells exhibited a single radially-symmetric microtubule array surrounding a clear central core, whereas paclitaxel-treated cells have tetra or tripolar spindles (Mooberry, Tien et al. 1999). In addition, differences in the morphology of stabilized microtubule bundles in drug-treated cells have also been reported. Paclitaxel resulted in long, thick microtubule bundles, whereas laulimalide induced short bundles of stabilized microtubules (Mooberry, Tien et al. 1999). Comparisons have been made between laulimalide and another taxoid drug, docetaxel (Bennett, Chan et al. 2012). This study looked at the effects of low concentrations of laulimalide on interphase and mitotic microtubules and compared it with docetaxel. Both laulimalide and docetaxel stabilized microtubules at a 30 nM concentration. However, the microtubule phenotypes observed with the two drugs were quite distinct. Microtubule bundles were observed in the docetaxel-treated cells, whereas microtubule bundles were not present in laulimalide-treated cells. Docetaxel-treated cells in metaphase showed distinct centrosome fragmentation, which was absent in laulimalide-treated cells. Another interesting phenotype observed in this study was during metaphase, the sister kinetochores in laulimalide-treated cells were farther apart than those in the controls or docetaxel-treated cells. The findings from this study suggest that low doses of laulimalide induce kinetochore stretching and an increase in kinetochore-pole tension in metaphase. However, the reason for this phenotype is not completely understood (Bennett, Chan et al. 2012).

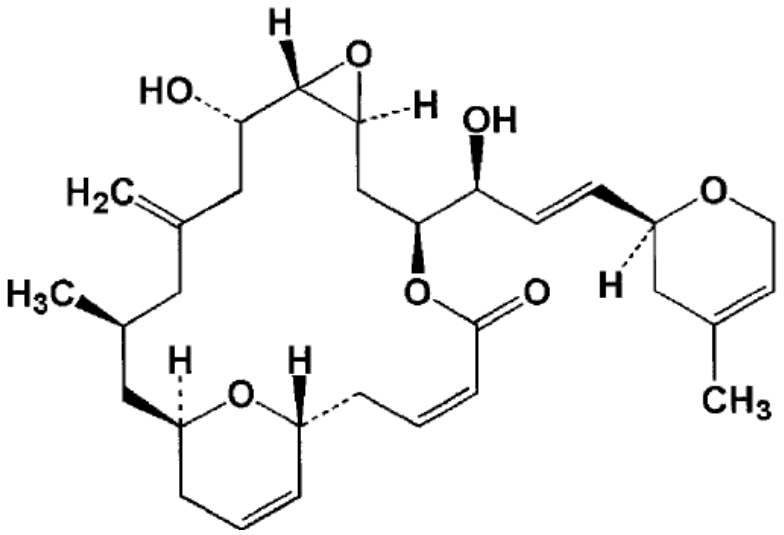

Figure 2.6 Structure of Laulimalide. Reprinted by permission from The American Society for Pharmacology and Experimental Therapeutics (ASPET). Copyright 2004. Eric J. Gapud, Ruoli Bai, Arun K.Ghosh, and Ernest Hamel, Laulimalide and Paclitaxel: A Comparison of Their Effects on Tubulin Assembly and Their Synergistic Action When Present Simultaneously, Mol Pharmacol 2004, 66(1):113-121; DOI: http://dx.doi.org/10.1124/mol.66.1.113

The initial study that identified the laulimalide-binding site was a competitive binding assay with drugs that have known binding sites on microtubules. These initial reports indicated that laulimalide failed to compete with paclitaxel for microtubule binding. Moreover, paclitaxel and laulimalide could bind simultaneously to tubulin (Pryor, O'Brate et al. 2002) and mass-shift perturbation studies showed that laulimalide binds to a distinct site on the exterior of the microtubule lattice near the charged C-terminal tail (Bennett, Barakat et al. 2010). Paclitaxel binds to the β-subunit of tubulin on the inner surface of microtubule lattice (Nogales, Wolf et al. 1995).

Despite the promising inhibitory effect of laulimalide on dividing cells in culture, *in vivo* data does not show significant tumor inhibition at any non-lethal dose (Liu, Towle et al. 2007). In addition, laulimalide exhibited a very narrow efficacy to toxicity ratio (Liu, Towle et al. 2007). In the *in vivo* mice model, laulimalide exhibited limited tumor regression accompanied by high toxicity and dose-dependent loss in body weight (Liu, Towle et al. 2007). However, the reason for high toxicity currently remains unknown. Due to this, laulimalide has limited value for therapeutic use. In spite of these limitations, it might be worthwhile to develop laulimalide as a molecular tool to study cell division. In order to develop it as a research tool to study cell division it is essential to study the acute effects of the drug on cells. The effects of laulimalide have been studied in mammalian cell culture; since these cells take a relatively long time to go through a single mitotic division (~18-24 hours depending on the cell line being used), the phenotypes observed could likely be secondary phenotypes due to lengthy periods of incubation in the drug. These secondary phenotypes might mask the acute effects of laulimalide on microtubules. The first cell division in the *C. elegans* embryo takes about 20 minutes for completion. This makes it an excellent system to investigate the acute effects of small molecules on the first mitotic division. In addition, the microtubule-based processes are highly stereotypical; drug application at a specific stage of mitosis provides a reliable and rapid method to identify distinct phenotypes resulting from different microtubule inhibitors. This makes the *C. elegans* embryo an attractive model for testing the acute effects of drugs.

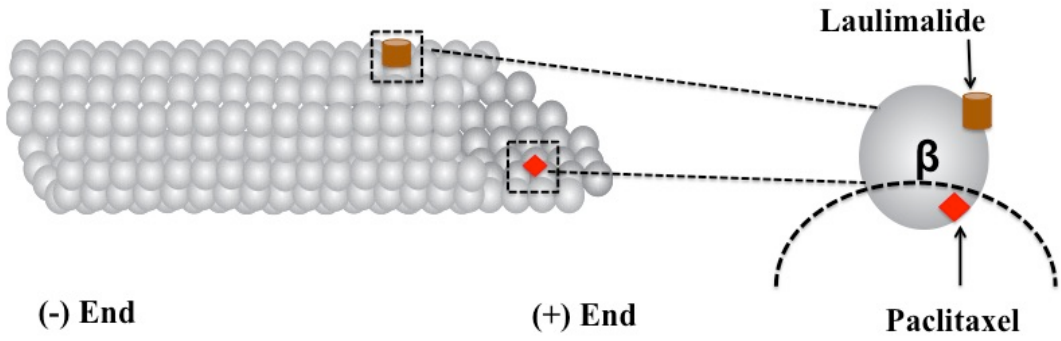

Figure 2.7 Binding sites of paclitaxel and laulimalide on microtubule.
The binding sites for laulimalide and paclitaxel are distinct. Laulimalide binds microtubule on the exterior lattice of microtubules. Paclitaxel binds microtubules on the inner surface of the lattice. Adapted from Bennett, J.M. *et al.* 2010. Chem. Biol.

2.2 Materials and Methods

2.2.1 *C. elegans* nomenclature

Characterized genes in *C. elegans* are given an italicized three or four letter name, which usually represents the function of the gene or a mutant phenotype, followed by a number (Horvitz, Brenner et al. 1979). For example, *nmy-1* encodes a non-muscle myosin chain. Italicized roman numbers indicate the chromosome number the gene is located on. Autosomes are designated by numbers *I-V* and *X* for the sex chromosome. Proteins are written as the gene, in all capital letters and not italicized. For example, NMY-1 is the protein produced by the *nmy-1* gene. Genes with the same properties are given the same three-lettered name followed by different numbers. For instance, the two non-muscle myosin genes are named *nmy-1* and *nmy-2*. A specific allele of a gene is included parenthetically after the gene name, example *paa-1(abc3),* where the letters of the allele refers to the laboratory where the allele was discovered; *abc* refers to the allele discovered in the Srayko lab in Alberta, Canada. A plus sign indicates wild-type alleles.

The phenotypes obtained by RNAi methods are also treated as genetic alleles. For example, *perm-1(RNAi)* indicates an embryo where *perm-1* gene has been knocked down via RNAi. Transgenes are designated by the lab allele nomenclature, followed by *Ex* if it is extra-chromosomal and *Is* if it is integrated, followed by a number. The genotype of the transgene is written in square brackets. Strains are given non-italicized names by the laboratory of origin; therefore, all the worm strains generated in Dr. Martin Srayko's laboratory are given an MAS designation.

2.2.2 *C. elegans* strain designations and maintenance

Table 2.1 *C. elegans* strain designations and genotypes used in this study.

Unless otherwise stated, all *C. elegans* strains were maintained at 25 °C on nematode growth medium (NGM) plates that were seeded with an auxotrophic *Escherichia coli* strain referred to as OP50. The MAS91 strain has a GFP-tubulin marker for visualizing microtubules and an mCherry histone marker to visualize DNA. N2 strain is the wild type strain that does not contain any fluorescent markers.

Strain	Genotype
MAS91	*itIs37[unc119(+),pie-1p::mCherry::his-58]IV;ruIs57[unc119(+),pie-1p::GFP::tbb-2]*
N2	Wild type (variation Bristol)

Table 2.2.1 *C. elegans* strain designations and genotypes used in this study.

2.2.3 Permeabilizing the egg shell for drug delivery using laser ablation

For laser ablation for drug delivery, 2 worms were dissected in a drop of 10 μL of egg buffer (188 mM NaCl, 48 mM KCl, 2 mM CaCl2 and 25 mM HEPES, ph 7.3) with 5% DMSO (dimethyl sulfoxide) or 10 μL of appropriate drug, on a coverslip. The coverslip was mounted on an agarose pad made with 2% agarose in egg buffer. Since all drugs were dissolved in DMSO, egg buffer with 5% DMSO was used as a negative control for all experiments. Embryos in early prophase were imaged in either 10 μL of egg buffer with 5% DMSO or appropriate drug. At this point the eggshell was not permeable and early mitosis events were imaged to ensure that the embryo exhibited a wild-type phenotype. At the pronuclei centering to nuclear envelope breakdown stage, the eggshell was pierced using an Olympus microscope. The ablation laser unit is a nitrogen laser-pumped dye laser. The laser dye used in the dye cell is BPBD (2-[1,1'-biphenyl]-4-yl-5-[4-(1,1-dimethylethyl)phenyl]-1,3,4-

oxadiazole; Butyl-PB), resulting in a wavelength of 365 nm, delivering approximately 120 μ Joules of energy in a 2-6 nanosecond pulse length. The eggshell was pierced once, either on the anterior or the posterior end to allow entry of the drug into the embryo

Table 2.2.2 List of drugs and concentrations used in the laser ablation method

Drug	Source	Concentrations used
Paclitaxel	Sigma	100 μM, 100 nM
Colchicine	Sigma	100 μM
Nocodazole	Sigma	100 μM
Laulimalide	Obtained from Dr. Schreimer, University of Calgary	100 nM

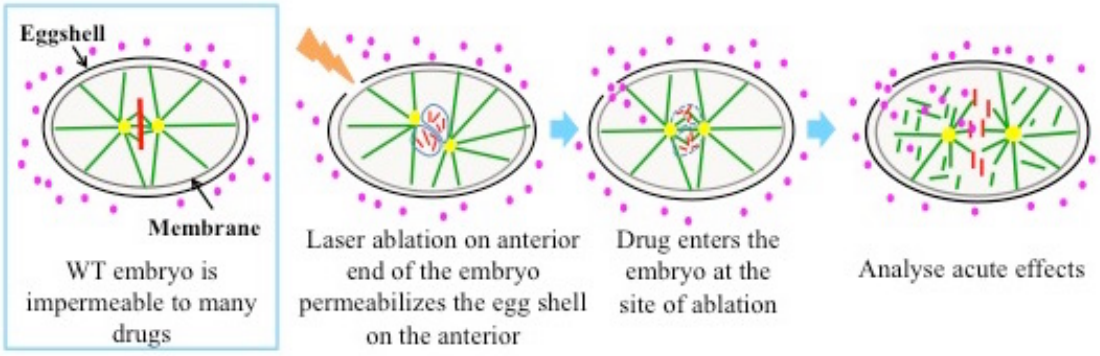

Figure 2.2.1 Drug delivery by laser ablation method. Worms were dissected in appropriate drug solution. The embryo was imaged before laser ablation. The embryo was ablated on one end, which allowed entry of the drug. Imaging was continued after laser ablation to look at acute effect of the drug on microtubules.

2.2.4 Permeabilizing the egg shell for drug delivery using RNA interference by feeding protocol

The *E. coli* strain HT115 (D3) and the L4440 vector (Addgene) were used for all RNAi feeding experiments (Kamath and Ahringer 2003). The HT115 (D3) strain carries the T7 RNA polymerase under the control of the IPTG-inducible promoter. The RNAi L4440 vector contains the T7 polymerase promoter flanking the multiple cloning site. The *E. coli* HT115 (D3) strain synthesizes dsRNA from any DNA that is inserted into this site. When *C. elegans* eat these bacteria, which contain the dsRNA; it induces the *C. elegans* endogenous RNAi machinery. This specifically knocks down any complementary transcript in the worm.

The RNAi feeding plates (NGM agar, 0.001 M IPTG [isopropyl b-D-1-thiogalactopyranoside], 25mg/ml carbenicillin) used in all experiments were poured no longer than one week before use and were stored at 4 °C until seeding. An RNAi based approach used for permeabilizing the *C. elegans* eggshell by knocking down the *perm-1* or *ptr-2* gene was used (Carvalho, Olson et al. 2011). The RNAi bacterial clone with the appropriate gene cloned into the L4440 vector were obtained from the RNAi feeding library (Kamath and Ahringer 2003). *E. coli* containing the desired RNAi vector were grown in 5 mL LB broth (Luria Bertani; 1.0mg/ml Bacto-Tryptone, 0.5 mg/mL yeast extract, 0.5 mg/mL NaCl) with 50 mg/mL ampicillin for 10-12 hours at 37 °C. The next day RNAi plates were seeded with the bacterial culture and left at room temperature for 7-8 hours to dry and express the double stranded RNA. 20-30 L4 hermaphrodites were then placed on the RNAi seeded plates and incubated for 10-20 hours at 20°C. The L4440 vector without an insert was used as a negative control in all RNAi feeding experiments.

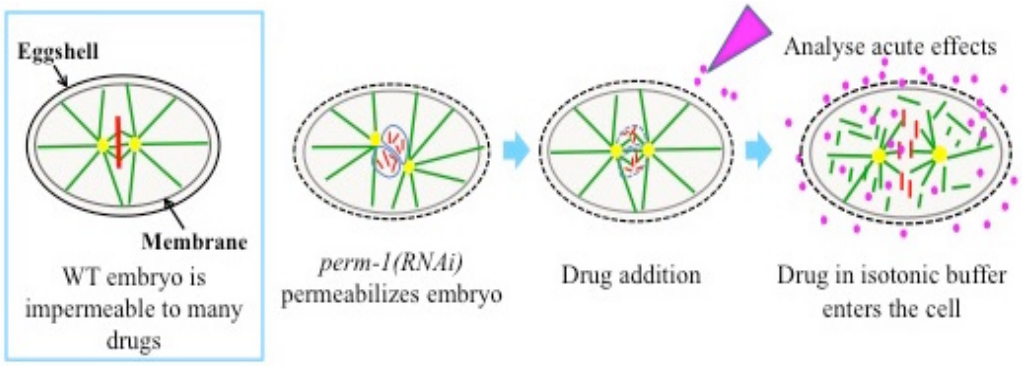

Figure 2.2.2 Drug delivery by RNAi feeding method. Worms are dissected in egg buffer. Permeable embryos are imaged before drug addition. After drug addition, imaging was continued to look at acute effect of the drug on microtubules.

For drug delivery, 2 worms were dissected in a drop of 10 μL of 60% egg buffer (188 mM NaCl, 48 mM KCl, 2 mM $CaCl_2$ and 25 mM HEPES, pH 7.3), which was mounted on a L-polylysine (Sigma-Aldrich) coated 22 mm x 22 mm coverslip. Embryos in early prophase were imaged in 10 μL of egg buffer, imaging at this point ensured that the permeabilized embryo shows a wild-type phenotype before drug addition. At approximately the time of nuclear envelope breakdown, 10 μL of appropriate drug was added while imaging. Live cell imaging was continued until the end of the first cell division for controls, and the appropriate stage for drug testing experimental samples. Since all drugs were dissolved in DMSO, egg buffer with 5% DMSO was used as a negative control for all experiments.

Table 2.2.3 List of drugs and concentrations used in the RNAi feeding method

Drug	Source	Concentrations used
Paclitaxel	Sigma	40 nM,50 nM, 100 nM, 200 nM, 500 nM,1μM
Nocodazole	Sigma	100 nM
Laulimalide	Obtained from Dr. Schreimer, University of Calgary	40 nM,50 nM, 100 nM, 200 nM, 500 nM, 1μM

2.2.5 Microscopy

Confocal microscopy was performed with an Olympus inverted microscope (IX81) with a 60X oil objective (NA 1.42) with a spinning disc confocal head (CSU10; Yokogawa) modified with a condenser lens in the optical path (Quorum Technologies). All images were acquired with an ORCA-R2 camera (Hamamtasu) controlled by MetaMorph software (Molecular Devices). Widefield microscopy was performed with an Olympus IX81 inverted microscope with a dry 10X (NA 0.3), dry 20X (NA 0.7), or oil 60X (NA 1.42) objective. Images were captured with a Hamamatsu ORCA-R2 camera controlled by MetaMorph software.

2.2.5.1 Live-cell imaging of embryos

For live-cell imaging GFP-tubulin and mCherry Histone two-colour Z-series stacks with 5 planes at 2 μm spacing were acquired every 15 seconds. The exposure time was 250 millisecond and 2x2 binning was used.

2.2.5.2 Imaging of fixed embryos

Z stacks with 61 planes at 0.2 μm spacing were acquired using equivalent exposure times, within the dynamic range of the camera for the control and experimental slides of the immunostaining experiment. No binning was used and maximum projections of image stacks were generated for the whole embryo using false colours for display using MetaMorph software.

2.2.6 Immunostaining of fixed embryos

RNAi feeding described in section 2.4 was used to permeabilize the wild-type (N2) embryo eggshell. For immunostaining, 20-30 gravid worms were placed in 5 μL of the appropriate drug solution on polylysine-coated slides. 5% DMSO in 60% egg buffer was used as the control for immunostaining experiments. A coverslip was placed on these worms and gentle pressure was applied to release the embryos in the solution. The released embryos were allowed to incubate in the drug for 5 minutes by leaving the slide at room temperature. The slides were then plunged into liquid nitrogen for 10 minutes after which each slide was retrieved. The coverslip was flicked off using a razor blade while the slide was still frozen. The slide was then incubated into methanol in a coplin jar at -20°C for 15 minutes. After incubation in methanol, slides were washed twice in a coplin jar containing phosphate-buffered saline (PBS). After the washing step, a total volume of 100 μL primary antibody solution (in PBS with 5% goat serum, 0.01% Triton X-100, primary antibody as per Table 2.3) was pipetted onto the fixed embryos on the slide. Slides were then incubated at room temperature in a humid (to prevent the slides from drying out) chamber for 45 minutes, followed by two 10-minute washes in PBS in a coplin jar. After this, secondary antibody solution (in PBS with 5% goat serum, 0.01% Triton X-100, secondary antibody as per Table 2.3) was applied onto the fixed embryos on the

slide and incubated for another 45 minutes in a humid chamber at room temperature. Embryos were then stained with DAPI (1μg/mL) for 5 minutes in order to stain chromatin. The embryos were then mounted with 5 μL glycerol- PPD media (90% glycerol, 20 mM Tris-HCl, pH 8.8, 0.5% p-phenylenediamine) and mixed well. A 22 x 22 mm coverslip was placed on the mounting media and the edges of the coverslip were sealed with nail polish. The slides were either used for imaging immediately or stored at -20 °C until further use.

Table 2.2.4 List of primary antibodies used in the immunostaining experiment

Antibody name and target	Source	Concentration (mg/mL)	Dilution used	Details
DM1A (primary α-tubulin)	Mouse	1	1:100	Sigma
Anti-TBG-1 (Gamma tubulin- C terminus)	Rabbit	3.89	1:200	O'Toole *et al*, 2012

2.2.7 Centrosome tracking

MetaMorph software track object application was used for tracking centrosomes. Centrosome tracking was started at nuclear envelope breakdown (NEBD) stage which was assigned time zero. Tracking was continued until the end of anaphase in control and appropriate stage in drug treated embryos. Three embryos of each drug treatment were used for tracking centrosomes and the average distance was used for making the graph. Distance between the two centrosomes was calculated using the formula $\sqrt{(x2-x1)^2}+\sqrt{(y2-y1)^2}$.

2.2.8 Plasmid extraction and Sanger sequencing of DNA

Plasmid extraction from bacteria was done using the Qiagen miniprep kit. Sequencing of extracted plasmids *perm-1* and *ptr-2* dsRNA vectors was performed at the University of Alberta, Molecular Biology Services Unit (MBSU). Reactions were

set up as follows: 2 μL BigDye terminator v3.1 premix, 6 μL 2.5x buffer (5 mM $MgCl_2$, 200 mM Tris pH 9.0), 1μL 10 mM primer, 250 ng of plasmid template, brought upto a volume of 20 μL with ddH_2O. The reaction was placed in a thermal cycler for 25 cycles of 96°C for 30 seconds, 50°C for 15 seconds and 60°C for 2 minutes. This was followed by ethanol precipitation of the sequencing sample in a 1.5 ml microfuge tube. The sequencing sample was added to 2 μL of NaOAc/EDTA (1.5 M sodium acetate, 250 mM EDTA) and 80 μL of cold 95% ethanol was then added. This was incubated for 15 minutes at 4 °C. The sample was centrifuged for 15 minutes at 4 °C and the supernatant was removed. This was followed by addition of 500 μL of cold 70% ethanol and centrifugation for 5 minutes at 4 °C. The supernatant was removed and the sample was allowed to air dry. The pellet was then delivered to MBSU for sequence analysis by their staff on the 3730 Genetic Analyzer (Applied Biosystems).

2.3 Results

2.3.1 Developing a drug-delivery assay

The first cell division in the *C. elegans* embryo takes about 20 minutes for completion. In addition, the microtubule-based processes are highly stereotypical; drug application at a specific stage of mitosis provides a reliable and rapid method to identify distinct phenotypes resulting from different microtubule inhibitors. This makes the *C. elegans* embryo an attractive model for testing the acute effects of drugs.

One of the biggest limitations of the one-cell embryo system for drug testing is the impermeability of the eggshell. The *C. elegans* embryo develops in an eggshell, which is a trilaminar structure composed of an outer vitelline layer, a middle chitin layer and an inner layer containing proteoglycans (Olson, Greenan et al. 2012). Following assembly of this trilaminar structure, a permeability barrier is formed which is composed of glycolipids (Olson, Greenan et al. 2012). Hence, I first worked towards setting up an assay for drug delivery into the embryo. I tested two different methods for drug delivery in the *C. elegans* embryo.

2.3.1.1 Laser ablation based drug delivery assay

The first method for drug delivery is an adaptation of piercing the eggshell using a laser micropoint. Using a high-energy UV laser is a common technique for piercing holes in the eggshell of early *C. elegans* embryos. The embryos with an ablated eggshell remain viable post-ablation and continue the process of normal development (Schierenberg and Wood 1985). In this method, the embryo was initially imaged at the pronuclear centration/nuclear envelope breakdown stage to visualize the microtubule dynamics before drug entry. At approximately nuclear envelope breakdown during mitosis, a laser micropoint was used to pierce a hole in the eggshell on either the anterior or posterior side of the egg. This method created a small hole in the eggshell and hence allowed drug entry at that location.

In order to test the efficiency of the laser ablation method for drug testing, known microtubule-targeting drugs paclitaxel, nocodazole and colchicine were initially used. The use of these known microtubule-effectors resulted in expected microtubule-based phenotypes (Fig 2.3.1).

Paclitaxel is a known stabilizer of microtubules (Schiff and Horwitz 1980). I started drug testing with 100 μM paclitaxel as other *C. elegans* labs have used this concentration earlier with the laser ablation method (Nguyen-Ngoc, Afshar et al. 2007). Upon paclitaxel application, fluorescent foci were observed in the embryos, indicated by white arrows (Figure 2.3.1 panel 2).

In addition, in the paclitaxel treated embryos, fluorescent foci first appeared and were more abundant on the side where the eggshell was pierced (Fig 2.3.1 panel 2, left, or anterior, side). Colchicine prevents microtubule polymerization by binding to free tubulin (Lambier and Engelborghs 1980) and nocodazole destabilizes microtubules (Vasquez, Howell et al. 1997). Treatment of embryos with 100 μM colchicine and nocodazole resulted in the loss of centrosome-based microtubule fibres within two minutes of drug entry (Fig 2.3.1 panel 3 and 4). A weak fluorescence signal (green) was observed at the centrosomes in these embryos (indicated by white arrows) within 2 minutes of drug application.

Laulimalide was initially tested at 100 nM using the laser ablation method. However, there was no effect of laulimalide at this concentration and the embryos underwent first mitotic division (Fig 2.3.2 panel 2). In contrast the 100 nM paclitaxel-treated embryos, which was used as a positive control, showed shorter microtubules, which looked stable within two minutes of laser ablation (Fig 2.3.2 panel 3).

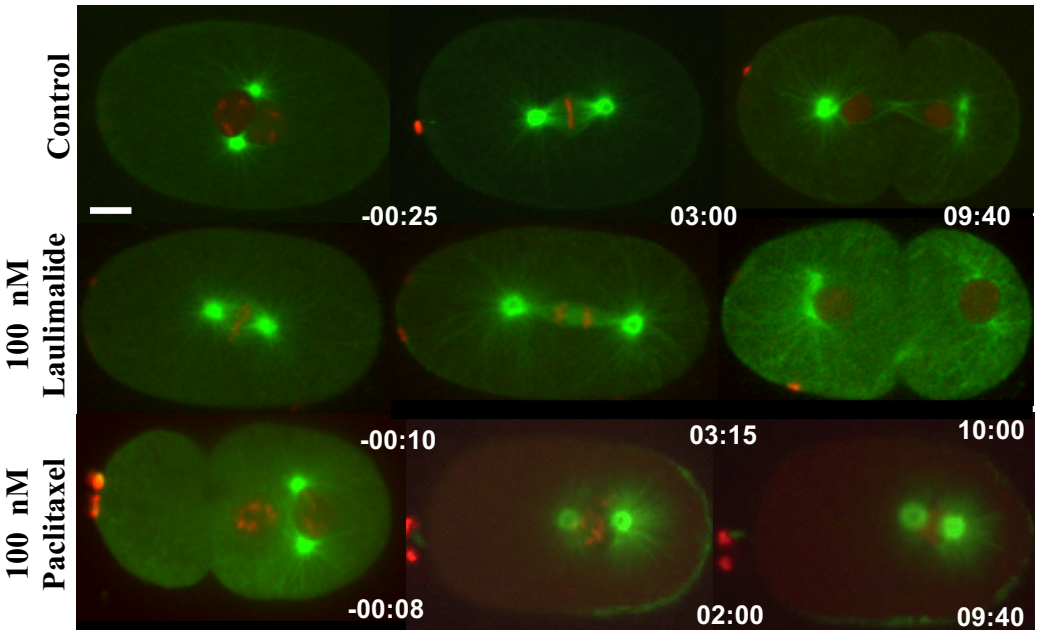

Figure 2.3.2. Laser ablation method for drug-delivery. The first image in all panels is before laser ablation. The second and third image in each panel was taken after laser ablation and drug entry in the embryo. Embryos treated with 5% DMSO (control) divided as expected. 100 μM laulimalide treated embryos divided and did not show any effect of the drug on microtubule dynamics. 100 nM paclitaxel-treated embryos show microtubule stabilization indicated by white arrows and did not undergo first mitotic division.

As seen in figure 2.3.1 and 2.3.2, the laser ablation method ruptures the eggshell only at a single site. Other *C. elegans* research groups have used the laser ablation method to create an imbalance in microtubule dynamics in the anterior and posterior sides (Nguyen-Ngoc, Afshar et al. 2007). Some early work done in the *C. elegans* embryo that looked at laser ablation of the eggshell reported that the inner lipid layer often reseals soon after the eggshell was ablated (Schierenberg and Wood 1985). Though this technique allowed drug entry into the embryo, the results obtained in this study using this assay were variable due to the temporary nature of the hole created by ablation as well as due to the inconsistency in its size. Therefore, it was necessary to use an alternative method for drug delivery and for testing laulimalide at low concentrations.

2.3.1.2 *perm-1/ptr-2* RNAi-feeding based drug delivery assay

An alternative method for drug delivery involves creating embryos that have a defective eggshell permeability barrier. This method was an adaptation of the one developed in the lab of Dr. Karen Oegema at the University of San Diego. Permeabilization of the entire eggshell occurs upon gene knockdown of *perm-1* or *ptr-2* using RNAi by feeding (Kamath, Martinez-Campos et al. 2001, Carvalho, Olson et al. 2011). Using a lipophilic dye present in the egg buffer, the authors demonstrated that the RNAi feeding method renders the entire eggshell permeable and allowed entry of the dye into the embryo, which labeled the plasma membrane (Carvalho, Olson et al. 2011). This RNAi feeding method was used for the rest of the experiments of this thesis for drug testing.

2.3.2 Laulimalide destabilizes microtubules at low concentrations using the *perm-1/ptr-2* RNAi drug delivery assay

Paclitaxel showed a robust microtubule-stabilization phenotype at 100 nM, thus laulimalide was initially tested at this concentration. In contrast to microtubule stabilization, embryos treated with 100 nM laulimalide exhibited defects that were more comparable to the microtubule destabilization phenotypes (Fig 2.3.3 panel 2).

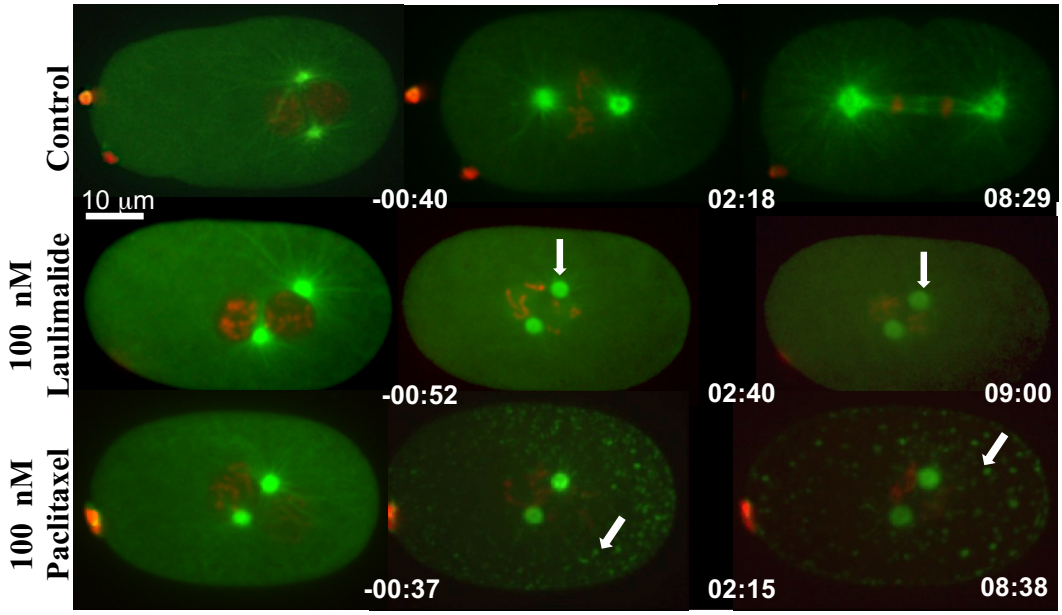

Figure 2.3.3. Laulimalide destabilizes microtubules at 100 nM. The first image in all panels is before drug addition. The second and third image in each panel was taken after drug addition and entry in the embryo. Embryos treated with 5% DMSO (control) divided as expected. In 100 µM laulimalide-treated embryos, fluorescence was observed only at the centrosomes after drug addition. 100 nM paclitaxel-treated embryos exhibit tubulin aggregates indicated by white arrows.

Within 2 minutes of drug administration, the fluorescence was only visible at the centrosomes after drug application (Fig 2.3.3 panel 2) shown by white arrows. This phenotype was similar to that which occurred with the application of nocodazole, a drug that is well established to depolymerize microtubules (Nocodazole panel in Fig 2.3.1 panel 4). On the other hand, the 100 nM paclitaxel-treated embryos exhibited stabilized tubulin aggregates in the cytoplasm (indicated by white arrows). These stabilized tubulin aggregates were not observed in the cytoplasm of 100 nM laulimalide-treated embryos.

In order to further characterize the microtubule defects, I performed live-cell imaging of a gfp-tubulin mCherry-histone strain and tracked the movements of the centrosomes during prometaphase to anaphase. Within 2 minutes of treatment with laulimalide, the anterior and posterior centrosomes drifted towards each other. In control embryos, anterior and posterior centrosomes maintained their relative positions during mitotic spindle assembly after nuclear envelope breakdown. Then centrosomes moved apart from each other just before chromatid separation, and continued to separate throughout anaphase, reaching a maximum separation of 18 μm at the end of anaphase (Fig 2.3.4). In comparison to other microtubule-binding drugs, laulimalide treatment resulted in centrosome movements that were most similar to the known microtubule depolymerizing drug nocodazole. In contrast, paclitaxel-treated embryos exhibited a slow separation of the centrosomes, to a maximal distance of 12 $\pm$ 2 μm. Together, the results suggested that laulimalide most closely resembles the effects caused by microtubule depolymerization, not stabilization (Fig 2.3.4).

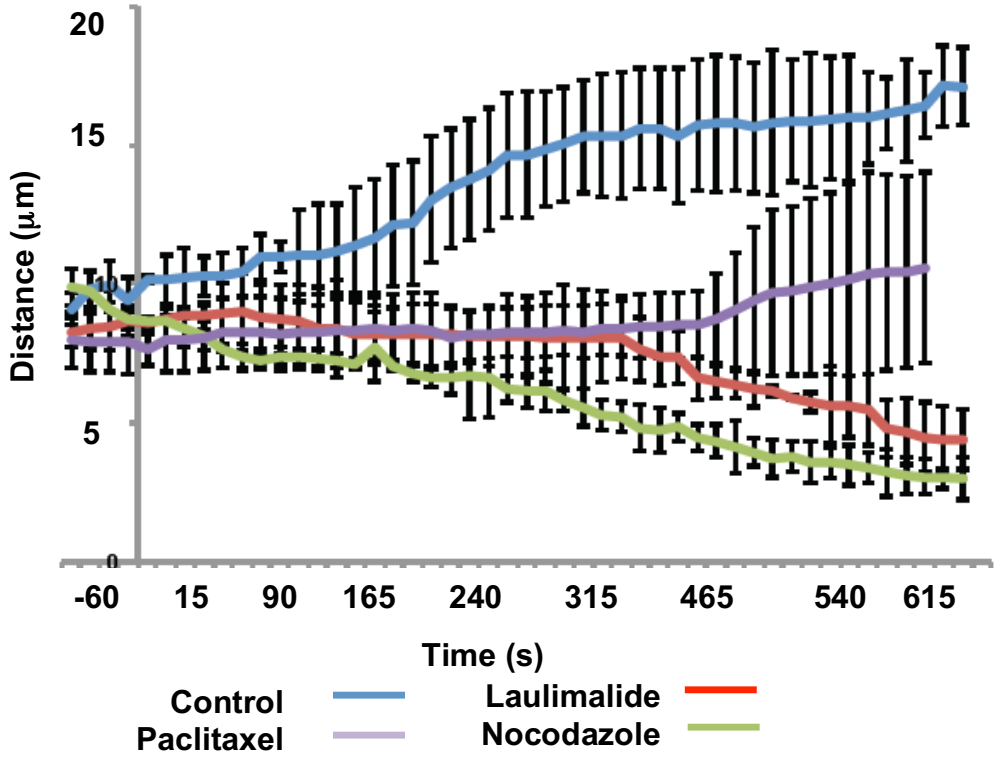

Figure 2.3.4. Centrosome tracking in control and drug-treated embryos. The graph shows the distance between centrosomes in control embryos, embryos treated with 100 nM laulimalide (red), paclitaxel (purple) and nocodazole (green). The data is an average of 3 embryos for each drug trial.

A transgenic beta-tubulin GFP strain was used in the live-cell imaging experiment. It was possible that the microtubule depolymerizaton phenotype observed with 100 nM laulimalide was because of the presence of GFP microtubules in the transgenic strain. For instance, the GFP tag itself could interfere with microtubule dynamics or the overexpression of beta tubulin could alter microtubule dynamics. In order to rule out this possibility, I also used the wild type N2 strain for immunostaining fixed, *perm-1(RNAi)* embryos. Similar to the transgenic strain used in live cell imaging, the fixed embryos also displayed phenotypes consistent with microtubule depolymerization when treated with 100 nM laulimalide and 100 nM nocodazole (Fig 2.3.5). As expected, microtubule stabilization was observed in embryos treated with 100 nM paclitaxel.

This experiment demonstrated that laulimalide caused microtubule destabilization at low concentration in wild-type embryos, which were subjected to immunofluorescence. In conclusion, the observed drug-induced phenotypes were not specific to the transgenic strain used for live-cell imaging experiments but could also be reproduced using the N2 wild-type strain by immunofluorescence

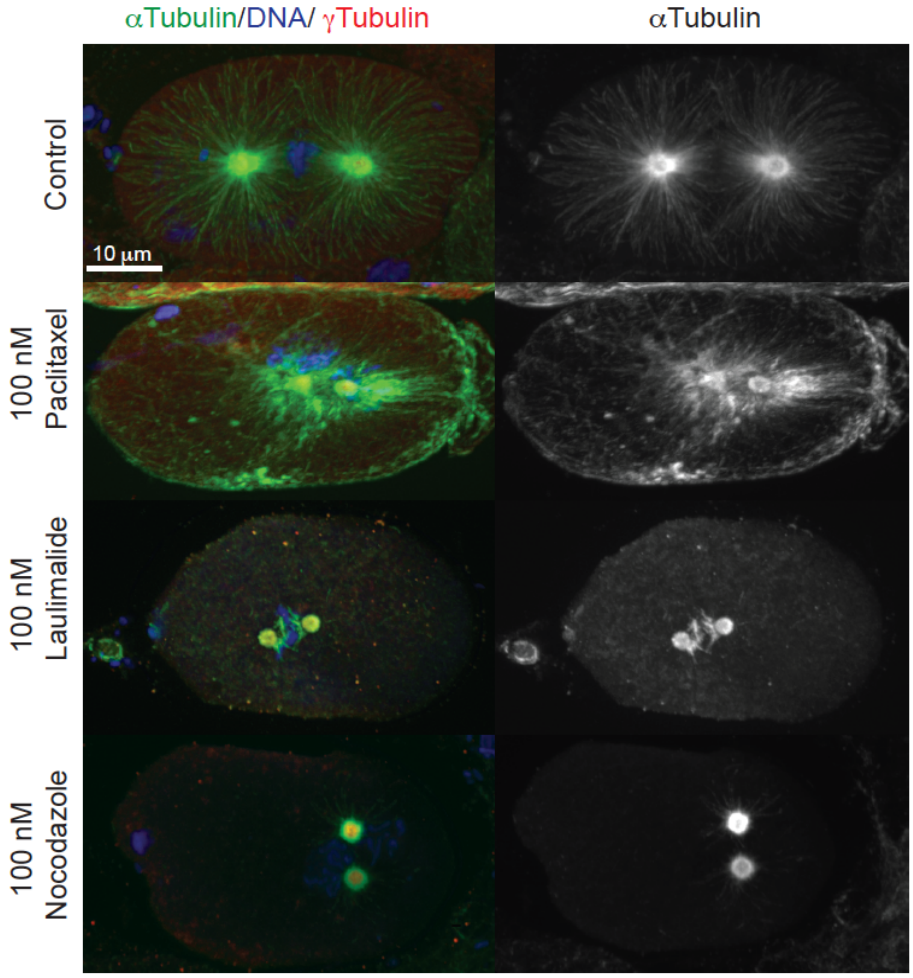

Figure 2.3.5. Antibody staining of fixed permeabilized embryos. Representative control and drug treated embryos stained with anti- α tubulin and anti-γ tubulin to observe the microtubules (in green) and centrosomes (in red) respectively. Chromatin was visualized using DAPI stain (shown in blue).

Laulimalide was also tested at 50 nM (figure 2.3.6) and phenotypes similar to that observed with 100 nM of the drug were observed. However, only 58% of the embryos (7/12) were obviously affected at this dose. At 50 nM, embryos exhibited phenotypes that were less severe than 100 nM laulimalide. For example, the embryos affected by 50 nM laulimalide progressed into anaphase; based on centrosome separation. However, chromosome segregation was not normal in these embryos. The chromosomes remained in the centre of the embryo and cytokinesis did not occur (Fig 2.3.6 panel 2).No microtubule-based phenotypes or other abnormalities were observed in embryos treated with 50 nM paclitaxel (Fig. 2.3.6 panel 3).

In the context of previously published work with laulimalide, my above experiments (Figure 2.3.3 and 2.3.6) suggest that 100 nM laulimalide results in destabilization of microtubules. This was unexpected, as laulimalide has been shown to be a microtubule-stabilizing drug (Mooberry, Tien et al. 1999, Gapud, Bai et al. 2004). The reason for microtubule destabilization like phenotype could be due to its administration at low concentration. In order to assess if laulimalide could affect the microtubule cytoskeleton distinctly at different concentrations, the drug was tested at a relatively high concentration of 1 μM.

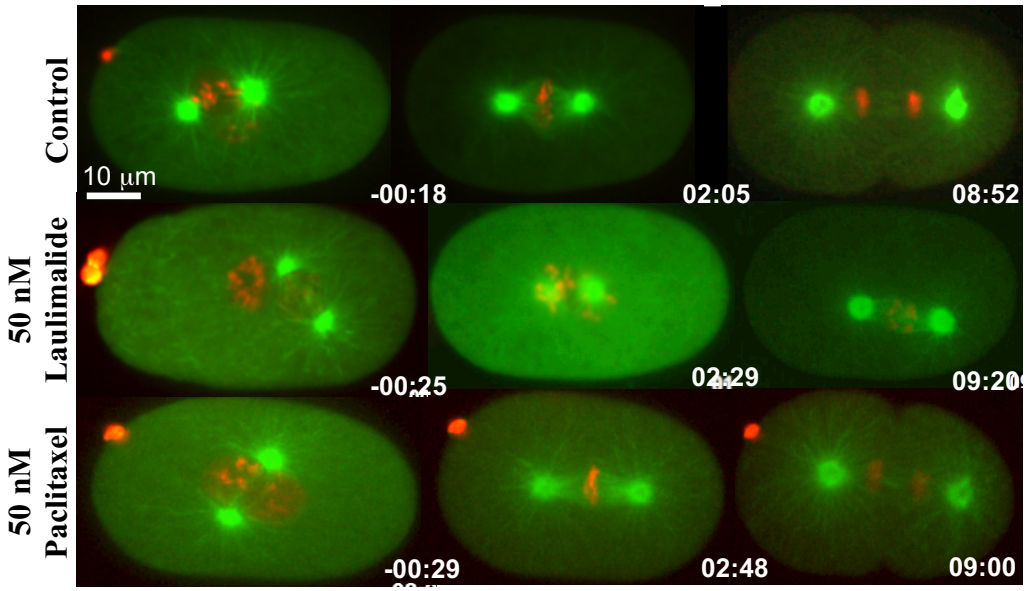

Figure 2.3.6. Laulimalide destabilizes microtubules at 50 nM. The first image in all panels is before drug addition. The second and third image in each panel was taken after drug addition and entry in the embryo. Embryos treated with 5% DMSO (control) and 50 nM paclitaxel divided normally. 50 nM laulimalide-treated embryos did not complete cell division.

2.3.3 Laulimalide stabilizes microtubules at high concentrations using the *perm-1/ptr-2* RNAi drug delivery assay

Application of either laulimalide or paclitaxel at 1 μM resulted in very prominent microtubule defects. Rapid microtubule stabilization was observed and the centrosomal tubulin fluorescence appeared brighter. Furthermore, both drugs resulted in the formation of fluorescent foci throughout the cytoplasm, likely representing stabilized tubulin aggregates (indicated by white arrows). These embryos did not complete the first cell division, but remained arrested at the stage at which the drug was administered. The chromosomes did not congress to form a metaphase plate in these embryos (Fig. 2.3.7 panel 2 and 3).

Laulimalide and paclitaxel also resulted in embryonic phenotypes consistent with microtubule stabilization at intermediate concentrations of 500 nM and 200 nM (Fig 2.3.8 and Fig 2.3.9 respectively).

Figure 2.3.10 shows a summary of phenotypes observed with various concentrations of laulimalide and paclitaxel. The lowest effective concentration of laulimalide was 50 nM, and paclitaxel was above 50 nM in *C. elegans* embryo as observed using the *perm-1 (RNAi)/ptr-2 (RNAi)* eggshell permeabilization method. The bar graph shows that in *C. elegans* embryos, laulimalide acted as a microtubule-stabilizing agent at concentrations of 200 nM- 1μM and a microtubule-destabilizer at concentrations of 50 nM-100 nM.

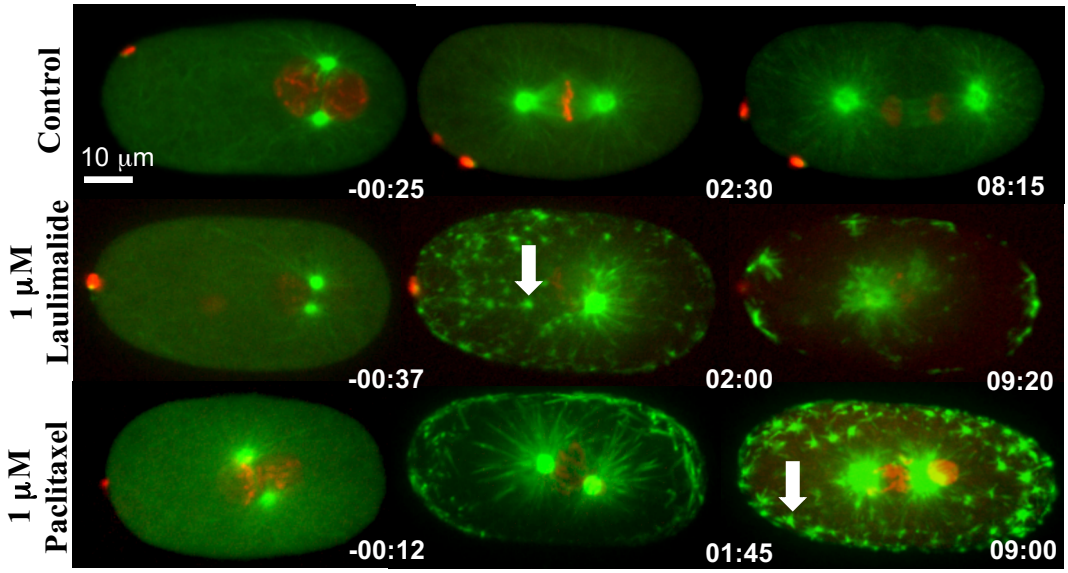

Figure 2.3.7. Laulimalide stabilizes microtubules at 1 μM. The first image in all panels is before drug addition. The second and third image in each panel was taken after drug addition and entry in the embryo. Embryos treated with 5% DMSO (control) divided normally. 50 nM laulimalide-treated embryos did not complete cell division.

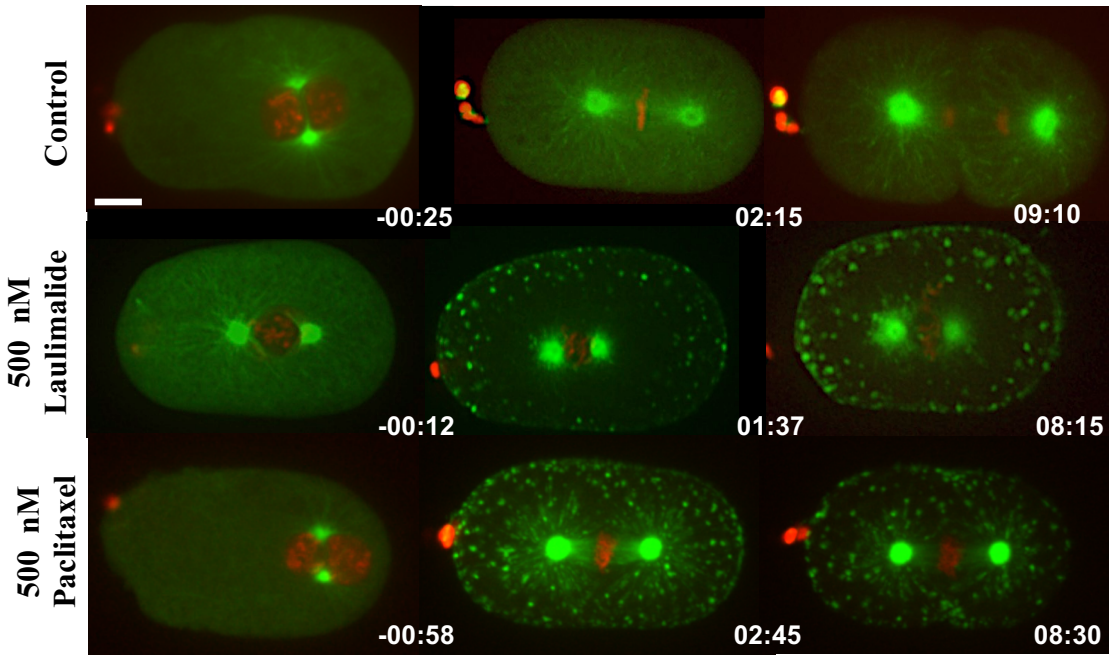

Figure 2.3.8. Laulimalide stabilizes microtubules at 500 nM. The first image in all panels is before drug addition. The second and third image in each panel was taken after drug addition and entry in the embryo. Embryos treated with 5% DMSO (control) divided normally. 500 nM laulimalide-and paclitaxel treated embryos did not complete cell division. At this concentration both drugs exhibit microtubule stabilization.

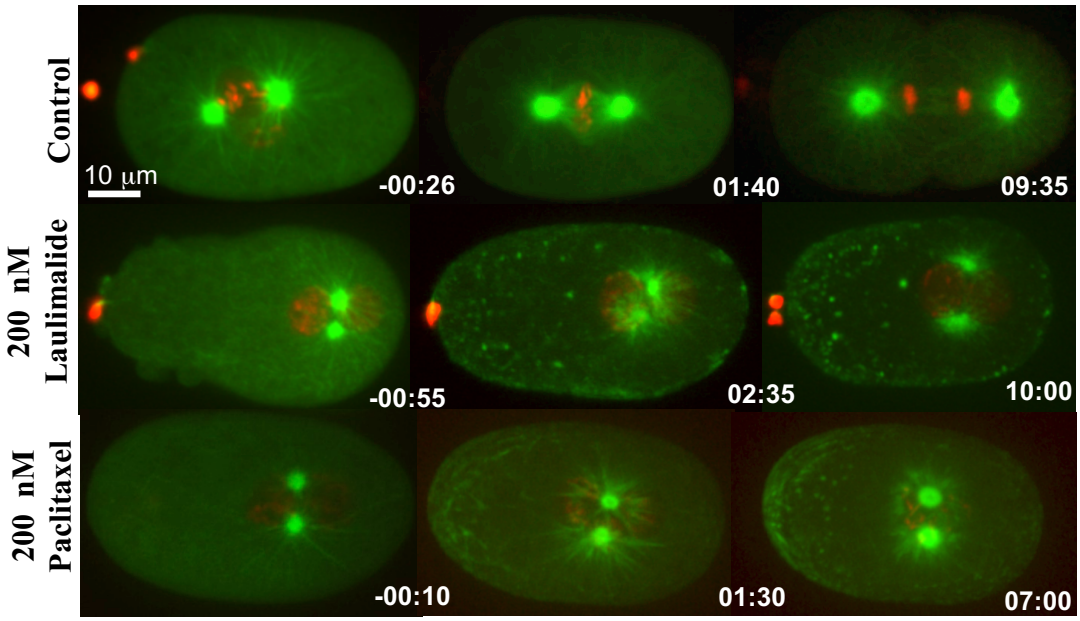

Figure 2.3.9. Laulimalide stabilizes microtubules at 200 nM. The first image in all panels is before drug addition. The second and third image in each panel was taken after drug addition and entry in the embryo. Embryos treated with 5% DMSO (control) divided normally. 200 nM laulimalide and paclitaxel treated embryos did not complete cell division. At this concentration both drugs exhibit microtubule stabilization.

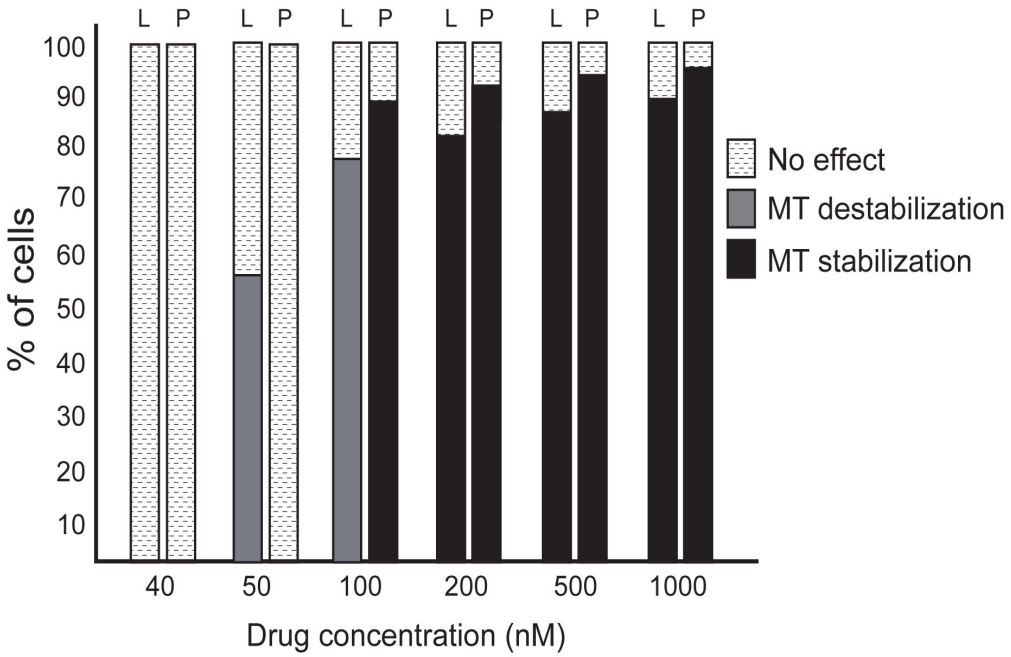

Figure 2.3.10. Dose response graph for laulimalide and paclitaxel. The graph shows the effect of various concentrations of drugs. N≥6 for each concentration tested. L= laulimalide and P=paclitaxel. Black bar indicates microtubule stabilization, grey bar is microtubule destabilization.

2.3.4 Effects of laulimalide in combination with paclitaxel

A combination of drugs when used together can have additive, antagonistic or synergistic effects. When two drugs are used in combination and the total effect is a sum of their individual effects then it is an additive effect. However, when two drugs used in combination generate an effect greater than the sum of their individual effect, then the drugs are said to be synergistic with each other. Paclitaxel and laulimalide bind to different sites on β–tubulin (Bennett, Barakat et al. 2010, Churchill, Klobukowski et al. 2015). Paclitaxel and laulimalide have been shown to work synergistically in mammalian cell culture (Gapud, Bai et al. 2004). Therefore, I decided to test if they can work synergistically when applied to the *C. elegans* embryo. Since laulimalide was sub-effective at 40 nM and paclitaxel was sub-effective at 50 nM, I tested embryos with a mixture of sub-effective concentrations of both the drugs. When 40 nM laulimalide and 50 nM paclitaxel were tested separately, microtubule phenotypes were not observed and 100% of the embryos that were tested exhibited normal cell division (Fig 2.3.11 panel 2 and 3). However, when a combination of 40 nM laulimalide and 50 nM paclitaxel was used, spindle formation occurred but spindle structure was not normal. These embryos had fewer microtubules than controls.

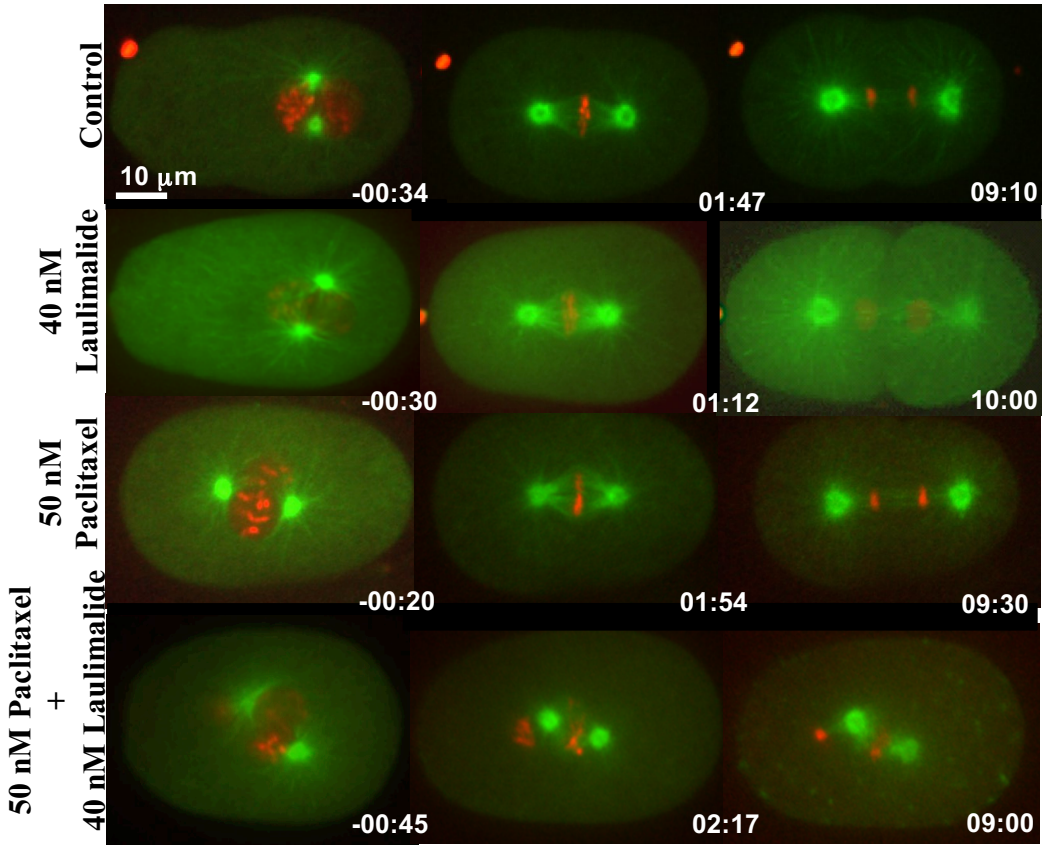

Figure 2.3.11 Laulimalide and paclitaxel act synergistically at sub-effective concentrations. The first image in all panels was acquired before drug addition. The second and third image in each panel was taken after drug addition. Embryos treated with 5% DMSO (control), 40 nM laulimalide or 50 nM paclitaxel divided normally. Embryos were also treated with 40 nM laulimalide and 50 nM paclitaxel mixture, which resulted in tubulin aggregates. A small spindle-like structure was observed however the morphology was abnormal and chromosome segregation did not occur. Microtubules are shown in green and histone in red.

After about 2 minutes of drug application, fluorescent foci were present in the cytoplasm, as observed with higher concentrations of laulimalide or paclitaxel (as seen in figure 2.3.8). 100% of the embryos tested did not undergo anaphase or complete cell division (Fig 2.3.11 panel 4).These results suggest that at sub-effective concentrations, laulimalide and paclitaxel can act synergistically to perturb spindle structure and disrupt the process of cell division in *C. elegans*.

I also tested the effect of both drugs at 100 nM, as each drug conferred different phenotypes at this concentration. This drug mixture resulted in phenotypes consistent with microtubule stabilization in 83% of the tested embryos.

Stabilization of the microtubules was observed within 2 minutes of drug application and the embryos did not recover even 9 minutes after drug application. After 9 minutes, fewer microtubule fibres remained and stabilized foci were present in the cytoplasm (Fig 2.3.12 panel 4).

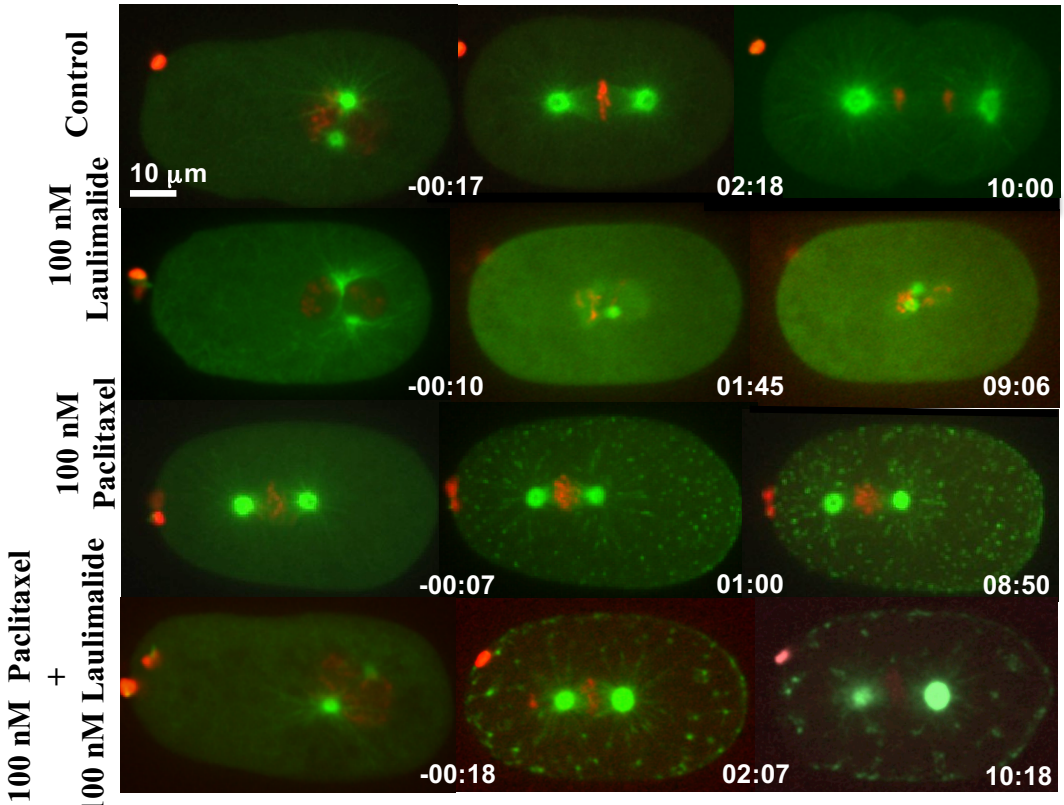

Figure 2.3.12. Laulimalide and paclitaxel act synergistically at 100 nM. Embryos treated with 5% DMSO (control) divided normally. Embryos treated with 100 nM paclitaxel and laulimalide show evidence of microtubule stabilization and destabilization, respectively. Embryos treated with a mixture of 100 nM paclitaxel and laulimalide displayed tubulin aggregates and phenotypes similar to high doses of paclitaxel alone. Microtubules are shown in green and histone in red.

2.4. Discussion and conclusion

2.4.1 Testing two methods for drug delivery in the *C. elegans* embryo

Laulimalide is considered a potent inhibitor of microtubule dynamics. Previous studies have shown that laulimalide and paclitaxel have strikingly similar properties in both *in vitro* and *in vivo* experiments (Mooberry, Tien et al. 1999, Gapud, Bai et al. 2004). Based on these studies, laulimalide has been classified as a microtubule-stabilizing agent, similar to paclitaxel. However, these studies also noted some important differences between the phenotypes conferred by laulimalide and paclitaxel. The objective of my work was to study the acute effects of laulimalide on microtubules. I started my drug-testing experiments using the laser ablation method. In my experiments paclitaxel was used as one of the controls. I observed localized microtubule stabilization on the side where the eggshell was ablated (see figure 2.3.1 & 2.3.2). Similar results of localized microtubule stabilization with 100 μM paclitaxel in the *C. elegans* embryo has been previously reported (Nguyen-Ngoc, Afshar et al. 2007). However, the other two control drugs, nocodazole and colchicine did not show any signs of localized effect on microtubules when used in the laser ablation experiment.

Laulimalide was only available in a limited quantity; hence I could not test laulimalide at a high concentration of 100 μM. At a concentration of 100 nM using the laser ablation method, laulimalide did not have any effect on microtubules and the embryos underwent normal mitotic division. This could have been a result of non-uniform distribution of the drug inside the embryo. The laser ablation technique makes a single hole in the eggshell. Previous work done using laser ablation of eggshell has indicated that soon after ablation the inner lipid layer often reseals (Schierenberg and Wood 1985). Therefore I used an alternative approach for drug delivery and for testing laulimalide at low concentrations.

In order to permeabilize the entire eggshell I used the method of knocking down *perm-1/ptr-2* by the RNAi feeding method (Carvalho, Olson et al. 2011). In *C. elegans* embryo, fertilization triggers the assembly of the eggshell. The eggshell provides mechanical rigidity, prevents polyspermy after fertilization and also keeps the embryo impermeable to its surrounding environment. Correlative light and electron microscopy studies revealed that one of the components of the eggshell – the permeability barrier; is a distinct layer of the eggshell. The assembly of the permeability barrier requires a sugar-modifying enzyme, PERM-1 for fatty acid synthesis (Olson, Greenan et al. 2012). PTR-2 belongs to the patched related family of proteins and has been implicated in the normal worm molting process and is also required for male tail development (Frand, Russel et al. 2005). The role of PTR-2 in eggshell development is still not clear (personal communication with Sara Olson) but an RNAi knockdown screen shows that *ptr-2(RNAi)* results into permeable embryos (Carvalho, Olson et al. 2011). The method of *perm-1/ptr-2 RNAi* worked better for testing laulimalide at a lower concentration.

2.4.2 Laulimalide induces dose-dependent modulation of microtubule behavior

My results with *perm-1/ptr-2 (RNAi)* indicate that laulimalide causes different effects on microtubules in a concentration dependent manner. Previous studies done using laulimalide, paclitaxel and its analogues have indicated that these drugs are able to stabilize microtubules both *in vivo* and *in vitro* (Jordan, Wendell et al. 1996, Mooberry, Tien et al. 1999). Therefore, it was not surprising that I observed similar cellular response in the *C. elegans* embryo using high concentrations of laulimalide (see figure 2.3.7). At higher concentrations, laulimalide acted as a microtubule stabilizer similar to paclitaxel. However, at lower concentrations it had a microtubule-destabilizing effect, which appeared similar to nocodazole and colchicine (figure 2.3.3). The microtubule-destabilization phenotype observed in my experiments was very interesting as all the previous drug tests done using laulimalide indicated that it

stabilizes microtubules similar to paclitaxel. A microtubule-destabilization phenotype using laulimalide has never been reported before.

One of the possible reasons for why low concentrations of laulimalide resulted in the destabilization of MTs could be that the binding site targeted by laulimalide on *C. elegans* differs from that presented by microtubules from mammalian cell lines used in previous experiments. However, there are no differences between the *C. elegans* and the bovine amino acid sequences within the critical region on β-tubulin that has been implicated in laulimalide binding (Bennett, Barakat et al. 2010). This suggests that the microtubule-depolymerization phenotype observed with low laulimalide concentrations was not due to any differences in the binding site for laulimalide on *C. elegans* β-tubulin.

Microtubules purified from *C. elegans* exhibit an unusual 11-protofilament arrangement compared to the canonical 13-protofilaments in mammalian microtubules (Aamodt and Culotti 1986), and this could alter polymer dynamics in the presence of small molecules. It is possible that the *C. elegans* 11-protofilament microtubule lattice might be more sensitive to low doses of laulimalide than the 13-protofilament counterpart. For instance, in situations where a small percentage of binding sites are occupied, 11-protofilament microtubules might become destabilized. At higher concentrations, the effect of multiple laulimalide molecules bound to multiple protofilaments of the same microtubule could instead stabilize the polymer. It is also possible that the *C. elegans* embryonic cellular environment contains a unique combination of microtubule-associated proteins (MAPs) and microtubule regulators that contribute to some of the laulimalide-induced phenotypes.

2.4.3 Laulimalide acts synergistically with paclitaxel

Laulimalide and paclitaxel have distinct binding sites on microtubules. The first study that identified a laulimalide binding site on β-tubulin showed that it binds on the

exterior of microtubules on β-tubulin in the seam between two protofilaments (Bennett, Barakat et al. 2010). Paclitaxel binds on the interior surface of microtubules within a pocket in the second globular domain of β-tubulin (Nogales, Wolf et al. 1995, Nogales, Whittaker et al. 1999). Since the two drugs have distinct binding sites on β-tubulin, they have been shown to work synergistically to prevent cell proliferation when applied to mammalian cells (Gapud, Bai et al. 2004, Clark, Hills et al. 2006). My results with a combination of laulimalide and paclitaxel also show a similar effect. The high dose combination of 100 nM laulimalide and 100 nM paclitaxel resulted in distinct microtubule-stabilization-like phenotypes indicated by the presence of tubulin aggregates in the embryo (figure 2.3.12). When both drugs were applied to the embryos at sub-effective concentrations, a MT-stabilization phenotype was also observed, indicated by accumulation of tubulin aggregates in the embryo (figure 2.3.11). This phenotype was not predicted, in part, because laulimalide and paclitaxel bind to different sites on β-tubulin. Furthermore, the two drugs have opposite phenotypes, individually, at 100 nM. Synergy between laulimalide and paclitaxel has been observed in earlier studies, which used mammalian cell culture (Gapud, Bai et al. 2004, Clark, Hills et al. 2006). If microtubule stabilization could be conferred by the occupation of either paclitaxel or laulimalide sites on the polymer, this would explain how low doses of paclitaxel can act synergistically with low doses of laulimalide to stabilize microtubules. The mechanism of this synergism between laulimalide and paclitaxel is currently not clearly understood. However, when used in combination, microtubules treated with paclitaxel and laulimalide together (either at sub-effective concentrations or at 100 nM of each drug) exhibit stabilization-like phenotypes. Thus, paclitaxel seemed dominant in affecting the dynamics of microtubules when used in combination with laulimalide.

In conclusion, my results indicate that the *C. elegans* microtubule network responds differentially to varying concentrations of laulimalide, compared with paclitaxel. At higher concentrations, laulimalide acts as a microtubule stabilizer similar to paclitaxel. This finding confirms that laulimalide belongs to a class of microtubule stabilizing drugs. However, at low concentrations laulimalide is able to

act as a microtubule destabilizer. This property of microtubule destabilization might be specific only to the *C. elegans* cellular environment. My results also demonstrate that laulimalide and paclitaxel can act synergistically at sub-effective concentrations. Further studies with laulimalide in combination with other anti-mitotic drugs can be done to understand the behavior of microtubules in the presence of other drugs and also for possible development of laulimalide for combination-drug therapies. It is possible that combining laulimalide with other microtubule-targeting drugs might have a clinical utility. In addition, my results also establish that laulimalide can be used as an important molecular tool to study microtubule dynamics in the *C. elegans* embryo and this single drug can be used as a powerful agent for conducting both microtubule stabilization and destabilization studies.

Andreu, J. M. and S. N. Timasheff (1986). "Tubulin-colchicine interactions and polymerization of the complex." Ann N Y Acad Sci **466**: 676-689.

Aamodt, E. J. and J. G. Culotti (1986). "Microtubules and microtubule-associated proteins from the nematode Caenorhabditis elegans: periodic cross-links connect microtubules in vitro." J Cell Biol **103**(1): 23-31.

Bennett, M. J., K. Barakat, J. T. Huzil, J. Tuszynski and D. C. Schriemer (2010). "Discovery and characterization of the laulimalide-microtubule binding mode by mass shift perturbation mapping." Chem Biol **17**(7): 725-734.

Bennett, M. J., G. K. Chan, J. B. Rattner and D. C. Schriemer (2012). "Low-dose laulimalide represents a novel molecular probe for investigating microtubule organization." Cell Cycle **11**(16): 3045-3054.

Bollag, D. M., P. A. McQueney, J. Zhu, O. Hensens, L. Koupal, J. Liesch, M. Goetz, E. Lazarides and C. M. Woods (1995). "Epothilones, a new class of microtubule-stabilizing agents with a taxol-like mechanism of action." Cancer Res **55**(11): 2325-2333.

Brogdon, C. F., F. Y. Lee and R. M. Canetta (2014). "Development of other microtubule-stabilizer families: the epothilones and their derivatives." Anticancer Drugs **25**(5): 599-609.

Carvalho, A., S. K. Olson, E. Gutierrez, K. Zhang, L. B. Noble, E. Zanin, A. Desai, A. Groisman and K. Oegema (2011). "Acute drug treatment in the early C. elegans embryo." PLoS One **6**(9): e24656
.

Clark, E. A., P. M. Hills, B. S. Davidson, P. A. Wender and S. L. Mooberry (2006). "Laulimalide and synthetic laulimalide analogues are synergistic with paclitaxel and 2-methoxyestradiol." Mol Pharm **3**(4): 457-467.

Chen, J., T. Liu, X. Dong and Y. Hu (2009). "Recent development and SAR analysis of colchicine binding site inhibitors." Mini Rev Med Chem **9**(10): 1174-1190.

Corley, D. G., R. Herb, R. E. Moore, P. J. Scheuer and V. J. Paul (1988). "Laulimalides. New potent cytotoxic macrolides from a marine sponge and a nudibranch predator." The Journal of Organic Chemistry **53**(15): 3644-3646.

D'Agostino, G., J. del Campo, B. Mellado, M. A. Izquierdo, T. Minarik, L. Cirri, L. Marini, J. L. Perez-Gracia and G. Scambia (2006). "A multicenter phase II study of the cryptophycin analog LY355703 in patients with platinum-resistant ovarian cancer." Int J Gynecol Cancer **16**(1): 71-76.

De Brabander, M., G. Geuens, R. Nuydens, R. Willebrords and J. De Mey (1981). "Taxol induces the assembly of free microtubules in living cells and blocks the organizing capacity of the centrosomes and kinetochores." Proc Natl Acad Sci U S A **78**(9): 5608-5612.

Desai, A. and T. J. Mitchison (1997). "Microtubule polymerization dynamics." Annu Rev Cell Dev Biol **13**: 83-117.

Dhamodharan, R., M. A. Jordan, D. Thrower, L. Wilson and P. Wadsworth (1995). "Vinblastine suppresses dynamics of individual microtubules in living interphase cells." Mol Biol Cell **6**(9): 1215-1229.

Don, S., N. M. Verrills, T. Y. Liaw, M. L. Liu, M. D. Norris, M. Haber and M. Kavallaris (2004). "Neuronal-associated microtubule proteins class III beta-tubulin and MAP2c in neuroblastoma: role in resistance to microtubule-targeted drugs." Mol Cancer Ther **3**(9): 1137-1146.

Dumontet, C. and M. A. Jordan (2010). "Microtubule-binding agents: a dynamic field of cancer therapeutics." Nat Rev Drug Discov **9**(10): 790-803.

Dumontet, C., M. A. Jordan and F. F. Lee (2009). "Ixabepilone: targeting betaIII-tubulin expression in taxane-resistant malignancies." Mol Cancer Ther **8**(1): 17-25.

Gapud, E. J., R. Bai, A. K. Ghosh and E. Hamel (2004). "Laulimalide and paclitaxel: a comparison of their effects on tubulin assembly and their synergistic action when present simultaneously." Mol Pharmacol **66**(1): 113-121.

Gerth, K., N. Bedorf, G. Hofle, H. Irschik and H. Reichenbach (1996). "Epothilons A and B: antifungal and cytotoxic compounds from Sorangium cellulosum (Myxobacteria). Production, physico-chemical and biological properties." J Antibiot (Tokyo) **49**(6): 560-563.

Gornstein, E. and T. L. Schwarz (2014). "The paradox of paclitaxel neurotoxicity: Mechanisms and unanswered questions." Neuropharmacology **76 Pt A**: 175-183.

Greene, L. M., M. J. Meegan and D. M. Zisterer (2015). "Combretastatins: More Than Just Vascular Targeting Agents?" Journal of Pharmacology and Experimental Therapeutics **355**(2): 212-227.

Hastie, S. B. (1991). "Interactions of colchicine with tubulin." Pharmacol Ther **51**(3): 377-401.

Horvitz, H. R., S. Brenner, J. Hodgkin and R. K. Herman (1979). "A uniform genetic nomenclature for the nematode Caenorhabditis elegans." Mol Gen Genet **175**(2): 129-133.

Johnson, I. S., J. G. Armstrong, M. Gorman and J. P. Burnett, Jr. (1963). "The Vinca Alkaloids: A New Class of Oncolytic Agents." Cancer Res **23**: 1390-1427.

Johnson, I. S., H. F. Wright, G. H. Svoboda and J. Vlantis (1960). "Antitumor principles derived from Vinca rosea Linn. I. Vincaleukoblastine and leurosine." Cancer Res **20**: 1016-1022.

Jordan, M. A., K. Wendell, S. Gardiner, W. B. Derry, H. Copp and L. Wilson (1996). "Mitotic block induced in HeLa cells by low concentrations of paclitaxel (Taxol) results in abnormal mitotic exit and apoptotic cell death." Cancer Res **56**(4): 816-825.

Kamath, R. S. and J. Ahringer (2003). "Genome-wide RNAi screening in Caenorhabditis elegans." Methods **30**(4): 313-321.

Kavallaris, M., A. S. Tait, B. J. Walsh, L. He, S. B. Horwitz, M. D. Norris and M. Haber (2001). "Multiple microtubule alterations are associated with Vinca alkaloid resistance in human leukemia cells." Cancer Res **61**(15): 5803-5809.

Lakhani, N. J., M. A. Sarkar, J. Venitz and W. D. Figg (2003). "2-Methoxyestradiol, a promising anticancer agent." Pharmacotherapy **23**(2): 165-172.

Lambier, A. and Y. Engelborghs (1980). "A quantitative analysis of tubulin-colchicine binding to microtubules." Eur J Biochem **109**(2): 619-624.

Leandro-Garcia, L. J., S. Leskela, I. Landa, C. Montero-Conde, E. Lopez-Jimenez, R. Leton, A. Cascon, M. Robledo and C. Rodriguez-Antona (2010). "Tumoral and tissue-specific expression of the major human beta-tubulin isotypes." Cytoskeleton (Hoboken) **67**(4): 214-223.

Liu, J., M. J. Towle, H. Cheng, P. Saxton, C. Reardon, J. Wu, E. A. Murphy, G. Kuznetsov, C. W. Johannes, M. R. Tremblay, H. Zhao, M. Pesant, F. G. Fang, M. W. Vermeulen, B. M. Gallagher, Jr. and B. A. Littlefield (2007). "In vitro and in vivo anticancer activities of synthetic (-)-laulimalide, a marine natural product microtubule stabilizing agent." Anticancer Res **27**(3B): 1509-1518.

Marty, M., P. Fumoleau, A. Adenis, Y. Rousseau, Y. Merrouche, G. Robinet, I. Senac and C. Puozzo (2001). "Oral vinorelbine pharmacokinetics and absolute bioavailability study in patients with solid tumors." Ann Oncol **12**(11): 1643-1649.

Mooberry, S. L., G. Tien, A. H. Hernandez, A. Plubrukarn and B. S. Davidson (1999). "Laulimalide and isolaulimalide, new paclitaxel-like microtubule-stabilizing agents." Cancer Res **59**(3): 653-660.

Nguyen-Ngoc, T., K. Afshar and P. Gonczy (2007). "Coupling of cortical dynein and G alpha proteins mediates spindle positioning in Caenorhabditis elegans." Nat Cell Biol **9**(11): 1294-1302.

Noble, R. L., C. T. Beer and J. H. Cutts (1958). "Role of chance observations in chemotherapy: Vinca rosea." Ann N Y Acad Sci **76**(3): 882-894.

Nogales, E., S. G. Wolf, I. A. Khan, R. F. Luduena and K. H. Downing (1995). "Structure of tubulin at 6.5 A and location of the taxol-binding site." Nature **375**(6530): 424-427.

Nogales, E., M. Whittaker, R. A. Milligan and K. H. Downing (1999). "High-resolution model of the microtubule." Cell **96**(1): 79-88.

Olson, S. K., G. Greenan, A. Desai, T. Muller-Reichert and K. Oegema (2012). "Hierarchical assembly of the eggshell and permeability barrier in C. elegans." J Cell Biol **198**(4): 731-748.

Owellen, R. J., C. A. Hartke, R. M. Dickerson and F. O. Hains (1976). "Inhibition of tubulin-microtubule polymerization by drugs of the Vinca alkaloid class." Cancer Res **36**(4): 1499-1502.

Poi, M. J., M. Berger, M. Lustberg, R. Layman, C. L. Shapiro, B. Ramaswamy, E. Mrozek, E. Olson and R. Wesolowski (2013). "Docetaxel-induced skin toxicities in breast cancer patients subsequent to paclitaxel shortage: a case series and literature review." Support Care Cancer **21**(10): 2679-2686.

Pryor, D. E., A. O'Brate, G. Bilcer, J. F. Diaz, Y. Wang, Y. Wang, M. Kabaki, M. K. Jung, J. M. Andreu, A. K. Ghosh, P. Giannakakou and E. Hamel (2002). "The microtubule stabilizing agent laulimalide does not bind in the taxoid site, kills cells resistant to paclitaxel and epothilones, and may not require its epoxide moiety for activity." Biochemistry **41**(29): 9109-9115.

Roberts, W. N., M. H. Liang and S. H. Stern (1987). "Colchicine in acute gout. Reassessment of risks and benefits." JAMA **257**(14): 1920-1922.
Rowinsky, E. K. and R. C. Donehower (1995). "Paclitaxel (taxol)." N Engl J Med **332**(15): 1004-1014.

Schierenberg, E. and W. B. Wood (1985). "Control of cell-cycle timing in early embryos of Caenorhabditis elegans." Dev Biol **107**(2): 337-354.

Schiff, P. B., J. Fant and S. B. Horwitz (1979). "Promotion of microtubule assembly in vitro by taxol." Nature **277**(5698): 665-667.

Smoter, M., L. Bodnar, R. Duchnowska, R. Stec, B. Grala and C. Szczylik (2011). "The role of Tau protein in resistance to paclitaxel." Cancer Chemother Pharmacol **68**(3): 553-557.

Tanaka, S., T. Nohara, M. Iwamoto, K. Sumiyoshi, K. Kimura, Y. Takahashi and N. Tanigawa (2009). "Tau expression and efficacy of paclitaxel treatment in metastatic breast cancer." Cancer Chemother Pharmacol **64**(2): 341-346.

Torres, K. and S. B. Horwitz (1998). "Mechanisms of Taxol-induced cell death are concentration dependent." Cancer Res **58**(16): 3620-3626.

Tozer, G. M., C. Kanthou, C. S. Parkins and S. A. Hill (2002). "The biology of the combretastatins as tumour vascular targeting agents." International Journal of Experimental Pathology **83**(1): 21-38.

van Vuuren, R. J., M. H. Visagie, A. E. Theron and A. M. Joubert (2015). "Antimitotic drugs in the treatment of cancer." Cancer Chemother Pharmacol **76**(6): 1101-1112.

Verdier-Pinard, P., S. Shahabi, F. Wang, B. Burd, H. Xiao, G. L. Goldberg, G. A. Orr and S. B. Horwitz (2005). "Detection of human betaV-tubulin expression in epithelial cancer cell lines by tubulin proteomics." Biochemistry **44**(48): 15858-15870.

Wani, M. C., H. L. Taylor, M. E. Wall, P. Coggon and A. T. McPhail (1971). "Plant antitumor agents. VI. Isolation and structure of taxol, a novel antileukemic and antitumor agent from Taxus brevifolia." Journal of the American Chemical Society **93**(9): 2325-2327.

Wendell, K. L., L. Wilson and M. A. Jordan (1993). "Mitotic block in HeLa cells by vinblastine: ultrastructural changes in kinetochore-microtubule attachment and in centrosomes." J Cell Sci **104 (Pt 2)**: 261-274.

Wilson, L., M. A. Jordan, A. Morse and R. L. Margolis (1982). "Interaction of vinblastine with steady-state microtubules in vitro." J Mol Biol **159**(1): 125-149.

Yvon, A. M., P. Wadsworth and M. A. Jordan (1999). "Taxol suppresses dynamics of individual microtubules in living human tumor cells." Mol Biol Cell **10**(4): 947-959.

3. CYK-1 maintains cortical rigidity and attenuates anaphase spindle forces in the *C. elegans* embryo

3.1 Introduction- CYK-1 and its function in *C. elegans*

In *C. elegans*, CYK-1 (cytokinesis defective) was originally characterized as a protein required for a late step in cytokinesis. In CYK-1 mutant embryos cytokinesis initiates normally; the cleavage furrow starts to ingress, but later regresses (Swan, Severson et al. 1998). In the original characterization of *cyk-1*, the authors also showed that CYK-1 co-localized with actin at the cytokinesis ring. Based on the results obtained by Swan *et al*, (1998) the authors hypothesized a model for CYK-1 function. Their model proposes that CYK-1 is involved in a late step during cytokinesis (Swan, Severson et al. 1998).

In contrast to the early characterization of CYK-1, more recent work sheds light on the function of CYK-1 early in cytokinesis (Davies, Jordan et al. 2014). This study performed a high-resolution temporal analysis of the function of CYK-1 during cytokinesis. A temperature-sensitive mutation in the FH2 domain of CYK-1 causes full loss-of-function phenotypes with no furrow ingression and a failure of cytokinesis. In this study, the temperature-sensitive mutant embryos were upshifted to high temperature at different time-points during cytokinesis. When the embryos were upshifted before initiation of constriction, there was no furrow formation at all and cytokinesis completely failed in these embryos. Embryos that were upshifted just after furrow formation, showed failed cytokinesis but the constriction of the actomyosin ring continued in these embryos. Embryos that were upshifted midway or late during furrow formation maintained ring closure and completed cytokinesis. This study indicated that CYK-1-mediated actin assembly is important in early cytokinesis but becomes dispensable midway during furrow formation (Davies, Jordan et al. 2014).

In addition to CYK-1 being involved in cytokinesis, research groups studying sarcomere formation have shown that CYK-1 is a component of the sarcomere and is

present in the worm body wall muscle (Mi-Mi, Votra et al. 2012). CYK-1 and another formin protein, FHOD-1, are present either on the Z-lines or near the Z-lines in sarcomeres. During larval growth, reduction of CYK-1 function resulted in stunted growth of the striated contractile lattice of the sarcomere. It also reduced the number of striations and number of sarcomeres in the muscle cell (Mi-Mi, Votra et al. 2012, Mi-Mi and Pruyne 2015).

3.1.1 CYK-1 is a formin protein

CYK-1 belongs to the formin family of proteins. Formins are actin polymerization proteins, which play an instrumental role in various cytoskeleton-based cellular processes, like cell division, cellular motility, muscle development and tissue morphogenesis (Kovar 2006, Chesarone, DuPage et al. 2010, Liu, Linardopoulou et al. 2010). The term 'formin' was introduced in 1990 to describe a limb deformity gene, which was suggested to have an important role in the formation of several organs in mouse (Mass, Zeller *et al*. 1990, Woychik, Maas *et al*. 1990). Four years later, the *Drosophila* formin homologue, *diaphanous,* was discovered (Castrillon and Wasserman 1994). The role of formins in cytokinesis was first discovered because *Drosophila dia* mutants failed in cytokinesis during spermatogenesis, rendering male flies sterile (Castrillon and Wasserman 1994). Cytokinesis failure was also reported in follicle cells, which surround the developing egg chamber during oogenesis. In addition, homozygous null mutants of *dia* showed pupal lethality and a failure in embryonic cell cytokinesis (Castrillon and Wasserman 1994). During *Drosophila* oogenesis, diaphanous is required for membrane invagination and cellularization and for the formation of pole cells (Afshar, Stuart et al. 2000). In addition, *diaphanous* also plays an important role in stabilizing adherens junctions by regulating both actin and myosin activity during gastrulation in the embryo (Homem and Peifer 2008).

3.1.2 Structure and function of formin proteins

3.1.2.1 Structure of formin proteins

A defining feature of all formin proteins is the presence of a domain that is ~ 400 amino acids in length, termed the FH2 (Formin homology 2) domain. FH2 domains mediate actin assembly by binding actin and stabilizing actin dimers and trimers. Many formin proteins contain two formin domains (FH1 and FH2). The FH1 domain is of variable length in different formin proteins. FH1 interacts with another actin-binding protein, profilin, and directs the actin-profilin complex to the plus end of the actin filament for elongation (Goode and Eck 2007). Thus the FH1 domain sequesters monomeric actin bound to the profilin protein and enhances actin filament assembly (Higgs 2005, Goode and Eck 2007).

In vivo, formins are auto-inhibited by intramolecular binding of the N and C termini. The N-terminus contains the DID (diaphanous inhibitory domain) and C-terminus contains DAD (diaphanous autoregulatory domain)(Chesarone, DuPage et al. 2010). This autoinhibition is released by the binding of active RhoA to a GTP binding domain (GBD) in the formin protein. Formins dimerize through the dimerization domain (DD) (Chesarone, DuPage et al. 2010). Although the overall structure can exhibit variability, the typical domain structure of formin proteins is shown in figure 3.1.1.

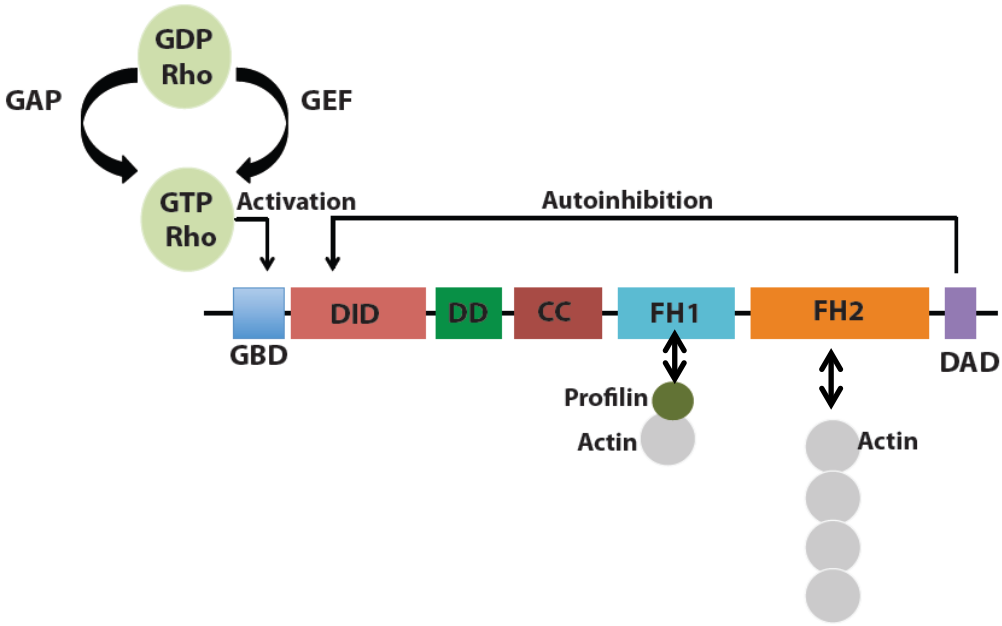

Figure 3.1.1 Domain structure of diaphanous-related formins. The domain structure of diaphanous related formins and the ligands that they bind to are shown. FH1 and FH2 domains are the characteristics of formin proteins. Both domain assist in actin polymerization. GBD is the GTPase binding domain. DID and DAD bind to each other and help I autoinhibition of formin proteins. DD is the dimerization domain- once formins are active they exist as a dimer. The CC is the coiled-coil domain of formin.

3.1.2.2 Formin proteins promote functional interactions between actin and microtubules

In addition to the established role of formin in nucleating and elongating actin filaments (Otomo, Tomchick et al. 2005), these proteins have also been implicated in regulating microtubules. Some formin proteins have been implicated in interacting with actin and microtubule structures simultaneously, thereby regulating cellular processes that require close collaboration of the two-cytoskeleton networks. Cappuccino (Capu) is a diaphanous-related formin in *Drosophila* which has been implicated in mediating the interactions between actin and microtubules during oogenesis (Rosales-Nieves, Johndrow et al. 2006). *In vitro* and *in vivo* data from this study has shown that Capu has microtubule and actin crosslinking activity. Loss-of-function mutations in Capu cause premature streaming of the cytoplasm during oogenesis, which disrupts the anterior-posterior and dorsal-ventral body axes in flies (Rosales-Nieves, Johndrow et al. 2006). Another example illustrating the importance of formin cross-linking actin and microtubules comes from fission yeast. Cdc12p formin is required for actin-myosin assembly and is also transported across microtubules during cell division (Lee, Klee et al. 1999). Cdc12p locates to the cell cortex, where, in combination with other actin nucleation proteins, it helps actin assemble at the cortex. Immunofluorescence experiments from this study indicated that, before localizing to the cortex, Cdc12p is transported on microtubules and actin tracks (Lee, Klee et al. 1999). These results suggest that the localization of Cdc12p to the cortex might require its interaction with both microtubule and actin cytoskeletons. In migrating breast cancer cell lines mDia1 works downstream of a receptor tyrosine kinase, ErbB2. mDia1 in these cells helps in the capture of microtubules at the cortex (Zaoui, Benseddik et al. 2010). A recent study has shown that mDia1-mediated actin

assembly and microtubule capture at the cortex are mediated by overlapping surfaces of the FH2 domain (Daou, Hasan et al. 2014).

Some mouse formin proteins show interesting differences in their ability to regulate microtubule and microfilament dynamics. An *in vitro* study using mouse formin proteins mDia1, mDia2 and INF2 show that they interact with both microtubules and microfilaments (Gaillard, Ramabhadran et al. 2011). The presence of microtubules partially inhibits actin nucleation by mDia1 and mDia2. mDia2 also brings about actin bundling and this activity is separate from its role in actin nucleation. There is no effect on actin bundling by mDia2 in the presence of microtubules. On the other hand, INF2 formin affects cytoskeletal dynamics differently. INF2 can bind microtubules and microfilaments simultaneously, and microtubules do not affect actin polymerization or depolymerization. Interestingly, the presence of actin monomers inhibits microtubule binding and bundling by INF2 (Gaillard, Ramabhadran et al. 2011). Thus, the mouse formin proteins provide some intriguing information on regulating cytoskeletal dynamics.

3.1.2.3 Formin proteins are implicated in diseases

Formins are important for cellular processes such as cell migration, cell division, intracellular transport and formation of adherens junction. These processes are often deregulated in pathological conditions. A study of colorectal cancer cells from patients showed that the expression of Formin like-2 (FMNL2) protein was higher compared to normal colorectal mucosa. Also, overexpression of FMNL2 in this study was associated with elevated lymphatic metastasis (Zhu, Liang et al. 2008). In another study involving murine prostate cancer cells, the mouse formin proteins mDia1 and mDia2 were implicated in microvesicle formation and thereby function in tumor growth and metastasis (Di Vizio, Kim et al. 2009). In the above-mentioned studies, the phenotypes were associated with an overexpression of formins, however, knock-down of formins has also been associated with some diseases. For example in myelodysplastic syndrome (MDS), a hematopoietic stem cell disease, expression of

mDia1 in mice was reduced. Loss of mDia1 and Rho in mice enhances the myeloproliferative disorder (DeWard, Leali et al. 2009).

The role of the formin protein FHOD-1 (formin homology domain-1) has been studied in bacterial invasion. A study done in HeLa cells shows that FHOD-1 plays an important role in invasion of *S. typhimurium (*Truong, Brabant et al. 2013). *S. typhimurium* invades the host cell by injecting virulence proteins, which induce formation of membrane ruffles in the host cell. These membrane ruffles are protrusions that extend from the host plasma membrane and are rich in actin. Formation of these membrane ruffles is important for invasion of the bacteria. In this study, it was shown that FHOD-1 is activated and localized at actin-rich invasion sites in the host cells (Truong, Brabant et al. 2013). The reorganization of actin at the host plasma membrane is essential for infection. This study shows that the formin protein FHOD-1 is phosphorylated by ROCK II (an isoform of Rho-associated protein kinase) of the host cell and this modification is critical for bacterial uptake by the host cell. As shown in figure 3.1.2, FHOD-1 knockdown restricts the formation of membrane ruffles and results in protrusions that are smaller in volume and less stable. This results in a decreased probability of *S. typhimurium* infection (Truong, Brabant et al. 2013).

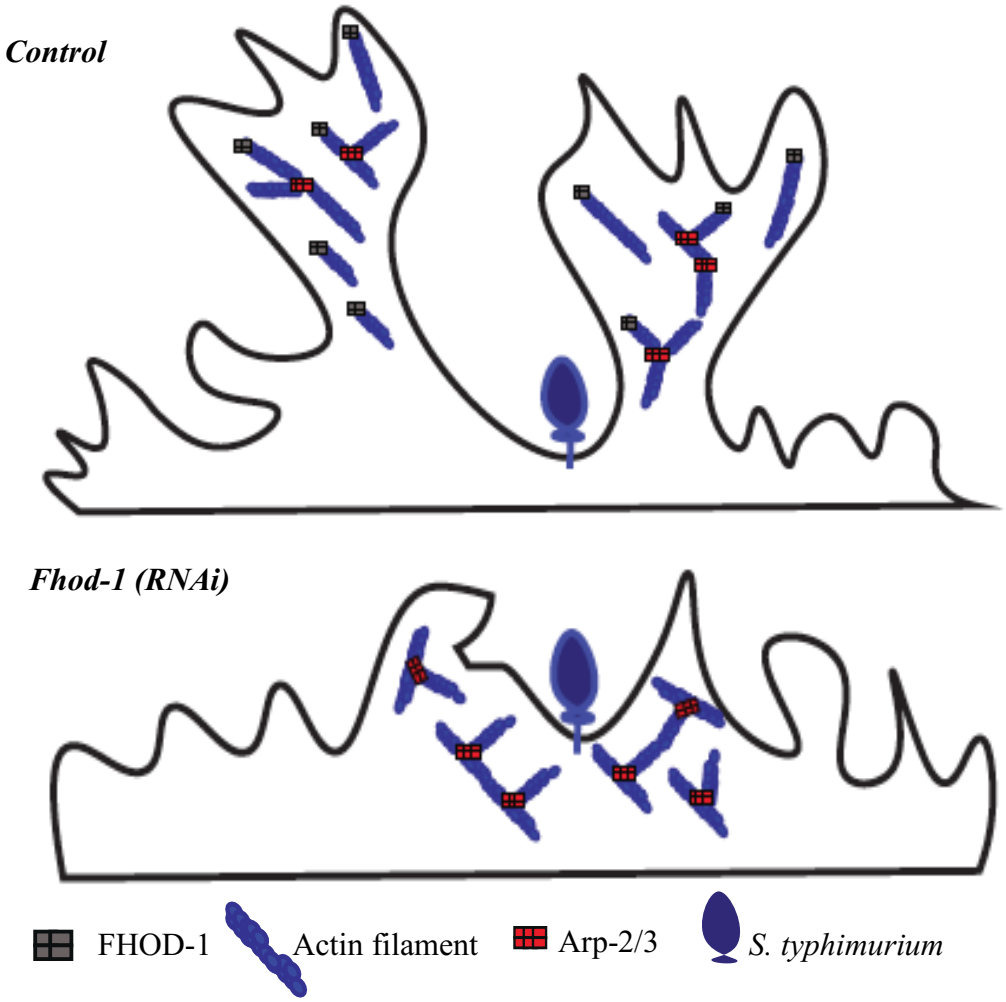

Figure 3.1.2 FHOD-1 contributes to *S. typhimurium* infection site.
S. typhimurium infection filopodia-like infection ruffles are shown. FHOD-1 and actin localize throughout the infection ruffle. Knockdown of FHOD-1 results into smaller invasion ruffles compared to the control. Adapted from (Truong, Copeland et al. 2014)

In *C. elegans* the FHOD-1 protein is expressed in lateral epidermal cells, which undergo cell-shape changes during development to facilitate embryonic elongation of the worm. Loss of FHOD-1 protein results in actin polymerization defects in lateral epidermal cells and limited elongation during development (Vanneste, Pruyne et al. 2013). In humans, an insertion mutation in the formin gene *diaph1* generates a stop codon and results in the production of a truncated DIAPH1 protein (Lynch, Lee et al. 1997). This mutation causes autosomal dominant sensorineural hearing loss. The DIAPH1 protein has been implicated in the proper functioning of the stereocilia of the mechanosensing organ of the inner ear. Actin filaments provide structural support and rigidity to the stereocilia, which are responsible for sound reception. Thus, DIAPH1 loss results into disruption of the structure of hair cells and of actin polymerization, which ultimately results in hearing loss (Lynch, Lee et al. 1997).

3.1.3 Current model of CYK-1 function in the *C. elegans* embryo

3.1.3.1 CYK-1 in *C. elegans* embryo cytokinesis

Reports from early characterization of CYK-1 have shown its role late in cytokinesis. Figure 3.1.3 (a) shows the model for CYK-1 function in the *C. elegans* embryo. During late cytokinesis, the actomyosin ring and the microtubules from the spindle mid-zone come into close proximity to one another. CYK-1 is possibly involved in bridging microtubules from the spindle mid-zone and microfilaments from the plasma membrane during cytokinesis (Swan, Severson et al. 1998). This bridging role of CYK-1 could be responsible for stabilization of the cytokinesis cleavage furrow by binding to microtubules at one end and actin in the plasma membrane on the other end. The defects observed in *cyk-1(RNAi)* embryos could be a result of disruption of a bridge between actin and microtubules at the leading edge of the furrow during late cytokinesis (Swan, Severson et al. 1998).

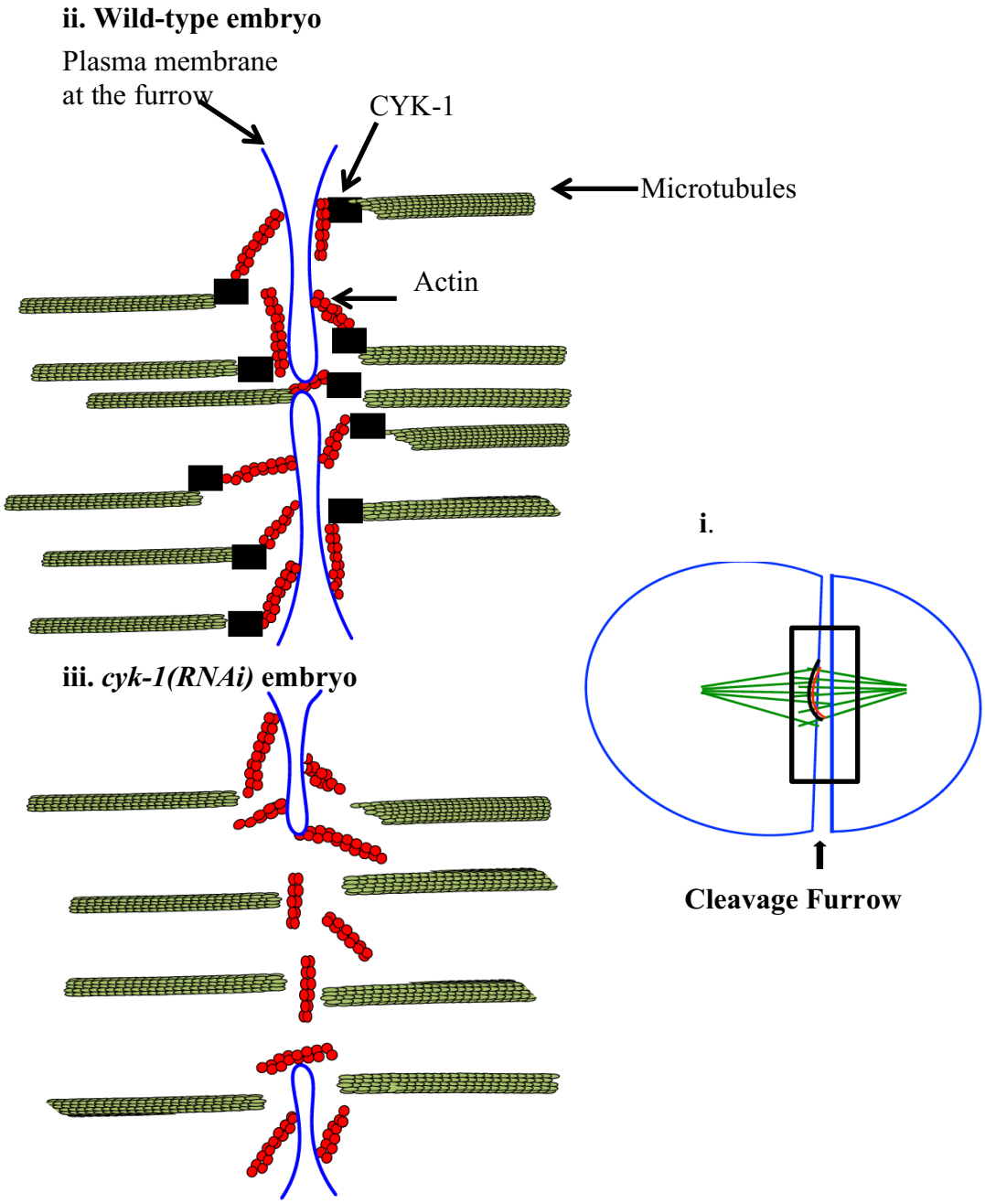

Figure 3.1.3 (a) A model for CYK-1 function in cytokinesis. i) CYK-1 is shown in black, actin is shown in red and microtubules are shown in green here. The inset is enlarged in ii and iii. ii) In wild type embryos CYK-1, the formin protein that is involved in actin polymerization, possibly bridges actin from the plasma membrane to microtubules at the cytokinesis furrow. iii) In *cyk-1(RNAi)* embryos, the cytokinesis furrow regresses possibly due to depletion of CYK-1 and no bridging between microtubules and actin.

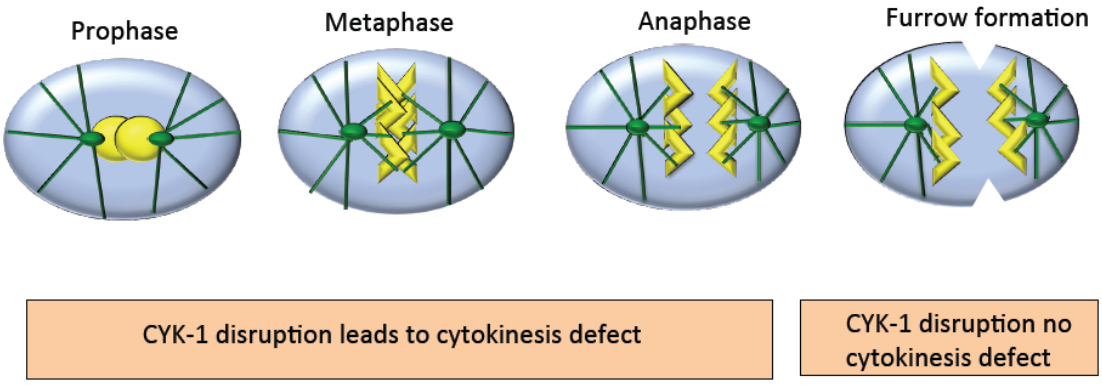

Figure 3.1.3 (b) A model for CYK-1 function in cytokinesis. Depletion of CYK-1 before initiation of furrow formation completely blocks cytokinesis. However, when CYK-1 was depleted at a later stage after furrow initiation, no cytokinesis defects were observed. Adapted from (Davies, Jordan et al. 2014)

As discussed before, more recent work indicated that the *C. elegans* formin protein CYK-1 is required for an early step in cytokinesis (Davies, Jordan et al. 2014). In contrast to the early study, this study indicates the role of CYK-1 protein in actin assembly and cytokinesis in early stages like metaphase and anaphase. Once cytokinesis furrow formation initiates, the role of CYK-1 in cytokinesis becomes dispensable. This is shown in figure 3.1.3 (b).

3.1.3.2 EVA assay and the role of CYK-1 in *C. elegans* embryo

Another potential role for CYK-1 came unexpectedly through a previous assay developed in the Srayko lab. This experiment was designed to uncover modulators of microtubule-based pulling forces in the early embryo. Specifically, an assay was developed to detect changes in dynein motor activity at the cell cortex. This assay determines if the dynein motors are differentially activated at the anterior and posterior cortex in the embryo(Gusnowski 2010). The assay is called EBP-2 (end-binding protein-2) velocity assay (EVA). EBP-2 binds specifically to the growing ends of microtubules (Srayko, Kaya et al. 2005). This assay measures the lateral contribution of dynein protein on EBP-2 velocities (which is a read-out of microtubule velocity) (figure 3.1.4). Various factors and their effect on the activity of dynein along the microtubule lattice were checked to test whether they could modulate the velocities of the EBP-2 particles. Thus, a methodical analysis of genes required for cortical force generation was performed with the EVA assay. Elimination of CYK-1 by RNAi increased the dynein-dependent microtubule velocities at the inner cortex. At this point we did not understand why *cyk-1(RNAi)* had this effect on dynein dependent microtubule velocities at the cortex. However, it suggested that CYK-1 played a role at the cortex for something other than cytokinesis. CYK-1 possibly modulates microtubule-based pulling forces. However, from the EVA assay it was not clear if CYK-1 really had an impact on cortical pulling forces and how did it regulate such forces in the embryo.

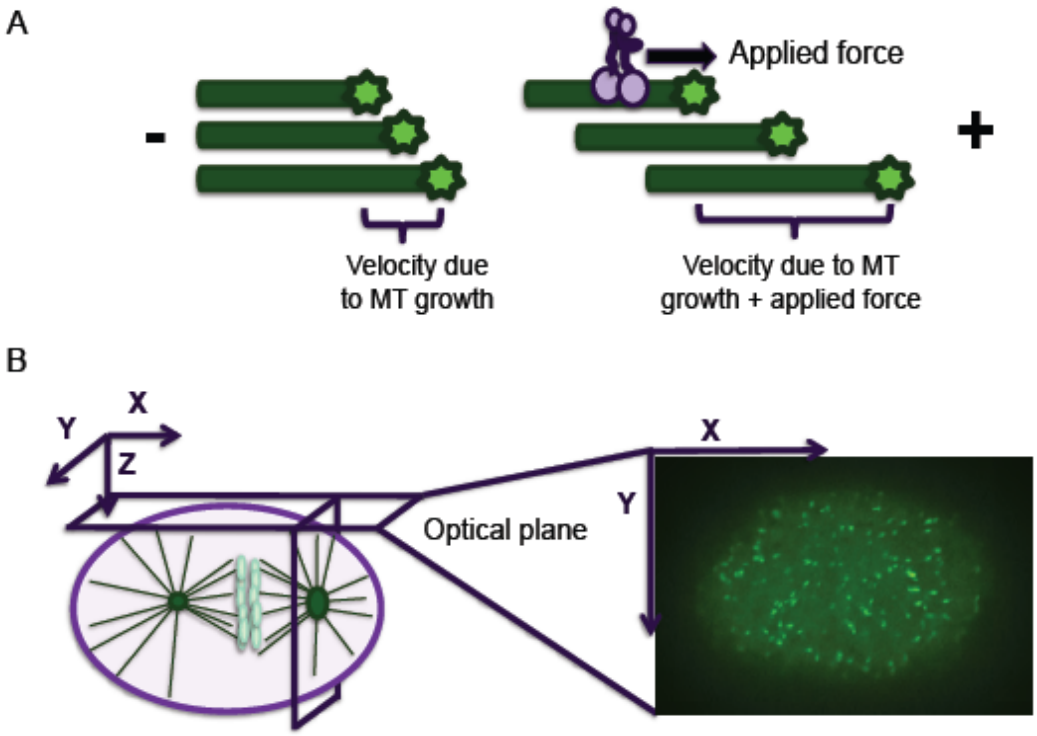

Figure 3.1.4 EVA assay. A) EBP-2 velocity is due to microtubule growth or microtubule growth plus applies force. B) EBP-2::GFP velocity is taken at the inner embryonic cortical plane. This figure is taken from Gusnowski E.M. 2010 thesis.

3.1.4 The goals of this chapter

The primary goal of this chapter is to elucidate the role of CYK-1 in mitosis in the *C. elegans* embryo. As discussed before, the role of CYK-1 in cytokinesis is well established. Previous inspection of *cyk-1(RNAi)* in the Srayko lab has revealed that depletion of CYK-1 increases the proportion of dynein-dependent microtubule velocities at the embryo cortex (Gusnowski 2010). This suggests that CYK-1 might have a role in modulating spindle-based pulling forces in the embryo cortex. The goal of this chapter is to elucidate the role of CYK-1 in regulating spindle-pulling forces during anaphase. Different assays were used to measure the rigidity of the cortex upon CYK-1 depletion. Based on the results obtained from this chapter a model has been put forth to explain the role of CYK-1 and its relation to dynein motor protein in modulating spindle-based pulling forces.

3.2 Materials and Methods

3.2.1 *C. elegans* strain designation and maintenance

Table 3.2.1 *C. elegans* strain designations and genotypes used in this study.

Strain	Genotype
MAS91	*unc-119(ed3) III; itIs37[unc119(+); pie-1p::mCherry::his-58]IV; ruIs57[unc119(+),pie-1p::GFP::tbb-2]*
EU144	*unc-119(ed3) III; orIs17 [dhc-1p::GFP::dhc-1; unc-119(+)]*
JJ1473	*unc-119(ed3) III; zuIs45 [nmy-2::NMY-2::GFP; unc-119(+)] V*
OD58	*unc-119(ed3) III; ltIs38 [(pAA1) pie-1::GFP::PH(PLC1delta1); unc-119(+)]*
PF100	*unc-119(ed3) III; nnIs1[unc-119(+) + Ppie-1::GFP::moesin]*

Unless otherwise stated, all *C. elegans* strains were maintained at 25 °C on nematode growth medium (NGM) plates that were seeded with an auxotrophic *Escherichia coli* strain referred to as OP50. Worm strains were generated in the Srayko lab or obtained from the *Caenorhabditis* Genetics Centre. The PF100 strain was a gift from Fabio Piano, New York University.

3.2.2 RNA interference by feeding

The *E. coli* strain HT115 (D3) and the L4440 vector (Addgene) were used for all RNAi feeding experiments (Kamath and Ahringer 2003). The HT115 (D3) strain expresses T7 RNA polymerase under the control of the IPTG-inducible promoter. The RNAi L4440 vector contains T7 polymerase promoters that flank the multiple cloning site. The *E. coli* HT115 (D3) strain synthesizes dsRNA from any DNA that is inserted into this site. When *C. elegans* eat these bacteria, which contain the dsRNA, it induces the *C. elegans* endogenous RNAi machinery. This specifically knocks down complementary transcripts in the worm, however, different genes exhibit different efficiencies of knock-down. Therefore, effective RNAi knockdown was confirmed using microscopy to verify the appropriate loss-of-function phenotype.

RNAi feeding plates (NGM agar, 0.001 M IPTG, 25 mg/mL carbenicillin) were prepared no longer than one week before use and were stored at 4 °C until seeding. The RNAi bacterial clones with the appropriate gene cloned into the L4440 vector were obtained from the RNAi feeding library (Kamath and Ahringer 2003). *E. coli* that contained the desired RNAi vector, were grown in 5 mL LB broth (Luria Bertani; 1.0 mg/mL Bacto-Tryptone, 0.5 mg/mL yeast extract, 0.5 mg/mL NaCl) with 50 mg/mL ampicillin for 10-18 hours at 37 °C. The next day, RNAi plates were seeded with the bacterial culture and left at room temperature for 7-8 hours to dry and express the double-stranded RNA. 20-30 L4 hermaphrodites were then placed on the RNAi seeded plates and incubated for 15-48 hours (the duration varied, depending on the gene) at 25°C. The L4440 vector without an insert was used as a negative control in all RNAi feeding experiments.

3.2.3 RNA interference by dsRNA injections

Some *C. elegans* genes are not effectively knocked down by the RNA-feeding technique. For example, feeding with a *rho-1* clone did not produce the expected phenotypes in one-cell embryos. Thus, RNAi against *rho-1* was performed by injecting dsRNA into the syncytial gonad of L4 hermaphrodite worms. The *rho-1* DNA template was amplified by PCR, gel extracted (QIAquick gel extraction kit-Qiagen) and precipitated with ethanol. RNA was *in vitro* transcribed by using the MEGAscript transcription system (Ambion) to give complementary ssRNA expressed from T3 and T7 promoters. Each ssRNA sample was DNAse digested by adding 1 Unit of DNAse enzyme and incubating it at 37 °C for 15 minutes. This was followed by RNA purification of the ssRNA using the RNAeasy kit (Qiagen).

To obtain dsRNA, 40 µL of the T3 and T7 -transcribed ssRNAs were mixed in a tube and incubated at 72 °C for 10 minutes. This was followed by incubation at room temperature for 20 minutes to allow annealing of complementary RNA. The T3 and T7 ssRNA after DNAse digestion and the dsRNA (after annealing) and T3 and T7

ssRNA were visualized on a gel as shown in figure 3.1. The dsRNA was injected in worms at 0.5 mg/mL for *rho-1*. Details of primer sequences are listed in table 3.2.2.

Table 3.2.2 *rho-1* primer sequences for generation of DNA template

Gene	Primer sequence
rho-1	T3 forward:5'- AATTAACCCTCACTAAAGGGATCGTCTGCGTCCACTCTCT-3' T7 reverse: 5'-TAATACGACTCACTATAGGGCTCGGCTGAAATTTCCAAAA-3'

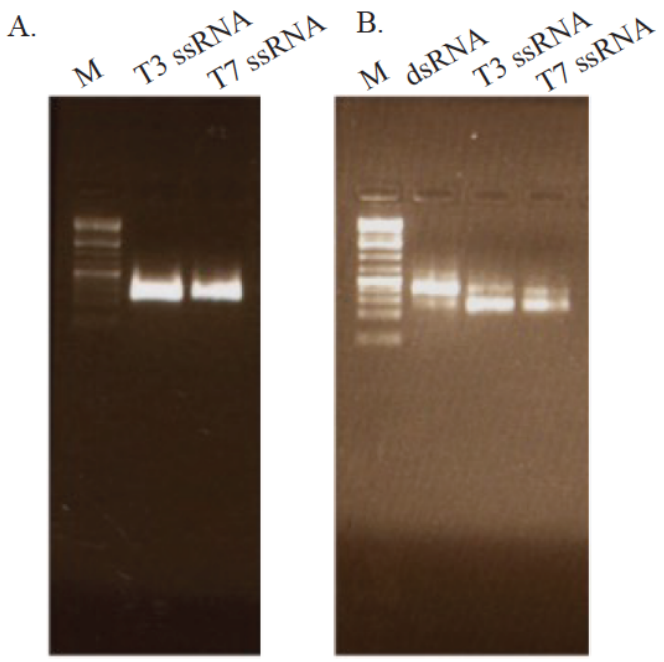

Figure 3.2.1. dsRNA generation for *rho-1* RNAi. A) DNAse digested T3 and T7 ssRNA. B) Annealed dsRNA is shown in second lane and T3 and T7 ssRNA were also run on the gel to compare the size.

3.2.4 Microscopy

Confocal microscopy was performed with an Olympus inverted microscope (IX81) with a 60X oil objective (NA 1.42) with a spinning disc confocal head (CSU10; Yokogawa) modified with a condenser lens in the optical path (Quorum Technologies). All images were acquired with an ORCA-R2 camera (Hamamatsu) controlled by MetaMorph software (Molecular Devices).

3.2.4.1 Measuring centrosome movements using the average peak velocity assay

3.2.4.1.1 Live-cell imaging for average peak velocity assay

Worms were dissected in egg buffer (188 mM NaCl, 48 mM KCl, 2 mM $CaCl_2$ and 25 mM HEPES, pH 7.3) and embryos were mounted using 2% agarose pads. For live-cell imaging of microtubules and chromatin, a strain expressing GFP-Tubulin and mCherry-Histone was used. For GFP-Tubulin, a short Z-stack (3 images at 1 μm spacing) was acquired every 1.5 seconds. For mCherry-Histone, a similar stack was acquired at every 5^{th} time point. A DIC image was acquired every 5 seconds from telophase to cytokinesis to confirm normal cytokinesis in wild type embryos and failure in cytokinesis in some of the RNAi treatments. This was done to ensure that RNAi worked and the embryos showed the expected phenotypes, consistent with previously published results. The exposure time was 150 msec, gain was 250 and 2x2 binning was used.

The imaging environment temperature was controlled by a water circulator (Haake) pumping through a collar on the 60x oil immersion objective (Tegha-Dunghu, Gusnowski et al. 2014). The temperature of the immersion oil on the coverslip was recorded immediately after the final image of each embryo and was maintained between 19.5 °C -20.5 °C. For the Latrunculin A experiment, the worms were dissected in 100 μm Latrunculin A (Sigma). 5% DMSO was used as control in this experiment. For drug-delivery the embryo was visualized using DIC optics and

the eggshell was pierced using a single laser shot at the anterior and a second shot at the posterior side of the embryo. The ablation laser unit was a nitrogen laser-pumped dye laser (from Photonics Instruments, now Andor Technology). The laser dye used in the dye cell was BPBD (2-[1,1'-biphenyl]-4-yl-5-[4-(1,1-dimethylethyl)phenyl]-1,3,4-oxadiazole; Butyl-PB) with a wavelength of 365 nm delivering approximately 120 m Joules of energy in a 2-6 nanosecond pulse length.

3.2.4.1.2 Centrosome tracking for average peak velocity assay

MetaMorph software was used to automatically track the movement of centrosomes. Centrosome tracking was started at the initiation of anaphase. Tracking was continued until the end of anaphase. In this experiment, n ≥ 10 for each control, RNAi or drug treatment and were used for tracking centrosomes and for making the average peak velocity graph. Distance between the two centrosomes in 3D was calculated using the distance formula $\sqrt{(x2-x1)^2}+\sqrt{(y2-y1)^2}+\sqrt{(z2-z1)^2}$; derived from the Pythagorean theorem. Velocity was calculated using the velocity formula: velocity=distance/time.

3.2.5 Average peak amplitude measurement

The displacement of the spindle poles in the transverse plane to Anterior-Posterior axis of the embryo was measured manually using MetaMorph software. Measurements were made at each time-point (every 1.5 second). The peak amplitude from each embryo was converted into % embryo width for each embryo (n ≥ 10 embryos for each RNAi treatment). The peak amplitude from all the embryos was used to plot the average peak amplitude graph.

3.2.6 GFP::NMY-2 live cell imaging and analysis

Worms were dissected in egg buffer and embryos were mounted using 2% agarose pads. DIC images were acquired every 5 seconds during the prophase stage up to nuclear envelope breakdown (NEBD), keeping one or both centrosomes in the focal plane. After NEBD, focus was moved to the cortical plane and DIC and GFP::NMY-2 images were acquired every 3 seconds. After the completion of the

cortical time-lapse imaging, focus was moved back to the centrosomal plane and DIC images were acquired to follow the progression of cytokinesis. The exposure time was 150 ms and gain was 250 ms, with 2x2 binning. Temperature was maintained between 19.5 °C -20.5 °C. n=14 embryos for control and *cyk-1(RNAi)* treatments. Kymographs were assembled from a series of single lines consisting of the maximum pixel intensity over a 10 pixel-wide line drawn along the A-P axis of the embryo.

3.2.7 GFP::Actin live cell imaging and analysis

Worms were dissected in egg buffer and embryos were mounted on 2% agarose pads. A DIC time-lapse was acquired every 5 seconds up to NEBD at the spindle plane. At anaphase initiation (3 minutes after NEBD), focus was moved to the cortical plane and GFP::MOE was acquired every 1 second for ~2 minutes. After the completion of the time-lapse, focus was moved back to the spindle plane to acquire DIC images to visualize cytokinesis. In order to mark the GFP::MOE foci and measure their size, the Metamorph application "Integrated Morphometry Analysis" was used. The MetaMorph application "Granularity" was used to apply an empirical threshold in order to identify GFP-MOE foci.

3.2.8 Membrane Invagination assay

The membrane invagination assay was adapted from (Redemann, Pecreaux et al. 2010). Worms were dissected in egg buffer (188 mM NaCl, 48 mM KCl, 2 mM CaCl2 and 25 mM HEPES, ph 7.3) and embryos were mounted using 2% agarose pads. Z-stacks of DIC and PH::GFP (membrane marker) were acquired every 5 seconds. For GFP stacks, exposure was 150 ms and gain was 250. For DIC, exposure and gain was 250 ms. NEBD was marked as time zero for cell cycle timing. Z-series stacks (3 planes, 1 μm spacing) were acquired every 5 s. Temperature was maintained between 19.5 °C -20.5 °C.

For drug tests, worms were dissected in egg buffer containing either 100 μm Nocodazole or Latrunculin A. 5% DMSO was used as a control for this experiment. Laser ablation was performed once on the anterior and once on the posterior side of

the eggshell for drug delivery. Membrane invaginations were counted manually during the anaphase stage (~3 minutes after NEBD) using MetaMorph software.

3.2.9 Cortical Laser Ablation Assay

The cortical laser ablation assay was based on (Mayer, Depken et al. 2010). GFP::NMY-2 time-lapse was acquired every 1 second with an exposure time of 150 ms and gain 250. Time of ablation was labeled time zero. The laser ablation was performed using a UV laser (micro-point) as described in section 3.5.1. Embryo cortices were targeted during the pronuclear migration stage. Point of ablation is shown in figure 3.2.2.

Only those embryos that survived and divided (for controls) were analyzed. The MetaMorph track object application was used to track the GFP-NMY-2 foci (5 foci each embryo surrounding the point of ablation) and to calculate velocity, 3 seconds before ablation and 7 seconds after ablation. As a negative control, 5 foci away from the point of ablation were also tracked in each embryo, and their velocities calculated. The mean velocity per embryo was averaged and plotted over time.

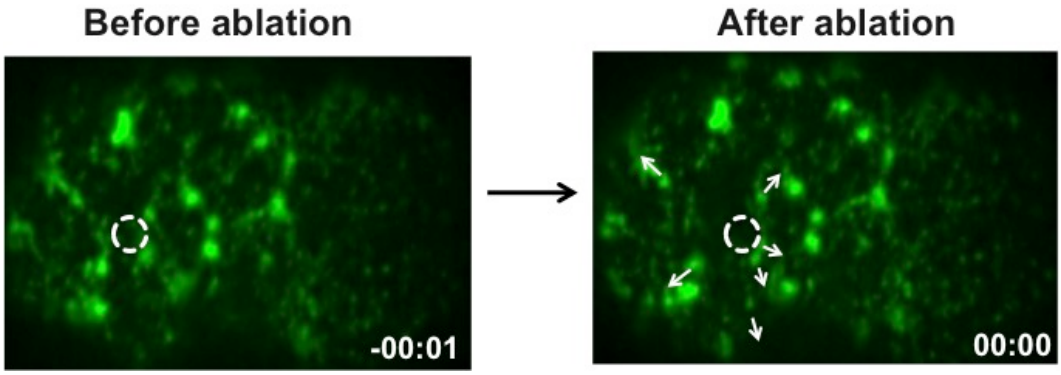

Figure 3.2.2 Cortical Laser Ablation. The point of ablation is shown with white dotted lines. The white arrows point to direction of movement of the GFP::NMY-2 foci after laser ablation.

3.2.10 Cortical GFP::Dynein imaging

3.2.10.1 Cortical dynein foci distribution

3 images of GFP::DHC-1 were acquired every 30 s after anaphase initiation. Nuclear envelope breakdown was used as a reference for cell-cycle timing. A time-lapse DIC movie was acquired before and after capturing the GFP::DHC-1 images. Nuclear envelope breakdown was used as a reference for cell-cycle timing. The spot detector plugin of the ICY image analysis tool (de Chaumont, Dallongeville et al. 2012) was used to count the number of DHC-1 foci in 10 *control (RNAi)* and *cyk-1(RNAi)* embryos . The size filter was used with a range of 0-17 pixels. The number of foci (foci/μm^2) on the embryo cortical surface was plotted in order to compare the distribution of foci in *control (RNAi)* and *cyk-1(RNAi)* embryos.

3.2.10.2 Cortical dynein residency time

A time-lapse DIC movie was acquired before the GFP::DHC-1 stream. Nuclear envelope breakdown was used as a reference for cell-cycle timing. GFP::DHC-1 was acquired every 100 msec for a total of 30 s starting at anaphase initiation. The GFP::DHC-1 stream was started at anaphase initiation (~3 minutes after nuclear envelope breakdown). After completion of the GFP stream, focus was moved back to the spindle plane to acquire DIC to visualize cytokinesis.

3.2.11 Immunoflourescence

For immunostaining, 30-40 gravid N2 worms were placed in 5 μL of egg buffer. A coverslip was placed on these worms and gentle pressure was applied to release the embryos in the solution. The slides were then plunged into liquid nitrogen for 10 minutes, after which each slide was retrieved. The coverslip was flicked off using a razor blade while the slide was still frozen. The slide was then incubated in methanol

in a coplin jar at -20 °C for 15 minutes. After incubation in methanol, slides were washed twice in a coplin jar containing phosphate-buffered saline (PBS). After the washing step, a total volume of 100 μL primary antibody solution (in PBS with 5% goat serum, 0.01% Triton X-100, primary antibody, as per Table 2.3) was pipetted onto the fixed embryos on the slide. Slides were then incubated at room temperature in a humid chamber for 45 minutes (to prevent the slides from drying out), followed by two 10-minute washes in PBS in a coplin jar. After this, secondary antibody solution (in PBS with 5% goat serum, 0.01% Triton X-100, secondary antibody, Table 2.3) was applied to the fixed embryos on the slide and incubated for another 45 minutes in a humid chamber at room temperature. Embryos were then stained with Fluoroshield with DAPI (Sigma) for 5 minutes in order to stain chromatin. A 22 mm x 22 mm coverslip was placed on the mounting media and the edges of the coverslip were sealed with nail polish. The slides were either used for imaging immediately or stored at 4°C until further use.

Table 3.2.3 List of primary antibodies used in the immunostaining experiment

Antibody name and target	Source	Concentration (mg/mL)	Dilution used	Details
DM1A (primary α–tubulin)	Mouse	1	1:100	Sigma
Anti-CYK-1	Rabbit	-	1:100	Swan *et al*, 1998

3.3 Results

CYK-1 is required for completion of a late step in cytokinesis in the *C. elegans* embryo. *cyk-1* encodes a protein homologous to the *Drosophila* Diaphonous (DIA) protein and belongs to the formin family of proteins. Previous inspection of *cyk-1(RNAi)* in our lab revealed that depletion of CYK-1 increased the proportion of dynein-dependent microtubule velocities at the embryo cortex (Gusnowski 2010). This suggested that CYK-1 might have a role in modulating spindle-based pulling forces in the embryo cortex. Therefore, in order to determine the role of CYK-1 in force generation, CYK-1 was depleted using feeding RNAi method followed by analysis of the knockdown phenotypes.

3.3.1 CYK-1 depletion increases transverse spindle pole amplitude and average spindle pole peak velocities

During anaphase, the spindle poles oscillate in a plane transverse to the anterior-posterior embryo axis. This movement occurs as the poles separate, which facilitates the segregation of chromosomes. The oscillations are maintained throughout anaphase, and arise as a product of the cortical microtubule-based pulling forces exerted on the spindle (Cowan and Hyman 2004). A computer model in *C. elegans* explains the mechanism of these oscillations. For example computer simulations have shown that increasing the attachment rate of force generators at the cortex and decreasing the rigidity of the cortex increased the oscillation speed (Kozlowski, Srayko et al. 2007). An *in vivo* study has shown that a threshold of force generator activity is required for the spindle to oscillate (Pecreaux, Roper et al. 2006). Using a time-course RNAi approach, which produces a series of phenotypes that correlate in severity with the amount of time that the worms spend on RNAi feeding plates, it was shown that oscillations were very sensitive to reduction of G-protein regulators, GPR-1/2 and the motor protein dynein. Interestingly, anaphase chromosome movement was not as sensitive to the reduction in cortical forces, which was also predicted by computer simulations. This supports the idea that a threshold of motor activity is required for the spindles to oscillate and maintain the oscillations during anaphase. Furthermore, the oscillations serve as a sensitive read-out for subtle changes to

cortical pulling forces in the one-cell embryo. As visualized by spinning disc confocal microscopy, RNAi depletion of *cyk-1* increased the posterior spindle pole oscillations. In order to quantify the phenotype, transverse amplitude of the anterior and posterior spindle poles was measured. As shown in figure 3.3.1-a, the posterior spindle pole oscillation amplitude is higher than the control embryos.

In order to measure relative microtubule-based pulling force in the embryo, the spindle pole trajectories were tracked and average peak velocities for each spindle pole were measured during the anaphase-rocking stage.

Velocity measurements indicated that the average peak velocity in *control(RNAi)* was 0.96 μm/s (anterior pole) and 1.27 μm/s (posterior pole), in *cyk-1(RNAi)* embryos, average peak velocity was 1.55 μm/s (anterior pole) and 1.85 μm/s (posterior pole). The average peak velocity in *cyk-1(RNAi)* embryos was significantly higher (p value < 0.001) than control embryos (Figure 3.3.1-b).

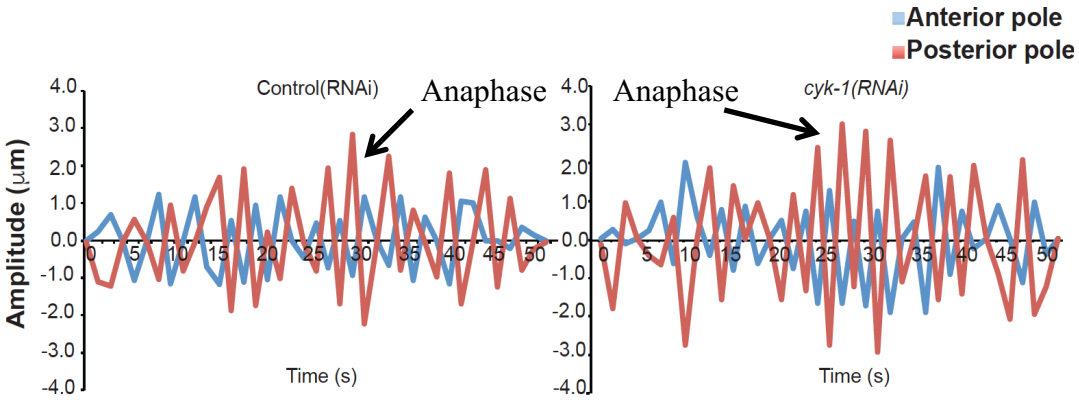

Figure 3.3.1-a Transverse amplitude in control and *cyk-1(RNAi)*. The transverse spindle amplitude is from one representative control and *cyk-1 (RNAi)* embryo is shown here. Posterior spindle amplitude is shown in red and anterior spindle amplitude is shown in blue.

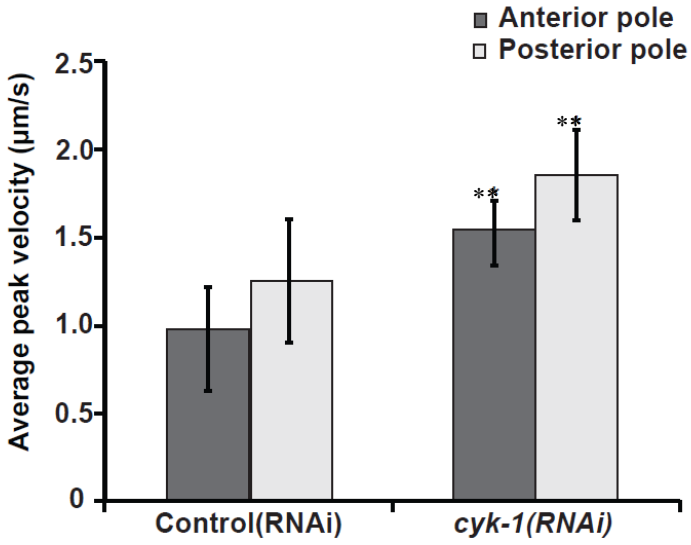

Figure 3.3.1-b Average peak spindle pole velocities of control and *cyk-1 (RNAi)* embryo. n=15 embryos for each sample set. Anterior spindle pole velocity is shown in grey and posterior spindle pole velocity is shown in white. Asterisk indicates p value <0.001. Error bars indicate standard deviation.

3.3.2 Effect of depleting known effectors of cytokinesis on spindle pole motion

cyk-1 (RNAi) increases spindle pole velocities as shown in Figure 3.3.1-b. However, because *cyk-1* is required for cytokinesis, it is possible that the effect of *cyk-1(RNAi)* on spindle pole motion could be an indirect consequence of an aberrant cytokinesis. If so, loss of function of other genes required for cytokinesis might be expected to change the spindle pole motion, similarly to *cyk-1(RNAi)*. Furthermore, the effect of perturbing other genes required for cytokinesis on cortical force generation has never been studied. Therefore, candidate genes (listed in table 3.3.1) that are involved in cytokinesis were depleted by either RNAi feeding or dsRNA injection methods. This was followed by measurements of amplitude in the transverse plane and analysis of average spindle pole peak velocities.

The microtubule and actin cytoskeleton components that contribute to cytokinesis in the *C. elegans* embryo were originally broadly divided into 3 classes. Class 1 includes proteins involved in the initiation of cytokinesis and contractile events (like CYK-1). The class 2 proteins are required for central spindle formation and completion of cytokinesis and class 3 proteins are the components of the chromosomal passenger complex, which are also required for central spindle formation (www.wormbook.org) (Glotzer 2005).

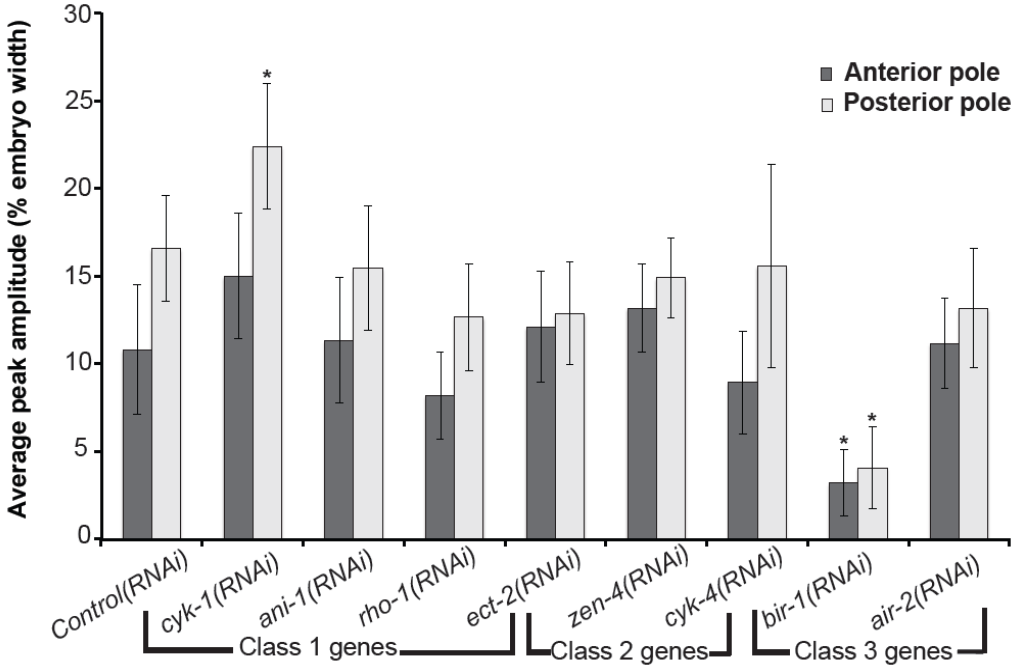

Figure 3.3.2 Average peak amplitude data. Average peak amplitude was measured in terms of percentage embryo width. n≥ 10 embryos for each RNAi treatment. Asterisk indicates p value < 0.01. Error bars indicate standard deviation.

The transverse amplitude was measured for each RNAi treatment and is expressed as a percentage of embryo width in figure 3.3.2. Only the posterior spindle pole in *cyk-1(RNAi)* treatment showed a statistically significant increase in average peak amplitude (23% embryo width) compared to the *control(RNAi)* treatment. The *bir-1(RNAi)* treatment showed a significant decrease (3% embryo width for anterior spindle pole and 4% embryo width for posterior spindle pole) in average peak amplitude as compared to the control.

The average peak velocity of the two spindle poles was also measured in the RNAi-treated embryos. A statistically significant increase in average peak velocity was observed only in *cyk-1(RNAi)*, *ani-1(RNAi)* and *rho-1(RNAi)* one-cell embryos, suggesting that these class 1 proteins have a similar effect on anaphase pulling forces.

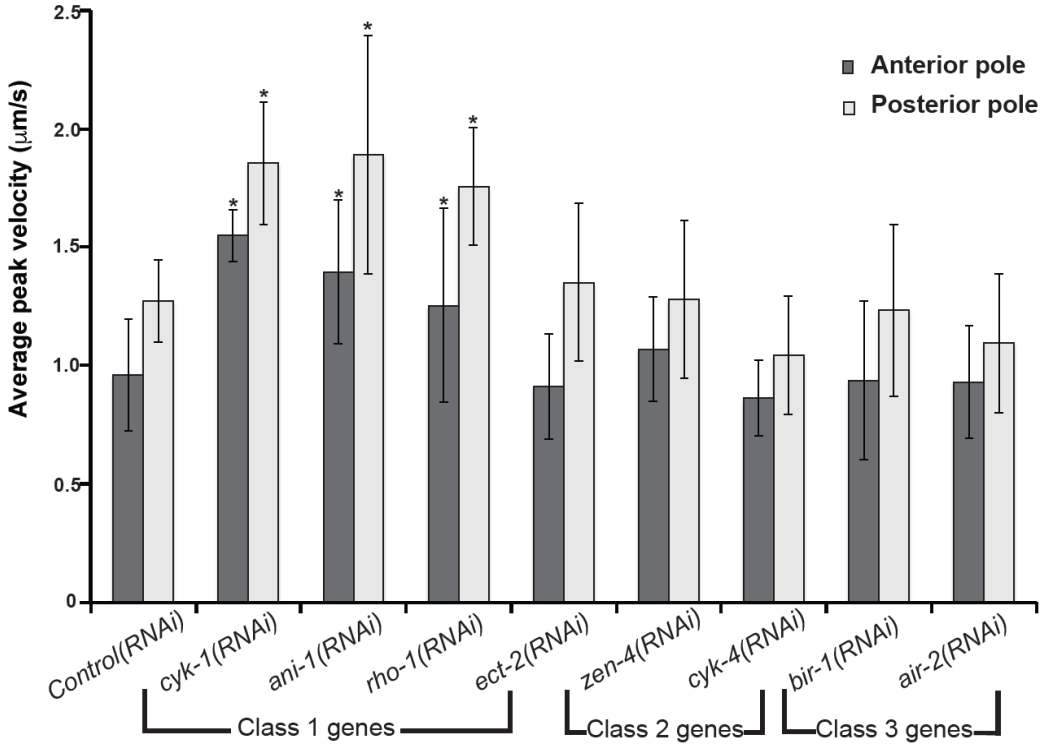

Figure 3.3.3 Average peak spindle pole velocities for each RNAi treatment. $n \geq 10$ embryos for each sample set. Anterior spindle pole velocity is shown in grey and posterior spindle pole velocity is shown in white. Asterisk indicates p value <0.01. Error bars indicate standard deviation.

3.3.3 Effect of CYK-1 depletion on the actomyosin cortex in the C. elegans embryo

3.3.3.1 CYK-1 depletion affects GFP:: NMY-2 dynamics

Previous work has shown that partial depletion of CYK-1 affects NMY-2 movement during the early stage of mitosis (Werner, Munro et al. 2007) indicating that CYK-1 depletion can affect the acto-myosin cortex. In order to study the effect of CYK-1 depletion on NMY-2 dynamics during anaphase, live cell imaging of GFP::NMY-2 was carried out at the embryo cortex. The kymograph in Figure 3.3.4 shows that CYK-1 depletion affects the movement and re-accumulation of NMY-2 foci during anaphase.

Phenotype	Number of embryos	% of total embryos
No rotation	10/14	72%
Wild-type like right-handed rotation	2/14	14%
Left-handed rotation	2/14	14%

Table 3.3.2 GFP::NMY-2 phenotypes of right-handed rotation in *cyk-1(RNAi)* embryos

.

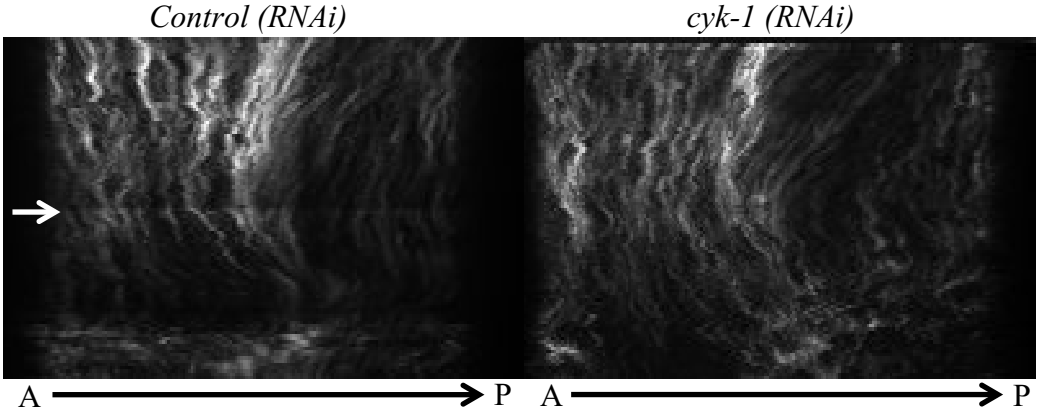

Figure 3.3.4 GFP::NMY-2 dynamics during anaphase. The kymograph shows GFP::NMY-2 movements across the A-P axis. First visible sign of cytokinesis was used as the reference t=0. Anaphase initiation is indicated by the white arrow on the kymograph and starts approximately 3 minutes before the first visible sign of cytokinesis furrow formation.

The cortex of the one-cell embryo undergoes a right-handed rotation around the dorso-ventral axis of the embryo during anaphase (Schonegg, Hyman et al. 2014). In the *cyk-1(RNAi)* experiments, I observed that 72% (10/14) of the embryos did not undergo the normal right-handed rotation. Of the remaining embryos, 2/14 exhibited a left-handed rotation (cortical movement opposite of the wild-type) and 2/14 underwent a normal right-handed rotation. 10 *control (RNAi)* embryos were tested and 100 % of these embryos show normal right-handed rotation of the cortex.

3.3.3.2 Effect of CYK-1 depletion on actin

Formin proteins are known to polymerize actin. An *in-vitro* study has shown that a CYK-1 construct with FH1-FH2 domains nucleates actin filament assembly and remains associated with the barbed end of assembled actin filament (Neidt, Skau et al. 2008) . Thus it is possible that CYK-1 might have a role in regulating actin dynamics in the *C. elegans* embryo. An indirect way to compare CYK-1 depletion and actin on the cortex is by using an actin-depolymerizing compound. This was done using Latrunculin A, a known actin-depolymerizing agent that has been shown to increase cortical forces in *C. elegans* one-cell embryo, when applied at low doses (Afshar, Werner et al. 2010, Berends, Munoz et al. 2013, Spiro, Thyagarajan et al. 2014). As shown in figure 3.3.5, upon treatment with 100 μM Latrunculin A, the average peak velocities of the anterior spindle pole was 1.27 μm/s and posterior spindle pole was 1.68 μm/s. These velocity values were significantly higher (p value <0.001) than the 5% DMSO control. Thus, Latrunculin A treatment resulted in an increase in the average peak spindle velocities, similar to the effect of CYK-1 depletion.

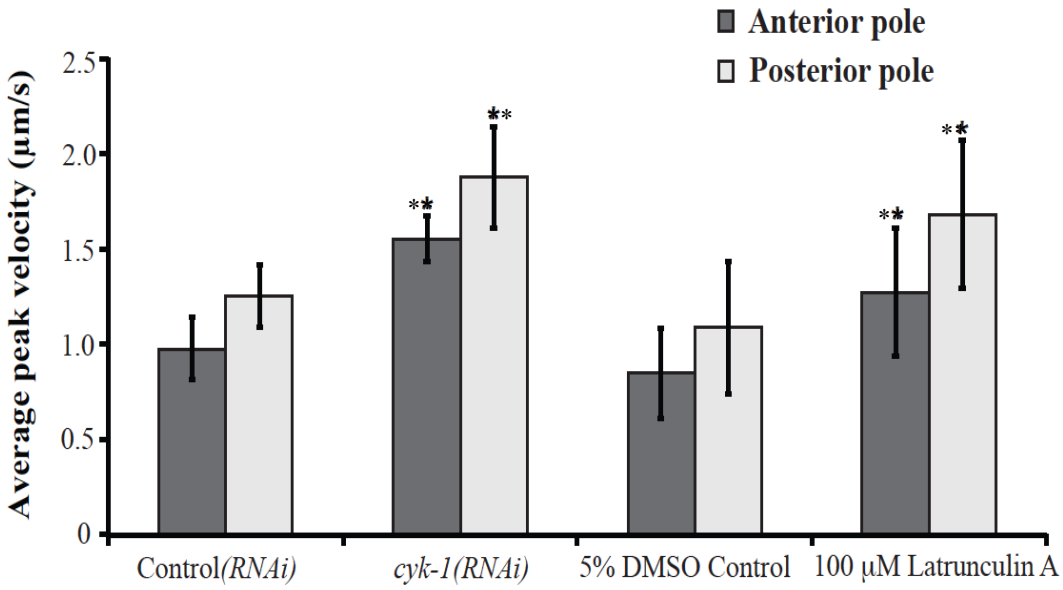

Figure 3.3.5 Average peak velocities with Latrunculin A treatment. Average peak spindle pole velocity for each treatment is shown. n ≥ 10 embryos for each sample set. Anterior spindle pole velocity is shown in grey and posterior spindle pole velocity is shown in white. Asterisk indicates p value <0.001. Error bars indicate standard deviation.

Since low-dose treatment with Latrunculin A resulted in an increase in spindle pole velocities during anaphase, I decided to examine the location of moesin, a factor that is required for proper F-actin distribution in the embryos. Moesin belongs to the ERM (Ezrin, radixin and moesin) family of proteins which link actin filaments to the plasma membrane (Jankovics, Sinka et al. 2002) and hence serves as a good marker for actin dynamics in the embryo. Spinning disk confocal microscopy was performed in live embryos expressing GFP::Moesin to visualize filamentous actin. The size of the F-actin foci was measured in *control (RNAi)* and *cyk-1(RNAi)* embryos.

As shown in figure 3.3.6, there was a slight increase in the number of F-actin foci bigger than 2 μm^2 in *cyk-1(RNAi)*, in the 1-2 μm^2 range there was a slight decrease in the number of actin foci, in the range of > 2μm^2 there was a decrease in the number of foci. However, there was no statistically significant difference in the overall number of F-actin foci between control and *cyk-1(RNAi)* treatment.

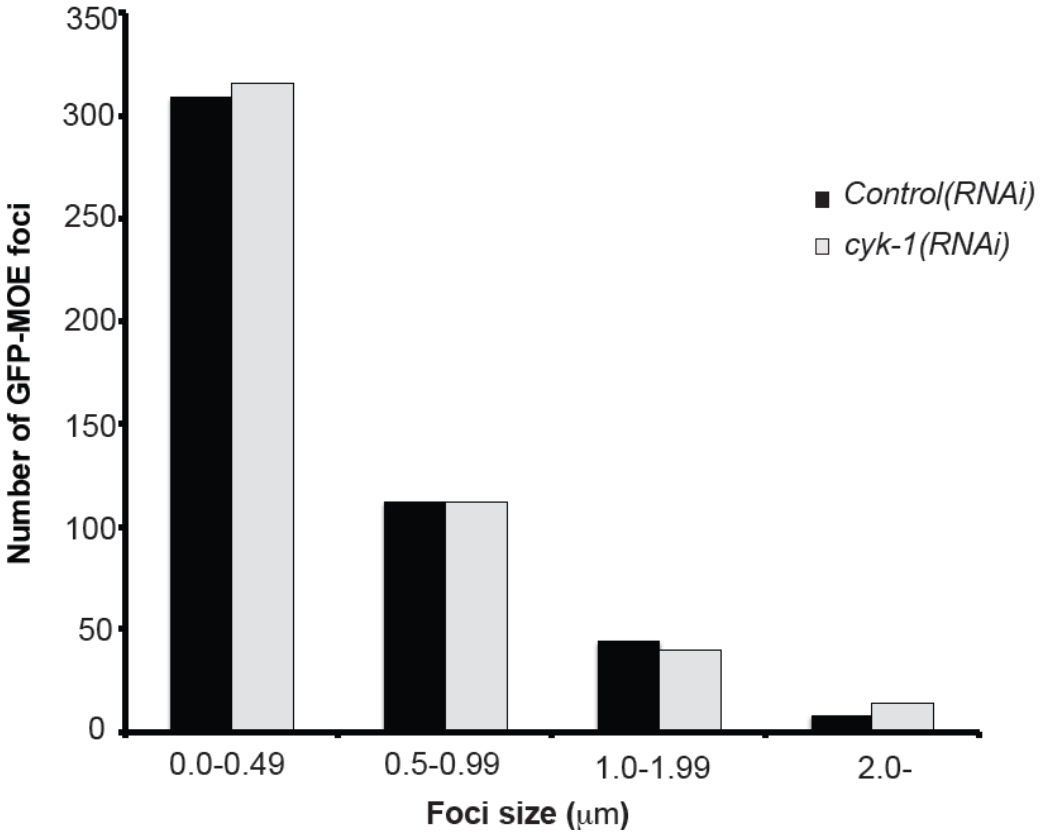

Figure 3.3.6 Quantification of GFP::MOE foci in control and *cyk-1(RNAi)* embryos. n=6 embryos for each treatment. The embryos were imaged from NEBD to anaphase. The foci size was measured at anaphase initiation.

3.3.4 Effect of CYK-1 depletion on cortical membrane invaginations in the *C. elegans* embryo

cyk-1(RNAi) resulted in a change in spindle pole movement during anaphase that was similar to the treatment of the embryos with medium doses of latrunculin (shown in figure 3.3.5). This suggested that depletion of CYK-1 affects actin dynamics in the embryo. Earlier work done in the *C. elegans* embryo has shown that a weakened acto-myosin cortex causes increased membrane invaginations. These invaginations are directed away from the membrane and towards the centrosome. Also, the membrane invaginations are caused by microtubule pulling forces and they disappear when treated with nocodazole, a microtubule-destabilizing drug (Redemann, Pecreaux et al. 2010), thus the invaginations reveal underlying microtubule-based pulling forces that are otherwise masked by the mechanically strong cortex. PH::GFP is known to specifically bind plasma membrane and does not label internal membranes. In addition, earlier work established that weakening the acto-myosin cortex increased the cortical elasticity and, in turn, increased the number of membrane invaginations at the embryo cortex (Redemann, Pecreaux et al. 2010). Hence, this assay was used to test if CYK-1 depletion increased the number of membrane invaginations.

In order to establish that the assay was working in my hands, drug testing was done using nocodazole. Since nocodazole is a microtubule-destabilizing agent, as shown in figure 3.3.7 (panel 3), the membrane invaginations disappeared upon nocodazole treatment. This result was similar to earlier published data (Redemann, Pecreaux et al. 2010) and confirmed that the assay worked as expected.

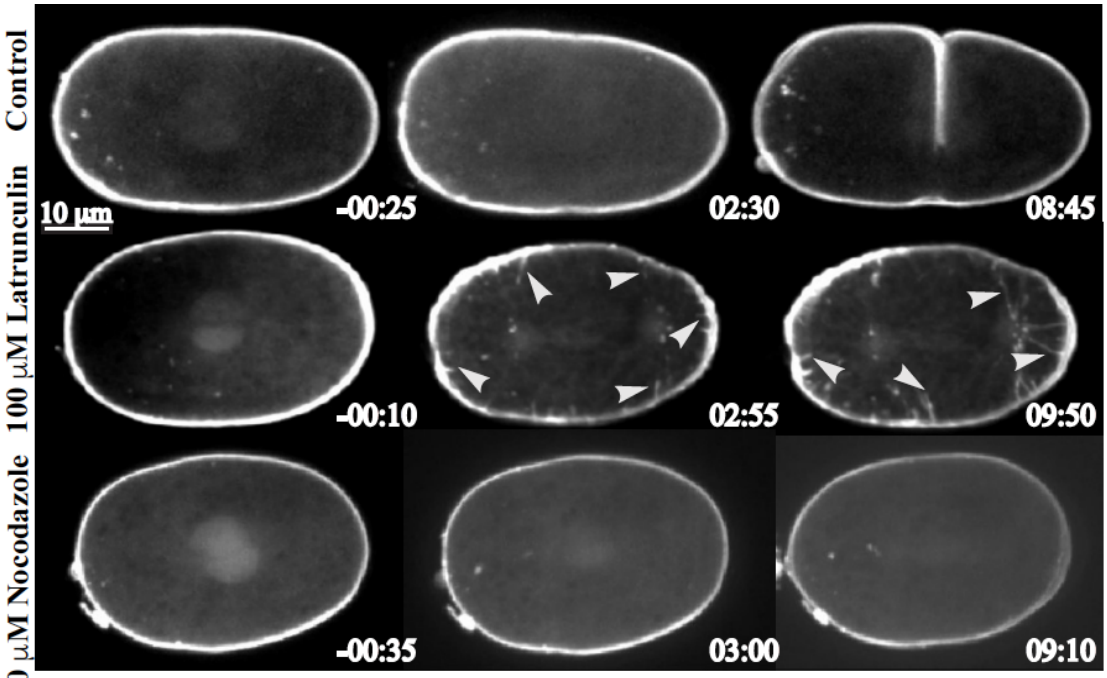

Figure 3.3.7 Membrane invaginations in control and drug-treated embryos. Embryos expressing the PH::GFP membrane marker are shown. White arrowheads mark the membrane invaginations. The control is 5% DMSO in egg buffer. Scale bar is 10 μm.

Latrunculin A is an actin-destabilizing drug and the number of invaginations increased upon latrunculin A application (as indicated in figure 3.3.7). Also, the average number of membrane invaginations (counted during the anaphase stage) in 5% DMSO control embryos was 1.2 on the anterior side and 1.8 on the posterior side, while the average number of membrane invaginations in latrunculin A treated embryos was 78 on the anterior side and 89 on the posterior side and that for nocodazole-treated embryos was 0.33 on the anterior side and 1.67 on the posterior side (data from five embryos for each trail). Quantification of the number of invaginations for each treatment is shown in figure 3.3.8 The box plot shows an increase in the number of membrane invaginations in latrunculin A treated embryos, both on the anterior and posterior side. The box-plot also shows the variability observed in the total number of membrane invaginations in each latrunculin A treated embryo.

Next, *cyk-1(RNAi)* was tested for the presence of membrane invaginations. As indicated by white arrows in figure 3.3.9, the number of membrane invaginations in *cyk-1(RNAi)* was higher than the *control(RNAi),* both on the anterior and posterior domains. Also, the average number of membrane invaginations (counted during the anaphase stage) in *control(RNAi)* embryos was 1.66 on the anterior side and 1.66 on the posterior side, while the average number of membrane invaginations in *cyk-1(RNAi)* embryos was 38.5 on the anterior side and 52.6 on the posterior side. For *cyk-1(RNAi)* embryos treated with 100μM nocodazole, the average number of invaginations was 1.26 on the anterior side and 1.55 on the posterior side. Quantification of the number of invaginations for each treatment is shown in figure 3.3.10 The box plot shows an increase in the number of membrane invaginations in *cyk-1(RNAi)* embryos, both on the anterior and posterior side. The number of invaginations was counted from 5 embryos for each data set. The box-plot also shows the variability observed in the total number of membrane invaginations in each *control(RNAi)*, *cyk-1(RNAi)* and *cyk-1(RNAi)* embryo treated with Nocodazole.

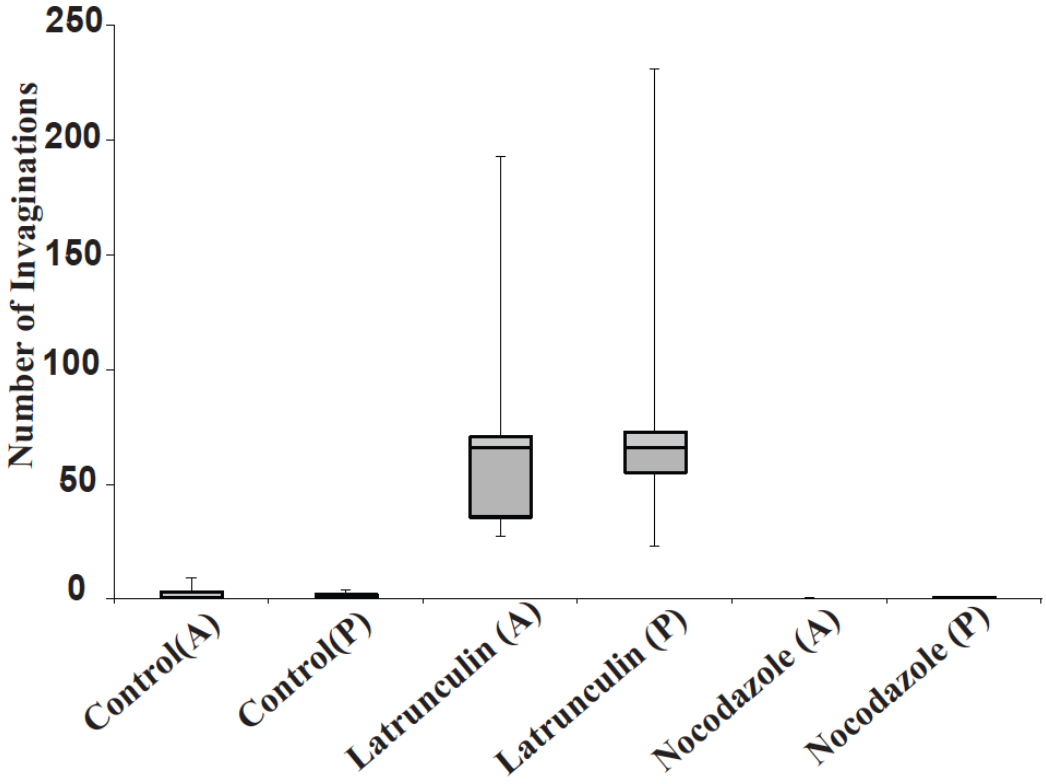

Figure 3.3.8 Effect of drug treatment on the number of membrane invaginations. The box-plot shows the number of membrane invaginations in control and drug treated embryos on the anterior (A) and posterior (P) side. The central mark in the box plot indicates the median value and the end of each box are the upper and lower quartile of the data range. Each data set is from 5 embryos.

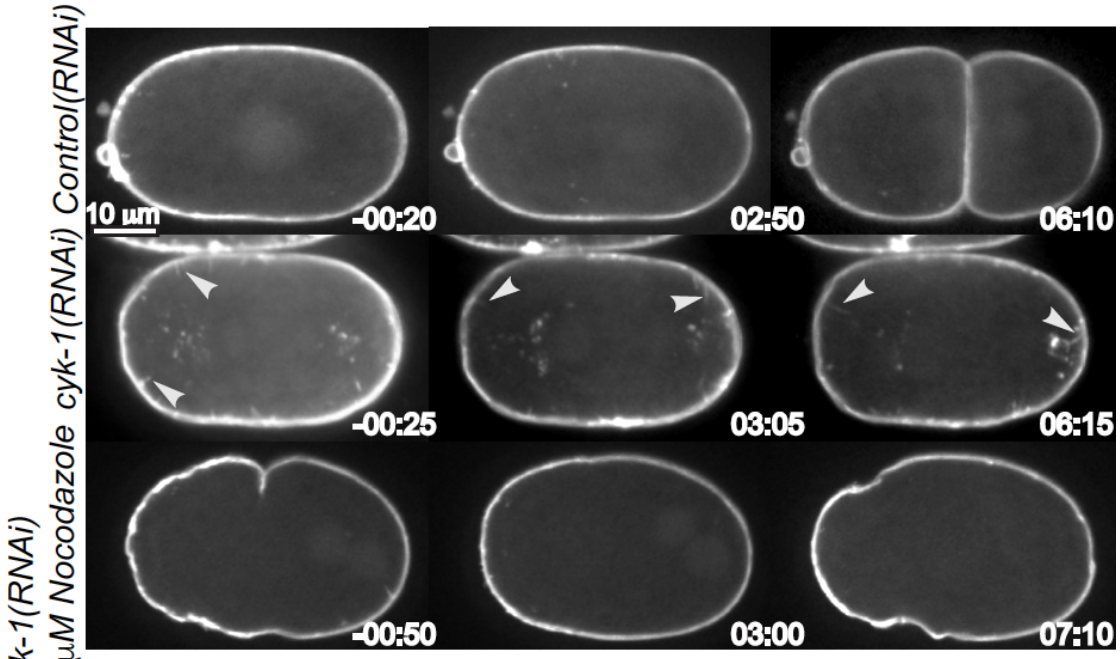

Figure 3.3.9 Membrane invaginations in control, *cyk-1(RNAi)* and *cyk-1(RNAi)* with Nocodazole. Embryos expressing the PH::GFP membrane marker are shown. White arrowheads mark the membrane invaginations.

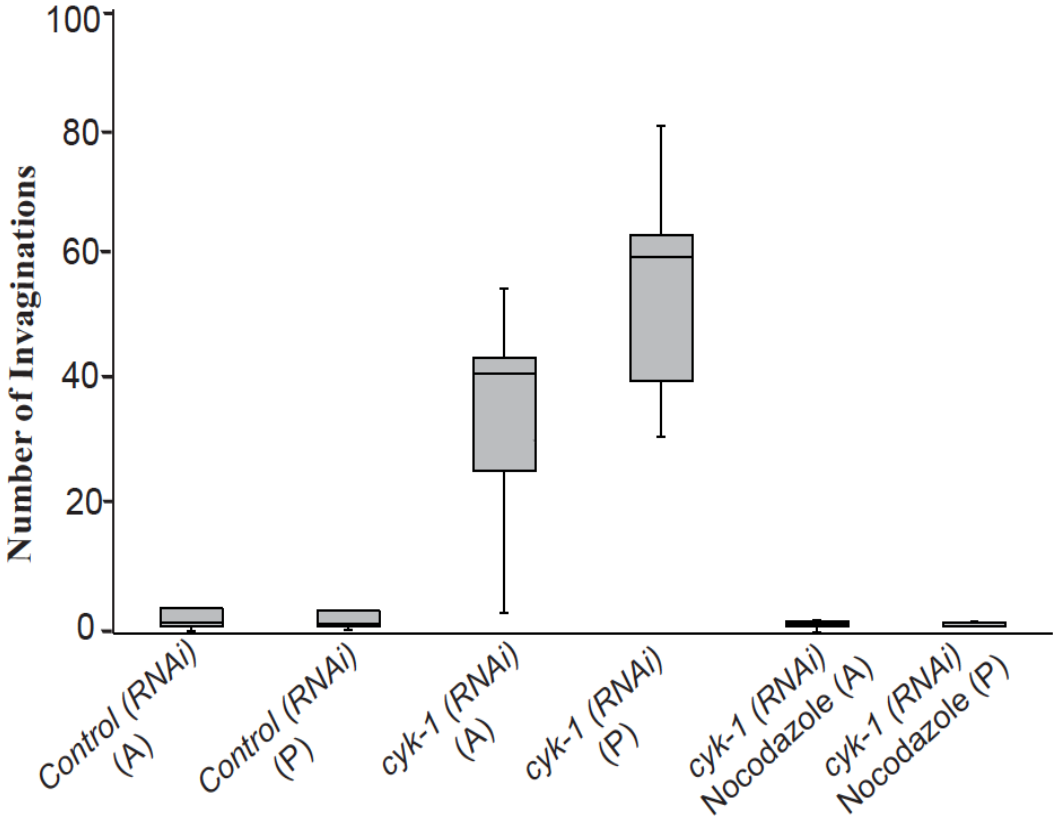

Figure 3.3.10 Effect of *cyk-1(RNAi)* on the number of membrane invaginations. The box-plot shows the number of membrane invaginations in control and drug treated embryos on the anterior (A) and posterior (P) side. The central mark in the box plot indicates the median value and the end of each box are the upper and lower quartile of the data range. Each data set is from 5 embryos.

3.3.5 Effect of CYK-1 depletion on cortical tension in the *C. elegans* embryo

cyk-1(RNAi) resulted in a change in spindle pole movement during anaphase and results from 3.3.4 indicate that the acto-myosin cortex is weakened by depletion of CYK-1. This results in an increase in the formation of the membrane invaginations in *cyk-1(RNAi)* embryos compared to the control. Therefore, I reasoned that, if the formation of membrane invaginations is an effect of acto-myosin weakening due to CYK-1 depletion, does it also affect the cortical tension in the acto-myosin cortex.

Therefore, the next thing I wanted to investigate was if the cortical tension in the acto-myosin cortex was changed by CYK-1 depletion. Cortical-laser ablation experiments have been previously developed to measure tension in the acto-myosin network in the *C. elegans* embryo (Mayer, Depken et al. 2010). In this way, the acto-myosin network can be locally disrupted using a pulsed ultraviolet laser (Mayer, Depken et al. 2010). I used a similar approach to disrupt the cortex and measure cortical tension. A micropoint laser was used to ablate the acto-myosin cortex which was visualized by the GFP::NMY-2 marker. Velocities of the GFP-NMY-2 foci were measured before and after laser ablation. The velocity in *control (RNAi)* and *cyk-1(RNAi)* before laser ablation (time point -3 second in the figure 3.3.11) was 0.05 μm/s and 0.18 μm/s respectively. As shown in Fig 3.3.11, the initial outward velocity of GFP::NMY-2 foci right after laser ablation (time point 0 second) in *control(RNAi)* was 0.935 μm/s and in *cyk-1(RNAi)* was 0.473 μm/s. Thus the GFP::NMY-2 foci in *cyk-1(RNAi)* embryos (indicated in red in figure 3.3.11) travel with lower velocities (p value < 0.0001) compared to controls, immediately after laser ablation. Another interesting phenotype observed here is that *cyk-1(RNAi)* embryos exhibited faster basal GFP::NMY-2 foci movements compared to the controls.

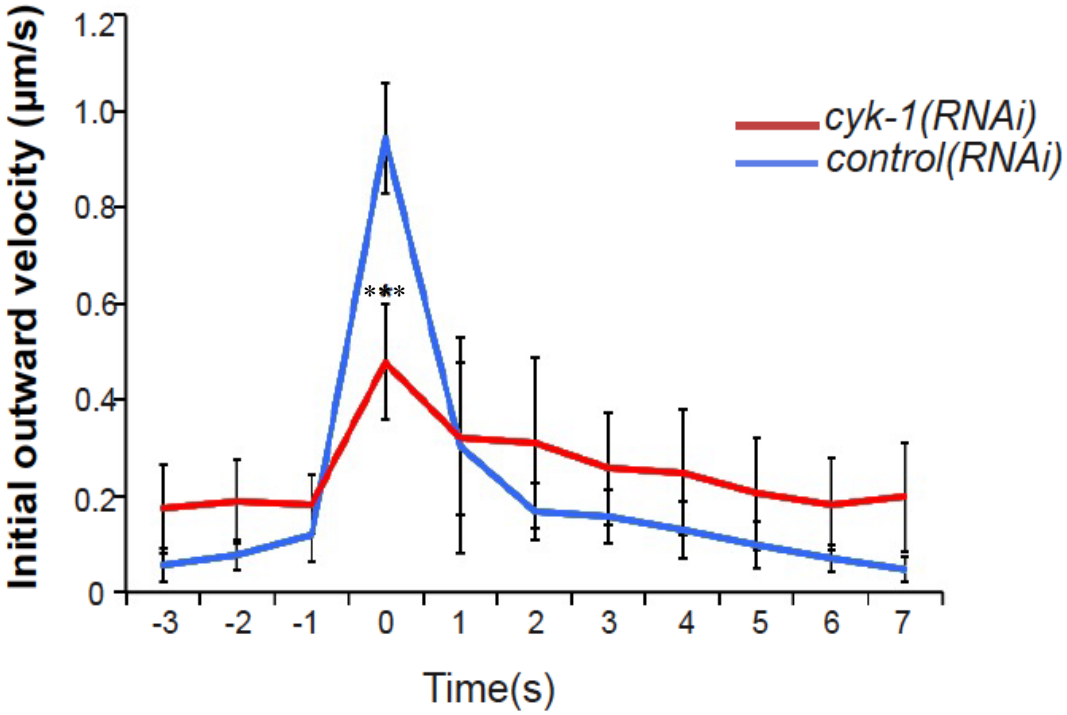

Figure 3.3.11 Effect of *cyk-1(RNAi)* on cortical tension. The velocities of GFP::NMY-2 foci at the cortex is shown. Time zero indicates the initial outward velocity right after laser ablation. 5 foci were tracked in each embryo. n=10 embryos for each group. p-value <0.0001

3.3.6 Effect of CYK-1 depletion on cortical dynein dynamics

Dynein is thought to influence microtubule assembly and regulate microtubule based spindle oscillations in the one-cell *C. elegans* embryo (Grill, Howard et al. 2003, Schmidt, Rose et al. 2005, Srayko, Kaya et al. 2005). Previous work has shown that embryos with reduced dynein activity lack spindle oscillations (Schmidt, Rose et al. 2005, Pecreaux, Roper et al. 2006). Since CYK-1-depleted embryos show increased spindle oscillations, the possibility that CYK-1 regulates the distribution and dynamics of dynein at the cortex was tested using a DHC-1::GFP strain (O'Rourke, Christensen et al. 2010).

The distribution of GFP::DHC-1 dots at the cortex during anaphase was determined and converted into a density plot. As shown in figure 3.3.12, the density of DHC-1 in *cyk-1(RNAi)* was 0.1 foci/μm^2 and *control(RNAi)* was 0.091 foci/μm^2. CYK-1 depletion did not show any significant increase ($p = 0.359$) in the density of DHC-1 on the cortex compared to the control. *dhc-1(RNAi)* embryos was used as a control and exhibited a density of 0.004 foci/μm^2. This significant reduction ($p < 0.0001$) compared to the *control (RNAi)* indicated that the foci represented dynein-GFP.

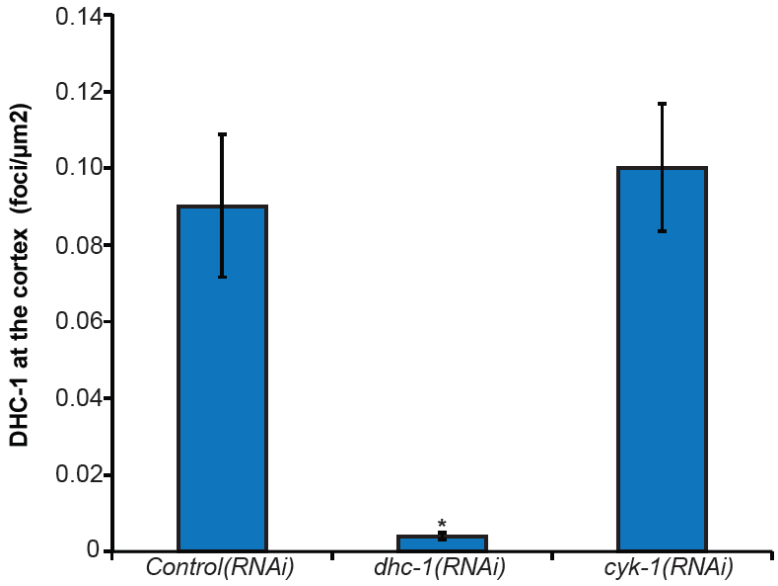

Figure 3.3.12 Effect of *cyk-1(RNAi)* on the number of DHC-1 spots on the cortex. The number of DHC-1 spots were counted on the cortical surface and converted into density (foci/μm^2). Error bars indicate standard deviation. n= 8 embryos for *control (RNAi)* and *cyk-1(RNAi)* and n=6 for *dhc-1(RNAi)*.

I also measured DHC-1 foci density in *lin-5(RNAi)* background. Previous work done in the *C. elegans* embryo showed that LIN-5 localizes dynein to the inner cortex and is required for anaphase pulling forces (Srinivasan, Fisk et al. 2003, Nguyen-Ngoc, Afshar et al. 2007, Gusnowski and Srayko 2011). Based on the results obtained for NuMA (mammalian homologue of LIN-5), the N-terminal domain mediates interaction with the dynein motor complex (Kotak, Busso et al. 2012). Therefore, it was expected that cortical dynein-GFP foci would be reduced or lost in a *lin-5(RNAi)* background. In addition, *lin-5(RNAi)* could serve as a useful negative control for experiments involving the quantification of dynein-GFP at the cortex.

Treatment of the dynein-GFP strain with *lin-5 (RNAi)* resulted in phenotypes expected for loss of LIN-5 function, for example, reduced spindle oscillations and symmetric cell division. However, the GFP::DHC-1 foci density plot in *lin-5(RNAi)* background revealed no reduction in the density compared to the control (Figure 3.3.13). This observation is contrary to the previously published results, where dynein motor protein localization at the cortex was abolished in the absence of LIN-5. Although the reason for this is not clear, it is possible that the GFP::DHC-1 strain reveals a population of "LIN-5 independent" dynein at the cortex. It is also possible that this dynein population at the cortex is not involved in anaphase pulling. DIC movies that were captured before and after the GFP-stream were used to confirm that the RNAi worked, which is indicated by the absence of anaphase oscillations in *lin-5(RNAi)*. Because *dhc-1(RNAi)* drastically reduced the GFP signal, it is likely that a DHC-1-GFP fusion protein is expressed in this strain, and that the GFP dots represent DHC-1 protein, however, the GFP dots may not represent active dynein motor in the embryo.

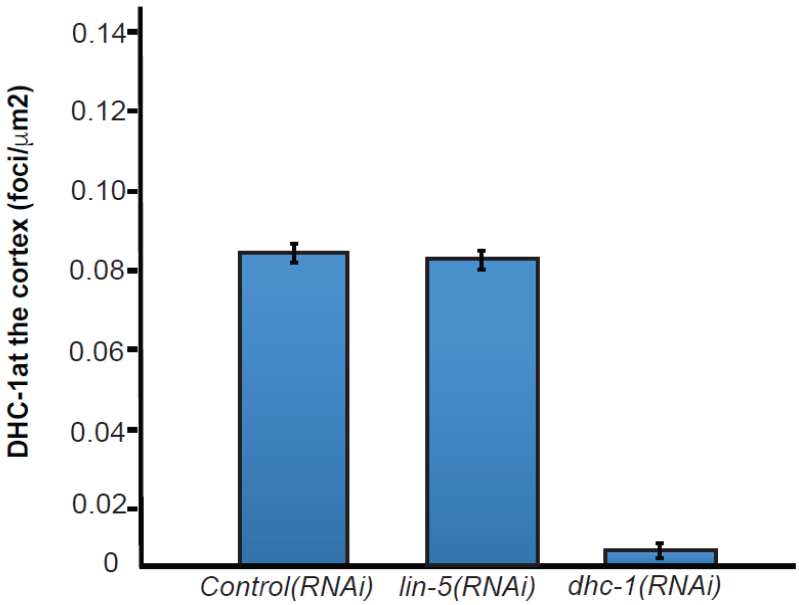

Figure 3.3.13 Effect of *lin-5(RNAi)* on the number of DHC-1 spots on the cortex. The number of DHC-1 spots were counted on the cortical surface and converted into density (foci/μm^2). Error bars indicate standard deviation. n= 6 embryos for *control (RNAi)* and *lin-5(RNAi)* and n=5 for *dhc-1(RNAi)*.

No changes were observed in the distribution of dynein foci at the cortex of *cyk-1(RNAi)* embryos. However, it was possible that CYK-1 could be involved in regulating a different aspect of dynein function, such as its residency time at the cortex. In this way, if dynein persisted at the cortex, it could, in theory, give rise to more prolonged pulling force and lead to the observed increase in pole oscillation velocity and amplitude. I measured the residency time for dynein foci at the cortex (*i.e.,* the time that DHC-1 foci spend at the cortex before getting detached) in *cyk-1(RNAi)* and control embryos. As shown in figure 3.3.14 the residency time of dynein at the cortex in control embryos was 1.28 s. Whereas, in *cyk-1(RNAi)* embryos, the residency time of cortical dynein was increased to 1.90 s. There was a statistically significant increase (p value <0.0001) in the residence time of dynein upon CYK-1 depletion.

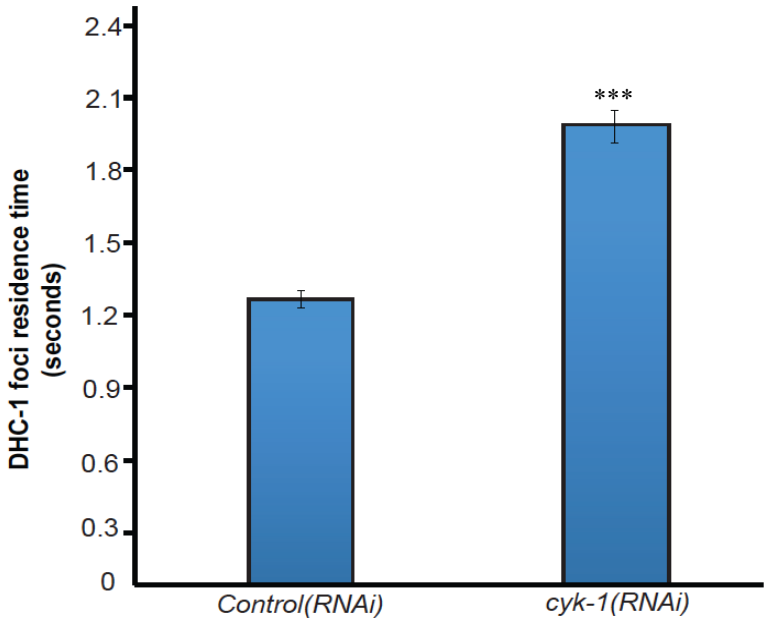

Figure 3.3.14 Effect of *cyk-1(RNAi)* on DHC-1 residence time at the cortex. The residence time of dynein was calculated by tracking the DHC-1 spots on the cortex over time. Error bars indicate standard deviation. n= 11 embryos for *control (RNAi)* and *cyk-1(RNAi)* and 20 DHC-1 spots were tracked in each embryo. p value <0.0001

3.3.7 CYK-1 localization in the *C. elegans* embryo

Previous work has shown localization of CYK-1 at the leading edge of the cytokinesis furrow (Swan, Severson et al. 1998). In order to determine if CYK-1 is present at the embryo cortex, I used CYK-1 antibodies (obtained from Bowerman lab, University of Oregon) to perform immuno-staining. Figure 3.3.15 shows maximum projection of the cortical stacks in *control (RNAi)* and *cyk-1(RNAi)* embryos. CYK-1 is present along the cytokinesis furrow in *control (RNAi)* embryos, indicated by white arrows. This localization is similar to previously published results (Swan, Severson et al. 1998). In *cyk-1 (RNAi)* embryos, cytokinesis fails and CYK-1 was not detectable at the furrow.

Other than the presence of CYK-1 at the cytokinesis furrow, the control images in figure 3.3.15 also show the presence of CYK-1 punctae (appear as red dots) at the cortex. These punctae appear to be distributed along the anterior and posterior domains of the two-cell stage control embryos. In *cyk-1(RNAi)* embryos, the CYK-1 punctae were not detected, which indicates that these dots represent CYK-1. In mammalian system, the formin protein, DIAPH1 (protein diaphanous homolog 1) has been shown to be associated with the cortex in HeLa cells (Fritzsche, Erlenkamper et al. 2016). Diaph1-GFP appeared as dots along the cortex, and treatment of the cells with the formin inhibitor, SMIFH2, interfered with localization along the cortex (Fritzsche, Erlenkamper et al. 2016). The presence of such CYK-1 punctae has been observed in earlier studies done in *C. elegans* embryo (Swan et al 1998 paper). However, the authors in this study argued that the presence of the cortical dots was not reproducible and not specific to CYK-1. However, in my experiments, I was able to detect the CYK-1 punctae in 100% of the embryos tested. This result suggests that, in addition to localizing along the cleavage furrow, CYK-1 is also distributed at the embryo cortex.

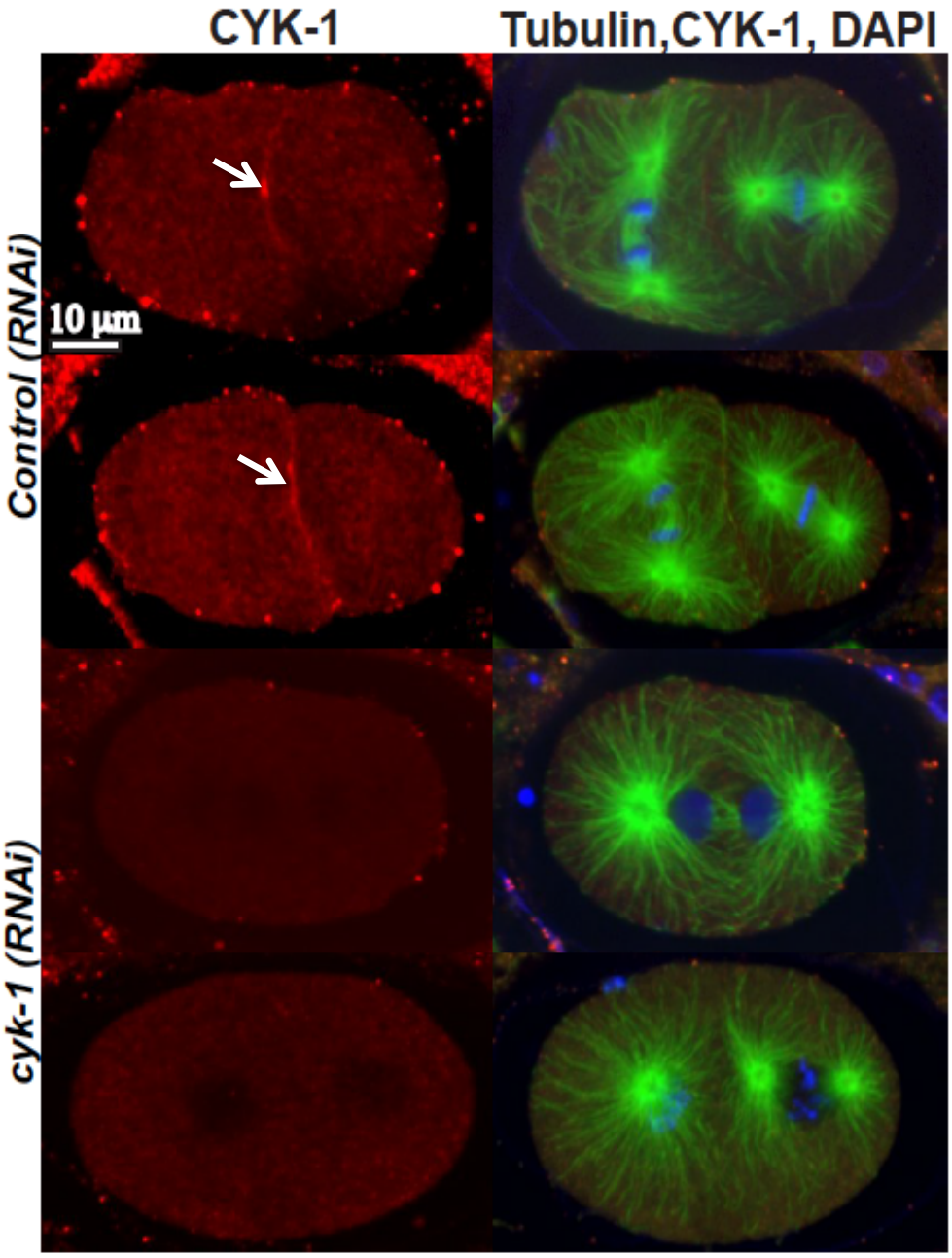

Figure 3.3.15 CYK-1 localization in the embryo. The localization of CYK-1 is shown in the *C. elegans* embryo. CYK-1 (shown in red) can be seen localized at the cytokinesis furrow. The DNA was stained by DAPI, which is shown in blue and tubulin is shown in green.

3.3.8 Effect of depleting members of the Heterotrimeric G protein complex in *cyk-1(RNAi)* background

In *C. elegans* embryos, heterotrimeric G-proteins play an important role in cortical force generation (Srinivasan, Fisk et al. 2003, Nguyen-Ngoc, Afshar et al. 2007, Park and Rose 2008) (see Introduction). The heterotrimeric G protein complex consists of Gα, Gβ, and Gγ subunits, where Gβγ act as a dimer. Depletion of Gα and GPR-1/2 by RNAi results in loss of spindle oscillations and greatly reduced anaphase spindle movement (Gotta and Ahringer 2001). On the other hand, depletion of Gβ protein causes an increase in spindle oscillations, which can be suppressed by *Gα(RNAi)* (Gotta and Ahringer 2001). *lin-5(RNAi)* reduces spindle oscillations. It is not known if the increased cortical forces observed in *cyk-1(RNAi)* embryos require the function of cortical force generators (*i.e*. the heterotrimeric G proteins and LIN-5). In order to test this, I simultaneously depleted CYK-1 and individual components of heterotrimeric G proteins and LIN-5 and measured average peak velocities. The phenotypes resulting from RNAi of individual G-protein components and *cyk-1* are distinguishable, which provided a ready method to confirm the effectiveness of the double RNAi. For example, *Gα(RNAi)*, *gpr-1/2(RNAi)* and *lin-5(RNAi)* resulted in a loss of spindle oscillations and a decrease in average peak velocity. *Gβ(RNAi)* caused an increase in spindle oscillations and average peak velocity compared to the control. *cyk-1(RNAi)* embryos showed cytokinesis defects. The double depletion with *cyk-1(RNAi)* of each gene also showed the cytokinesis defect and the phenotype associated with the depletion of the G-protein component. As shown in figure 3.3.16, depletion of Gα, GPR-1/2 and LIN-5 all suppressed excess cortical forces in *cyk-1(RNAi)* embryos during anaphase. There was no significant difference observed between the average peak velocities when each member of the G-protein family was depleted individually or in combination with CYK-1. Also, the depletion of G β protein in *cyk-1(RNAi)* embryos during anaphase did not show any significant difference in the average peak velocities of individual and double knockdown.

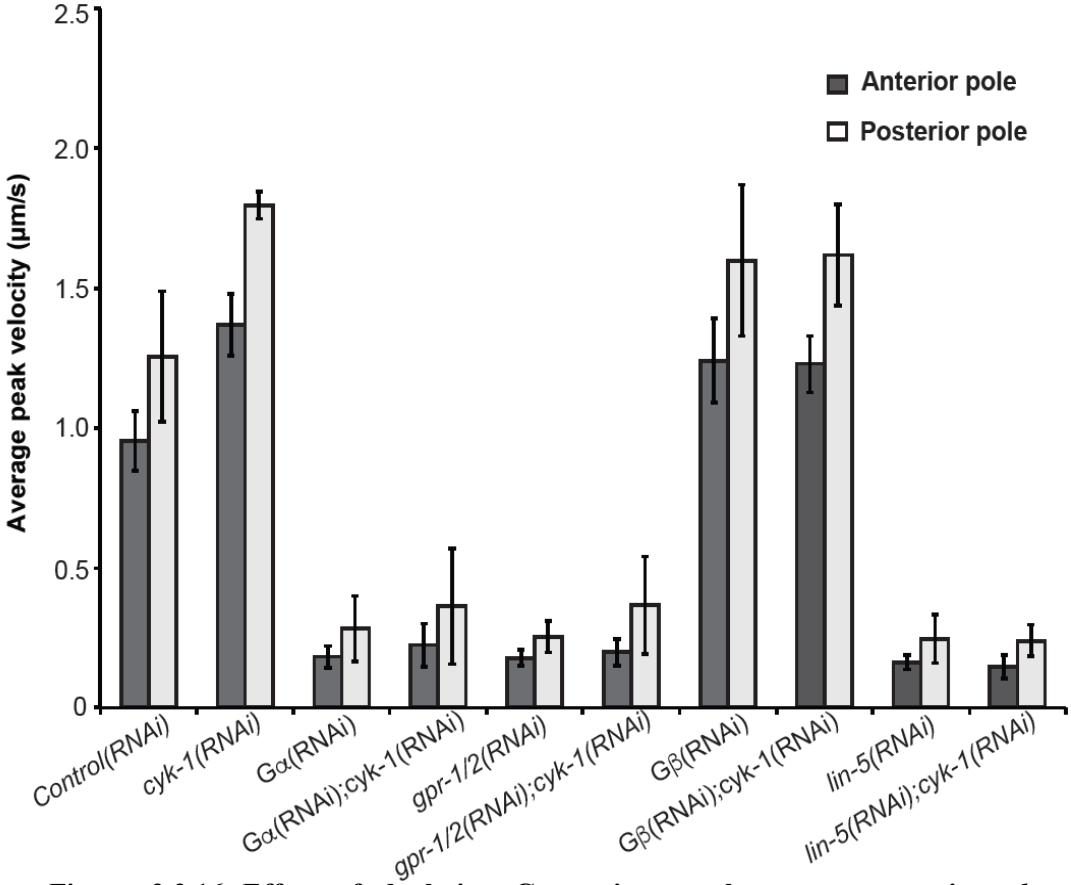

Figure 3.3.16 Effect of depleting G-protein complex components in *cyk-1(RNAi).*

Average peak velocity is shown here for single and double RNAi treatments. . n≥10 embryos for each treatment. Error bars indicate standard deviation.

3.4. Discussion

3.4.1 Summary of depleting known effectors of cytokinesis

CYK-1 is a formin protein that has an important role in cytokinesis in the *C. elegans* one-cell embryo (Swan, Severson et al. 1998). However, in my *cyk-1(RNAi)* experiments, in addition to cytokinesis failure, I also observed hyperactive movements of the mitotic spindle (section 3.3.1) during anaphase. The results from section 3.3.1 indicate that *cyk-1(RNAi)* results in higher spindle pulling forces. Despite the increased anaphase spindle pulling force in CYK-1-depleted embryos, the positioning of the anaphase spindle was not affected. This is consistent with earlier published results (Kozlowski, Srayko et al. 2007), which showed that oscillations were sensitive to changes in other variables, but spindle skewing and orientation were more robust. These results indicate that CYK-1 normally limits cortical spindle-pulling forces in the embryo during anaphase.

It has been hypothesized that CYK-1 functions in the one-cell embryo by bridging the actin and microtubule cytoskeleton at the cytokinesis furrow (Swan, Severson et al. 1998). Previous work in our lab on the motor activity of dynein has shown that CYK-1 depletion increases the proportion of dynein-dependent microtubule velocities at the embryo cortex (Gusnowski 2010). However previously, it was not clear if CYK-1 had any role, prior to cytokinesis, in the first mitotic division in the one-cell embryo. This is the first report of CYK-1 protein affecting spindle-pulling forces in the *C. elegans* embryo during first mitotic division.

The RNAi survey to study the effect of perturbing other candidate cytokinesis genes provided some interesting results. Only a subset of candidate proteins required for cytokinesis affected cortical forces upon depletion. In addition to *cyk-1(RNAi)*

treatment, cortical pulling forces were increased only in *ani-1(RNAi)* and *rho-1(RNAi)*. All three genes belong to class 1 group of cytokinesis effectors. ANI-1 is involved in crosslinking cytoskeletal components by interacting with both actin and non-muscle myosin. ANI-1 is specifically required for contractile events in the one-cell embryo like pseudocleavage formation, polar body extrusion, cortical ruffling and for targeting septins to the contractile ring during mitotic cytokinesis (Maddox, Habermann et al. 2005, Maddox, Lewellyn et al. 2007, Piekny and Glotzer 2008). RHO-1 is a small GTPase, which has been shown to have a major role in controlling actomyosin contractility, and the organization of the NMY-2 network in the one-cell embryo (Schonegg and Hyman 2006). The class one family of cytokinesis proteins are involved in maintaining the actomysoin cortex and embryo contractility (Severson, Baillie et al. 2002, Maddox, Habermann et al. 2005). Hence, it is possible that CYK-1-depletion perturbs the actomysoin cortex in the one-cell embryo. This hypothesis was tested and discussed in section 4.2.

ect-2 also belongs to class 1 protein but the RNAi treatment did not have any impact on the average peak velocity (section 3.3.2). ECT-2 is an evolutionarily conserved guanine exchange factor, which activates the GTPase RHO-1 (Prokopenko, Brumby et al. 1999, Tatsumoto, Xie et al. 1999). Both ECT-2 and RHO-1 are considered to be the main regulators controlling cortical contractility in the one-cell embryo (Piekny, Werner et al. 2005, Motegi and Sugimoto 2006). *ect-2(RNAi)* perturbed cytokinesis as expected, indicating that lack of an obvious spindle oscillation phenotype was not a result of ineffective RNAi. This indicates that though ECT-2 and RHO-1 are both involved in regulating cortical contractility and cytokinesis, it is likely that RHO-1 can be activated in the absence of ECT-2, possibly by a currently unknown factor, to maintain normal cortical tension. Another interpretation of this result is that the RNAi conditions did not allow complete depletion of ECT-2. It is possible that a low amount of ECT-2 could still activate RHO-1 to a level that allows normal spindle pulling force, but not normal cytokinesis.

Class 2 genes did not show any significant differences in anaphase cortical pulling forces (figure 3.3.2 and 3.3.3). From the class 3 candidate genes, *bir-1(RNAi)* showed a significant decrease in average peak amplitude (figure 3.3.2). Bir-1 encodes a homologue of the human gene Survivin (Fraser, James et al. 1999). The Survivin protein is upregulated in many tumors and interference in its expression leads to polyploidy. Survivin also possesses mitotic functions. In mammalian cells, survivin localizes to the kinetochores until metaphase, redistributes to the spindle midzone during anaphase-telophase and then localizes to the midbody during cell cleavage and functions as a chromosome passenger protein (Skoufias, Mollinari et al. 2000). Mutants in the BIR domain failed to localize at the kinetochore and spindle midzone but showed normal cytokinesis (Skoufias, Mollinari et al. 2000). In contrast, the Drosophila gene *scapolo* encodes a survivin homologue that, when mutated, behaves in the opposite manner. The *scapolo* mutant displays normal recruitment and function of the chromosomal passenger complex during metaphase, no delay in the metaphase-to-anaphase transition, and normal chromosome segregation during anaphase (Szafer-Glusman, Fuller et al. 2011). However, cytokinesis failed in these mutants, which indicates that the function of Survivin during metaphase and cytokinesis can be separated during different stages of mitosis in Drosophila (Szafer-Glusman, Fuller et al. 2011). In case of *S. cerevisiae*, Bir-1 is required for kinetochore tension checkpoint function (Shimogawa, Widlund et al. 2009). One of the functions of Bir-1 in yeast is to properly localize Ipl-1(aurora kinase) to kinetochores. Thus, Bir-1 functions to regulate chromatin stretching and detachment of individual kinetochores by maintaining tension with the adjacent chromatin (Shimogawa, Widlund et al. 2009).

In *C. elegans* BIR-1 localizes AIR-2 (aurora-like kinase) to chromosomes. BIR-1 depletion also results into chromosome misalignment; defects in chromosome condensation and segregation during mitosis (Speliotes, Uren et al. 2000). Based on these defects associated with BIR-1 depletion in *C. elegans*, a reduction in the amount of BIR-1 protein possibly results in a reduced kinetochore-chromosome tension similar to the one seen in yeast. This could be the reason that the movement of the spindle pole in the Y-axis and the measured amplitude in my experiments was

reduced significantly compared to the controls. However, there was not a significant decrease in spindle pole velocity upon BIR-1 depletion. This result shows that spindle pole velocity is not only governed by forces acting between the central spindle and tension between the kinetochores. The cortical forces, which are acting outside the spindle pole, also affect spindle pole velocity. In the case of *ani-1(RNAi)*, *rho-1(RNAi)* and *cyk-1(RNAi)* which perturb the actomyosin cortex, spindle pole velocities were increased (discussed above).

3.4.2 CYK-1 maintains proper organization of the actomyosin network

The results presented in section 3.3.3, 3.3.4 and 3.3.5 indicate that CYK-1 depletion perturbs the function of the acto-myosin cortex, at least in part, by disrupting the distribution of NMY-2 and by impacting the right-handed rotation of the embryo cortex during anaphase. Previous work done in *C. elegans* showed that perturbation of the actomyosin cytoskeleton could affect cortical forces (Kozlowski, Srayko et al. 2007, Spiro, Thyagarajan et al. 2014); however the molecular mechanism currently remains unknown.

3.4.2.1 Elimination of CYK-1 significantly affects NMY-2 dynamics during anaphase

As shown in section 3.3.1, depletion of CYK-1 affected the re-accumulation of NMY-2 patches and the rotation of the embryo cortex during anaphase. The embryo cortex is composed of both actin and non-muscle myosin, which interact and affect its contractility (Munro, Nance et al. 2004, Cowan and Hyman 2007). Previous work done in the *C. elegans* embryo has shown that movement of the NMY-2 foci during pseudocleavage and anaphase was determined by myosin-mediated contractility (Cowan and Hyman 2004, Cowan and Hyman 2007). It is possible that depletion of CYK-1 affects the interaction between NMY-2 and F-actin bundles at the embryo cortex. This could explain why CYK-1-depleted embryos do not undergo the normal right-handed rotation of the cortex during anaphase. NMY-2 itself is a mechanosensitive motor and its attachment to actin fibres is affected by force. It is

therefore possible that tension modulates the mechanochemical cycle of NMY-2 motor during right-handed rotation. During *Drosophila* gastrulation, RhoA signaling functions to activate Myosin II and promotes movement of Myosin II during apical constriction and tissue invagination (Mason, Tworoger et al. 2013).

In the *C. elegans* embryo, it has been reported that the knockdown of genes involved in actomyosin organization and microtubule function can completely inhibit rotation of the embryo cortex (Schonegg, Hyman et al. 2014). In addition, it was also reported that genes required for cytokinesis did not affect the right-handed rotation of the cortex (Schonegg, Hyman et al. 2014). However, CYK-1 was not tested in this study. Therefore, my results with *cyk-1(RNAi)* provide new evidence that a gene required for cytokinesis can affect rotation of the embryo cortex. However, what is different about CYK-1 as discussed above is that it is also required for the normal organization of actomyosin in the embryo. Also, previous work shows that CYK-1 might be involved in bridging the actin and microtubule cytoskeleton (Swan, Severson et al. 1998). Therefore, it is possible that CYK-1 connects the microtubule to actin in the actomyosin cortex and thus co-ordinates normal right-handed rotation of the embryo. When CYK-1 is depleted, the connection between microtubules and actin is lost, which disrupts the right-handed cortical rotation.

3.4.2.2 CYK-1 maintains tension in the actomyosin network

Since CYK-1 depletion affects normal organization of the actomyosin network, I wanted to test if this is also accompanied by alteration in cortical tension. Cortical laser ablation experiment (COLA) has been used in previous studies to measure cortical tension (Mayer, Depken et al. 2010). I found that cortical tension was reduced in *cyk-1(RNAi)*. This decrease in tension could be due to an overall perturbation of the actomyosin network upon CYK-1 depletion. Because formins are required for polymerization of F-actin filaments it is possible that the decrease in tension in the actomyosin network is a result of insufficient actin filament polymerization. A balanced level of cortical tension mediated by actomyosin is also required in

mammalian system. In HeLa cells, perturbation of actomyosin by depleting myosin, affects spindle positioning during mitosis (Toyoshima and Nishida 2007). However, in my experiments I did not see any defects associated with the position of the mitotic spindle. In HeLa cells, depletion of myosin causes abnormal rounding during metaphase and anaphase. This was accompanied by defects in actin organization (Toyoshima and Nishida 2007). Mitotic cell rounding is required to maintain proper geometry of cell division in mammalian cells. The actomyosin network based tension also helps mammalian cell to contract against the intracellular osmotic pressure (Stewart, Helenius et al. 2011).

3.4.2.3 CYK-1 is required to maintain rigidity of the embryo cortex

CYK-1 is a formin protein and is involved in actin polymerization. When embryos are treated with the actin-depolymerizing drug Latrunculin A, an increased net pulling force was observed on the anterior spindle (Afshar, Werner et al. 2010, Berends, Munoz et al. 2013). My results with Latrunculin A (figure 3.3.5) are consistent with these observations. However, when the cortical actin cytoskeleton was visualized (figure 3.3.6) using the GFP::MOE strain, I did not see any significant difference in the size of foci in CYK-1 depleted embryos. One of the reasons for this could be that CYK-1 depletion only causes a subtle change in the actin cytoskeleton which might not be detectable by the GFP::MOE marker used in this study.

The inner cortex of the *C. elegans* embryo is characterized by the actomyosin network which provides a rigid surface for proteins to anchor to (Redemann, Pecreaux et al. 2010). Redemann *et al.,* showed that when the cortex is made softer (by various RNAi and drug treatments), it causes the plasma membrane to invaginate towards the centrosomes. The plasma membrane invaginates due to microtubule pulling forces (Redemann, Pecreaux et al. 2010). In this study depletion of NMY-2 and PFN-1 (profilin) by RNAi revealed more invaginations compared to the wild type embryo.

NMY-2 is required for proper cortical contractility and cytokinesis (Munro, Nance et al. 2004, Werner, Munro et al. 2007) and PFN-1 functions in actin polymerization. In addition, a computer modeling study looked at the effect of changing cortical elasticity on mitotic spindle oscillations (Kozlowski, Srayko et al. 2007). In this study it was shown that an increase in rigidity of the cortex resulted in decrease in the speed of spindle pole oscillations during anaphase. Based on the results it was postulated that a softer posterior cortex prevents detachment of cortical force generators and hence allows for more sustained pulling forces acting on the posterior spindle (Kozlowski, Srayko et al. 2007).

My results of visualizing membrane invaginations upon CYK-1 depletion show similar results. As indicated in figure 3.3.9 and 3.3.10, a significant increase in the number of membrane invaginations was observed in *cyk-1(RNAi)* embryos. Since CYK-1 is required for maintaining the proper organization of the actomyosin network, these results indicate that the cortex becomes softer upon its depletion. The force generators, which are attached at the plasma membrane, pull on the microtubules or hold on to depolymerizing microtubules, which generate cortical force (Grill, Howard et al. 2003, Schmidt, Rose et al. 2005, Nguyen-Ngoc, Afshar et al. 2007). In wild type embryos, the cortical network of actomyosin provides sufficient stiffness to the plasma membrane during cortical force generation. However, upon CYK-1 depletion, the acto-myosin cortex is perturbed and the cortex is more elastic. In this situation the cortical pulling forces are excessively strong which might make the plasma membrane to get pulled towards the centrosomes and form an invagination. Consistent with my results, a recent study done using HeLa cells show that the formin/DIAPH1-generated actin filaments are the primary determinants of cortical elasticity (Fritzsche, Erlenkamper et al. 2016). The DIAPH1 nucleated actin filaments were longer compared to the Arp2/3 (actin-related protein 2/3) nucleated actin filaments. With the help of Atomic Force Microscopy, this study also characterized the elasticity of the cortex. The DIAPH1-based actin filaments were 10 times longer than the Arp2/3 nucleated filaments. Though both long and short filaments contribute to cortical elasticity, the longer filaments regulate macro scale

mechanical properties of the cortex to a large extent. The longer filaments are under constant tension and hence they are able to spread the mechanochemical cortical force over longer lengths and distances within the cell compared to the shorter actin filaments. This helps the longer filaments in significantly increasing elasticity of the cortex. In addition, when the cortex was perturbed using a small molecule inhibitor of formin, SMIFH2, a 50% decrease in elasticity was observed. This value was consistent with cortical elasticity measured upon treatment with the actin depolymerizer, cytochalasin D (Fritzsche, Erlenkamper et al. 2016). In addition recent work done to study epithelial morphogenesis using *Drosophila* embryo indicates that the cellular cortex of the fly embryo is elastic (Doubrovinski, Swan et al. 2017). The elastic response was measured in this study by subjecting the tissue to controlled externally applied force and then measuring the deformation in the tissue. Upon treatment with Cytochalasin D (an actin-destabilizing agent), the elastic response of the cortex was majorly disrupted which shows that the elasticity of the cortex is maintained by filamentous actin. However, the role of the proteins cross-linking the actin filaments or nucleating the actin filaments was not tested in this study. Thus, my data and the work in mammalian cell culture support the idea that formin proteins are the main regulators of actin-based cortical elasticity.

3.4.3 Effect of CYK-1 depletion on dynein at the cortex

The dynein motor protein is required for force generation in the *C. elegans* embryo (Gonczy, Pichler et al. 1999, Schmidt, Rose et al. 2005). It is thought that cortically localized dynein can either pull on astral microtubules approaching the cortex or hold onto depolymerizing microtubules at the cortex and this contributes to the cortical forces in the embryo (Schmidt, Rose et al. 2005, Kozlowski, Srayko et al. 2007, Gusnowski and Srayko 2011). Moreover, embryos with reduced dynein activity lack spindle oscillations (Schmidt, Rose et al. 2005, Pecreaux, Roper et al. 2006). Since CYK-1 depletion increased spindle oscillations, I tested whether the distribution and dynamics of dynein was affected in these embryos. I used DHC-1::GFP strain for this experiment (O'Rourke, Christensen et al. 2010). One mechanism to increase

cortical forces in *cyk-1(RNAi)* embryos, at least theoretically, could be through an increase in the number of dynein motor proteins in these embryos. However, as shown in figure 3.3.12, the number of dynein foci (DHC-1 foci) remained unaltered at the cortex. Thus, there was no increase in the number of dynein motor proteins. The GFP foci were greatly reduced upon *dhc-1(RNAi)*, indicating that these dots were composed of DHC-1-GFP, however, a caveat of this experiment is that these dots may not represent functional DHC-1 complexes, or active force-generators

Another potential mechanism to increase cortical force in *cyk-1(RNAi)* embryos could invoke a change in the contact time of cortical force generators with the cortex (Kozlowski, Srayko et al. 2007). The duration of time that the force generator remains at the cortex during anaphase could cause a change in the amount of net force on the spindle pole. As shown in figure 3.3.13, the residency time of dynein was increased significantly upon CYK-1 depletion. As discussed in section 3.4.2.3, CYK-1 depletion rendered the cortex more elastic. Therefore, it is possible that due to the increase in elasticity in *cyk-1(RNAi)*, dynein is able to interact with the depolymerizing microtubules for a longer time. This might be responsible for generating excessive cortical force upon CYK-1 depletion.

3.4.4 Localization of CYK-1 at the embryo cortex

As shown in figure 3.3.15, CYK-1 localizes to the leading edge of the furrow during cytokinesis. This is similar to previously published results (Swan, Severson et al. 1998) In addition, CYK-1 localizes dramatically at the contractile ring as furrow ingression progresses (Swan, Severson et al. 1998). This could mean that CYK-1 is present at the cortex during anaphase but is not detectable by the antibodies used in this study. The localization of CYK-1 at the cortex supports the model of Swan *et al.* (1998), which hypothesizes that CYK-1, a formin protein might be responsible for bridging the actin and microtubule cytoskeleton at the cytokinesis furrow. Importantly a recent study done in *Dictyostelium discoideum* cells showed that mDia1 colocalizes with actin and myosin II protein at the cortex of migrating cells (Ramalingam, Franke et al. 2015).

Work done in other systems has shown that formin proteins play an integral role in mediating actin-microtubule interactions (Ishizaki, Morishima et al. 2001, Daou, Hasan et al. 2014). In addition, work done in Drosophila shows that Cappucino, a diaphanous-related formin protein mediates an interaction between microtubules and the actin cytoskeleton during oogenesis (Rosales-Nieves, Johndrow et al. 2006). *In vitro* and *in vivo* data from this study suggests that Cappucino regulates the interaction between actin and microtubules during early stages of Drosophila germline development (Rosales-Nieves, Johndrow et al. 2006). Therefore, it is plausible that CYK-1 formin protein cross-links microtubules and the actin cytoskeleton at the cortex. This connection helps in maintaining "normal" or "wild-type" spindle oscillations and cortical forces during anaphase. As a formin protein, CYK-1 is predicted to play a role in actin polymerization. Therefore, it is conceivable that the depletion of CYK-1 from the inner cortex reduces the density of actin from the actomyosin network, which might contribute in making the cortex of the embryo more elastic.

3.4.5 Higher cortical forces in CYK-1 depleted embryos are dependent on the G-protein ternary complex

The Gα- GPR-1/2-LIN-5 ternary complex plays an important role in asymmetric cell division in the *C. elegans* embryo (Gotta and Ahringer 2001, Srinivasan, Fisk et al. 2003, Tsou, Hayashi et al. 2003, Nguyen-Ngoc, Afshar et al. 2007, Gusnowski and Srayko 2011). Despite information about the components involved in cortical pulling forces, there is more work to be done to fully understand the regulation of these forces. I set out to address if the hyperactive spindle oscillations observed in *cyk-1(RNAi)* were dependent on the G-protein components. Previous work established that depleting Gα, GPR-1/2 or LIN-5 decreases cortical forces in the one-cell embryo (Gotta and Ahringer 2001, Srinivasan, Fisk et al. 2003). In addition, depletion of GPB-1(Gβ protein) results in increased cortical forces (Tsou, Hayashi et al. 2003). As shown in figure 3.3.16, simultaneous depletion of CYK-1 and either Gα, GPR-1/2 or

LIN-5 resulted in decreased average peak spindle pole velocities. There was no statistically significant difference between the cortical forces in *Gα(RNAi)*, *gpr-1/2(RNAi)* or *lin-5(RNAi)* alone or in the double depletion of these genes in *cyk-1(RNAi)* background. Since *cyk-1(RNAi)* alone results in an increase in cortical forces, the double RNAi experiment indicates that depletion of Gα, GPR-1/2 or LIN-5 is epistatic to the *cyk-1(RNAi)* phenotype. This data shows that the increase in cortical force observed in CYK-1 depleted embryos is completely dependent on the G-protein-microtubule interaction. Earlier work done in many systems shows that G*α* protein links to cortical plasma membrane via hydrophobic anchors. Without any G-protein there is limited contact of microtubules with the cortex, therefore depletion of G*α* and GPR-1/2 alone causes a decrease in cortical force. My data indicates that without any G*α* and GPR-1/2 protein, it does not matter if CYK-1 is depleted; cortical forces remain low, presumably, because the contact of the cortex with microtubules has been abolished. CYK-1 affects the actomyosin surface of the cortex and depletion of CYK-1 increases the elasticity of the cortex (discussed in section 3.4.2.3).

It is conceivable that the ability of the G-protein components to maintain contact with a microtubule end could be influenced by the elasticity of the cortex. However, in my experiments, in the absence of these force generators (Gα, GPR-1/2 and LIN-5), even when the cortex is made more elastic (by depleting CYK-1), this phenomenon alone cannot cause spindle oscillations and increase cortical force.

3.4.6 Model for CYK-1 function

3D simulations of *C. elegans* anaphase pulling forces predicted that increased cortical elasticity could cause an increase in oscillations of the spindle pole and increased cortical pulling forces (Kozlowski, Srayko et al. 2007). In addition, another study done in the *C. elegans* embryos indicated that perturbing the rigidity of the cortex, results into stretching of the cortex. In this case the interaction between the depolymerizing microtubules and cortical force generator can be sustained for a

longer period of time (Spiro, Thyagarajan et al. 2014). My results indicate that the rigidity of the cortex is perturbed upon CYK-1 depletion and the residency time of dynein is also increased. Based on these results a model for the function of CYK-1 is shown in figure 3.3.17. CYK-1, the formin protein is normally required for assembly of the actomyosin network at the cortex. In the presence of CYK-1, the rigidity of the cortex is maintained. In this condition, the G-protein complex and dynein which are present at the cortex interact with orthogonally approaching microtubule plus ends. This interaction assists in chromosome segregation during anaphase, which is accompanied by spindle pole oscillations and cortical forces. In the absence of CYK-1, the interaction between dynein and the depolymerizing microtubules is sustained for a longer time, either through an intrinsic change in dynein turnover at the cortex, or via an increase in cortical elasticity, which, in turn, could allow prolonged interaction between microtubule plus end tips and the dynein complex.

The role of formin proteins in actin polymerization has been well studied. However, reports in other systems indicate formin proteins can also regulate microtubule dynamics (Gaillard, Ramabhadran et al. 2011, Daou, Hasan et al. 2014). Based on these studies and my data, it is possible that CYK-1 could regulate microtubule dynamics in many systems. However, previous examination indicates that CYK-1 likely has limited or no effect on microtubule growth in the one-cell *C. elegans* embryo (Gusnowski 2010). Nonetheless, as shown in figure 3.3.18, CYK-1 could interact with microtubules via the FH2 domain. Thus, this could explain how CYK-1 might be involved in bridging actin and microtubule cytoskeleton at the embryo cortex. Such molecular interactions between different structural components of the cortex could account for changes in cortical elasticity observed in the *cyk-1(RNAi)* experiments described herein.

Is the function of CYK-1 in cytokinesis separate from its role in maintaining the cortical rigidity and attenuating anaphase-pulling forces? A definite answer to this question is difficult to obtain because of CYK-1's role in actin polymerization. Actin is present at both the cytokinetic furrow as well as at the cortex and is important in a

number of cytoskeletal processes in the cell. However, in the future it might be useful to generate mutants of the FH1 and FH2 domains of CYK-1 protein using CRISPR-Cas9 system. It would first be important to establish if cortical forces are affected in these mutants during anaphase. In addition, it will be important to identify if these mutants also cause failure in cytokinesis. Also, this will help in identifying if cortical forces are regulated either by one of the domains or both. It might also be useful to generate CYK-1::GFP strains to identify the subcellular localization of CYK-1 in the embryo cortex. The CYK-1::GFP strain might be able to better detect the protein compared to immuno-staining experiments done in this study. Imaging experiments with this strain would reveal if CYK-1 localizes at the acto-myosin cortex and this will help in understanding the role of CYK-1 in the *C. elegans* embryo.

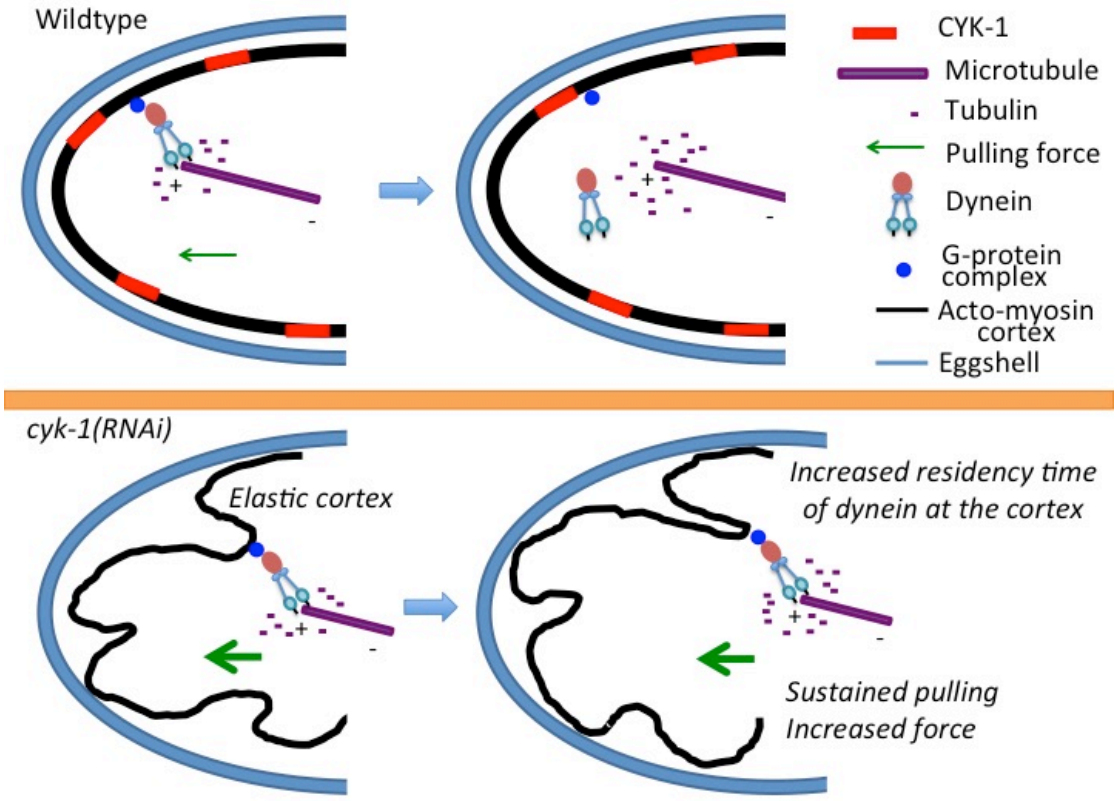

Figure 3.3.17 Model for CYK-1 function at the embryo cortex. Force generators hold onto depolymerizing microtubules, which generates cortical pulling forces. In *cyk-1(RNAi),* the cortex is more elastic due to perturbation of the actomyosin network. Due to the increased elasticity, the cortex can stretch more compared to the wild type embryos. This increased stretch can possibly increase the time the force generators interact with a depolymerizing microtubule. Thus the increased elasticity of the cortex could increase the residency time of dynein at the cortex before it detaches from the depolymerizing microtubule end. This in turn causes sustained pulling and translates into higher cortical forces in CYK-1 depleted embryos. The elasticity of the cortex has been exaggerated in this figure so it is easy to visualize.

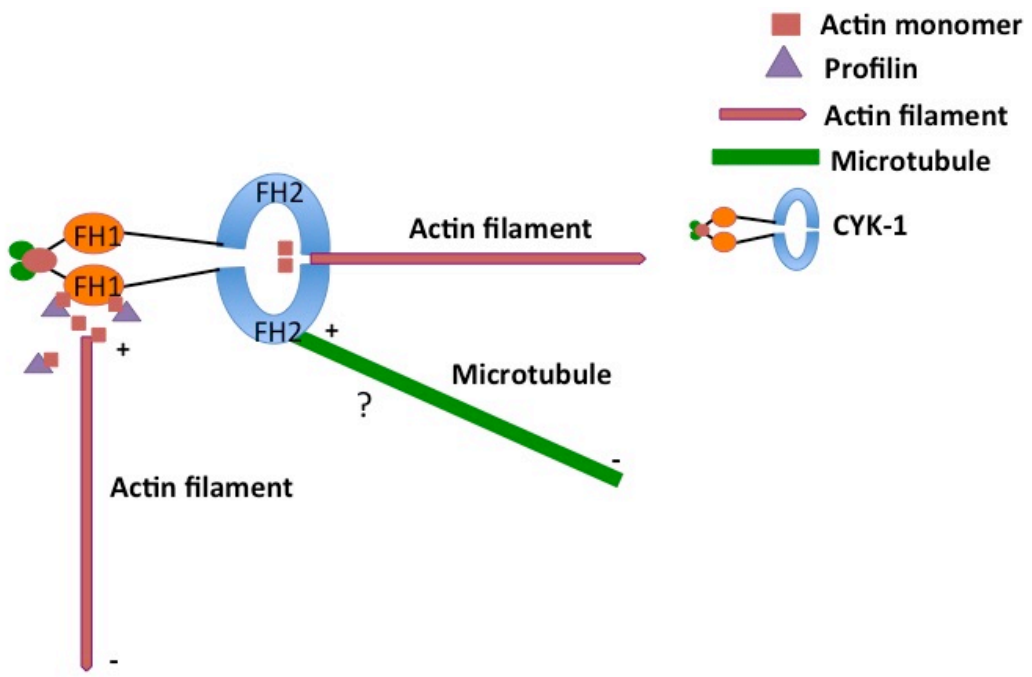

Figure 3.3.18 Model of CYK-1 function in bridging actin and microtubules . FH1 and FH2 domains are both known to interact with actin filament and help in polymerization of actin. It is possible that the FH2 domain of CYK-1 interacts with microtubules and this CYK-1 at the cortex has a function in bridging actin and microtubule cytoskeleton.

4. Summary and conclusion

The microtubule-binding agents have high structural diversity and bind microtubules at different binding sites. These naturally occurring microtubule-binding agents and their synthetic analogues can affect microtubule dynamics, inhibit cellular proliferation and hence continue to be effective for cancer-therapy. Though laulimalide has been tested in mammalian cells before, my experiments in the *C. elegans* embryo provide some unique results. In the context of previously published work (Mooberry, Tien et al. 1999), my results confirm that laulimalide is a microtubule stabilizer at higher concentrations. However, one of the interesting phenotypes I report in my study is that laulimalide behaves as a microtubule destabilizing agent at concentrations between 50 nM-500 nM.

Previous work has reported that laulimalide and paclitaxel have distinct binding sites (Bennett, Barakat et al. 2010). My results show that laulimalide and paclitaxel can act synergistically at sub-effective concentrations. It might be worthwhile to conduct further combination studies with laulimalide and other drugs that affect micrtotubule dynamics. Combination studies can be done at lower doses or sub-effective concentrations of the drugs, which can help in reducing the toxicity of individual drug. Based on the microtubule-associated phenotypes, the information could be useful to develop effective combination therapies to treat cancer.

The study of microtubule-binding agents is critical in the area of drug discovery for cancer therapy. However, microtubule-binding agents also serve as vital research tools to address several molecular mechanisms in the cell. For example, in the *C. elegans* embryo, a recent study used nocodazole to investigate the recovery of the kinesin-like motor protein, KLP-7 at the centrosome (Han, Adames et al. 2015). Another study

used nocodazole to examine if the cortical localization of the force generator protein, LIN-5 is dependent on microtubule dynamics (Berends, Munoz et al. 2013). These are just two examples where microtubule-binding agents were used as tools to study molecular mechanisms in *C. elegans* mitosis. Many microtubule-binding agents have been previously used and continue to be explored in other model systems to dissect various regulatory pathways in the cell.

The understanding of molecular mechanisms that contribute to microtubule-based forces during mitosis has significantly improved in the last decade. In *C. elegans*, the interaction between the microtubules and the embryo cortex has been studied extensively by various groups (Grill, Howard et al. 2003, Srinivasan, Fisk et al. 2003, Cowan and Hyman 2004, Labbe, McCarthy et al. 2004, Munro, Nance et al. 2004, Kozlowski, Srayko et al. 2007, Gusnowski and Srayko 2011). In addition, previous work indicates that a stiff actin cortex is vital to balance the forces produced by the combination of microtubule depolymerization and pulling forces (Redemann, Pecreaux et al. 2010). Thus due to the contribution of multiple pathways for cortical force generation, we are currently only at the cusp of understanding the importance of the acto-myosin cortex in this pathway.

My recent work sheds light on the role of CYK-1 (a formin protein) in maintaining microtubule-mediated pulling forces in the *C. elegans* one-cell embryo. CYK-1 in *C. elegans* has been extensively studied previously in cytokinesis. Interestingly, this is the first study to report the role of CYK-1 protein in maintaining the normal microtubule-based pulling forces. Our model hypothesizes that CYK-1, a formin protein in *C. elegans* maintains normal microtubule-based pulling forces by preserving the rigidity of the cortical acto-myosin network.

In other systems, formin proteins have been shown to either bind to microtubule-associated protein or bind directly to microtubules to modulate its dynamics (Watanabe, Kato et al. 1999, Feierbach, Verde et al. 2004). In adddition, a lot of research has been done that relates formin to various diseases. For example, a study of colorectal cancer cells from patients showed that the expression of Formin like-2

(FMNL2) protein was higher compared to normal colorectal mucosa (Zhu, Liang et al. 2008). Also, overexpression of FMNL2 in this study was associated with elevated lymphatic metastasis. In another study on prostrate cancer cells, the mouse formin proteins mDia1 and mDia2 are implicated in microvesicle formation and thereby function in tumor growth and metastasis (Di Vizio, Kim et al. 2009). An insertion mutation in another formin gene *diaph1* has been shown to generate a stop codon and expression of a truncated DIAPH1 protein in humans. This mutation causes an autosomal dominant, sensorineural hearing loss (Lynch, Lee et al. 1997).

My work shows that CYK-1 plays an important role in maintaining the integrity of the embryo cortex, which in turn regulates microtubule-mediated pulling forces in the first mitotic division. It shows how microtubules and the actin cytoskeleton coordinately determine subtle differences in force generation during asymmetric cell division. It is possible that formin proteins in other model organisms might differentially regulate cortical forces. Whether modulation of cortical forces occurs in disease conditions currently remains uncharacterized. Answers to these and other questions will help increase our knowledge of formin proteins and how their misregulation can lead to disease. The discoveries made in such fundamental processes might also lead to the potential development of novel therapeutic tools in the future.

Bibliography

Aamodt, E. J. and J. G. Culotti (1986). "Microtubules and microtubule-associated proteins from the nematode Caenorhabditis elegans: periodic cross-links connect microtubules in vitro." J Cell Biol **103**(1): 23-31.

Adames, N. R. and J. A. Cooper (2000). "Microtubule interactions with the cell cortex causing nuclear movements in Saccharomyces cerevisiae." J Cell Biol **149**(4): 863-874.

Afshar, K., B. Stuart and S. A. Wasserman (2000). "Functional analysis of the Drosophila diaphanous FH protein in early embryonic development." Development **127**(9): 1887-1897.

Afshar, K., M. E. Werner, Y. C. Tse, M. Glotzer and P. Gonczy (2010). "Regulation of cortical contractility and spindle positioning by the protein phosphatase 6 PPH-6 in one-cell stage C. elegans embryos." Development **137**(2): 237-247.

Andreu, J. M. and S. N. Timasheff (1986). "Tubulin-colchicine interactions and polymerization of the complex." Ann N Y Acad Sci **466**: 676-689.

Ayloo, S., J. E. Lazarus, A. Dodda, M. Tokito, E. M. Ostap and E. L. Holzbaur (2014). "Dynactin functions as both a dynamic tether and brake during dynein-driven motility." Nat Commun **5**: 4807.

Bajaj, M. and M. Srayko (2013). "Laulimalide induces dose-dependent modulation of microtubule behaviour in the C. elegans embryo." PLoS One **8**(8): e71889.

Bennett, M. J., K. Barakat, J. T. Huzil, J. Tuszynski and D. C. Schriemer (2010). "Discovery and characterization of the laulimalide-microtubule binding mode by mass shift perturbation mapping." Chem Biol **17**(7): 725-734.

Bennett, M. J., G. K. Chan, J. B. Rattner and D. C. Schriemer (2012). "Low-dose laulimalide represents a novel molecular probe for investigating microtubule organization." Cell Cycle **11**(16): 3045-3054.

Berends, C. W., J. Munoz, V. Portegijs, R. Schmidt, I. Grigoriev, M. Boxem, A. Akhmanova, A. J. Heck and S. van den Heuvel (2013). "F-actin asymmetry and the endoplasmic reticulum-associated TCC-1 protein contribute to stereotypic spindle movements in the Caenorhabditis elegans embryo." Mol Biol Cell **24**(14): 2201-2215.

Betschinger, J., K. Mechtler and J. A. Knoblich (2006). "Asymmetric segregation of the tumor suppressor brat regulates self-renewal in Drosophila neural stem cells." Cell **124**(6): 1241-1253.

Bishop, J. D. and J. M. Schumacher (2002). "Phosphorylation of the carboxyl terminus of inner centromere protein (INCENP) by the Aurora B Kinase stimulates Aurora B kinase activity." J Biol Chem **277**(31): 27577-27580.
Bollag, D. M., P. A. McQueney, J. Zhu, O. Hensens, L. Koupal, J. Liesch, M. Goetz, E. Lazarides and C. M. Woods (1995). "Epothilones, a new class of microtubule-stabilizing agents with a taxol-like mechanism of action." Cancer Res **55**(11): 2325-2333.
Bonaccorsi, S., M. G. Giansanti and M. Gatti (1998). "Spindle self-organization and cytokinesis during male meiosis in asterless mutants of Drosophila melanogaster." J Cell Biol **142**(3): 751-761.
Bringmann, H. and A. A. Hyman (2005). "A cytokinesis furrow is positioned by two consecutive signals." Nature **436**(7051): 731-734.
Brogdon, C. F., F. Y. Lee and R. M. Canetta (2014). "Development of other microtubule-stabilizer families: the epothilones and their derivatives." Anticancer Drugs **25**(5): 599-609.
Brouhard, G. J., J. H. Stear, T. L. Noetzel, J. Al-Bassam, K. Kinoshita, S. C. Harrison, J. Howard and A. A. Hyman (2008). "XMAP215 is a processive microtubule polymerase." Cell **132**(1): 79-88.
Burns, K. M., M. Wagenbach, L. Wordeman and D. C. Schriemer (2014). "Nucleotide exchange in dimeric MCAK induces longitudinal and lateral stress at microtubule ends to support depolymerization." Structure **22**(8): 1173-1183.
Carminati, J. L. and T. Stearns (1997). "Microtubules orient the mitotic spindle in yeast through dynein-dependent interactions with the cell cortex." J Cell Biol **138**(3): 629-641.
Carvalho, A., S. K. Olson, E. Gutierrez, K. Zhang, L. B. Noble, E. Zanin, A. Desai, A. Groisman and K. Oegema (2011). "Acute drug treatment in the early C. elegans embryo." PLoS One **6**(9): e24656.
Castrillon, D. H. and S. A. Wasserman (1994). "Diaphanous is required for cytokinesis in Drosophila and shares domains of similarity with the products of the limb deformity gene." Development **120**(12): 3367-3377.
Chen, J., T. Liu, X. Dong and Y. Hu (2009). "Recent development and SAR analysis of colchicine binding site inhibitors." Mini Rev Med Chem **9**(10): 1174-1190.
Chesarone, M. A., A. G. DuPage and B. L. Goode (2010). "Unleashing formins to remodel the actin and microtubule cytoskeletons." Nat Rev Mol Cell Biol **11**(1): 62-74.
Churchill, C. D., M. Klobukowski and J. A. Tuszynski (2015). "The Unique Binding Mode of Laulimalide to Two Tubulin Protofilaments." Chem Biol Drug Des **86**(2): 190-199.
Clark, E. A., P. M. Hills, B. S. Davidson, P. A. Wender and S. L. Mooberry (2006). "Laulimalide and synthetic laulimalide analogues are synergistic with paclitaxel and 2-methoxyestradiol." Mol Pharm **3**(4): 457-467.
Corley, D. G., R. Herb, R. E. Moore, P. J. Scheuer and V. J. Paul (1988). "Laulimalides. New potent cytotoxic macrolides from a marine sponge and a nudibranch predator." The Journal of Organic Chemistry **53**(15): 3644-3646.
Cowan, C. R. and A. A. Hyman (2004). "Asymmetric cell division in C. elegans: cortical polarity and spindle positioning." Annu Rev Cell Dev Biol **20**: 427-453.

Cowan, C. R. and A. A. Hyman (2007). "Acto-myosin reorganization and PAR polarity in C. elegans." Development **134**(6): 1035-1043.
D'Agostino, G., J. del Campo, B. Mellado, M. A. Izquierdo, T. Minarik, L. Cirri, L. Marini, J. L. Perez-Gracia and G. Scambia (2006). "A multicenter phase II study of the cryptophycin analog LY355703 in patients with platinum-resistant ovarian cancer." Int J Gynecol Cancer **16**(1): 71-76.
Dacheux, D., B. Roger, C. Bosc, N. Landrein, E. Roche, L. Chansel, T. Trian, A. Andrieux, A. Papaxanthos-Roche, R. Marthan, D. R. Robinson and M. Bonhivers (2015). "Human FAM154A (SAXO1) is a microtubule-stabilizing protein specific to cilia and related structures." J Cell Sci **128**(7): 1294-1307.
Daou, P., S. Hasan, D. Breitsprecher, E. Baudelet, L. Camoin, S. Audebert, B. L. Goode and A. Badache (2014). "Essential and nonredundant roles for Diaphanous formins in cortical microtubule capture and directed cell migration." Mol Biol Cell **25**(5): 658-668.
Davies, T., S. N. Jordan, V. Chand, J. A. Sees, K. Laband, A. X. Carvalho, M. Shirasu-Hiza, D. R. Kovar, J. Dumont and J. C. Canman (2014). "High-resolution temporal analysis reveals a functional timeline for the molecular regulation of cytokinesis." Dev Cell **30**(2): 209-223.
De Brabander, M., G. Geuens, R. Nuydens, R. Willebrords and J. De Mey (1981). "Taxol induces the assembly of free microtubules in living cells and blocks the organizing capacity of the centrosomes and kinetochores." Proc Natl Acad Sci U S A **78**(9): 5608-5612.
de Chaumont, F., S. Dallongeville, N. Chenouard, N. Herve, S. Pop, T. Provoost, V. Meas-Yedid, P. Pankajakshan, T. Lecomte, Y. Le Montagner, T. Lagache, A. Dufour and J. C. Olivo-Marin (2012). "Icy: an open bioimage informatics platform for extended reproducible research." Nat Methods **9**(7): 690-696.
Dechant, R. and M. Glotzer (2003). "Centrosome separation and central spindle assembly act in redundant pathways that regulate microtubule density and trigger cleavage furrow formation." Dev Cell **4**(3): 333-344.
Desai, A., P. S. Maddox, T. J. Mitchison and E. D. Salmon (1998). "Anaphase A chromosome movement and poleward spindle microtubule flux occur At similar rates in Xenopus extract spindles." J Cell Biol **141**(3): 703-713.
Desai, A. and T. J. Mitchison (1997). "Microtubule polymerization dynamics." Annu Rev Cell Dev Biol **13**: 83-117.
DeWard, A. D., K. Leali, R. A. West, G. C. Prendergast and A. S. Alberts (2009). "Loss of RhoB expression enhances the myelodysplastic phenotype of mammalian diaphanous-related Formin mDia1 knockout mice." PLoS One **4**(9): e7102.
Dhamodharan, R., M. A. Jordan, D. Thrower, L. Wilson and P. Wadsworth (1995). "Vinblastine suppresses dynamics of individual microtubules in living interphase cells." Mol Biol Cell **6**(9): 1215-1229.
di Pietro, F., A. Echard and X. Morin (2016). "Regulation of mitotic spindle orientation: an integrated view." EMBO Rep **17**(8): 1106-1130.
Di Vizio, D., J. Kim, M. H. Hager, M. Morello, W. Yang, C. J. Lafargue, L. D. True, M. A. Rubin, R. M. Adam, R. Beroukhim, F. Demichelis and M. R. Freeman (2009).

"Oncosome formation in prostate cancer: association with a region of frequent chromosomal deletion in metastatic disease." Cancer Res **69**(13): 5601-5609.
Don, S., N. M. Verrills, T. Y. Liaw, M. L. Liu, M. D. Norris, M. Haber and M. Kavallaris (2004). "Neuronal-associated microtubule proteins class III beta-tubulin and MAP2c in neuroblastoma: role in resistance to microtubule-targeted drugs." Mol Cancer Ther **3**(9): 1137-1146.
Doubrovinski, K., M. Swan, O. Polyakov and E. F. Wieschaus (2017). "Measurement of cortical elasticity in Drosophila melanogaster embryos using ferrofluids." Proc Natl Acad Sci U S A **114**(5): 1051-1056.
Dumontet, C. and M. A. Jordan (2010). "Microtubule-binding agents: a dynamic field of cancer therapeutics." Nat Rev Drug Discov **9**(10): 790-803.
Dumontet, C., M. A. Jordan and F. F. Lee (2009). "Ixabepilone: targeting betaIII-tubulin expression in taxane-resistant malignancies." Mol Cancer Ther **8**(1): 17-25.
Feierbach, B., F. Verde and F. Chang (2004). "Regulation of a formin complex by the microtubule plus end protein tea1p." J Cell Biol **165**(5): 697-707.
Frand, A. R., S. Russel and G. Ruvkun (2005). "Functional genomic analysis of C. elegans molting." PLoS Biol **3**(10): e312.
Fraser, A. G., C. James, G. I. Evan and M. O. Hengartner (1999). "Caenorhabditis elegans inhibitor of apoptosis protein (IAP) homologue BIR-1 plays a conserved role in cytokinesis." Curr Biol **9**(6): 292-301.
Fritzsche, M., C. Erlenkamper, E. Moeendarbary, G. Charras and K. Kruse (2016). "Actin kinetics shapes cortical network structure and mechanics." Sci Adv **2**(4): e1501337.
Gadea, B. B. and J. V. Ruderman (2006). "Aurora B is required for mitotic chromatin-induced phosphorylation of Op18/Stathmin." Proc Natl Acad Sci U S A **103**(12): 4493-4498.
Gaillard, J., V. Ramabhadran, E. Neumanne, P. Gurel, L. Blanchoin, M. Vantard and H. N. Higgs (2011). "Differential interactions of the formins INF2, mDia1, and mDia2 with microtubules." Mol Biol Cell **22**(23): 4575-4587.
Gapud, E. J., R. Bai, A. K. Ghosh and E. Hamel (2004). "Laulimalide and paclitaxel: a comparison of their effects on tubulin assembly and their synergistic action when present simultaneously." Mol Pharmacol **66**(1): 113-121.
Gerth, K., N. Bedorf, G. Hofle, H. Irschik and H. Reichenbach (1996). "Epothilons A and B: antifungal and cytotoxic compounds from Sorangium cellulosum (Myxobacteria). Production, physico-chemical and biological properties." J Antibiot (Tokyo) **49**(6): 560-563.
Gibbons, I. R. (1963). "Studies on the Protein Components of Cilia from Tetrahymena Pyriformis." Proc Natl Acad Sci U S A **50**: 1002-1010.
Gibbons, I. R. and A. J. Rowe (1965). "Dynein: A Protein with Adenosine Triphosphatase Activity from Cilia." Science **149**(3682): 424-426.
Glotzer, M. (2003). "Cytokinesis: progress on all fronts." Curr Opin Cell Biol **15**(6): 684-690.
Glotzer, M. (2005). "The molecular requirements for cytokinesis." Science **307**(5716): 1735-1739.

Gonczy, P., S. Pichler, M. Kirkham and A. A. Hyman (1999). "Cytoplasmic dynein is required for distinct aspects of MTOC positioning, including centrosome separation, in the one cell stage Caenorhabditis elegans embryo." J Cell Biol **147**(1): 135-150.
Goode, B. L. and M. J. Eck (2007). "Mechanism and function of formins in the control of actin assembly." Annu Rev Biochem **76**: 593-627.
Gornstein, E. and T. L. Schwarz (2014). "The paradox of paclitaxel neurotoxicity: Mechanisms and unanswered questions." Neuropharmacology **76 Pt A**: 175-183.
Gotta, M. and J. Ahringer (2001). "Distinct roles for Galpha and Gbetagamma in regulating spindle position and orientation in Caenorhabditis elegans embryos." Nat Cell Biol **3**(3): 297-300.
Greene, L. M., M. J. Meegan and D. M. Zisterer (2015). "Combretastatins: More Than Just Vascular Targeting Agents?" Journal of Pharmacology and Experimental Therapeutics **355**(2): 212-227.
Grill, S. W., P. Gonczy, E. H. Stelzer and A. A. Hyman (2001). "Polarity controls forces governing asymmetric spindle positioning in the Caenorhabditis elegans embryo." Nature **409**(6820): 630-633.
Grill, S. W., J. Howard, E. Schaffer, E. H. Stelzer and A. A. Hyman (2003). "The distribution of active force generators controls mitotic spindle position." Science **301**(5632): 518-521.
Grill, S. W., K. Kruse and F. Julicher (2005). "Theory of mitotic spindle oscillations." Phys Rev Lett **94**(10): 108104.

Gusnowski, E. M. (2010). "Analysis of microtubule motor proteins at the cortex of Caenorhabditis elegans one-cell embryos." Thesis

Gusnowski, E. M. and M. Srayko (2011). "Visualization of dynein-dependent microtubule gliding at the cell cortex: implications for spindle positioning." J Cell Biol **194**(3): 377-386.
Han, X., K. Adames, E. M. Sykes and M. Srayko (2015). "The KLP-7 Residue S546 Is a Putative Aurora Kinase Site Required for Microtubule Regulation at the Centrosome in C. elegans." PLoS One **10**(7): e0132593.
Hastie, S. B. (1991). "Interactions of colchicine with tubulin." Pharmacol Ther **51**(3): 377-401.
Haydar, T. F., E. Ang, Jr. and P. Rakic (2003). "Mitotic spindle rotation and mode of cell division in the developing telencephalon." Proc Natl Acad Sci U S A **100**(5): 2890-2895.
Higgs, H. N. (2005). "Formin proteins: a domain-based approach." Trends Biochem Sci **30**(6): 342-353.
Homem, C. C. and M. Peifer (2008). "Diaphanous regulates myosin and adherens junctions to control cell contractility and protrusive behavior during morphogenesis." Development **135**(6): 1005-1018.
Horvitz, H. R., S. Brenner, J. Hodgkin and R. K. Herman (1979). "A uniform genetic nomenclature for the nematode Caenorhabditis elegans." Mol Gen Genet **175**(2): 129-133.

Hubbard, E. J. and D. Greenstein (2000). "The Caenorhabditis elegans gonad: a test tube for cell and developmental biology." Dev Dyn **218**(1): 2-22.
Hyman, A. A., D. Chretien, I. Arnal and R. H. Wade (1995). "Structural changes accompanying GTP hydrolysis in microtubules: information from a slowly hydrolyzable analogue guanylyl-(alpha,beta)-methylene-diphosphonate." J Cell Biol **128**(1-2): 117-125.
Ishizaki, T., Y. Morishima, M. Okamoto, T. Furuyashiki, T. Kato and S. Narumiya (2001). "Coordination of microtubules and the actin cytoskeleton by the Rho effector mDia1." Nat Cell Biol **3**(1): 8-14.
Jankovics, F., R. Sinka, T. Lukacsovich and M. Erdelyi (2002). "MOESIN crosslinks actin and cell membrane in Drosophila oocytes and is required for OSKAR anchoring." Curr Biol **12**(23): 2060-2065.
Jantsch-Plunger, V., P. Gonczy, A. Romano, H. Schnabel, D. Hamill, R. Schnabel, A. A. Hyman and M. Glotzer (2000). "CYK-4: A Rho family gtpase activating protein (GAP) required for central spindle formation and cytokinesis." J Cell Biol **149**(7): 1391-1404.
Johnson, I. S., J. G. Armstrong, M. Gorman and J. P. Burnett, Jr. (1963). "The Vinca Alkaloids: A New Class of Oncolytic Agents." Cancer Res **23**: 1390-1427.
Johnson, I. S., H. F. Wright, G. H. Svoboda and J. Vlantis (1960). "Antitumor principles derived from Vinca rosea Linn. I. Vincaleukoblastine and leurosine." Cancer Res **20**: 1016-1022.
Jordan, M. A., K. Wendell, S. Gardiner, W. B. Derry, H. Copp and L. Wilson (1996). "Mitotic block induced in HeLa cells by low concentrations of paclitaxel (Taxol) results in abnormal mitotic exit and apoptotic cell death." Cancer Res **56**(4): 816-825.
Jourdain, L., P. Curmi, A. Sobel, D. Pantaloni and M. F. Carlier (1997). "Stathmin: a tubulin-sequestering protein which forms a ternary T2S complex with two tubulin molecules." Biochemistry **36**(36): 10817-10821.
Kaitna, S., M. Mendoza, V. Jantsch-Plunger and M. Glotzer (2000). "Incenp and an aurora-like kinase form a complex essential for chromosome segregation and efficient completion of cytokinesis." Curr Biol **10**(19): 1172-1181.
Kaltschmidt, J. A. and A. H. Brand (2002). "Asymmetric cell division: microtubule dynamics and spindle asymmetry." J Cell Sci **115**(Pt 11): 2257-2264.
Kamath, R. S. and J. Ahringer (2003). "Genome-wide RNAi screening in Caenorhabditis elegans." Methods **30**(4): 313-321.
Kamath, R. S., M. Martinez-Campos, P. Zipperlen, A. G. Fraser and J. Ahringer (2001). "Effectiveness of specific RNA-mediated interference through ingested double-stranded RNA in Caenorhabditis elegans." Genome Biol **2**(1): RESEARCH0002.
Kavallaris, M., A. S. Tait, B. J. Walsh, L. He, S. B. Horwitz, M. D. Norris and M. Haber (2001). "Multiple microtubule alterations are associated with Vinca alkaloid resistance in human leukemia cells." Cancer Res **61**(15): 5803-5809.
Kemphues, K. J., J. R. Priess, D. G. Morton and N. S. Cheng (1988). "Identification of genes required for cytoplasmic localization in early C. elegans embryos." Cell **52**(3): 311-320.

Kimura, A. and S. Onami (2005). "Computer simulations and image processing reveal length-dependent pulling force as the primary mechanism for C. elegans male pronuclear migration." Dev Cell **8**(5): 765-775.
King, S. J. and T. A. Schroer (2000). "Dynactin increases the processivity of the cytoplasmic dynein motor." Nat Cell Biol **2**(1): 20-24.
Kotak, S., C. Busso and P. Gonczy (2012). "Cortical dynein is critical for proper spindle positioning in human cells." J Cell Biol **199**(1): 97-110.
Kotak, S. and P. Gonczy (2013). "Mechanisms of spindle positioning: cortical force generators in the limelight." Curr Opin Cell Biol **25**(6): 741-748.
Kovar, D. R. (2006). "Cell polarity: formin on the move." Curr Biol **16**(14): R535-538.
Kozlowski, C., M. Srayko and F. Nedelec (2007). "Cortical microtubule contacts position the spindle in C. elegans embryos." Cell **129**(3): 499-510.
Kraut, R. and J. A. Campos-Ortega (1996). "inscuteable, a neural precursor gene of Drosophila, encodes a candidate for a cytoskeleton adaptor protein." Dev Biol **174**(1): 65-81.
Laan, L., N. Pavin, J. Husson, G. Romet-Lemonne, M. van Duijn, M. P. Lopez, R. D. Vale, F. Julicher, S. L. Reck-Peterson and M. Dogterom (2012). "Cortical dynein controls microtubule dynamics to generate pulling forces that position microtubule asters." Cell **148**(3): 502-514.
Labbe, J. C., E. K. McCarthy and B. Goldstein (2004). "The forces that position a mitotic spindle asymmetrically are tethered until after the time of spindle assembly." Journal of Cell Biology **167**(2): 245-256.
Lakhani, N. J., M. A. Sarkar, J. Venitz and W. D. Figg (2003). "2-Methoxyestradiol, a promising anticancer agent." Pharmacotherapy **23**(2): 165-172.
Lambier, A. and Y. Engelborghs (1980). "A quantitative analysis of tubulin-colchicine binding to microtubules." Eur J Biochem **109**(2): 619-624.
Leandro-Garcia, L. J., S. Leskela, I. Landa, C. Montero-Conde, E. Lopez-Jimenez, R. Leton, A. Cascon, M. Robledo and C. Rodriguez-Antona (2010). "Tumoral and tissue-specific expression of the major human beta-tubulin isotypes." Cytoskeleton (Hoboken) **67**(4): 214-223.
Lee, C. Y., B. D. Wilkinson, S. E. Siegrist, R. P. Wharton and C. Q. Doe (2006). "Brat is a Miranda cargo protein that promotes neuronal differentiation and inhibits neuroblast self-renewal." Dev Cell **10**(4): 441-449.
Lee, L., S. K. Klee, M. Evangelista, C. Boone and D. Pellman (1999). "Control of mitotic spindle position by the Saccharomyces cerevisiae formin Bni1p." J Cell Biol **144**(5): 947-961.
Liebmann, J. E., J. A. Cook, C. Lipschultz, D. Teague, J. Fisher and J. B. Mitchell (1993). "Cytotoxic studies of paclitaxel (Taxol) in human tumour cell lines." Br J Cancer **68**(6): 1104-1109.
Liu, J., M. J. Towle, H. Cheng, P. Saxton, C. Reardon, J. Wu, E. A. Murphy, G. Kuznetsov, C. W. Johannes, M. R. Tremblay, H. Zhao, M. Pesant, F. G. Fang, M. W. Vermeulen, B. M. Gallagher, Jr. and B. A. Littlefield (2007). "In vitro and in vivo anticancer activities of synthetic (-)-laulimalide, a marine natural product microtubule stabilizing agent." Anticancer Res **27**(3B): 1509-1518.

Liu, R., E. V. Linardopoulou, G. E. Osborn and S. M. Parkhurst (2010). "Formins in development: orchestrating body plan origami." Biochim Biophys Acta **1803**(2): 207-225.
Lu, B., M. Rothenberg, L. Y. Jan and Y. N. Jan (1998). "Partner of Numb colocalizes with Numb during mitosis and directs Numb asymmetric localization in Drosophila neural and muscle progenitors." Cell **95**(2): 225-235.
Lu, M. S. and C. A. Johnston (2013). "Molecular pathways regulating mitotic spindle orientation in animal cells." Development **140**(9): 1843-1856.
Lynch, E. D., M. K. Lee, J. E. Morrow, P. L. Welcsh, P. E. Leon and M. C. King (1997). "Nonsyndromic deafness DFNA1 associated with mutation of a human homolog of the Drosophila gene diaphanous." Science **278**(5341): 1315-1318.
Maddox, A. S., B. Habermann, A. Desai and K. Oegema (2005). "Distinct roles for two C. elegans anillins in the gonad and early embryo." Development **132**(12): 2837-2848.
Maddox, A. S., L. Lewellyn, A. Desai and K. Oegema (2007). "Anillin and the septins promote asymmetric ingression of the cytokinetic furrow." Dev Cell **12**(5): 827-835.
Marty, M., P. Fumoleau, A. Adenis, Y. Rousseau, Y. Merrouche, G. Robinet, I. Senac and C. Puozzo (2001). "Oral vinorelbine pharmacokinetics and absolute bioavailability study in patients with solid tumors." Ann Oncol **12**(11): 1643-1649.
Mason, F. M., M. Tworoger and A. C. Martin (2013). "Apical domain polarization localizes actin-myosin activity to drive ratchet-like apical constriction." Nat Cell Biol **15**(8): 926-936.
Mass, R. L., R. Zeller, R. P. Woychik, T. F. Vogt and P. Leder (1990). "Disruption of formin-encoding transcripts in two mutant limb deformity alleles." Nature **346**(6287): 853-855.
Mayer, M., M. Depken, J. S. Bois, F. Julicher and S. W. Grill (2010). "Anisotropies in cortical tension reveal the physical basis of polarizing cortical flows." Nature **467**(7315): 617-621.
Meunier, S. and I. Vernos (2011). "K-fibre minus ends are stabilized by a RanGTP-dependent mechanism essential for functional spindle assembly." Nat Cell Biol **13**(12): 1406-1414.
Mi-Mi, L. and D. Pruyne (2015). "Loss of Sarcomere-associated Formins Disrupts Z-line Organization, but does not Prevent Thin Filament Assembly in Caenorhabditis elegans Muscle." J Cytol Histol **6**(2).
Mi-Mi, L., S. Votra, K. Kemphues, A. Bretscher and D. Pruyne (2012). "Z-line formins promote contractile lattice growth and maintenance in striated muscles of C. elegans." J Cell Biol **198**(1): 87-102.
Mitchison, T. and M. Kirschner (1984). "Dynamic instability of microtubule growth." Nature **312**(5991): 237-242.
Mitchison, T. J. (1993). "Localization of an exchangeable GTP binding site at the plus end of microtubules." Science **261**(5124): 1044-1047.
Monen, J., P. S. Maddox, F. Hyndman, K. Oegema and A. Desai (2005). "Differential role of CENP-A in the segregation of holocentric C. elegans chromosomes during meiosis and mitosis." Nat Cell Biol **7**(12): 1248-1255.

Mooberry, S. L., G. Tien, A. H. Hernandez, A. Plubrukarn and B. S. Davidson (1999). "Laulimalide and isolaulimalide, new paclitaxel-like microtubule-stabilizing agents." Cancer Res **59**(3): 653-660.
Moores, C. A., M. Yu, J. Guo, C. Beraud, R. Sakowicz and R. A. Milligan (2002). "A mechanism for microtubule depolymerization by KinI kinesins." Mol Cell **9**(4): 903-909.
Moorhouse, K. S. and D. R. Burgess (2014). "How to be at the right place at the right time: the importance of spindle positioning in embryos." Mol Reprod Dev **81**(10): 884-895.
Morton, D. G., D. C. Shakes, S. Nugent, D. Dichoso, W. Wang, A. Golden and K. J. Kemphues (2002). "The Caenorhabditis elegans par-5 gene encodes a 14-3-3 protein required for cellular asymmetry in the early embryo." Dev Biol **241**(1): 47-58.
Motegi, F. and A. Sugimoto (2006). "Sequential functioning of the ECT-2 RhoGEF, RHO-1 and CDC-42 establishes cell polarity in Caenorhabditis elegans embryos." Nat Cell Biol **8**(9): 978-985.
Munro, E., J. Nance and J. R. Priess (2004). "Cortical flows powered by asymmetrical contraction transport PAR proteins to establish and maintain anterior-posterior polarity in the early C. elegans embryo." Dev Cell **7**(3): 413-424.
Neidt, E. M., C. T. Skau and D. R. Kovar (2008). "The cytokinesis formins from the nematode worm and fission yeast differentially mediate actin filament assembly." J Biol Chem **283**(35): 23872-23883.
Nguyen-Ngoc, T., K. Afshar and P. Gonczy (2007). "Coupling of cortical dynein and G alpha proteins mediates spindle positioning in Caenorhabditis elegans." Nat Cell Biol **9**(11): 1294-1302.
Noble, R. L., C. T. Beer and J. H. Cutts (1958). "Role of chance observations in chemotherapy: Vinca rosea." Ann N Y Acad Sci **76**(3): 882-894.
Nogales, E., M. Whittaker, R. A. Milligan and K. H. Downing (1999). "High-resolution model of the microtubule." Cell **96**(1): 79-88.
Nogales, E., S. G. Wolf, I. A. Khan, R. F. Luduena and K. H. Downing (1995). "Structure of tubulin at 6.5 A and location of the taxol-binding site." Nature **375**(6530): 424-427.
O'Rourke, S. M., C. Carter, L. Carter, S. N. Christensen, M. P. Jones, B. Nash, M. H. Price, D. W. Turnbull, A. R. Garner, D. R. Hamill, V. R. Osterberg, R. Lyczak, E. E. Madison, M. H. Nguyen, N. A. Sandberg, N. Sedghi, J. H. Willis, J. Yochem, E. A. Johnson and B. Bowerman (2011). "A survey of new temperature-sensitive, embryonic-lethal mutations in C. elegans: 24 alleles of thirteen genes." PLoS One **6**(3): e16644.
O'Rourke, S. M., S. N. Christensen and B. Bowerman (2010). "Caenorhabditis elegans EFA-6 limits microtubule growth at the cell cortex." Nat Cell Biol **12**(12): 1235-1241.
O'Rourke, S. M., M. D. Dorfman, J. C. Carter and B. Bowerman (2007). "Dynein modifiers in C. elegans: light chains suppress conditional heavy chain mutants." PLoS Genet **3**(8): e128.

O'Toole, E., G. Greenan, K. I. Lange, M. Srayko and T. Muller-Reichert (2012). "The role of gamma-tubulin in centrosomal microtubule organization." PLoS One **7**(1): e29795.
Oakley, B. R., V. Paolillo and Y. Zheng (2015). "gamma-Tubulin complexes in microtubule nucleation and beyond." Mol Biol Cell **26**(17): 2957-2962.
Oegema, K., A. Desai, S. Rybina, M. Kirkham and A. A. Hyman (2001). "Functional analysis of kinetochore assembly in Caenorhabditis elegans." J Cell Biol **153**(6): 1209-1226.
Oegema, K. and T. J. Mitchison (1997). "Rappaport rules: cleavage furrow induction in animal cells." Proc Natl Acad Sci U S A **94**(10): 4817-4820.
Ohi, R., T. Sapra, J. Howard and T. J. Mitchison (2004). "Differentiation of cytoplasmic and meiotic spindle assembly MCAK functions by Aurora B-dependent phosphorylation." Mol Biol Cell **15**(6): 2895-2906.
Olson, S. K., G. Greenan, A. Desai, T. Muller-Reichert and K. Oegema (2012). "Hierarchical assembly of the eggshell and permeability barrier in C. elegans." J Cell Biol **198**(4): 731-748.
Otomo, T., D. R. Tomchick, C. Otomo, S. C. Panchal, M. Machius and M. K. Rosen (2005). "Structural basis of actin filament nucleation and processive capping by a formin homology 2 domain." Nature **433**(7025): 488-494.
Owellen, R. J., C. A. Hartke, R. M. Dickerson and F. O. Hains (1976). "Inhibition of tubulin-microtubule polymerization by drugs of the Vinca alkaloid class." Cancer Res **36**(4): 1499-1502.
Park, D. H. and L. S. Rose (2008). "Dynamic localization of LIN-5 and GPR-1/2 to cortical force generation domains during spindle positioning." Dev Biol **315**(1): 42-54.
Pearson, C. G. and K. Bloom (2004). "Dynamic microtubules lead the way for spindle positioning." Nat Rev Mol Cell Biol **5**(6): 481-492.
Pecreaux, J., J. C. Roper, K. Kruse, F. Julicher, A. A. Hyman, S. W. Grill and J. Howard (2006). "Spindle oscillations during asymmetric cell division require a threshold number of active cortical force generators." Curr Biol **16**(21): 2111-2122.
Piekny, A., M. Werner and M. Glotzer (2005). "Cytokinesis: welcome to the Rho zone." Trends Cell Biol **15**(12): 651-658.
Piekny, A. J. and M. Glotzer (2008). "Anillin is a scaffold protein that links RhoA, actin, and myosin during cytokinesis." Curr Biol **18**(1): 30-36.
Piekny, A. J. and P. E. Mains (2002). "Rho-binding kinase (LET-502) and myosin phosphatase (MEL-11) regulate cytokinesis in the early Caenorhabditis elegans embryo." J Cell Sci **115**(Pt 11): 2271-2282.
Poi, M. J., M. Berger, M. Lustberg, R. Layman, C. L. Shapiro, B. Ramaswamy, E. Mrozek, E. Olson and R. Wesolowski (2013). "Docetaxel-induced skin toxicities in breast cancer patients subsequent to paclitaxel shortage: a case series and literature review." Support Care Cancer **21**(10): 2679-2686.
Prokopenko, S. N., A. Brumby, L. O'Keefe, L. Prior, Y. He, R. Saint and H. J. Bellen (1999). "A putative exchange factor for Rho1 GTPase is required for initiation of cytokinesis in Drosophila." Genes Dev **13**(17): 2301-2314.
Pryor, D. E., A. O'Brate, G. Bilcer, J. F. Diaz, Y. Wang, Y. Wang, M. Kabaki, M. K. Jung, J. M. Andreu, A. K. Ghosh, P. Giannakakou and E. Hamel (2002). "The microtubule

stabilizing agent laulimalide does not bind in the taxoid site, kills cells resistant to paclitaxel and epothilones, and may not require its epoxide moiety for activity." Biochemistry **41**(29): 9109-9115.
Ramalingam, N., C. Franke, E. Jaschinski, M. Winterhoff, Y. Lu, S. Bruhmann, A. Junemann, H. Meier, A. A. Noegel, I. Weber, H. Zhao, R. Merkel, M. Schleicher and J. Faix (2015). "A resilient formin-derived cortical actin meshwork in the rear drives actomyosin-based motility in 2D confinement." Nat Commun **6**: 8496.
Rappaport, R. (1961). "Experiments concerning the cleavage stimulus in sand dollar eggs." J Exp Zool **148**: 81-89.
Rappaport, R. (1983). "Cytokinesis: Effects of blocks between the mitotic apparatus and the surface on furrow establishment in flattened echinoderm eggs." Journal of Experimental Zoology **227**: 213-227.
Rappaport, R. (1996). "Cytokinesis in Animal Cells." Cambridge: Cambridge University Press.
Rappaport, R. (1997). "Cleavage furrow establishment by the moving mitotic apparatus." Dev Growth Differ **39**(2): 221-226.
Redemann, S., J. Pecreaux, N. W. Goehring, K. Khairy, E. H. Stelzer, A. A. Hyman and J. Howard (2010). "Membrane invaginations reveal cortical sites that pull on mitotic spindles in one-cell C. elegans embryos." PLoS One **5**(8): e12301.
Roberts, W. N., M. H. Liang and S. H. Stern (1987). "Colchicine in acute gout. Reassessment of risks and benefits." JAMA **257**(14): 1920-1922.
Rodriguez, O. C., A. W. Schaefer, C. A. Mandato, P. Forscher, W. M. Bement and C. M. Waterman-Storer (2003). "Conserved microtubule-actin interactions in cell movement and morphogenesis." Nat Cell Biol **5**(7): 599-609.
Romano, A., A. Guse, I. Krascenicova, H. Schnabel, R. Schnabel and M. Glotzer (2003). "CSC-1: a subunit of the Aurora B kinase complex that binds to the survivin-like protein BIR-1 and the incenp-like protein ICP-1." J Cell Biol **161**(2): 229-236.
Rosales-Nieves, A. E., J. E. Johndrow, L. C. Keller, C. R. Magie, D. M. Pinto-Santini and S. M. Parkhurst (2006). "Coordination of microtubule and microfilament dynamics by Drosophila Rho1, Spire and Cappuccino." Nat Cell Biol **8**(4): 367-376.
Rowinsky, E. K. and R. C. Donehower (1995). "Paclitaxel (taxol)." N Engl J Med **332**(15): 1004-1014.
Salbreux, G., G. Charras and E. Paluch (2012). "Actin cortex mechanics and cellular morphogenesis." Trends Cell Biol **22**(10): 536-545.
Schierenberg, E. and W. B. Wood (1985). "Control of cell-cycle timing in early embryos of Caenorhabditis elegans." Dev Biol **107**(2): 337-354.
Schiff, P. B., J. Fant and S. B. Horwitz (1979). "Promotion of microtubule assembly in vitro by taxol." Nature **277**(5698): 665-667.
Schiff, P. B. and S. B. Horwitz (1980). "Taxol stabilizes microtubules in mouse fibroblast cells." Proc Natl Acad Sci U S A **77**(3): 1561-1565.
Schmidt, D. J., D. J. Rose, W. M. Saxton and S. Strome (2005). "Functional analysis of cytoplasmic dynein heavy chain in Caenorhabditis elegans with fast-acting temperature-sensitive mutations." Mol Biol Cell **16**(3): 1200-1212.

Schmidt, H. and A. P. Carter (2016). "Review: Structure and mechanism of the dynein motor ATPase." Biopolymers **105**(8): 557-567.
Schonegg, S. and A. A. Hyman (2006). "CDC-42 and RHO-1 coordinate acto-myosin contractility and PAR protein localization during polarity establishment in C. elegans embryos." Development **133**(18): 3507-3516.
Schonegg, S., A. A. Hyman and W. B. Wood (2014). "Timing and mechanism of the initial cue establishing handed left-right asymmetry in Caenorhabditis elegans embryos." Genesis **52**(6): 572-580.
Severson, A. F., D. L. Baillie and B. Bowerman (2002). "A Formin Homology protein and a profilin are required for cytokinesis and Arp2/3-independent assembly of cortical microfilaments in C. elegans." Curr Biol **12**(24): 2066-2075.
Severson, A. F., D. R. Hamill, J. C. Carter, J. Schumacher and B. Bowerman (2000). "The aurora-related kinase AIR-2 recruits ZEN-4/CeMKLP1 to the mitotic spindle at metaphase and is required for cytokinesis." Curr Biol **10**(19): 1162-1171.
Shaye, D. D. and I. Greenwald (2011). "OrthoList: a compendium of C. elegans genes with human orthologs." PLoS One **6**(5): e20085.
Shelton, C. A., J. C. Carter, G. C. Ellis and B. Bowerman (1999). "The nonmuscle myosin regulatory light chain gene mlc-4 is required for cytokinesis, anterior-posterior polarity, and body morphology during Caenorhabditis elegans embryogenesis." J Cell Biol **146**(2): 439-451.
Shimogawa, M. M., P. O. Widlund, M. Riffle, M. Ess and T. N. Davis (2009). "Bir1 is required for the tension checkpoint." Mol Biol Cell **20**(3): 915-923.
Skop, A. R. and J. G. White (1998). "The dynactin complex is required for cleavage plane specification in early Caenorhabditis elegans embryos." Curr Biol **8**(20): 1110-1116.
Skoufias, D. A., C. Mollinari, F. B. Lacroix and R. L. Margolis (2000). "Human survivin is a kinetochore-associated passenger protein." J Cell Biol **151**(7): 1575-1582.
Smoter, M., L. Bodnar, R. Duchnowska, R. Stec, B. Grala and C. Szczylik (2011). "The role of Tau protein in resistance to paclitaxel." Cancer Chemother Pharmacol **68**(3): 553-557.
Spana, E. P., C. Kopczynski, C. S. Goodman and C. Q. Doe (1995). "Asymmetric localization of numb autonomously determines sibling neuron identity in the Drosophila CNS." Development **121**(11): 3489-3494.
Speliotes, E. K., A. Uren, D. Vaux and H. R. Horvitz (2000). "The survivin-like C. elegans BIR-1 protein acts with the Aurora-like kinase AIR-2 to affect chromosomes and the spindle midzone." Mol Cell **6**(2): 211-223.
Spiro, Z., K. Thyagarajan, A. De Simone, S. Trager, K. Afshar and P. Gonczy (2014). "Clathrin regulates centrosome positioning by promoting acto-myosin cortical tension in C. elegans embryos." Development **141**(13): 2712-2723.
Srayko, M., A. Kaya, J. Stamford and A. A. Hyman (2005). "Identification and characterization of factors required for microtubule growth and nucleation in the early C. elegans embryo." Dev Cell **9**(2): 223-236.
Srayko, M., T. O'Toole E, A. A. Hyman and T. Muller-Reichert (2006). "Katanin disrupts the microtubule lattice and increases polymer number in C. elegans meiosis." Curr Biol **16**(19): 1944-1949.

Srinivasan, D. G., R. M. Fisk, H. Xu and S. van den Heuvel (2003). "A complex of LIN-5 and GPR proteins regulates G protein signaling and spindle function in C elegans." Genes Dev **17**(10): 1225-1239.
Stewart, M. P., J. Helenius, Y. Toyoda, S. P. Ramanathan, D. J. Muller and A. A. Hyman (2011). "Hydrostatic pressure and the actomyosin cortex drive mitotic cell rounding." Nature **469**(7329): 226-230.
Swan, K. A., A. F. Severson, J. C. Carter, P. R. Martin, H. Schnabel, R. Schnabel and B. Bowerman (1998). "cyk-1: a C. elegans FH gene required for a late step in embryonic cytokinesis." J Cell Sci **111 (Pt 14)**: 2017-2027.
Szafer-Glusman, E., M. T. Fuller and M. G. Giansanti (2011). "Role of Survivin in cytokinesis revealed by a separation-of-function allele." Mol Biol Cell **22**(20): 3779-3790.
Tabuse, Y., Y. Izumi, F. Piano, K. J. Kemphues, J. Miwa and S. Ohno (1998). "Atypical protein kinase C cooperates with PAR-3 to establish embryonic polarity in Caenorhabditis elegans." Development **125**(18): 3607-3614.
Tanaka, S., T. Nohara, M. Iwamoto, K. Sumiyoshi, K. Kimura, Y. Takahashi and N. Tanigawa (2009). "Tau expression and efficacy of paclitaxel treatment in metastatic breast cancer." Cancer Chemother Pharmacol **64**(2): 341-346.
Tatsumoto, T., X. Xie, R. Blumenthal, I. Okamoto and T. Miki (1999). "Human ECT2 is an exchange factor for Rho GTPases, phosphorylated in G2/M phases, and involved in cytokinesis." J Cell Biol **147**(5): 921-928.
Tegha-Dunghu, J., E. M. Gusnowski and M. Srayko (2014). "Measuring microtubule growth and gliding in Caenorhabditis elegans embryos." Methods Mol Biol **1136**: 103-116.
Torres, K. and S. B. Horwitz (1998). "Mechanisms of Taxol-induced cell death are concentration dependent." Cancer Res **58**(16): 3620-3626.
Toyoshima, F. and E. Nishida (2007). "Integrin-mediated adhesion orients the spindle parallel to the substratum in an EB1- and myosin X-dependent manner." EMBO J **26**(6): 1487-1498.
Tozer, G. M., C. Kanthou, C. S. Parkins and S. A. Hill (2002). "The biology of the combretastatins as tumour vascular targeting agents." International Journal of Experimental Pathology **83**(1): 21-38.
Truong, D., D. Brabant, M. Bashkurov, L. C. Wan, V. Braun, W. D. Heo, T. Meyer, L. Pelletier, J. Copeland and J. H. Brumell (2013). "Formin-mediated actin polymerization promotes Salmonella invasion." Cell Microbiol **15**(12): 2051-2063.
Truong, D., J. W. Copeland and J. H. Brumell (2014). "Bacterial subversion of host cytoskeletal machinery: hijacking formins and the Arp2/3 complex." Bioessays **36**(7): 687-696.
Tse, Y. C., A. Piekny and M. Glotzer (2011). "Anillin promotes astral microtubule-directed cortical myosin polarization." Mol Biol Cell **22**(17): 3165-3175.
Tse, Y. C., M. Werner, K. M. Longhini, J. C. Labbe, B. Goldstein and M. Glotzer (2012). "RhoA activation during polarization and cytokinesis of the early Caenorhabditis elegans embryo is differentially dependent on NOP-1 and CYK-4." Mol Biol Cell **23**(20): 4020-4031.

Tsou, M. F., A. Hayashi and L. S. Rose (2003). "LET-99 opposes Galpha/GPR signaling to generate asymmetry for spindle positioning in response to PAR and MES-1/SRC-1 signaling." Development **130**(23): 5717-5730.
Uemura, T., S. Shepherd, L. Ackerman, L. Y. Jan and Y. N. Jan (1989). "numb, a gene required in determination of cell fate during sensory organ formation in Drosophila embryos." Cell **58**(2): 349-360.
Vallee, R. B., J. C. Williams, D. Varma and L. E. Barnhart (2004). "Dynein: An ancient motor protein involved in multiple modes of transport." J Neurobiol **58**(2): 189-200.
van Vuuren, R. J., M. H. Visagie, A. E. Theron and A. M. Joubert (2015). "Antimitotic drugs in the treatment of cancer." Cancer Chemother Pharmacol **76**(6): 1101-1112.
Vanneste, C. A., D. Pruyne and P. E. Mains (2013). "The role of the formin gene fhod-1 in C. elegans embryonic morphogenesis." Worm **2**(3): e25040.
Vasquez, R. J., B. Howell, A. M. Yvon, P. Wadsworth and L. Cassimeris (1997). "Nanomolar concentrations of nocodazole alter microtubule dynamic instability in vivo and in vitro." Mol Biol Cell **8**(6): 973-985.
Verdier-Pinard, P., S. Shahabi, F. Wang, B. Burd, H. Xiao, G. L. Goldberg, G. A. Orr and S. B. Horwitz (2005). "Detection of human betaV-tubulin expression in epithelial cancer cell lines by tubulin proteomics." Biochemistry **44**(48): 15858-15870.
Vinzenz, M., M. Nemethova, F. Schur, J. Mueller, A. Narita, E. Urban, C. Winkler, C. Schmeiser, S. A. Koestler, K. Rottner, G. P. Resch, Y. Maeda and J. V. Small (2012). "Actin branching in the initiation and maintenance of lamellipodia." J Cell Sci **125**(Pt 11): 2775-2785.
Walker, R. A., E. T. O'Brien, N. K. Pryer, M. F. Soboeiro, W. A. Voter, H. P. Erickson and E. D. Salmon (1988). "Dynamic instability of individual microtubules analyzed by video light microscopy: rate constants and transition frequencies." J Cell Biol **107**(4): 1437-1448.
Wani, M. C., H. L. Taylor, M. E. Wall, P. Coggon and A. T. McPhail (1971). "Plant antitumor agents. VI. Isolation and structure of taxol, a novel antileukemic and antitumor agent from Taxus brevifolia." Journal of the American Chemical Society **93**(9): 2325-2327.
Watanabe, N., T. Kato, A. Fujita, T. Ishizaki and S. Narumiya (1999). "Cooperation between mDia1 and ROCK in Rho-induced actin reorganization." Nat Cell Biol **1**(3): 136-143.
Watanabe, S., K. Okawa, T. Miki, S. Sakamoto, T. Morinaga, K. Segawa, T. Arakawa, M. Kinoshita, T. Ishizaki and S. Narumiya (2010). "Rho and anillin-dependent control of mDia2 localization and function in cytokinesis." Mol Biol Cell **21**(18): 3193-3204.
Watts, J. L., B. Etemad-Moghadam, S. Guo, L. Boyd, B. W. Draper, C. C. Mello, J. R. Priess and K. J. Kemphues (1996). "par-6, a gene involved in the establishment of asymmetry in early C. elegans embryos, mediates the asymmetric localization of PAR-3." Development **122**(10): 3133-3140.

Wendell, K. L., L. Wilson and M. A. Jordan (1993). "Mitotic block in HeLa cells by vinblastine: ultrastructural changes in kinetochore-microtubule attachment and in centrosomes." J Cell Sci **104 (Pt 2)**: 261-274.
Werner, M., E. Munro and M. Glotzer (2007). "Astral signals spatially bias cortical myosin recruitment to break symmetry and promote cytokinesis." Curr Biol **17**(15): 1286-1297.
Widlund, P. O., J. H. Stear, A. Pozniakovsky, M. Zanic, S. Reber, G. J. Brouhard, A. A. Hyman and J. Howard (2011). "XMAP215 polymerase activity is built by combining multiple tubulin-binding TOG domains and a basic lattice-binding region." Proc Natl Acad Sci U S A **108**(7): 2741-2746.
Wilson, L., M. A. Jordan, A. Morse and R. L. Margolis (1982). "Interaction of vinblastine with steady-state microtubules in vitro." J Mol Biol **159**(1): 125-149.
Wolfe, B. A., T. Takaki, M. Petronczki and M. Glotzer (2009). "Polo-like kinase 1 directs assembly of the HsCyk-4 RhoGAP/Ect2 RhoGEF complex to initiate cleavage furrow formation." PLoS Biol **7**(5): e1000110.
Woychik, R. P., R. L. Maas, R. Zeller, T. F. Vogt and P. Leder (1990). "'Formins': proteins deduced from the alternative transcripts of the limb deformity gene." Nature **346**(6287): 850-853.
Yang, C. P. and S. S. Fan (2008). "Drosophila mars is required for organizing kinetochore microtubules during mitosis." Exp Cell Res **314**(17): 3209-3220.
Yvon, A. M., P. Wadsworth and M. A. Jordan (1999). "Taxol suppresses dynamics of individual microtubules in living human tumor cells." Mol Biol Cell **10**(4): 947-959.
Zaoui, K., K. Benseddik, P. Daou, D. Salaun and A. Badache (2010). "ErbB2 receptor controls microtubule capture by recruiting ACF7 to the plasma membrane of migrating cells." Proc Natl Acad Sci U S A **107**(43): 18517-18522.
Zhu, X. L., L. Liang and Y. Q. Ding (2008). "Overexpression of FMNL2 is closely related to metastasis of colorectal cancer." Int J Colorectal Dis **23**(11): 1041-1047.

Appendix

Generating FH1 domain point mutants for CYK-1 using CRISPR-Cas9 system:
The DNA sequence of CYK-1 FH1 domain is shown below. The three PAM sites have been highlighted in blue. The sgRNA sequence for each PAM site is highlighted in "bold".

TCTACCGCCAATAACTGGAGGTCCACCACCACCTCCAG
GTCTCCCACCAATCACAGGAGGGCCGCCTCCACCTC
CTCCTCCTG**GTGGTCTTCCTCCAATCAC**CGGAGGACC
CCCGCCGCCGCCTCCACCGG**GAGGATTGCCTCCAATA**
TCTGGAGGTCCTCCACCACCTCCGCCGCCTCCTGGAG
GATGTCCACCTCCACCTCCTCCACCACCACCGGGAGGG
TTCAAGGGCGGACCGCCACCACCACCTCCTCCA

Cyk-1 F sgRNA#1	5'GTCTCCCACCAATCACAGGTTTTAGAGCTAGA AATAGCAAGTTA-3'
Cyk-1 R sgRNA#1	5'CCTGTGATTGGTGGGAGACAAACATTTAGATT TGCAATTCAATTATATATAG-3'
Cyk-1 F sgRNA#2	5'GTGGTCTTCCTCCAATCACTTTTAGAGCTAGA AATAGCAAGTTA-3'
Cyk-1 R sgRNA#2	5'GTGATTGGAGGAAGACCACAAACATTTAGAT TTGCAATTCAATTATATATAG-3'
Cyk-1 F sgRNA#3	5'GAGGATTGCCTCCAATATCTTTTAGAGCTAGA AATAGCAAGTTA-3'
Cyk-1 R sgRNA#3	5'GATATTGGAGGCAATCCTCAAACATTTAGATT TGCAATTCAATTATATATAG-3'

Cyk-1 FH1 domain sgRNA primer sequences:

Primer name	Primer sequence
U6 promoter EcoRI F primer	5'-CGG**GAATTC**CTCCAAGAACTCGTACAAAAATGCTCT-3'
U6 promoter HindIII R primer	5'-CGG**AAGCTT**CACAGCCGACTATGTTTGGCGT-3'

U6 promoter primer sequences:

The EcoRI and HindIII restriction sites are bold and underlined

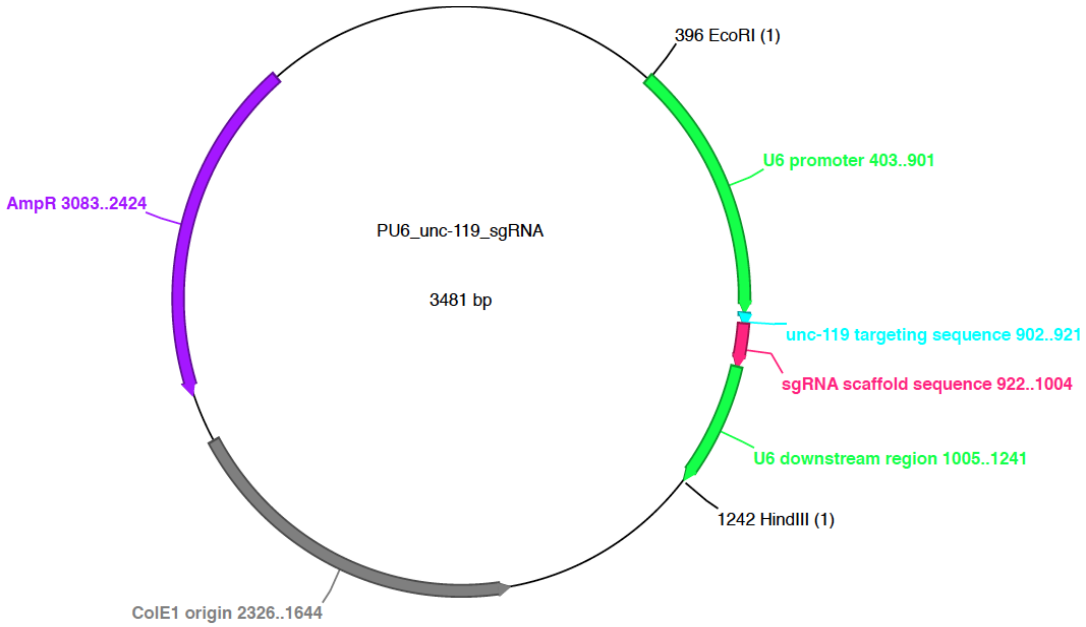

Starting plasmid with unc-119 sequence

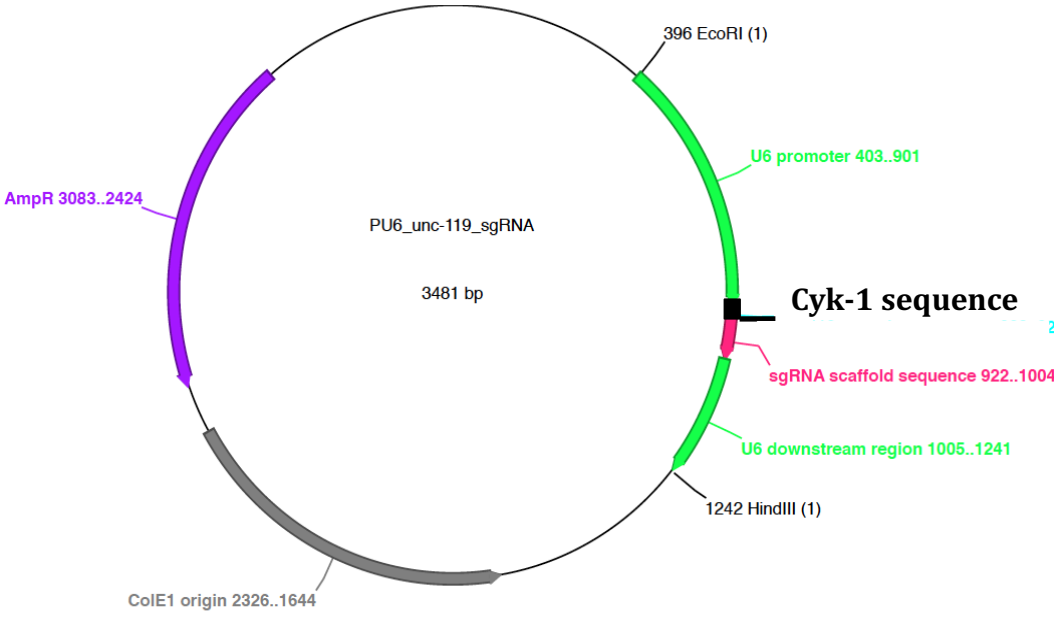

End product after PCR with CYK-1 sequence swapped in

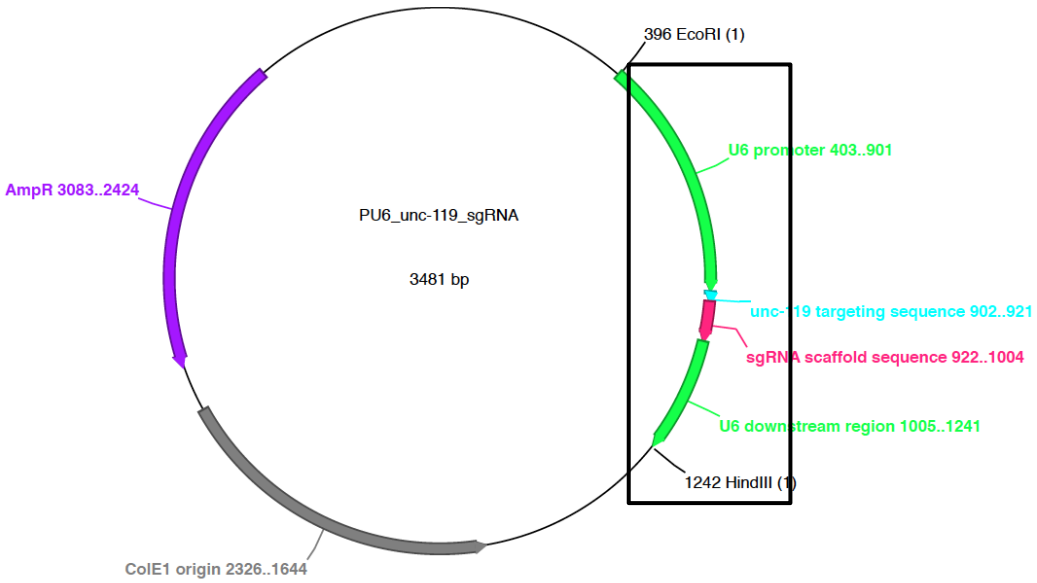

Addgene plasmid # 46169. Addgene PU6_unc119_sgRNA plasmid. Images adapted from https://www.addgene.org/46169/

Steps for PCR reaction:

1. Swap out the Unc-119 targeting sequence and insert the region of interest (the 3 different cyk-1sgRNA sequences). Two PCR reactions (PCR#1 and PCR#2) are performed to achieve this step as shown in the figure below. Only the highlighted section of the plasmid is shown in the PCR steps below.
2. Mix the two PCR fragments (a 500 bp fragment and a 300 bp fragment) and perform PCR#3 to get a fragment of ~800 bp in length.
3. Gel extract PCR#3 (~800 bp), RE digest, ligate & transform
4. Colony PCR to check the clones
5. Plasmid extraction and sequencing of the positive clones.

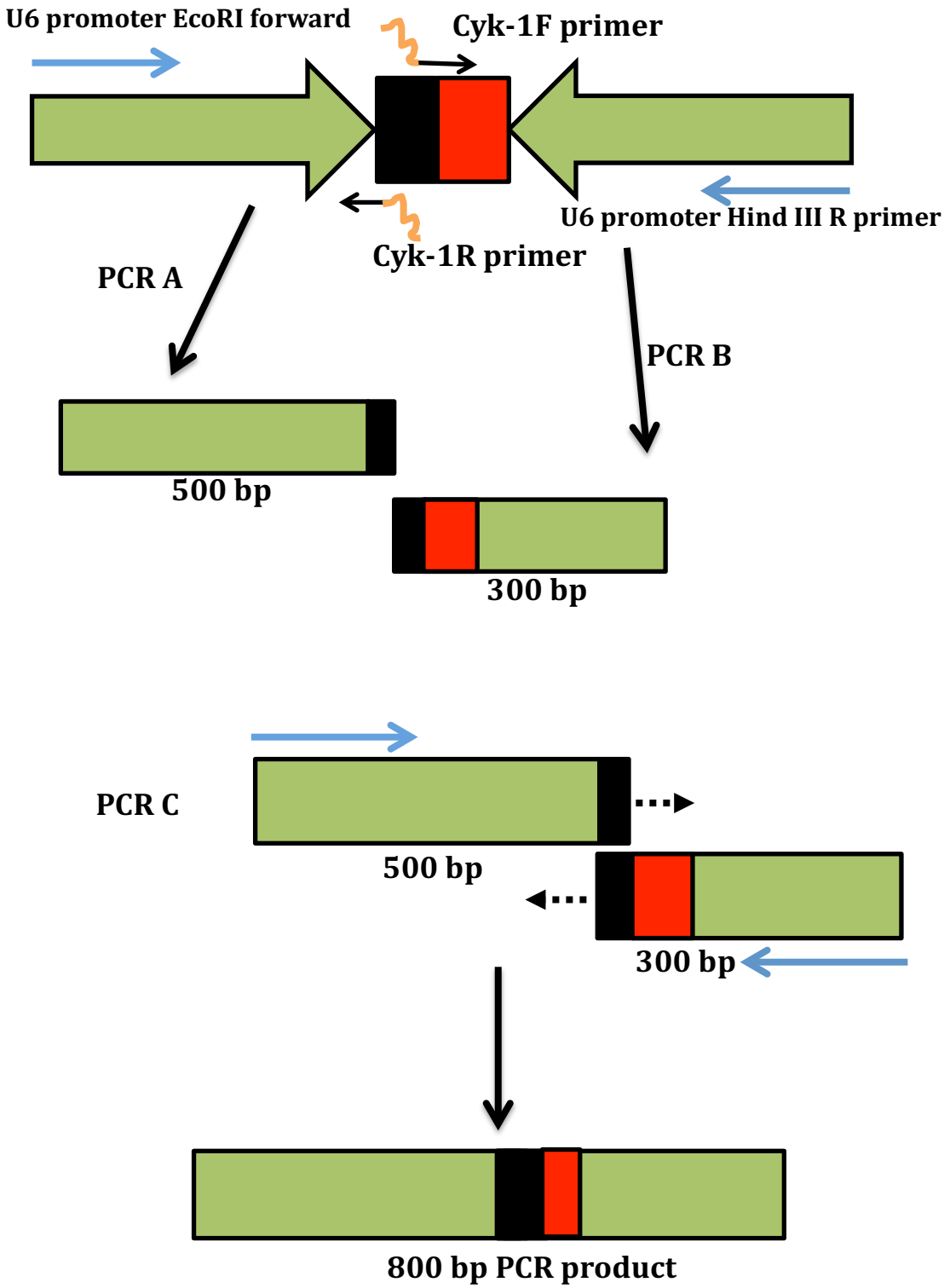
U6 promoter EcoRI forward
Cyk-1F primer
U6 promoter Hind III R primer
Cyk-1R primer
PCR A
PCR B
500 bp
300 bp
PCR C
500 bp
300 bp
800 bp PCR product

800 bp PCR product

Gel extraction of the RE digested products

Ligation reaction

Transformation

Colony PCR to check the clones, plasmid extraction and sequencing

1. Amplifying the 500 bp and 300 bp regions to swap out the sgRNA scaffold from the plasmid. 50 µl PCR A & B reactions were performed with 5ng plasmid DNA as template. Annealing temperature was optimized at 60 °C. Extension times were estimated based on predicted product size for the reaction. Gel extraction was done using Qiagen Gel Extraction kit.

PCR cycle for 500 bp product	PCR cycle for 300 bp product	
94°C x 2 minutes	94°C x 2 minutes	
94°C x 15 seconds	94°C x 15 seconds	30 cycles
60°C x 30 seconds	60°C x 30 seconds	
72°C x 50 seconds	72°C x 30 seconds	
4°C x ∞	4°C x ∞	

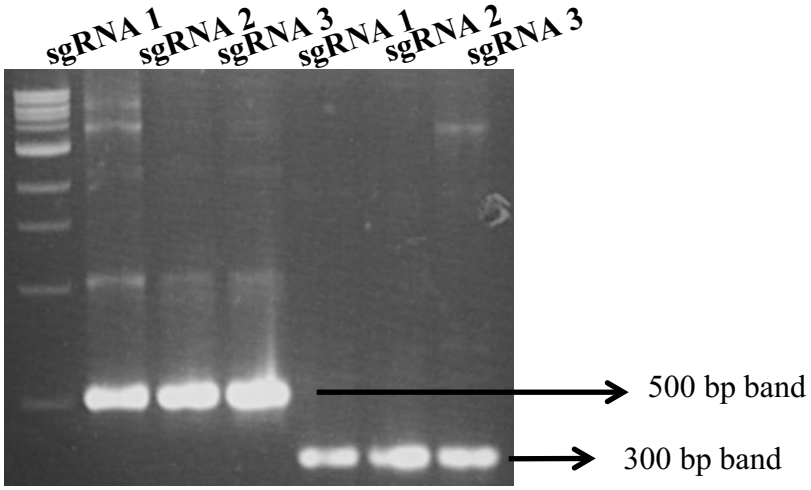

2. PCR C to get the 800bp product. The primers used are listed below.

PCR cycle for 800 bp product	
94°C x 2 minutes	
94°C x 15 seconds	30 cycles
60°C x 30 seconds	
72°C x 1 minute	
4°C x ∞	

The EcoRI and HindIII restriction sites are bold and underlined

Primer name	Primer sequence
U6 promoter EcoRI Forward primer	5'-CGG**GAATTCC**TCCAAGAACTCGTACAAAAATGCTCT-3'
U6 promoter HindIII Reverse primer	5'-CGG**AAGCTT**CACAGCCGACTATGTTTGGCGT-3'

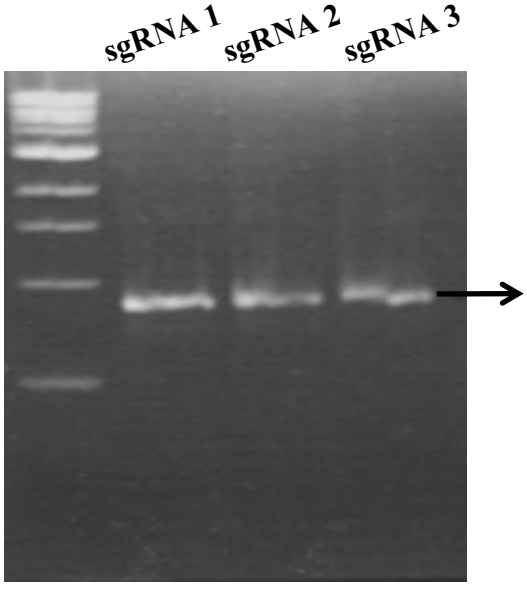

3. Restriction digestion of PCR product and plasmid DNA

800 bp PCR product restriction digestion mix

DNA	3.7 µl (0.24 µg)
EcoRI	1 µl
HindIII	1 µl
Buffer	2 µl
MilliQ	22.3 µl
	30 µl

PCR products were restriction digested for 20 minutes at 37 °C, followed by heat inactivation at 80 °C for 10 minutes.

pU6-unc119-sgRNA plasmid restriction digestion mix

DNA	3µl (1µg)
EcoRI	1 µl
HindIII	1 µl
Buffer	2 µl
MilliQ	13 µl
	20 µl

Plasmid DNA was restriction digested for 60 minutes at 37 °C, followed by heat inactivation at 80 °C for 10 minutes.

Cloning was done using standard techniques. Colonies were scored by colony PCR. The following primers were used for colony PCR.

Primer name	**Primer sequence**
M13 Forward primer	5'CCTGTGATTGGTGGGAGACAAACATTTAGATTT GCAATTCAATTATATATAG-3'
Cyk-1 sgRNA reverse primer	5'CCTGTGATTGGTGGGAGACAAACATTTAGATTT GCAATTCAATTATATATAG-3'